Title
Development of Chemical Probes for Studying Redox-Active Metals in Biology

Author
Aron, Allegra Tess

Publication Date
2018

Peer reviewed|Thesis/dissertation

Development of Chemical Probes for Studying Redox-Active Metals in Biology

By

Allegra Tess Aron

A dissertation submitted in partial satisfaction of the

requirements for the degree of

Doctor of Philosophy

in

Chemistry

in the

Graduate Division

of the

University of California, Berkeley

Committee in charge:

Professor Christopher J. Chang, Chair

Professor Evan Miller

Professor Daniel K. Nomura

Professor Andreas Stahl

Spring 2018

Development of Chemical Probes for Studying Redox-Active Metals in Biology

by Allegra Tess Aron

Abstract

Development of Chemical Probes for Studying Redox-Active Metals in Biology

By Allegra Tess Aron

Doctor of Philosophy in Chemistry

University of California, Berkeley

Professor Christopher J. Chang, Chair

Metals are necessary for sustaining life and play essential roles in each aspect of the central dogma of biology (DNA, RNA, and proteins). While many roles of redox-inactive metals in cellular signaling have been extensively characterized, the ability of redox-active transition metals like copper and iron to act as signals has been less explored. As these metals can aberrantly produce reactive oxygen species (ROS)[1], most research has considered redox-active transition metals as cofactors sequestered within enzyme active sites, despite the intricate cellular machinery regulating their concentration in exchangeable forms. Recently, new roles for redox-active metals in their exchangeable (or labile) forms have been elucidated; however, visualizing redox-active metals in real-time (with spatial and temporal resolution) and identifying their protein binding partners remain formidable challenges. This dissertation chronicles the design and applications of novel imaging probes and chemoproteomic strategies for probing redox-active metals in biology. This work describes both the first fluorescence resonance energy transfer (FRET) probe for imaging cellular Fe^{2+} and the first bioluminescence probe for imaging iron *in vivo*; both probes utilize an adamantyl-endoperoxide as the iron-reactive moiety. Additionally, this work describes new metalloproteomic methods aimed at identifying novel metal-binding proteins. Taken as a whole, this dissertation describes the development and application of new chemical methods for probing redox-active metals in biology by imaging and/or proteomics.

Dedication

To my parents,
for unwavering love and support.

Table of Contents

Acknowledgments		iii
Chapter 1	Synthetic Probes for Studying Transition Metal Signaling in Living Systems	1
Chapter 2	Design, synthesis, and application of an endoperoxide reactivity-based FRET probe for ratiometric fluorescence imaging of labile iron pools in living cells	22
Chapter 3	Design and synthesis of a luciferin-based probe for *in vivo* bioluminescence imaging of labile iron and application to a murine model of Acinetobacter baumannii infection	57
Chapter 4	Development of a chemoproteomic platform for the identification of copper-dependent cysteines	78
Appendix 1	Towards the development of fluorescent copper sensors targeted to subcellular organelles	110
Appendix 2	New methods for *in vitro* characterization of fluorescent copper sensors and control sensors	137
Appendix 3	Development of a panel of capped Fe(II)-reactive fluorescent probes	147
Appendix 4	Development of a platform for identification of metalloproteins using promiscuous photocrosslinking probes	180

Acknowledgments

Graduate school has been the most consistently challenging endeavor I've undertaken to date, and the constant love and encouragement of those around me have been essential for my success and happiness. I would like to thank my family for supporting me throughout the past six years, particularly my parents Ken and Felicia. I was lucky to attend graduate school close to home, and seeing my parents regularly sustained me over the past six years. I am indebted to them for countless dinners, for unwavering emotional support, and for always providing advice, a shoulder to cry on, or a place to stay in the city. I would also like to thank my sister, Zoe; even though we are very different, I appreciate her unwavering confidence in me.

Thank you to Professor Chris Chang for mentoring me over the past six years. I am so appreciative that Chris allowed me to pursue my diverse scientific interests. Chris has been an excellent mentor, providing countless resources for my success, setting up exciting and fruitful collaborations, providing invaluable career advice, and pushing me to be my best. I am additionally grateful for the support of Professor Eunsuk Kim, my undergraduate mentor at Brown. Eunsuk inspired me to pursue a Ph.D. in chemistry and continuously cheered me on with her praise and confidence in me. I am also indebted to Professor Carolyn Bertozzi, who provided me with advice as I was starting graduate school and who continues to inspire me.

The support of the Chang laboratory has also been essential to my graduate success. I feel at home in the Chang lab and am thankful to have made a number of lifelong friendships. I would especially like to thank Lakshmi Krishnamoorthy, Marie Heffern Thom Brewer, Eva Nichols, Cheri Ackerman, Karla Ramos-Torres, Mark Vander Wal, Joey Cotruvo, Brian Michel, Shixian Lin, Sumin Lee, Tyler Detomasi, Kevin Bruemmer, Jean-Marc Grandjean and Ryan Walvoord for their guidance, training, and/or friendship. The postdocs in the Chang lab taught me nearly all I know about how to do science, design experiments, think about data etc., so to them I am forever indebted. Thom, Lakshmi, and Marie each deserve a special thank you. Thom was my rock throughout graduate school. Not only did he provide me with the best chemistry advice, he also provided the most unwavering and non-judgmental friendship and encouraged me to be confident in myself. I am so lucky to have met a friend like Thom in graduate school. Additionally, Lakshmi and Marie have both been mentors to me throughout graduate school; I really look up to them for their strength, character, and will-power. I cherish their advice and friendship. I also am thankful for the constant friendship of my classmate Zach Hallberg.

Climbing has been a source of great happiness to me throughout graduate school. I am grateful to Eva and Jean-Marc for introducing me to climbing. Climbing has provided balance to my life over the past four years, as the mountains remind me that graduate school stresses are minor and relatively insignificant. Through climbing, I was able to meet a number of inspiring, supportive, amazing friends. Kerstin Lindstrom, Morgan Weiler, Katie Sieverman, Julian Bigi, Kim Keller, and Nicole Repina have made my time in Berkeley really special; I have enjoyed countless gym sessions, trips to Yosemite and Tahoe, and have developed a special trust with these friends. I will truly miss these friendships. I also want to thank my roommates, Katie Sieverman and Ross Pedersen. Living at 817 Kains Ave often felt like a safe haven during graduate school.

Finally, I am thankful that I have been able to keep in touch with a number of my friends from college. My friendships with Joanna Wohlmuth, Madeleine Heldman, Sarah Glick, Sameer Iyer, Elise & James Fishelson, Sam Baker, Dakota Gruener, and Joelle Murphy have sustained me and provided balance and perspective over the past six years.

Chapter 1

Synthetic Probes for Studying Transition Metal Signaling in Living Systems

Portions of this work were published in the following scientific journals:

Aron, A. T.; Reeves, A. G.; Chang, C. J.; "Activity-based sensing fluorescent probes for iron in biological systems", *Curr. Opin. Chem. Biol.* **2018**, *43*, 113-118.

Aron, A. T.; * Ramos-Torres, K. M.; * Cotruvo, Jr., J. A.; Chang, C. J. "Recognition- and Reactivity-Based Fluorescent Probes for Studying Transition Metal Signaling in Living Systems", *Acc. Chem. Res.* **2015**, *48*, 2434-2442.

Cotruvo, Jr., J. A.; Aron, A. T.; Ramos-Torres, K. M.; Chang, C. J. "Synthetic fluorescent probes for studying copper in biological systems", *Chem. Soc. Rev.* **2015**, *44*, 4400-4414.

* denotes equal contribution

1.1. Background and Motivation

Metals are necessary for sustaining all life, playing essential roles in all aspects of the central dogma of biology (e.g., DNA to RNA to proteins), as exemplified by the requirement of metal cofactors for function of all nucleic acids and an estimated one-third to one-half of all proteins, including DNA and RNA polymerases[1]. The biological chemistry of metals is remarkably versatile; metal ions provide permanent and transient structural reinforcement, mediate electron transfer, transport small-molecules, and act as Lewis-acid and redox catalysts. In most cases, a specific metal is required for a particular role, so it is critical that the proper level of that metal be present in the right place at the right time. This process of metal homeostasis is inherently dynamic because metals, unlike organic products, can neither be created nor destroyed under ambient biological conditions.

Accordingly, rapid changes in concentration gradients of metal ions can be used to mediate signaling processes; redox-inactive alkali, alkaline earth, and transition metals−especially calcium, sodium, potassium, and zinc−have been extensively studied in this regard. In contrast, the ability of redox-active transition metals like copper and iron to act as signals has been relatively less explored. As these metals can aberrantly produce reactive oxygen species (ROS)[1], most research has considered redox- active transition metals as cofactors sequestered within enzyme active sites, despite the intricate cellular machinery regulating their concentration in labile forms.

Iron is the most abundant transition metal in the human body and its capacity to cycle between various oxidation states is required for oxygen transport in globins, electron transfer in iron-sulfur (FeS) clusters and cytochromes, C-H functionalization by P450 oxygenases and non-heme congeners, and nucleotide synthesis by ribonucleotide reductase[2-6]. As such, iron homeostasis is precisely controlled from cellular to whole body level (Figure 1.1), with local and global overload and/or deficiency being detrimental. At the systemic whole body level, the hormone hepcidin is a main driver of iron homeostasis in mammals, regulating absorption of dietary iron, release of hepatic iron stores, and recycling of iron by macrophages[7-8]. At the cellular level, the transferrin receptor and divalent metal transporter-1 import proteins, iron storage protein ferritin, and ferroportin-1 export protein are in dynamic equilibrium with a "labile iron pool" (LIP) that exists in the center of this network and refers to a predominantly cytosolic pool of Fe^{2+} that is weakly bound to cellular ligands. Indeed, imbalances in LIPs are implicated in diseases ranging from cancer[9-12] to cardiovascular[13] and prion/neurodegenerative disorders to aging[14] and inflammation[15]. For example, proliferating cancer cells accumulate elevated concentrations of labile iron compared to normal cells owing to their increased metabolic activity, yet this expanded iron pool may also sensitize cancer cells to death by ferroptosis, a newly recognized iron-dependent cell-death pathway[16-17].

After iron, copper is the second most abundant redox-active transition metal in biology, and like iron, copper serves as a cofactor in a number of redox enzymes. Cuproenzymes are involved in a variety of essential processes, including electron transfer and substrate oxidation, iron uptake[18], and antioxidant defense[19-20]. Additional roles of copper include neurotransmitter synthesis/metabolism, epigenetic modifications[21], and handling of dietary amines[22-23]. In addition to this tightly-bound pool of copper, evidence for the presence of a “labile” pool of copper in cells, likely bound to ligands such as glutathione (GSH), is accumulating. Recently, copper has also been found to potentiate tumor growth in cancers that operate through mutations in BRAF, promoting MEK1/2 kinase activity in the MAPK pathway[24-25]. Like iron, copper homeostasis must also be precisely maintained (Figure 1.2); copper overload has been implicated in genetic

disorders like Wilson's disease[26], metabolic disorders[27], and neurodegenerative diseases like Alzheimer's, Parkinson's, and prion diseases[28], while copper deficiency has been implicated in genetic disorders like Menkes disease[29].

Our laboratory is interested in developing novel chemical tools to better understand the roles of transition metals in biology. Specifically, we are interested in understanding how labile (or chelatable/exchangeable) metal pools can act as dynamic signals in cells or whole animals. Towards this end, I have developed small-molecule fluorescent and bioluminescent sensors for visualizing labile iron chemoproteomics workflows for identification of novel metalloproteins. This dissertation summarizes progress on the development of chemical probes for transition metals and application to identify principles of transition metal signaling.

1.2. Fluorescent Probes: Recognition and Reactivity Approaches for Visualizing Iron and Copper in Biological Systems

1.2.1 Approaches for designing transition metal-sensing fluorescent probes

Metals in biology can be divided into two general pools: a static pool where metals are tightly bound by proteins and other macromolecules, and a labile pool where metals are bound relatively weakly to cellular ligands, including proteins and low-molecular weight ligands (Figure 1.1a). These smaller ligands include glutathione for copper[30], and citrate, phosphate, and glutathione for iron[31]. Exchange can occur between static and labile metal pools, and tightly-bound metal can exchange with variable kinetic parameters[32]. In some cases, this dynamic exchange can be transduced into cellular signaling events, such as the role of copper in neuronal activity (Figure 1.1b). In this context, fluorescent probes offer a potentially powerful set of tools for mapping labile metal pools with spatial and temporal resolution. However, as with any tool, there is no one-size-fits-all reagent; the diversity and chemical complexity of biological systems – including heterogeneities in pH, hydrophobicity, and local ligand concentrations – means that it is important, but not sufficient, to characterize these probes in a controlled in vitro chemical setting. As no synthetic buffer or additives can faithfully mimic all aspects of a biological specimen, *in vitro* characterization should not be relied upon solely for interpretation of probe efficacy. Application of a probe in a native biological context requires supporting experiments, including metal supplementation and chelation, genetic models of metal hyperaccumulation and depletion, bulk analysis of metal concentrations (e.g., XFM, Nano-SIMS, ICP), and comparative use of control dyes where the fluorophore scaffold is identical but has minimal to no metal response.

Useful probes for imaging transition metal dynamics in living systems must meet several criteria. First and foremost is a selective response to the metal of interest. For transition metals, this criterion is especially challenging, because these metals are far less abundant compared to their alkali/alkaline earth counterparts; for redox-active metals, specificity for a particular oxidation state is also required [e.g., Cu^{+} vs Cu^{2+}]. Probes must also have a dissociation constant (K_d) appropriate to compete with the predominant ligand(s) in a given biological context, which in many cases is in flux or even uncertain. Suitable photophysical properties – a large turn-on response and high optical brightness, and excitation and emission in the visible region – minimize potential disruption of cellular homeostasis because lower probe concentrations are needed for imaging experiments. Transition metals pose an additional challenge for turn-on detection as they can act as potent quenchers of fluorescence through a variety of mechanisms, including quenching by an unfilled d shell via electron or energy transfer[33-34]. Finally, probes

must be compatible with biological specimens (e.g., be non-toxic and water-compatible and exhibit predictable biodistribution).

We have pursued two general strategies for metal detection, termed "recognition" and "reactivity" (Fig. 1.2). Recognition-based sensing utilizes a fluorophore attached to a chelating group (receptor) specific to the metal of interest. Binding of analyte to the receptor results in a readily visualized optical change that is reversed upon analyte dissociation. A suitable receptor can often be designed based on coordination chemistry fundamentals, including hard-soft acid-base theory and preferred donor numbers and ligand field geometries. This strategy is best known for its successes in Ca^{2+} [35] and Zn^{2+} sensing[36-37], and we have applied it most extensively to Cu^{+} detection[36, 38-39]. Alternatively, a reactivity approach can be taken when receptor selectivity is challenging and/or when binding of metal of interest quenches fluorophore emission. In this approach, selectivity is derived from the ability of the analyte of interest to uniquely carry out chemistry that results in an optical change. Because this approach most commonly makes use of an irreversible reaction, the fluorescent signal accumulates over time, but reversible sensing is not possible. We have employed this reactivity-based approach for the detection of transient biological analytes such as hydrogen peroxide,[40] carbon monoxide,14 and hydrogen sulfide,15 as well as redox-active Co^{2+} and Fe^{2+} [41]. In both recognition- and reactivity-based modes, the probe provides information based on a chemical interaction rather than on an intrinsic property of the metal.

1.2.2 Reactivity-based sensing fluorescent probes for iron in biological systems

The broad contributions of iron status in health, aging, and disease provide motivation to develop new methods for biological iron detection[39, 42-43], particularly in its labile Fe^{2+} forms. Fluorescence detection in particular offers the convenience of a real-time optical readout that can enable biological study across a variety of length scales. Because Fe^{2+} is a potent fluorophore quencher by energy and electron transfer[33-34] and a weak binder on the Irving-Williams series, [44] conventional chelation-based probes for iron detection (Figure 2) suffer largely from a turn-off response and/or limitations in metal ion selectivity [45-50]. To address these issues, we[51-52] and others [53-56] have recently developed reagents for "turn-on" detection of labile Fe^{2+}. These probes share a general design approach that we term "activity-based sensing" (ABS), which relies on molecular reactivity, rather than molecular recognition, to achieve high chemical selectivity in complex biological systems. As such, "activity" refers to the ability of the moiety present in a probe to confer reactivity with Fe^{2+}.

Design considerations for fluorescent Fe^{2+} probes

Detection of biological Fe^{2+} presents a number of difficulties, including sensitivity to labile iron pools that span a wide range of potential concentrations (high nM - low μM)[46, 57], the need for metal and oxidation state specificity, particularly over Fe^{3+} and divalent metals that are abundant in biological systems or stronger in the Irving-Williams series, and a turn-on or ratiometric response to avoid non-specific quenching by electron and/or energy transfer. ABS is well-suited to meet these challenges, and recent advances have largely exploited the redox activity of Fe^{2+} for its selective detection (Figure 1.2 and Table 1.1). The following sections describe currently available reaction-based probes for detecting Fe^{2+} in biological systems.

Iron probes via N-oxide reduction

Hirayama and Nagasawa introduced RhoNox-1, the first member in a series of reagents that harness Fe^{2+}-mediated N-oxide reduction for iron detection [53]. The N-oxide moiety quenches RhoNox-1 through both twisted internal charge transfer (TICT) and photo-induced electron transfer (PET) processes, which are relieved after reaction with Fe^{2+} to produce the parent rhodamine dye. RhoNox-1 is capable of detecting exogenous addition of Fe^{2+} to HepG2 liver cells in addition to visualizing decreases in basal Fe^{2+} upon 2,2'-bipyridine treatment. More recently, RhoNox-1 has been successfully applied to detect elevations in Fe^{2+} in A549 lung carcinoma cells treated with plasma-activated medium[58], in addition to a number of other biological models.[59-62]

The N-oxide reduction strategy has proved broadly useful for developing an expanded toolbox of fluorescent Fe^{2+} probes through ABS. For example, HMRhoNox-M and related hydroxymethylrhodamine and hydroxymethylrhodol derivatives exhibit improved turn-on responses with reduced pH sensitivity, enabling visualization of iron uptake via transferrin endocytosis [54] and iron accumulation in ovarian endometriosis[63], along with other applications[64]. In addition, SiRhoNox-1 is the most red-shifted and sensitive probe of an expanded color palette that is capable of detecting endogenous iron pools by both microscopy and flow cytometry [55]. This reagent also reveals a shift in intracellular redox equilibrium towards labile iron in response to hypoxia in both living cells and in 3D tumor spheroids, an increase that appears to be independent of iron uptake pathways. Finally, a related Fe^{2+}-dependent nitroxide reduction reaction has been employed for ABS of ferrous ions[65]. Fe^{2+}-mediated reduction of the 2,2,6,6-tetramethylpiperidine 1-oxyl (TEMPO) radicals of CouT and RhT triggers both a fluorescence turn-on and a change in electron paramagnetic resonance (EPR) signal.

A fluorescent iron probe utilizing biomimetic oxygen activation

In parallel, our laboratory developed an alternative ABS strategy for Fe^{2+} detection by exploiting a biomimetic iron-binding motif to activate oxygen for oxidative C-O cleavage and release of a fluorescent product. Indeed, prior work by Taki [66] and our laboratory [67] on creation of fluorescent indicators for copper and cobalt, respectively, presaged the general utility of this strategy for redox-active metal detection.[68] Inspired by heme P450, mononuclear non-heme enzymes containing a 2-His-1-carboxylate motif, and their corresponding model complexes, the first-generation reagent Iron Probe 1 (IP1) employs a receptor with a mixed nitrogen/oxygen donor set for Fe^{2+} coordination with an open site for O_2 binding and activation.[51] Binding of Fe^{2+} and O_2 at this recognition motif results in an oxidative cleavage of the C-O bond and release of a fluorescent fluorescein alcohol[67]. The Fe^{2+}-triggered turn-on response for IP1 is highly selective over other biologically relevant metals (aside from Co^{2+}, noting that mammalian Co^{2+} exists primarily in tightly-bound vitamin B12/cobalamin forms).[69]

IP1 is capable of detecting changes in iron status with iron supplementation and chelation in HepG2/C3A liver cells, as well as endogenous changes in labile Fe^{2+} upon treatment of these cells with ascorbic acid, a vitamin known to promote redox cycling and mobilization of iron. Interestingly, an increase in IP1 fluorescence was also observed upon treatment with hepcidin, the key iron regulatory hormone responsible for degrading iron export protein (ferroportin). The largely lysosomal localization of this probe in HepG2 models can potentially limit its signal-to-noise responses but also makes it attractive for reporting on LIPs in these cellular storage compartments.

ABS iron probes based on peroxide activation

IP-1 relies on an oxygen-dependent, three-component sensing mechanism (probe, Fe^{2+}, and O_2) for iron detection. As such, our laboratory has sought to explore alternative ABS strategies that would utilize a direct reaction between a probe and Fe^{2+} for sensing purposes. Inspired by endoperoxide motifs that are a common feature of natural product anticancer and antimalarial drugs such as artemisinin[70-74], as well as synthetic compounds that enable specific targeting of tumors or parasites via local iron-dependent drug release[75-78], we turned our attention to developing ABS probes that exploit peroxide activation. Indeed, recent work by our laboratory and Renslo has established the efficacy of this approach for Fe^{2+} detection.

Trx-puro is a puromycin-based probe that utilizes an endoperoxide-caged puromycin to report on intracellular iron levels in fixed samples through an immunofluorescence readout [56]. Specifically, Fe^{2+}-dependent cleavage of Trx-puro yields puromycin, which is incorporated into growing polypeptide chains to yield a covalent tag that can be detected with puromycin-specific antibodies upon cellular fixation. Trx-puro exhibits high selectivity for Fe^{2+} over a variety of biologically-relevant metals, reductants, and oxidants and can be used to compare intracellular Fe^{2+} levels across a variety of cell types, including identification of expanded labile iron pools in cancer cell lines as compared to their non-cancerous counterparts. The high sensitivity of this probe also enabled detection of changes in intracellular iron status when expression of the major iron storage protein (ferritin heavy chain, FHC) or export protein (ferroportin, FPN) was altered.

In parallel, our laboratory reported FRET Iron Probe 1 (FIP-1), a first-generation endoperoxide probe for use in live-cell settings.[52] This thesis presents a description of FIP-1, a unique ratiometric indicator for Fe^{2+}. As described in this thesis, this dye makes use of an Fe^{2+}-cleavable endoperoxide linker to regulate FRET between donor and acceptor dyes. In the absence of Fe^{2+}, efficient FRET occurs between the covalently-linked 5-aminomethyl fluorescein (5-AMF) donor dye and the Cy3 acceptor dye; in the presence of Fe^{2+}, the endoperoxide linker is cleaved to separate the dyes into two fragments, reducing FRET efficiency. Owing to its endoperoxide ABS trigger, FIP-1 retains high selectivity and sensitivity for Fe^{2+} over a variety of biologically-relevant metal ions, oxidants, and reductants and is capable of detecting both increases and decreases in LIPs in HEK 293T cells and other models upon iron supplementation and/or depletion. Moreover, application of FIP-1 provides, to the best of our knowledge, the first direct imaging evidence for changes in labile iron levels during ferroptosis, opening the door to identifying and studying iron fluxes involved in other cell signaling pathways.

1.3 Chemoproteomic Tools: isoTOP-APBB and Photocrosslinking Approaches

The aforementioned imaging probes allow us to visualize changes in the location and levels of labile metals in a cell. We hypothesize that metal redistributions occur in the cell for a reason; perhaps labile metals can bind to target proteins to elicit some response. Recently, two examples of this have emerged. Our laboratory uncovered a novel role for Cu^+ in regulating lipolysis by modulating the activity of phosphodiesterase PDE3B.[79] Additionally, a role for copper in the mitogen activated protein kinase (MAPK) pathway has also been recently elucidated; cellular copper influx enhances phosphorylation of ERK1/2 through an interaction between copper and MEK1/2[24-25]. These key examples suggest an important and emerging role for copper as a dynamic signaling entity that can interact with cellular proteins to modulate

function. We hypothesized that in addition to these two recent examples, a number of other cellular proteins may bind metals in a way that alters activity or function. In order to gain insight into the physiological consequences of movement of labile metals, we envisioned developing a strategy to profile uncharacterized copper-binding proteins.

A variety of strategies have been taken to profile metalloproteins; these strategies include bioinformatics/*in silico* methodologies, enrichment strategies, traditional protein separation followed by metal detection, and the use of metal-directed separation followed by protein identification. Bioinformatic approaches have been performed by searching known protein sequences (and perhaps incorporating 3D protein structure) for metal binding domains; however, these approaches are difficult due to the lack of metal-binding consensus sequences[80-81]. Immobilized metal affinity chromatography (IMAC) has also been used to enrich for metal-binding proteins, which are subsequently identified. In these approaches, cell lysate is typically run over a metal loaded affinity column and these proteins are then separated by 1D or 2D gel electrophoresis and subjected to protein identification by mass spectrometry[82-83]. Alternatively, traditional approaches for separation followed by protein and metal identification have also been performed[84-86]. For these approaches, proteins are first separated by 1D or 2D gel electrophoresis. Coomassie staining is carried out to locate proteins on the gel, then x-ray fluorescence or laser ablation inductively coupled mass spectrometry (LA-ICP-MS) is performed to analyze the metal content of each spot. Each spot can subsequently be cut out, digested, and identified by mass spectrometry. Finally, Adams et al developed a novel method for metal-directed separation and protein ID[87].

ABPP, pioneered by Ben Cravatt, makes use of reactive small-molecule probes to report on enzyme function in native biological samples on a whole proteome level[88-89]. ABPP has been utilized to profile the reactivity of specific enzyme classes and amino acid residues. Briefly, ABPP probes have been used to profile a diverse range of enzyme classes such as serine hydrolases and metallohydrolases, cysteine proteases, and phosphatases as well as specific amino acids like cysteines and lysines (Figure 1.6b)[89]. While genomics can provide a complete list of proteins in an organism, ABPP technology can uniquely provide information about enzyme function. For example, ABPP can be instrumental in hinting at the function of proteins that lack annotated function. Additionally, ABPP can uniquely report on protein post-translational modifications (PTMs); genomics is incapable of yielding this information. ABPP has been used to profile PTMs ranging from S-sulfenylation[90] to S-nitrosylation[91] to palmitoylation[92].

ABPP probes are made up of three important components (Figure 1.6a) – a reactive "warhead", a spacer, and a tag or handle for pull-down. The reactive "warhead" gives the probe its specificity; for example, a "warhead" can be an electrophilic group, such as iodoacetamide or maleimide for cysteine-reactive probes. For active-site-directed covalent probes, this "warhead" may resemble an active-site inhibitor, such as using a phosphonate electrophile to target serine hydrolases. The tag or handle for pulldown is either a fluorophore, a biotin, or an alkyne. The alkyne handle can be used to append a fluorophore or biotin through Cu-catalyzed Click chemistry. The spacer separates the reactive group from the tag/handle. ABPP has made use of both gel electrophoresis platforms and liquid chromatography-mass spectrometry (LC-MS) platforms. Using gel electrophoresis, labeled proteins can be visualized using a Cu-catalyzed reaction between the alkyne and a fluorophore-azide and can be resolved by a one-dimensional (1D) or two-dimensional (2D) sodium dodecyl sulfate polyacrylamide gel electrophoresis (SDS-PAGE) experiment. This strategy can be limited by the poor resolution on an SDS-PAGE gel; as such, LC-MS can be used instead by appending a biotin-azide to labeled proteins through Click

chemistry for subsequent enrichment of targets of interest. Both strategies have been used for a number of applications, and numerous reviews have extensively covered these applications[88-89].

More recently, this workflow has been adapted to quantitatively profile reactivity of and modifications on specific amino acids[93]. The use of ABPP for quantitative mass spectrometry was pioneered by Weerapana & Cravatt in a workflow called isotopic Tandem Orthogonal Proteolysis (isoTOP)-ABPP.[93] This workflow makes use of isotopically-heavy and light probe (or tag) in parallel treatments so that two treatments can be directly compared by mass spectrometry. Using this approach, Weerapana profiled functional cysteines in the proteome; more recently, this approach has been used to identify zinc-binding cysteine residues.[94] Toward this end, we envisioned employing quantitative chemoproteomics to map cysteine reactivity of exogenously added copper in complex biological lysates. More specifically, we envisioned using activity-based protein profiling (ABPP) for this goal.

1.4. Dissertation Overview

An interest in the role of labile redox-active metals in biology has inspired the design of (1) probes for *in cellulo* and *in vivo* detection of redox-active metals and (2) chemoproteomic workflows for the identification of novel metalloproteins. This dissertation focuses on the design, synthesis, and application of a diverse set of probes for the detection of biological Fe^{2+} and the development of a chemoproteomic strategy for identification of novel copper-binding proteins.

Chapter 2 presents the design, synthesis, characterization, and application of FRET Iron Probe 1 (FIP-1), the first ratiometric probe of its type for Fe^{2+}. This chapter highlights the use of this probe to visualize labile iron release during ferroptosis, a novel form of cell death.

Chapter 3 details the extension of this Fe^{2+}-sensing strategy toward *in vivo* detection of Fe^{2+}. This chapter presents the design, synthesis, and characterization of Iron Caged Luficerin 1 (ICL-1) probe. Application of this probe to proof-of-concept imaging experiments in living mice and application of this probe to an *Acinetobacter baumannii* infection model was demonstrated.

Chapter 4 discusses a chemoproteomic workflow developed to identify uncharacterized copper-binding proteins. This workflow makes use of isoTOP-ABPP; a cysteine-reactive probe is used along with quantitative mass spectrometry to generate a list of potential-copper binding proteins. Efforts to validate this list of proteins are presented.

Appendices detail the development of targetable copper probes (Appendix 1) and new strategies for assessing copper-response *in vitro* (Appendix 2), a panel of turn-on probes for *in vitro* detection of Fe^{2+} (Appendix 3), and strategies for identification of novel metalloproteins (Appendix 4).

Figures

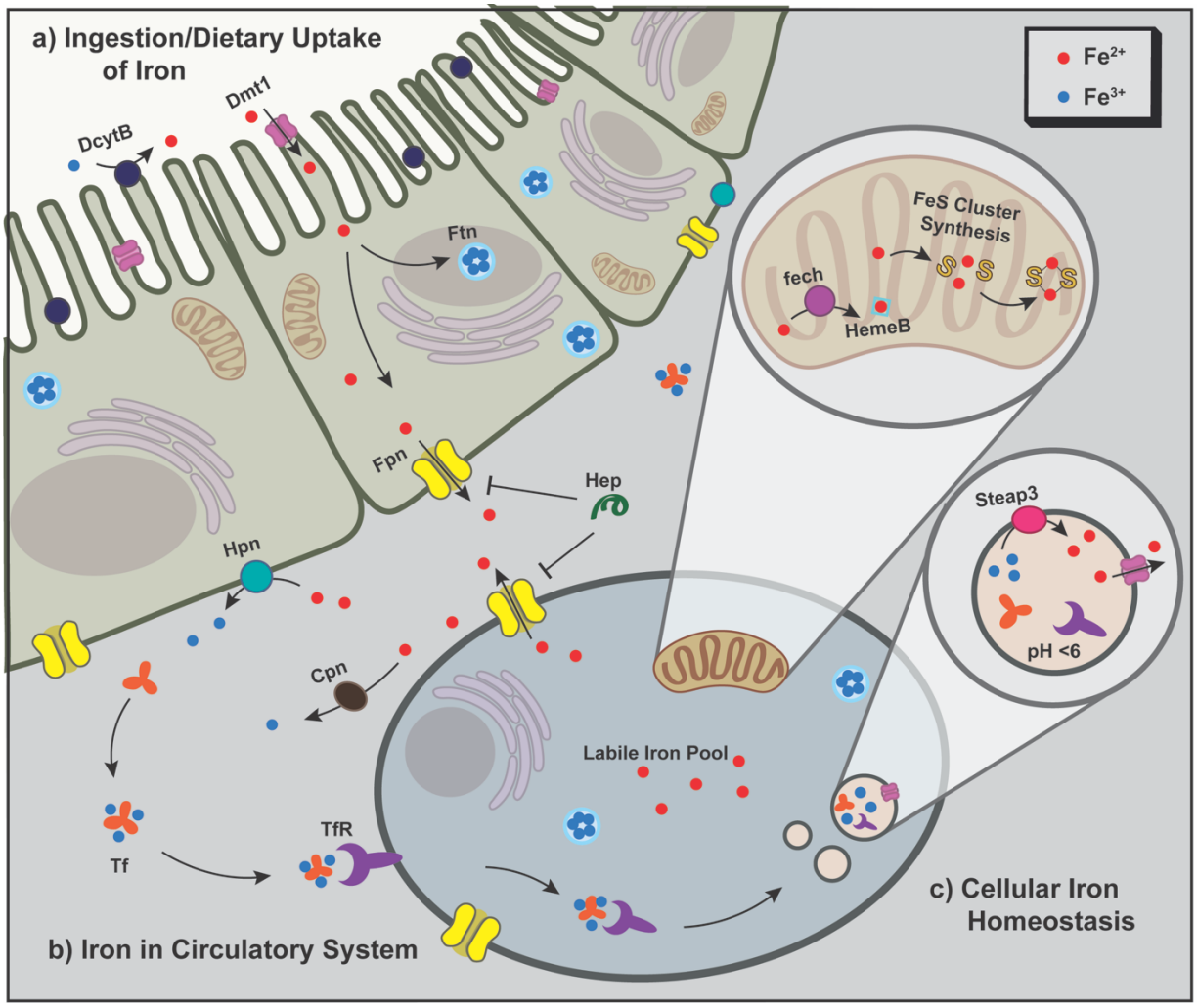

Figure 1.1. Iron homeostasis is highly regulated at both systemic whole body and cellular levels. (a) Iron from the diet is absorbed in the intestine. (b) Once in circulation, iron is bound to transferrin (Tf) as Fe^{3+}. (c) From the circulation system, iron can enter cells, which maintain iron homeostasis through a complex network of proteins. While Hepcidin (Hep) is a hormone that controls systemic homeostasis, cellular homeostasis is maintained through a dynamic network of import proteins including transferrin (Tf)/transferrin receptor (TfR) and divalent metal transporter-1 (Dmt1), storage proteins like ferritin (Ftn), and export proteins like ferroportin-1 (Fpn), in dynamic exchange with a central labile iron pool (LIP) that is comprised predominantly of Fe^{2+} coordinated to weakly-bound ligands.

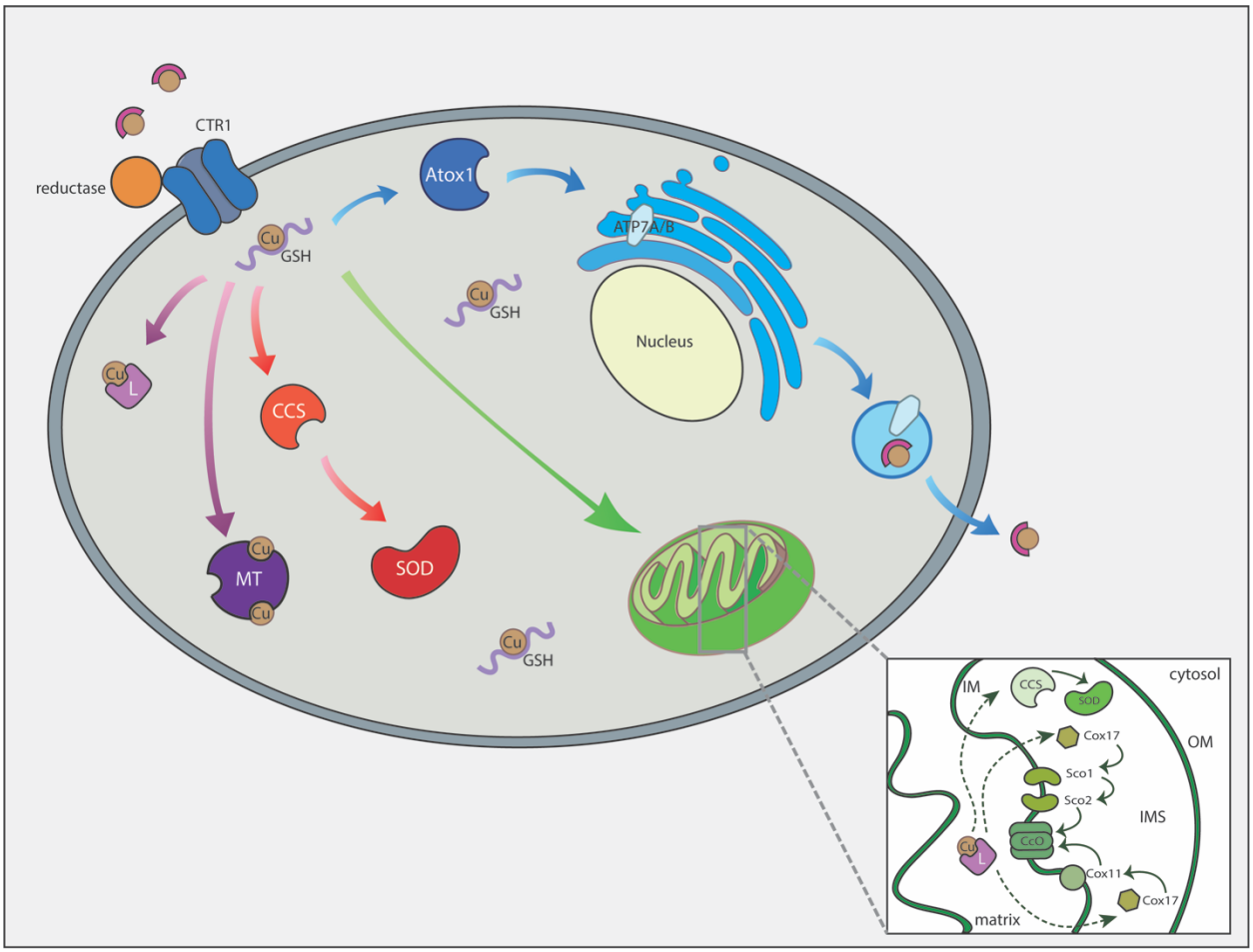

Figure 1.2. A simplified overview of copper handling pathways in a eukaryotic cell. Cu^{2+} is reduced to Cu^{+} then can enter the cell through CTR1, the principal high-affinity copper importer. Upon entry, copper interacts with cellular ligands and with chaperones that mediate its delivery to specific proteins. Glutathione (GSH) can buffer Cu^{+} pools and mediate Cu^{+} transfer between CTR1 and metallochaperones. Atox1 is the chaperone responsible for copper delivery to ATP7A and ATP7B, which reside in the trans-Golgi network. This is where the majority of cuproproteins are metallated. These ATPases are also involved in copper efflux from the cell. Delivery of copper to cytosolic SOD1 proceeds through the metallochaperone CCS. In the mitochondrion, an ensemble of mitochondrial proteins is required for metallation of the cytochrome c oxidase (CcO) complex. Cox17 delivers copper to Cox11 for the CuB site of CcO, while also delivering copper to Sco1 and Sco2 for the CuA site. CCS present in the intermembrane space (IMS) provides copper to a mitochondrial pool of SOD1. The small copper ligand (L) is proposed to buffer copper in the mitochondrion and may also be involved in copper delivery to that organelle. Metallothioneins (MTs) bind Cu tightly and protect the cell against copper overload and oxidative stress. Whereas XFM data show the presence of copper in the nucleus, its mechanism of transport and its nuclear ligands are currently unknown.

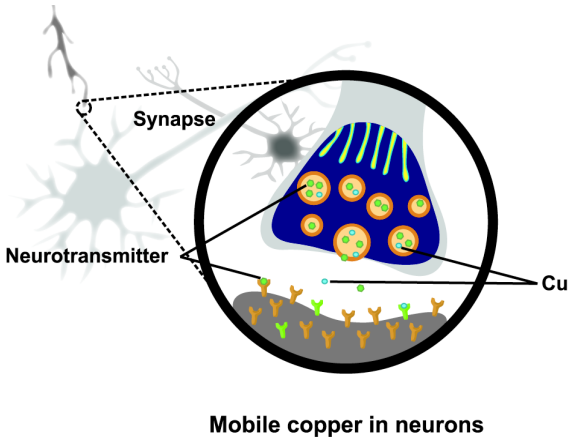

Figure 1.3. Mobile copper in neurons as an example of transition metal signaling.

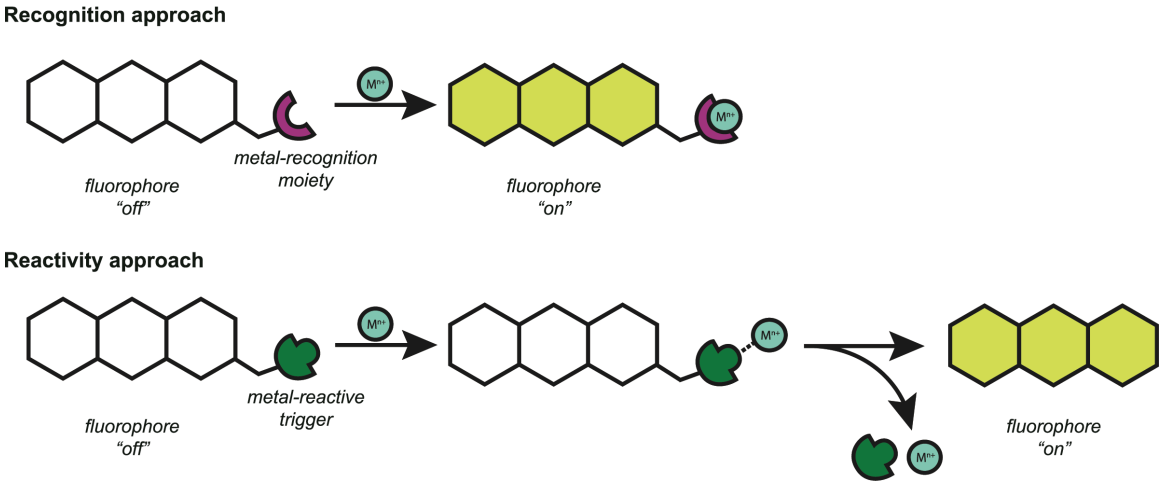

Figure 1.4. Recognition- and reactivity-based approaches for fluorescent metal probes.

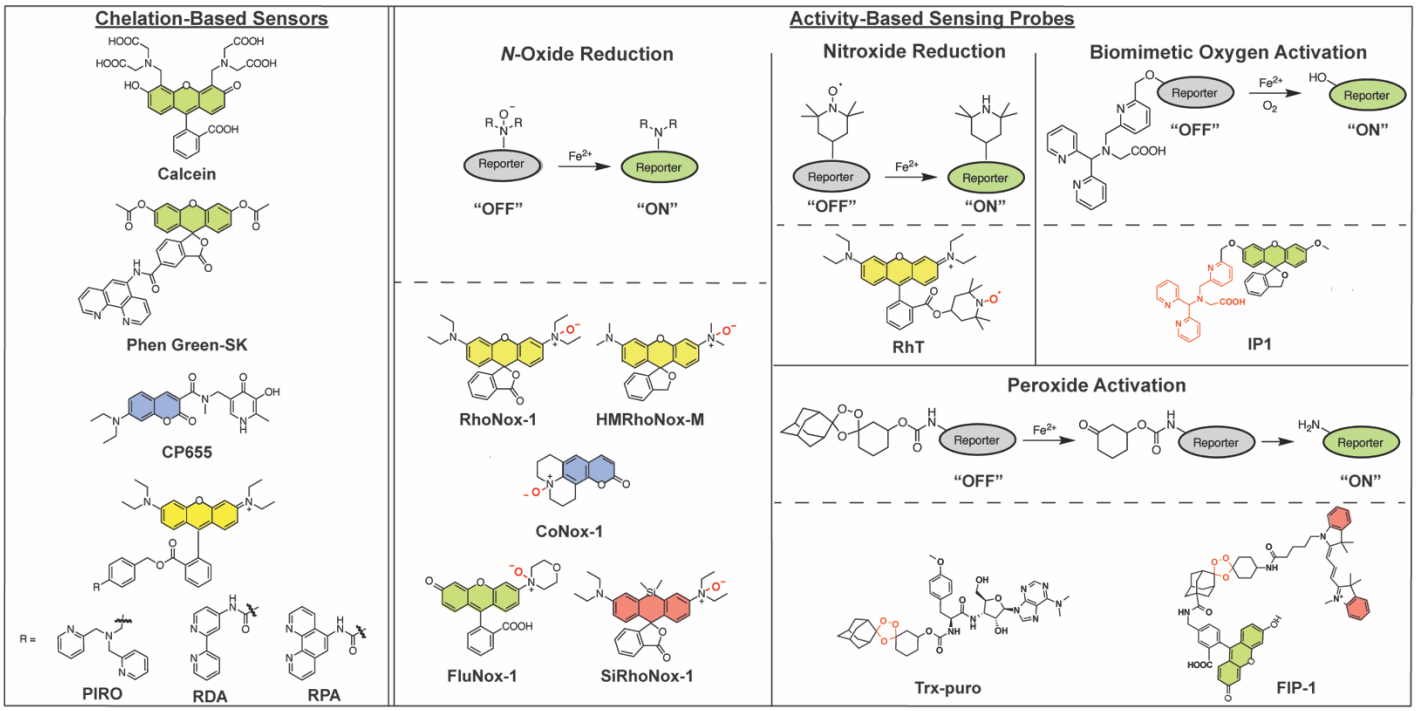

Figure 1.5. Chemical probes for fluorescent Fe^{2+} detection, divided into chelation-based probes (left) and activity-based sensing (ABS) probes (right), with iron-reactive triggers highlighted in red.

Table 1: Summary of Activity-Based Sensing Fluorescent Fe probes				
	λ_{ex} (nm)	λ_{em} (nm)	Response to Fe *in vitro*	Biological System Examined
***N*-oxide reduction probes**				
RhoNox-1 [31]	540	575	30-fold turn-on to 20 μM Fe (2 μM probe, 1 h, 50 mM HEPES)	Cells (HEPG2, A549)
HMRhoNox-M [32]	550	575	60-fold turn-on to 20 μM Fe (2 μM probe, 1 h, 50 mM HEPES)	Cells (HEPG2, endometrial stromal, epithelial, mesothelioma, fibroblast)
CoNox-1 [33]	295/405	495	10-fold turn-on to 20 μM Fe (2 μM probe, 1 h, 50 mM HEPES)	Cells (HEPG2)
FluNox-1 [33]	450/488	530	30-fold turn-on to 20 μM Fe (2 μM probe, 1 h, 50 mM HEPES)	Cells (HEPG2)
SiRhoNox-1 [33]	575/630	660	60-fold turn-on to 20 μM Fe (2 μM probe, 1 h, 50 mM HEPES)	Cells (HEPG2)
Nitroxide reduction probes				
RhT [43]	557	580	2.5-fold turn-on to 24 μM Fe (10 mM MOPS)	Cells (Ws1 fibroblasts)
Biomimetic oxygen activation probes				
IP1 [29]	470	508	6-fold turn-on to 20 μM (1 μM probe, 1 h, 50 mM Tris)	Cells (HEPG2/C3A)
Perxoide activation probes				
Trx-puro [34]	N/A	N/A	N/A - immunofluorescent readout *in cellulo*	Cells (U2OS, PC3)
FIP-1 [30]	495 and 545	515 and 556	1.7-fold ratio-change to 10 μM Fe (1 μM probe, 1 h, 50 mM HEPES)	Cells (HEK293T, MDA-MB 231, U2OS, MCF10A)

Table 1.1. Summary of Activity-Based Sensing Fluorescent Fe^{2+} probes.

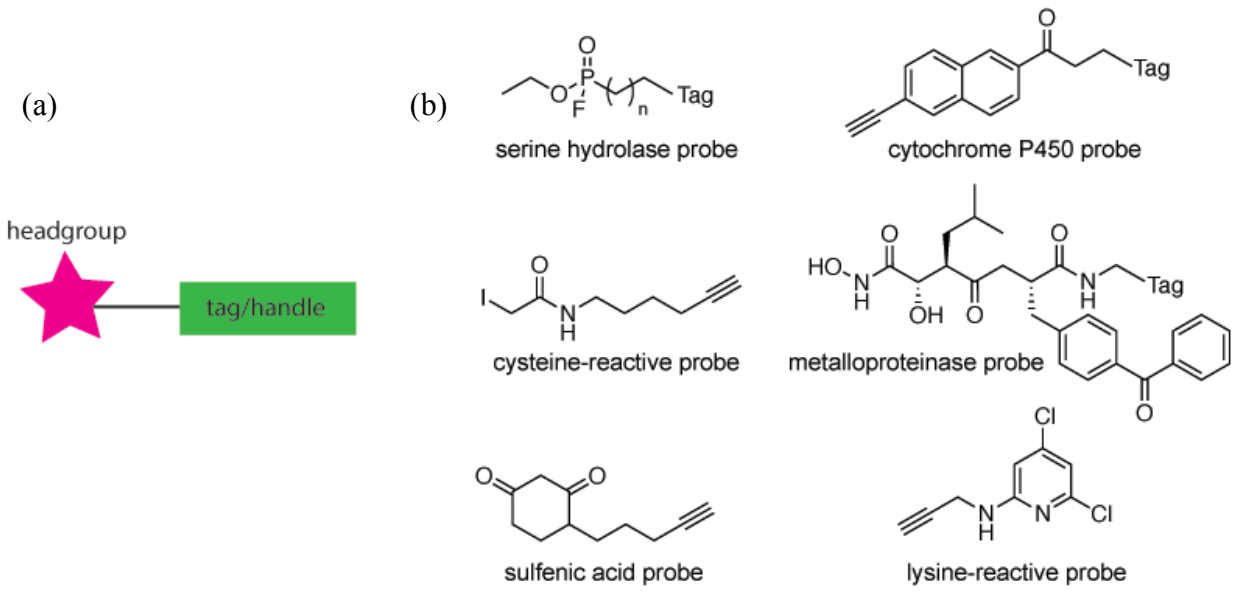

Figure 1.6. (a) ABPP probes contain three main components – a headgroup (or "warhead"), a linker, and a tag or handle for "Click" chemistry. (b) Examples of ABPP probes.

1.5. References

1. Lippard, S. J.; Berg, J. M., *Principles of Bioinorganic Chemistry*. University Science Books: Mill Valley, CA,: Mill Valley, CA, 1994.
2. Cammack, R.; Wrigglesworth, J. M.; Baum, H., *Transport and Storage*. CRC Press: 1989.
3. Johnson, D. C.; Dean, D. R.; Smith, A. D.; Johnson, M. K., Structure, function, and formation of biological iron-sulfur clusters. *Annu Rev Biochem* **2005,** *74*, 247-81.
4. Andrews, N. C., Iron homeostasis: insights from genetics and animal models. *Nat Rev Genet* **2000,** *1* (3), 208-17.
5. Xu, W.; Barrientos, T.; Andrews, N. C., Iron and copper in mitochondrial diseases. *Cell Metab* **2013,** *17* (3), 319-28.
6. Lippard, S. J.; Berg, J. M., *Principles of Bioinorganic Chemistry*. University Science Book: Mill Valley, 1994.
7. Ganz, T., Systemic Iron Homeostasis. *Phys Rev* **2013,** *93* (4), 1721-1741.
8. Ganz, T.; Nemeth, E., Hepcidin and iron homeostasis. *Biochim Biophys Acta* **2012,** *1823*, 1434-1443.
9. V., T. S.; M., T. F., Iron and cancer: more ore to be mined. *Nat Rev Cancer* **2013,** *13* (5), 342-55.
10. Wu, K. J.; Polack, A.; Dala-Favera, R., Coordinated regulation of iron-controlling genes, H-ferritin and IRP2, by c-MYC. *Science* **1999,** *283*, 676-9.
11. Pinnix, Z. K.; Miller, L. D.; Wang, W.; D'Agostino, R. J.; Kute, T.; Willingham, M. C.; Hatcher, H.; Tesfay, L.; Sui, G.; Di, X.; Torti, S. V.; Torti, F. M., *Sci. Transl. Med.* **2010,** *2* 43ra56.
12. Toyokuni, S., Role of iron in carcinogenesis: cancer as a ferrotoxic disease. *Cancer Sci.* **2009,** *100* (1), 9-16.
13. von Haehling, S.; Jankowska, E. A.; van Veldhuisen, D. J.; Ponikowski, P.; Anker, S. D., *Nat. Rev. Cardiol.* **2015,** *12*, 659-669.
14. James, S. A.; Robert, B. R.; Hare, D. J.; de Jonge, M. D.; Birchall, I. E.; Jenkin, N. L.; Cherny, R. A.; Bush, A. I.; McColl, G., *Chem. Sci.* **2015,** *6*, 2952-2962.
15. Wessling-Resnick, M., Iron Homeostasis and the Inflammatory Response. *Ann Rev Nutr* **2010,** *30*, 105-122.
16. Dixon, S. J.; Lemberg, K. M.; Lamprecht, M. R.; Skouta, R.; Zaitsev, E. M.; Gleason, C. E.; Patel, D. N.; Bauer, A. J.; Cantley, A. M.; Yang, W. S.; Morrison, B. I.; Stockwell, B. R., *Cell* **2012,** *149* (1060-72).
17. Stockwell, B. R.; Angeli, J. P. F.; Bayir, H.; Bush, A. I.; Conrad, M.; Dixon, S. J.; Fulda, S.; Gasco, S.; Hatzios, S. K.; Kagan, V. E.; Noel, K.; Jiang, X.; Linkermann, A.; Murphy, M. E.; Overholtzer, M.; Oyagi, A.; Pagnussat, G. C.; Park, J.; Ran, Q.; Rosenfeld, C. S.; Salnikow, K.; Tang, D.; Torti, F. M.; Torti, S. V.; Toyokuni, S.; Woerpel, K. A.; Zhang, D. D., Ferroptosis: A Regulated Cell Death Nexus Linking Metabolism, Redox Biology, and Disease. *Cell* **2017,** *171* (2), 273-285.
18. Hellman, N. E.; Gitlin, J. D., Ceruloplasmin metabolism and function. *Annu. Rev. Nutr.* **2002,** *22*, 439-458.
19. McCord, J. M.; Fridovich, I., Superoxide Dismutase: An Enzymuc Function for Erythrocuprein (Hemocuprein). *J. Biol. Chem.* **1969,** *244*, 6049-6055.

20. Reddi, A. R.; Culotta, V. C., SOD1 Integrates Signals from Oxygen and Glucose to Repress Respiration. *Cell* **2013,** *152*, 224-235.
21. Herranz, N.; Dave, A.; Millanes-Romero, A.; Morey, L.; Diaz, V. M.; Lorenz-Fonfria, V.; Gutierrez-Gallego, R.; Jeronimo, C.; Di Croce, L.; de Herreros, A.; Peiro, S., Lysyl oxidase-like 2 deaminates lysine 4 in histone H3. *Mol. Cell* **2012,** *46*, 369-376.
22. Klinman, J. P., The multi-functional topa-quinone copper amine oxidases. *Biochim. Biophys. Acta* **2003,** *1637*, 131-137.
23. Dawkes, H. C.; Phillips, S. E., Copper amine oxidase: Cunning cofactor and controversial copper. *Curr. Opin. Struct. Biol.* **2001,** *11*, 666-673.
24. Brady, D. C.; Crowe, M. S.; Turski, M. L.; Hobbs, G. A.; Yao, X.; Chaikuad, A.; Knapp, S.; Xiao, K.; Campbell, S. L.; Thiele, D. J.; Counter, C. M., Copper is required for oncogenic BRAF signalling and tumorigenesis. *Nature* **2014,** *509*, 492-496.
25. Turski, M. L.; Brady, D. C.; Kim, H. J.; Kim, B.-E.; Nose, Y.; Counter, C. M.; Winge, D. R.; Thiele, D. J., A Novel Role for Copper in Ras/Mitogen-Activated Protein Kinase Signaling. *Mol Cell Biol* **2012,** *32* (7), 1284-1295.
26. Lutsenko, S., Atp7b-/- mice as a model for studies of Wilson's disease. *Biochem. Soc. Trans.* **2008,** *36*, 1233-1238.
27. Huster, D.; Purnat, T. D.; Burkhead, J. L.; Ralle, M.; Fiehn, O.; Stuckert, F.; Olson, N. E.; Teupser, D.; Lutsenko, S., High Copper Selectively Alters Lipid Metabolism and Cell Cycle Machinery in the Mouse Model of Wilson Disease. *J. Biol. Chem.* **2007,** *282*, 8343-8355.
28. Que, E. L.; Domaille, D. W.; Chang, C. J., Metals in Neurobiology: Probing Their Chemistry and Biology with Molecular Imaging. *Chem. Rev.* **2008,** *108* (5), 1517-1549.
29. Vulpe, C.; Levinson, B.; Whitney, S.; Packman, S.; Gitschier, J., Isolation of a candidate gene for Menkes disease and evidence that it encodes a copper-transporting ATPase. *Nat Genet.* **1993,** *3* (1), 7-13.
30. Maryon, E. B.; Molloy, S. A.; Kaplan, J. H., Cellular glutathione plays a key role in copper uptake mediated by human copper transporter 1. . *Am. J. Physiol. Cell. Physiol.* **2013,** *304*, C768-C779.
31. Brissot, P.; Ropert, M.; Le Lan, C.; Loréal, O., Non-transferrin bound iron: A key role in iron overload and iron toxicity. . *Biochim. Biophys. Acta.* **2012,** *1820*, 403-410.
32. Banci, L.; Bertini, I.; Ciofi-Baffoni, S.; Kozyreva, T.; Zovo, K.; Palumaa, P., Affinity gradients drive copper to cellular destinations. *Nature* **2010,** *465*, 645-648.
33. Kemlo, J. A.; Shepherd, T. M., Quenching of Excited Singlet States by Metal Ions. *Chem. Phys. Lett.* **1977,** *47* (1), 158-162.
34. Varnes, A. W.; Dodson, R. B.; Wehry, E. L., Interactions of transition-metal ions with photoexcited states of flavines. Fluorescence quenching studies. *J. Am. Chem. Soc.* **1972,** *94* (3), 946-950.
35. Tsien, R. Y., ed. by E. Carafoli and C. Klee. New York: Oxford University Press, 28-54., *Calcium as a Cellular Regulator*. Oxford University Press: New York, p 28-54.
36. Que, E. L.; Domaille, D. W.; Chang, C. J., Metals in neurobiology: probing their chemistry and biology with molecular imaging. *Chem. Rev.* **2008,** *108*, 1517-1549.
37. Carter, K. P.; Young, A. M.; Palmer, A. E., Fluorescent Sensors for Measuring Metal Ions in Living Systems *Chem. Rev.* **2014,** *114* (8), 4564–4601.
38. Cotruvo, J. A.; Aron, A. T.; Ramos-Torres, K. M.; Chang, C. J., Synthetic fluorescent probes for studying copper in biological systems. *Chemical Society Reviews* **2015,** *44* (13), 4400-4414.

39. Domaille, D. W.; Que, E. L.; Chang, C. J., Sythetic Fluorescent Sensors for Studying to Cell Biology of Metals. *Nat. Chem. Biol.* **2008,** *4*, 168-175.
40. Lippert, A. R.; Van de Bittner, G. C.; Chang, C. J., Boronate Oxidation as a Bioorthogonal Reaction Approach for Studying the Chemistry of Hydrogen Peroxide in Living Systems. *Acc. Chem. Res.* **2011,** *44*, 793-804.
41. Chan, J.; Dodani, S. C.; Chang, C. J., Reaction-based small-molecule fluorescent probes for chemoselective bioimaging. *Nat. Chem.* **2012,** *4*, 973-984.
42. Carter, K. P.; Young, A. M.; Palmer, A. E., Fluorescent Sensors for Measuring Metal Ions in Living Systems *Chem Rev.* **2014,** *114* (8), 4564–4601.
43. Ackerman, C. M.; Lee, S.; Chang, C. J., Analytical Methods for IAmging Metals in Biology: From Transition Metal Metabolism to Transition Metal Signaling. *Anal. Chem.* **2017,** *89*, 22-41.
44. Irving, H.; Williams, R. J. P., *J. Chem. Soc.* **1953,** *3192*.
45. Breuer, W.; Epsztejn, S.; Millgram, P.; Cabantchik, I. Z., Transport of iron and other transition metals into cells as revealed by a fluorescent probe. *J. Am. Phys. Soc.* **1995,** *268*, C1354-C1361.
46. Petrat, F.; Rauen, U.; de Groot, H., Determination of the chelatable iron pool of isolated rat hepatocytes by digital fluorescence microscopy using the fluorescent probe, phen green SK. *Hepatology* **1999** *29* (4), 1171-1179.
47. Ma, Y.; de Groot, H.; Liu, Z.; Hider, R. C.; Petrat, F., Chelation and determination of labile iron in primary hepatocytes by pyridinone fluorescent probes. *Biochem. J.* **2006,** *395*, 49-55.
48. Ma, Y.; Liu, Z.; Hider, R. C.; Petrat, F., Determination of the Labile Iron Pool of Human Lymphocytes using the Fluorescent Probe, CP655. *Anal. Chem. Insights* **2007,** *2*, 61-67.
49. Petrat, F.; Weisheit, D.; Lensen, M.; de Groot, H.; Sustmann, R.; Rauen, U., Selective determination of mitochondrial chelatable iron in viable cells with a new fluorescent sensor. *Biochem. J.* **2002,** *362*, 137-147.
50. Rauen, U.; Springer, A.; Weisheit, D.; Petrat, F.; Korth, H.; de Groot, H.; Sustmann, R., Assessment of Chelatable Mitochondrial Iron byUsing Mitochondrion-Selective Fluorescent IronIndicators with Different Iron-Binding Affinities. *ChemBioChem* **2007,** *8*, 341-352.
51. Au-Yeung, H. Y.; Chan, J.; Chantarojsiri, T.; Chang, C. J., Molecular Imaging of Labile Iron(II) Pools in Living Cells with a Turn-On Fluorescent Probe. *J. Am. Chem. Soc.* **2013,** *135*, 15165-15173.
52. Aron, A. T.; Loehr, M. O.; Bogena, J.; Chang, C. J., An Endoperoxide Reactivity-Based FRET Probe for Ratiometric Fluorescence Imaging of Labile Iron Pools in Living Cells. *J. Am. Chem. Soc.* **2016,** *138* (43), 14338-14346.
53. Hirayama, T.; Okuda, K.; Nagasawa, H., A highly selective turn-on fluorescent probe for iron(II) to visualize labile iron in living cells. *Chem. Sci.* **2013,** *4*, 1250-1256.
54. Niwa, M.; Hirayama, T.; Okuda, K.; Nagasawa, H., *Org. Biomol. Chem.* **2014,** *12*, 6590-6597.
55. Hirayama, T.; Tsuboi, H.; Niwa, M.; Miki, A.; Kadota, S.; Ikeshita, Y.; Okuda, K.; Nagasawa, H., A universal fluorogenic switch for Fe(II) ion based on N-oxide chemistry permits the visualization of intracellular redox equilibrium shift towards labile iron in hypoxic tumor cells. *Chem. Sci.* **2017,** *8* (7), 4858-4866.

56. Spangler, B.; Morgan, C. W.; Fontaine, S. D.; Vander Wal, M. N.; Chang, C. J.; Wells, J. A.; Renslo, A. R., A reactivity-based probe of the intracellular labile ferrous iron pool *Nat. Chem. Biol.* **2016,** *12*, 680-685.
57. Petrat, F., de Groot, H. and Rauen, U. , Subcellular distribution of chelatable iron: a laser scanning microscopic study in isolated rat hepatocytes and rat liver endothelial cells. . *Biochem. J.* **2001,** *356*, 61-69.
58. Adachi, T.; Nonomura, S.; Horiba, M.; Hirayama, T.; Kamiya, T.; Nagasawa, H.; Hara, H., Iron stimulates plasma-activated medium-induced A549 cell injury. *Sci. Rep.* **2016,** *6*, 20928.
59. Ikeda, Y.; Horinouchi, Y.; Hamano, H.; Hirayama, T.; Kishi, S.; Izawa-Ishizawa, Y.; Imanishi, M.; Zamami, Y.; Takechi, K.; Miyamoto, L.; Ishizawa, K.; Aihara, K.; Nagasawa, H.; Tsuchiya, K.; Tamaki, T., Dietary iron restriction alleviates renal tubulointerstitial injury induced by protein overload in mice. *Sci Rep* **2017,** *7*, 10621.
60. Takenaka, M.; Suzuki, N.; Mori, M.; Hirayama, T.; Nagasawa, H.; Ken-ichiro Morishige, M., PhD, Iron regulatory protein 2 in ovarian endometrial cysts. *Biochem and Biophys Res Comm* **2017,** *487* (4), 789-794.
61. Itoa, F.; Nishiyamaa, T.; Shia, L.; Moria, M.; Hirayamad, T.; Nagasawad, H.; Yasuie, H.; Toyokuni, S., Contrasting intra- and extracellular distribution of catalytic ferrous iron in ovalbumin-induced peritonitis. *Biochem and Biophys Res Comm* **2016,** *476* (4), 600-606.
62. Wang, B.; Zhang, J.; Song, F.; Tian, M.; Shi, B.; Jiang, H.; Xu, W.; Wang, H.; Zhou, M.; Pan, X.; Gu, J.; Yang, S.; Jiang, L.; Li, Z., EGFR regulates iron homeostasis to promote cancer growth through redistribution of transferrin receptor 1. *Cancer Lett.* **2016,** *381* (2), 331-340.
63. Mori, M.; Ito, F.; Shi, L.; Wang, Y.; Ishida, C.; Hattori, Y.; Niwa, M.; Hirayama, T.; Nagasawa, H.; Iwase, A.; Kikkawa, F.; Toyokuni, S., *Redox Biol.* **2015,** *6*, 578−586.
64. Shi, L.; Ito, F.; Wang, Y.; Okazaki, Y.; Tanaka, H.; Mizuno, M.; Hori, M.; Hirayama, T.; Nagasawa, H.; Des R. Richardson, D. R.; Toyokuni, S., Non-thermal plasma induces a stress response in mesothelioma cells resulting in increased endocytosis, lysosome biogenesis and autophagy. *Free Rad Biol and Med* **2017,** *108*, 904-917.
65. Maiti, S.; Aydin, Z.; Zhang, Y.; Guo, M., Reaction-based turn-on fluorescent probes with magnetic responses for Fe2+ detection in live cells. *Dalton Trans.* **2015,** *44*, 8942-8949.
66. Taki, M.; Iyoshi, S.; Ojida, A.; Hamachi, I.; Yamamoto, Y., Development of Highly Sensitive Fluorescent Probes for Detection of Intracellular Copper(I) in Living Systems. *J. Am. Chem. Soc.* **2010,** *132* (17), 5938-5939.
67. Au-Yeung, H. Y.; New, E. J.; Chang, C. J., A selective reaction-based fluorescent probe for detecting cobalt in living cells. *Chem. Commun.* **2012,** *48*, 5268-5270.
68. Aron, A. T.; Ramos-Torres, K. M.; Cotruvo, J., J. A.; Chang, C. J., *Acc. Chem. Res.* **2015,** *48*, 2434-2442.
69. Stahlberg, K. G.; Radner, S.; Nordeń, A., Liver B12 in Subjects With and Without Vitamin BI 2 Deficiency. A Quantitative and Qualitative Study. *Scand. J.Haemat.* **1967,** *4*, 312-320.
70. Borstnik, K.; Paik, I. H.; Shapiro, T. A.; Posner, G. H., Antimalarial chemotherapeutic peroxides: artemisinin, yingzhaosu A and related compounds. *Int. J. Parasitol.* **2002,** *32* (13), 1661-1667.
71. Wang, X.; Creek, D. J.; Schiaffo, C. E.; Dong, Y.; Chollet, J.; Scheurer, C.; Wittlin, S.; Charman, S. A.; Dussault, P. H.; Wood, J. K.; Vennerstrom, J. L., Spiroadamantyl 1,2,4-trioxolane, 1,2,4-trioxane, and 1,2,4-trioxepane pairs: Relationship between peroxide bond

iron(II) reactivity, heme alkylation efficiency, and antimalarial activity. *Bioorg & Med Chem Lett* **2009,** *19* (16), 4542-4545.
72. Creek, D. J.; Charman, W. N.; Chiu, F. C.; Prankerd, R. J.; Dong, Y.; Vennerstrom, J. L.; Charman, S. A., Relationship between Antimalarial Activity and Heme Alkylation for Spiro- and Dispiro-1,2,4-Trioxolane Antimalarials. *Antimicrob. Agents Chemother.* **2008,** *52*, 1291.
73. Creek, D. J.; Charman, W. N.; Chiu, F. C.; Prankerd, R. J.; McCullough, K. J.; Dong, Y.; Vennerstrom, J. L.; Charman, S. A., Iron-mediated degradation kinetics of substituted dispiro-1,2,4-trioxolane antimalarials. *J. Pharm. Sci.* **2007,** *96* (11), 2945-2956.
74. Tang, Y.; Dong, Y.; Wang, X.; Sriraghavan, K.; Wood, J. K.; Vennerstrom, J. L., Dispiro-1,2,4-trioxane Analogues of a Prototype Dispiro-1,2,4-trioxolane: Mechanistic Comparators for Artemisinin in the Context of Reaction Pathways with Iron(II). *J. Org. Chem.* **2005,** *70* (13), 5103–5110.
75. Deu, E.; Chen, I. T.; Lauterwasser, E. M.; Valderramos, J.; Li, H.; Edgington, L. E.; Renslo, A. R.; Bogyo, M., Ferrous iron-dependent drug delivery enables controlled and selective release of therapeutic agents in vivo. *Proc Natl Acad Sci USA* **2013,** *110* (45), 18244-18249.
76. Fontaine, S. D.; Spangler, B.; Gut, J.; Lauterwasser, E. M. W.; Rosenthal, P. J.; Renslo, A. R., Drug Delivery to the Malaria Parasite Using an Arterolane-Like Scaffold. *ChemMedChem* **2015,** *10*, 47-51.
77. Fontaine, S. D.; DiPasquale, A. G.; Renslo, A. R., Efficient and Stereocontrolled Synthesis of 1,2,4-Trioxolanes Useful for Ferrous Iron-Dependent Drug Delivery. *Org. Lett. 16* (16), 5776-9.
78. Abrams, R. P.; Carroll, W. L.; Woerpel, K. A., Five-Membered Ring Peroxide Selectively Initiates Ferroptosis in Cancer Cells. *ACS Chem Biol 11*, 1305-1312.
79. Krishnamoorthy, L.; Cotruvo, J. A. J.; Chan, J.; Kaluarachchi, H.; Muchenditsi, A.; Pendyala, V. S.; Jia, S.; Aron, A. T.; Ackerman, C. M.; Vander Wal, M. N.; Guan, T.; Smaga, L. P.; Farhi, S. L.; New, E. J.; Lutsenko, S.; Chang, C. J., Copper regulates cyclic-AMP-dependent lipolysis. *Nat. Chem. Biol.* **2016,** *12*, 586-592.
80. Andreini, C.; Bertini, I.; Rosato, A., Metalloproteomes: A Bioinformatic Approach. *Acc. Chem. Res.* **2009,** *42* (10), 1471-1479.
81. Zhao, W.; Xu, M.; Liang, Z.; Ding, B.; Niu, L.; Liu, H.; Teng, M., Structure-based de novo prediction of zinc-binding sites in proteins of unknown function, . *Bioinformatics* **2011,** *27*, 1262-1268.
82. Smith, C. L., Stauber, J. L., Wilson, M. R. & Jolley, D. F. , The use of immobilised metal affinity chromatography (IMAC) to compare expression of copper-binding proteins in control and copper-exposed marine microalgae. *Anal and Bioanal Chem* **2014,** *406*, 305-315.
83. Song, Y.; Zhang, H.; Chen, C.; Wang, G.; Zhuang, K.; Cui, J.; Shen, Z., Proteomic analysis of copper-binding proteins in excess copper-stressed rice roots by immobilized metal affinity chromatography and two-dimensional electrophoresis. *BioMetals* **2014,** *27*, 265-276.
84. Raimunda, D.; Khare, T.; Giometti, C.; Vogt, S.; Argüelloa, J. M.; Finney, L., Identifying metalloproteins through X-ray fluorescence mapping and mass spectrometry. *Metallomics* **2012,** *4*, 921-927.
85. Chassaigne, H.; Chery, C. C.; Bordin, G.; Vanhaecke, F.; Rodriguez, A. R.; Dubikovskaya, E., 2-Dimensional gel electrophoresis technique for yeast selenium-containing proteins—sample preparation and MS approaches for processing 2-D gel protein spots. *J. Anal. At. Spectrom.* **2004,** *19*, 85-95.

86. Finney, L.; Chishti, Y.; Khare, T.; Giometti, C.; Levina, A.; Lay, P. A.; Vogt, S., Imaging Metals in Proteins by Combining Electrophoresis with Rapid X-ray Fluorescence Mapping. *ACS Chem Biol* **2010,** *5*, 577-587.
87. Cvetkovic, A.; Menon, A. L.; Thorgersen, M. P.; Scott, J. W.; Poole, F. L. I.; Jenney, F. E. J.; Lancaster, W. A.; Praissman, J. L.; Shanmukh, S.; Vaccaro, B. J.; Trauger, S. A.; Kalisiak, E.; Apon, J. V.; Siuzdak, G.; Yannone, S. M.; Tainer, J. A.; Adams, M. W. W., Microbial metalloproteomes are largely uncharacterized. *Nature* **2010,** *466*, 779-782.
88. Cravatt, B. F.; Wright, A. T.; Kozarich, J. W., Activity-Based Protein Profiling: From Enzyme Chemistry to Proteomic Chemistry. *Annu. Rev. Biochem.* **2008,** *77*, 383-414.
89. Roberts, A. M.; Ward, C. C.; Nomura, D. K., Activity-based protein profiling for mapping and pharmacologically interrogating proteome-wide ligandable hotspots. *Curr. Opin. Biochem.* **2017,** *43*, 25-33.
90. Yang, J.; Gupta, V.; Tallman, K. A.; Porter, N. A.; Carroll, K. S.; Liebler, D. C., Global, in situ, site-specific analysis of protein S-sulfenylation. *Nat. Protoc.* **2015,** *10*, 1022-1037.
91. Majmudar, J. D.; Konopko, A. M.; Labby, K. J.; Tom, C. T. M. B.; Crellin, J. E.; Prakash, A.; Martin, B. R., Harnessing Redox Cross-Reactivity To Profile Distinct Cysteine Modifications. *J. Am. Chem. Soc.* **2016,** *138*, 1852–1859.
92. Martin, B. R.; Wang, C.; Adibekian, A.; Tully, S. E.; Cravatt, B. F., Global profiling of dynamic protein palmitoylation. *2012* **2012,** *9*, 84-89.
93. Weerapana, E.; Wang, C.; Simon, G. M.; Richter, F.; Khare, S.; Dillon, M. B. D.; Bachovchin, D. A.; Mowen, K.; Baker, D.; Cravatt, B. F., Quantitative reactivity profiling predicts functional cysteines in proteomes. *Nature* **2010,** *468*, 790-795.
94. Pace, N. J.; Weerapana, E., A Competitive Chemical-Proteomic Platform to Identify Zinc-Binding Cysteines. *ACS Chem. Biol.* **2014,** *9* (1), 258-265.

Chapter 2

Design, synthesis, and application of an endoperoxide reactivity-based FRET probe for ratiometric fluorescence imaging of labile iron pools in living cells

Portions of this work were published in the following scientific journal:

Aron, A. T.; Loehr, M. O.; Bogena, J.; Chang, C. J. "An Endoperoxide Reactivity-Based FRET Probe for Ratiometric Fluorescence Imaging of Labile Iron Pools in Living Cells", *J. Am. Chem. Soc.* **2016**, *138*, 14338-14346.

Abstract

Iron is an essential nutrient for sustaining life, as its ability to cycle between multiple oxidation states is critical for catalyzing unique chemical transformations in biological systems. However, without proper regulation, this same redox capacity can trigger oxidative stress events that contribute to aging along with diseases ranging from cancer to cardiovascular and neurodegenerative disorders. Despite the central importance of iron to both normal physiology as well as disease, methods for monitoring biological iron that is bound weakly to cellular ligands - the labile iron pool - remain limited, owing to the difficulties of overcoming iron as a potent fluorescent quencher to generate a response that preserves spatial and temporal information. We now report the design, synthesis, and biological evaluation of FRET Iron Probe 1 (FIP-1), a unique reactivity-based probe that enables ratiometric fluorescence imaging of labile iron pools in living systems. Inspired by antimalarial natural products and related therapeutics, FIP-1 links two fluorophores (fluorescein and Cy 3) through an Fe^{2+}-cleavable endoperoxide bridge, where Fe^{2+}-triggered peroxide cleavage leads to a decrease in fluorescence resonance energy transfer (FRET) from the fluorescein donor to the Cy 3 acceptor by splitting these two dyes into separate fragments. FIP-1 is responsive to Fe^{2+} in aqueous buffer with selectivity over competing biological metal ions and is capable of detecting changes in labile iron pools within living cells with iron supplementation and/or depletion. Moreover, application of FIP-1 to a model of ferroptosis reveals a direct change in labile iron pools during this recently identified form of cell death, providing a starting point to study iron signaling in living systems.

2.1. Introduction

Iron is a required element for all living organisms and the most abundant transition metal in the human body[1-4]. Its ability to cycle between multiple oxidation states is essential for carrying out a diverse array of unique functions in biological systems, spanning nucleotide synthesis to oxygen transport to electron transfer[5-6]. However, this same potent redox activity makes iron in unregulated forms potentially toxic to the cell, owing to its ability to promote oxidative stress by participating in processes like the Fenton reaction where iron-catalyzed disproportionation of hydrogen peroxide can generate hydroxyl radical and other harmful reactive oxygen species[7]. Indeed, misregulation of iron levels has been linked to diseases associated with aging,[8] including cardiovascular[9] and neurodegenerative disorders[10-11] and a variety of cancers[12-15]. As such, the cell employs intricate systems for maintaining iron homeostasis, and a ferrous iron pool that is bound weakly to cellular ligands - defined as the labile iron pool - exists at the center of this dynamic network.

Despite its central importance, methods for non-invasive detection of labile Fe(II) within living cells and other intact biological specimens remain limited,[16-17] owing to intrinsic properties of Fe^{2+} as a weak binder on the Irving-Williams series[18] and as a potent fluorescence quencher by electron and/or energy transfer[19-20]. Indeed, the majority of sensors and probes for Fe^{2+} either lack selectivity for Fe^{2+}over other biologically relevant metal ions as well as oxidation state specificity over Fe^{3+}, and/or lose spatial resolution due to their "turn-off" fluorescence readout[21-22]. To address the dual issues of selectivity and Fe(II)-dependent quenching, we[23] and others[24-26] have pursued reactivity-based approaches[27-31] to labile iron detection by a "turn-on" response, where an Fe^{2+}-selective reaction with a caged dye leads to release of the parent fluorophore without permanent iron binding. Inspired by bioinorganic oxidations mediated by heme and non-heme iron enzymes, our laboratory reported Iron Probe 1 (IP-1), a reactivity-based probe for Fe^{2+} that makes use of an iron-mediated, oxygen-dependent dealkylation to trigger a turn-on response[23]. While this probe was highly metal and oxidation state specific for Fe^{2+} and capable of monitoring changes in endogenous labile iron pools, it required three components (probe, Fe^{2+}, and O2) to produce a change in signal. We envisioned an improved detection platform that could exhibit oxygen-independent reactivity and give a fluorescence response through direct reaction with Fe^{2+}. In addition, we sought to introduce a ratiometric readout[32-35], which enables internal self-calibration through multiple excitation/emission profiles to minimize interferences arising from analyte-independent phenomena such as sample thickness, heterogeneity and/or variations in light intensity.

In this chapter, we report the design, synthesis, and biological evaluation of a first-generation ratiometric fluorescent probe for Fe^{2+} by modulating fluorescence resonance energy transfer (FRET) between two dyes linked by an Fe^{2+}-responsive trigger. Specifically, FRET Iron Probe 1 (FIP-1) exploits an Fe^{2+}-cleavable endoperoxide linker inspired by antimalarial and anticancer drug scaffolds, which achieve specificity for parasites and tumors via elevations in local iron concentrations,[36-44] to control FRET between donor and acceptor dyes. This chemical design strategy is generally applicable to a broad range of ratiometric or turn-on probes for selective detection of iron or other chemical analytes that are potent fluorescent quenchers. FIP-1 features high selectivity and sensitivity to Fe^{2+} over competing biologically relevant metals and is capable of monitoring changes in labile iron pools in living cells in situations of iron excess and/or deficiency. The ratiometric readout of this probe also facilitates comparative screening of labile iron levels across a variety of cell types, identifying cancer cell types that possess higher resting levels of labile iron. Finally, the application of FIP-1 to a model of ferroptosis enables, to the best of our knowledge, the first direct imaging evidence of changes in labile iron stores upon induction of this emerging form of cell death. This result pro-vides a starting point for further studies of iron as a transition metal signal in biology[456].

2.2. Methods

2.2.1. General synthetic methods

Reactions using moisture- or air-sensitive reagents were carried out in flame-dried glassware under an inert atmosphere of N2. Solvent was passed over activated alumina and stored over activated 3Å molecular sieves before use when dry solvent was required. All other commercially purchased chemicals were used as received (without further purification). 2-adamantanone-5-carboxylic acid was purchased from Oakwood Products, Inc. (Estill, SC);

hydroxylamine methyl ester hydrochloride and 1,4-cyclohexanedione were purchased from AK Scientific (Union City, CA); all other reagents were purchased from Sigma-Aldrich (St. Louis, MO). 5-aminomethyl fluorescein (5-AMF) was prepared according to published procedures.50 Cy3 was prepared according to published procedures. (51) SiliCycle 60 F254 silica gel (pre-coated sheets, 0.25 mm thick) were used for analytical thin layer chromatography and visualized by fluorescence quenching under UV light. Silica gel P60 (SiliCycle) was used for column chromatography. ^{1}H and ^{13}C NMR NMR spectra were collected at 298 K in CDCl3 or CD3OD (Cambridge Isotope Laboratories, Cambridge, MA) at 25 °C on Bruker AVQ-400, AVB-400, AV-500, or AV-600 at the College of Chemistry NMR Facility at the University of California, Berkeley or on Bruker 900 at the QB3 Central California 900 MHz NMR Facility. All chemical shifts are reported in the standard notation of δ parts per mil-lion relative to residual solvent peak at 7.26 ($CDCl_3$) or 3.31 (CD_3OD) for ^{1}H and 77.16 ($CDCl_3$) or 49.00 (CD_3OD) for ^{13}C as an internal reference. Splitting patterns are indicated as follows: br, broad; s, singlet; d, doublet; t, triplet; m, multiplet; dd, doublet of doublets. Low-resolution electrospray mass spectral analyses were carried out using a LC-MS (Agilent Technology 6130, Quadrupole LC/MS and Advion expression-L Compact Mass Spectrometer). High-resolution mass spectral analyses (ESI-MS) were carried out at the College of Chemistry Mass Spectrometry Facility at the University of California, Berkeley.

2.2.2. Probe synthesis and new compound characterization

5-(Methoxycarbonyl)-2-adamantanone, 2. Thionyl chloride (0.450 mL, 6.17 mmol, 2.4 equiv) was added slowly to dry MeOH (26 mL) at 0 °C, and this was stirred for 15 minutes at this temperature. 2-adamantanone-5-carboxylic acid (0.5 g, 2.57 mmol, 1 equiv) was then added portion-wise over 5 minutes, also at 0 °C. The reaction mixture was allowed to warm to room temperature and was further stirred overnight. The reaction was then concentrated and loaded directly on silica gel for purification by flash column chromatography (0 → 35% EtOAc/Hex) to yield **2** (415 mg, 78% yield) as a white solid. ^{1}H NMR (400 MHz, $CDCl_3$) δ (ppm): 3.48 (s, 3 H), 2.38 (s, 2 H), 2.00 - 1.77 (m, 11 H). ^{13}C NMR (101 MHz, $CDCl_3$) δ (ppm): 215.88, 175.71, 51.63, 45.47, 39.82, 37.98, 37.51, 26.98. LRMS calcd. for $C_{12}H_{16}O_3$ $[M + H]^+$ 209.11, found 209.2.

Oxime Ether 3. 5-(Methoxycarbonyl)-2-adamantanone (0.114 g, 0.55 mmol, 1 equiv) and hydroxylamine methyl ester hydrochloride (0.050 g, 0.6 mmol, 1.1 equiv) were added in pyridine (2 mL), and the reaction mixture was stirred at room temperature for 3 hours. After 3 hours, the reaction was neutralized by addition of 1 M HCl, then ethyl acetate was added. The organic layer was washed with 1 M aq HCl (2 x 15 mL) and the combined aq layer was then extracted with EtOAc (3 x 15 mL), washed with brine, dried over Na_2SO_4 filtered and concentrated in vacuo to yield **3** (0.130 g, 100%).^{1}H NMR (400 MHz, $CDCl_3$) δ (ppm): 3.76 (s, 3 H), 3.60 (s, 3 H), 3.49 (s, 1 H), 2.57 (s, 1 H), 2.05 - 1.78 (m, 12 H). ^{13}C NMR (101 MHz, $CDCl_3$) δ (ppm): 176.75, 165.48, 61.07, 51.85, 40.73, 40.00, 38.66, 38.00, 36.57, 35.57, 28.76, 27.65. LRMS calcd. for $C_{13}H_{19}NO_3$ $[M + H]^+$ 238.14, found 238.2.

Endoperoxide 4. Oxime ether **3** (1.4620, 6.16 mmol, 1 equiv) and 1,4-cyclohexanedione (1.384, 12.32 mmol, 2 equiv) were dried then were added to a flame-dried 100 mL Schlenk flask. Dry CCl_4 (50 mL) and dry CH_2Cl_2 (25 mL) were added and the reaction mixture was stirred at 0 °C for 5 minutes before bubbling ozone through solution for 2.5 hours at this temperature. At this

point, the reaction was purged of ozone, warmed to room temperature, and concentrated. The concentrate was loaded directly on silica gel for purification by silica chromatography (0 → 25% EtOAc/Hex) to yield **4** (680 mg, 33%) as a pale-yellow solid. **4** was isolated as a mixture of diastereomers. ^{1}H NMR (400 MHz, $CDCl_3$) δ (ppm): 3.67 – 3.64 (m, 3 H), 2.51 (t, 3 H), 2.22 – 2.10 (m, 8 H), 2.03 – 1.83 (m, 7 H), 1.75 - 1.65 (m, 2 H). ^{13}C NMR (101 MHz, $CDCl_3$) δ (ppm): 209.25, 209.20, 177.18, 177.10, 111.46, 111.42, 107.44, 107.41, 51.92, 45.91, 40.27, 39.95, 39.55, 38.46, 38.23, 38.16, 37.89, 36.44, 36.26, 36.03, 35.88, 33.85, 33.75, 33.14, 33.12, 27.41, 26.62, 26.22. LRMS calcd. for $C_{18}H_{24}O_6$ $[M + H]^+$ 337.16, found 337.2.

Endoperoxide Amine 5. Endoperoxide **4** (0.1485 g, 0.4415 mmol, 1 equiv) and NH_4OAc (0.340 g, 4.415 mmol, 10 equiv) were added in dry MeOH (8 mL), and this was stirred for 5 minutes at room temperature before adding $NaBH_3CN$ (0.0194 g, 0.31 mmol, 0.7 equiv). The reaction mixture was stirred at room temperature overnight. The reaction was quenched by addition of 150 mL water and the MeOH was removed. At this point, the reaction mixture was basified (brought to pH 8) by addition of 5 M NaOH then was extracted three times with $CHCl_3$, washed with aq sat NaCl, dried over Na_2SO_4, filtered and the solvent was removed by rotary evaporation. Silica chromatography was run (50 → 100% ethyl acetate in hexanes → 0 → 10% MeOH in CH_2Cl_2) to yield **5** (0.085 g, 56%). ^{1}H NMR (600 MHz, $CDCl_3$) δ (ppm): 3.643 (t, 3 H), 2.524 (m, 1 H), 2.232 – 1.493 (m, 23 H). LRMS calcd. for $C_{18}H_{27}NO_5$ $[M + H]^+$ 338.19, found 338.2.

Endoperoxide Carboxylic Acid 6. Endoperoxide-free amine **5** (0.1377 g, 0.41 mmol, 1 equiv) was dissolved in 2 mL THF, then lithium hydroxide (0.015 g, 0.612 mmol, 1.5 equiv) was added in 2 mL water. This was stirred overnight, then was concentrated to yield **6** (0.140 g, 100%) which was carried on to the next step without without further purification. ^{1}H NMR (600 MHz, CD_3OD) δ (ppm): 2.708 (m, 1 H), 2.205 – 1.369 (m, 27 H) ^{13}C NMR (101 MHz, $CDCl_3$) 185.88, 109.46, 58.29, 42.36, 40.47, 38.49, 38.02, 37.92, 35.13, 18.42. LRMS calcd. for $C_{12}H_{16}O_3$ $[M + H]^+$ 324.17, found 324.2.

Cy3 NHS Ester 8. Cy3 (520 mg, 0.91 mmol, 1.0 equiv) was dried under high vacuum for 30 minutes and dissolved in 10 mL dry DMF. Disuccinimidyl carbonate (DSC) (350 mg, 1.37 mmol, 1.5 equiv), DMAP (2.1 mg, 0.02 mmol, 0.02 equiv) and NEt_3 (254 µL, 184 mg, 1.82 mmol, 2.0 equiv) were added and the dark red solution was stirred at room temperature overnight. 20 mL CH_2Cl_2 were added and the organic phases were washed with slightly acidic water (3 x 10 mL). The aqueous phases were re-extracted with CH_2Cl_2 (15 mL). Combined organic phases were dried over $MgSO_4$, filtered and the solvent was removed by rotary evaporation. Purification by flash column chromatography (5% IPA in CH_2Cl_2) yielded Cy3-NHS ester as a dark purple solid. ^{1}H NMR (600 MHz, $CDCl_3$) δ (ppm): 8.35 (t, 1H), 7.33 (t, 4H), 7.15 (m, 6H), 4.22 (t, 2H), 3.72 (s, 3H), 2.77 (s, 4 H), 1.92 (d, 4H), 1.65 (s, 12H). ^{13}C NMR (101 MHz, $CDCl_3$) 174.15, 173.62, 169.11, 168.33, 150.77, 142.56, 141.78, 140.39, 140.34, 128.85, 128.74, 125.26, 125.21, 122.03, 121.96, 110.93, 110.77, 104.87, 104.59, 53.43, 48.85, 48.81, 44.14, 32.06, 30.46, 28.07, 27.97, 26.25, 25.57,21.86. LRMS calcd. for $C_{33}H_{38}O_4N_3$ $[M + H]^+$ 540.3 found 540.5.

Cy3 Linker 7. Endoperoxide-carboxylic acid **6** (48 mg, 0.15 mmol, 1.0 equiv) and Cy3-NHS ester **8** (100 mg, 0.15 mmol, 1.0 equiv) were dried under high vacuum for 10 minutes and dissolved in 1 mL dry DMF. Dry NEt_3 (42 µL, 30 mg, 0.30 mmol, 2.0 equiv) was added and the

dark red solution was warmed to 30 °C and stirred overnight. The solvent was removed by vacuum distillation and the crude concentrate was purified by flash column chromatography (gradient of 0 → 20% MeOH in CH_2Cl_2) to yield Cy3-linker **7** (38 mg, 0.04 mmol, 29%) as a dark red solid and as a mixture of diastereomers. ^{1}H NMR (500 MHz, CD_3OD) δ (ppm): 8.56 (t, 1H), 7.57 (d, 2H), 7.46 (m, 2H), 7.42 – 7.28 (m, 4H), 6.50 (m, 2H), 4.19 (bt, 2H), 3.73 (m, 3 H), 2.29 (bt, 2 H), 2.21 (m, 2 H), 2.11 – 1.42 (m, 46) ^{13}C NMR (226 MHz, CD_3OD) 176.97, 176.21, 175.98, 175.04, 152.34, 152.20, 144.26, 143.71, 142.39, 142.34, 130.19, 127.02, 126.90, 123.76, 123.60, 112.62, 112.52, 111.95, 109.44, 104.24, 104.0, 103.94, 103.82, 45.08, 44.81, 41.18, 39.70, 38.06, 37.78, 37.70, 37.57, 36.73, 36.38, 34.93, 34.76, 33.89, 33.66, 33.27, 32.05, 30.98, 30.63, 30.54, 30.37, 28.54, 28.37, 28.05, 27.91, 27.62, 27.12,24.33, 23.94. LRMS calcd. for $C_{46}H_{58}O_6N_3$ $[M + H]^+$ 748.43, found 749.

FRET Iron Probe 1 (FIP-1). Cy3-linker **7** (35 mg, 0.040 mmol, 1.0 equiv) and HBTU (17 mg, 0.044 mmol, 1.1 equiv) were dried under high vacuum for 1 h and dissolved in 1 mL dry DMF. After addition of dry DIPEA (10µL, 7.2 mg, 0.56 mmol, 1.4 equiv), the solution was stirred for 1 h. 5-aminomethyl fluorescein (22 mg, 0.06 mmol, 1.5 equiv) was dried under high vacuum for 90 minutes, dissolved in 1 mL dry DMF and dry DIPEA (20 µL, 14.5 mg, 1.1 mmol, 2.8 equiv) then transferred to the solution containing the activated ester. The resulting solution was stirred overnight. 10 mL of saturated, aqueous NH_4Cl and 10 mL water were added and the aqueous phase was extracted with EtOAc (4 x 10 mL). The combined organic phases were washed with water (2 x 10 mL) and brine. The solvent was removed by rotary evaporation and purified by flash column chromatography (gradient of 0 →15% MeOH in CH_2Cl_2). Final purification was achieved by UHPLC (gradient of 53% H_2O supplemented with 0.05% formic acid (FA) in MeCN supplemented with FA → 47% H_2O supplemented with 0.05% formic acid (FA) in MeCN supplemented with FA over 13 minutes → 100% MeCN supplemented with FA over 2 minutes, from 13 minutes to 15 minutes). FRET Iron Probe 1 (FIP-1) (3.41 mg, 0.0028 mmol/2.8µmol, 7%) was obtained as a red film. ^{1}H NMR (500 MHz, CD_3OD) δ (ppm): 7.87 (s, 1 H), 7.55 (d, 2 H), 7.49 (d, 1 H), 7.44 (t, 2H), 7.37 (t, 2 H), 7.31 (t, 2H), 7.16 (d, 1 H), 7.00 (s, 2 H), 6.65 (s, 2 H), 6.59 (dd, 2 H), 6.39 (m, 2 H), 4.62 (s, 1 H), 4.50 (s, 2 H), 4.15 (t, 2 H), 3.70 (s, 3 H), 2.24 (t, 2 H), 2.10 (d, 2 H), 1.87 – 1.73 (m, 29 H), 1.62 (d, 2 H), 1.54 (d, 2 H), 1.44 (m, 2 H). ^{13}C NMR (226 MHz, CD_3OD) 179.77, 176.75, 176.04, 175.83, 174.82, 170.19, 169.38, 163.24, 163.09, 162.93, 152.00, 144.12, 144.02, 143.51, 143.35, 142.15, 132.42, 131.37, 130.00, 129.83, 126.91, 126.74, 112.44, 112.26, 111.56, 111.82, 103.78, 103.91, 103.73, 103.6, 69.95, 60.95, 50.67, 50.63, 50.44, 48.15, 44.88, 44.62, 43.48, 39.26, 37.57, 37.52, 37.50, 36.21, 34.84, 34.48, 33.69, 33.40, 33.09, 30.79, 30.36, 30.48, 3040, 30.15, 28.33, 28.17, 27.80, 27.47, 24.96, 24.19, 24.15, 23.75, 14.44, 11.40. HRMS calcd. for $C_{67}H_{71}O_{10}N_4$ $[M + H]^+$ 1091.517, found 1091.518

2.2.3. Spectroscopic materials and methods

All aqueous solutions were prepared using Milli-Q water, and all spectroscopic experiments were carried out in 50 mM HEPES, pH 7.4, unless otherwise noted. All spectroscopic experiments were prepared using freshly prepared aliquots and were prepared in an anaerobic chamber (MBraun), unless otherwise noted. Water and buffer used for spectroscopic measurements were deoxygenated in three freeze-pump-thaw cycles on a Schlenk line. Absorption spectra were acquired on a Varian Cary 50 spectrophotometer, and fluorescence spectra were acquired using a Photon Technology International Quanta Master 4 L-format scan spectro-fluorometer equipped with an LPS-220B 75-W xenon lamp and power supply, A-1010B lamp housing with integrated igniter, switchable 814 photocounting/analog photomultiplier detection unit, and MD5020 motor driver. 1-cm × 1-cm quartz cuvettes (1.4-mL volume, Starna, capped) were used for obtaining absorption and fluorescence spectra. For all fluorescence response to iron(II) studies, aqueous solutions of $Fe(NH_4)_2(SO_4)_2(H_2O)_6$ (FAS) (Sigma) were used. For metal selectivity studies, aqueous metal solutions of $MgCl_2 \bullet 4H_2O$ (EMD Millipore), $CaCl_2 \bullet 2H_2O$ (EMD Millipore), $NiCl_2 \bullet 6H_2O$ (Sigma), $ZnCl_2$ (Sigma), $CuCl_2 \bullet 2H_2O$ (Baker & Adamson), $CoCl_2 \bullet 6H_2O$ (Sigma), $MgCl_2 \bullet 6H_2O$ (Sigma), NaCl (Sigma), $[Cu(CH_3CN)_4]PF_6$ (Sigma), KCl (Sigma), and $FeCl_3$ (Sigma) were used. GSH (Sigma) was used for selectivity studies

2.2.4. Fluorescence Responses to Iron

999 µL of a 1 µM solu-tion of FIP-1 was prepared by diluting a 1 mM DMSO stock solution of FIP-1 into 50 mM HEPES (pH 7.4) in a 1-cm × 1-cm capped quartz cuvette. The probe solution was incubated at 37 °C for 5 minutes, then 1 µL of 10 mM stock solution of ferrous ammonium sulfate (FAS) (freshly prepared by diluting FAS into deoxygenated MilliQ water) was added to yield a final concentration of 10 µM. The mixture was then vortexed in the capped cuvette, then the t = 0 spectrum was acquired. Emission spectra (λex = 488 nm, λem = 500-600 nm) were collected at t = 0, 5, 10, 15, 20, 30, 45, 60, and 90 minutes. Temperature was maintained at 37 °C throughout the experiment by submerging cuvettes in a heated water bath.

2.2.5. Dose Dependence In Vitro.

999 µL of a 1 µM solution of FIP-1 was prepared by diluting a 1 mM DMSO stock solution of FIP-1 into 50 mM HEPES (pH 7.4) in a 1-cm × 1-cm capped quartz cuvette. The probe solution was incubated at 37 °C for 5 minutes. Then 1 µL or 5 µL of a 1 mM stock solution of FAS (freshly prepared by diluting FAS into deoxygenated MilliQ water) was added to yield a final concentration of 1 or 5 µM and 1 µL or 2 µL of a 10 mM stock solution of FAS (freshly prepared by diluting FAS into deoxygenated MilliQ water) was added to yield a final concentration of 10 or 20 µM. The mixture was then vortexed in the capped cuvette, then the t = 0 spectrum was acquired. Emission spectra (λ_{ex} = 488 nm, λ_{em} = 500-600 nm) were collected at t = 0, 5, 10, 15, 20, 30, 45, 60, and 90 minutes. Temperature was maintained at 37 °C throughout the experiment by submerging cuvettes in a heated water bath.

2.2.6. Metal and GSH Selectivity Experiments.

A 2 μM solution of FIP-1 was prepared by diluting a 1 mM DMSO stock solution of probe into 4.990 mL HEPES. 500 μL of this solution were added to ten 1-cm × 1-cm capped quartz cuvettes, then the cuvettes were placed in a 37 °C water bath for 5 minutes. After 5 minutes, 500 μL of the metal of interest was added to the cuvette to bring the concentration of transition metals to 10 μM and the concentration of alkaline earth/alkali metals to 1 mM. For GSH experiments, a 10 mM solution of GSH was prepared in HEPES buffer and this was brought to neutral pH by adding 1 M NaOH. 500 μL of this solution was added to 500 μL FIP-1 in HEPES solution for a final GSH concentration of 5 mM. 500 μL of buffer was added to one cuvette, and this sample served as the blank throughout the experiment. The mixture was then vortexed in the capped cuvette, then the t = 0 spectrum was acquired for the blank sample. Spectra were taken at t = 60 minutes.

2.2.7. LC-MS Assays for Characterization of Fe(II) Reaction.

100 μM FIP-1 was prepared in deoxygenated 10 mM HEPES (pH 7.4). Then ferrous ammonium sulfate (FAS) was added (from a 10mM stock in deoxygenated MilliQ water) to yield a final concentration of 1 mM FAS. This was stirred at 25 ºC for 2.5 hours, then the sample was lyophilized overnight. The sample was reconstituted in MeOH, was filtered, then subjected to LC-MS analysis. LC-MS method was a linear gradient from 5 % MeOH / 95 % H2O / 0.05 % formic acid to 95 % MeOH / 5 % H2O / 0.05% formic acid over 50 minutes using an Agilent 300 extend-C18, 3.5 μm, 4.6 x 100mm column, monitoring UV at 254 nm. LRMS calcd. for 5-AMF-lactone C32H27NO8 (Scheme 1) [M + H]+ 554.2, found 554.5. LRMS calcd. for Cy3-ketone C35H44N3O2+ (Scheme 1) [M]+ 538.3, found 538.4.

2.2.8. Cell Culture Procedures.

Cells were maintained by the UC Berkeley Tissue Culture Facility. HEK 293T, MDA-MB-231, and U-2OS cells were maintained as a monolayer in exponen-tial growth at 37 °C in a 5% CO2 atmosphere in Dulbecco's Modified Eagle Medium (DMEM, Gibco) supplemented with 10% fetal bovine serum (FBS, Hyclone), and glutamax (Gibco). One day before imaging, HEK 293T cells were passaged and plated in phenol red-free medium on poly-d-lysine-coated 4-well Lab Tek borosilicate chambered coverglass slides (Nunc) at 1.8 x 105 per well. HEK 293T cells were allowed to grow to between 60-70% confluence before imaging. MCF-10A cells were maintained in DMEM/F12 (500 mL, Invitrogen) with 5% horse serum (25 mL, Invitrogen), insulin (500 μL from 10 mg/mL stock), cholera toxin (50 μL, from 1 mg/mL stock), hydrocortisone (250 μL, from 1 mg/mL stock), EGF (100 μL, from 100μg/mL stock) and HEPES. One day before imaging, MCF-10A, MDA-MB-231, and U-2OS cells cells were passaged and plated on 4-well Lab Tek borosilicate chambered cover-glass slides (Nunc) and allowed to grow to between 60-80% confluence before imaging.

2.2.9. Confocal Fluorescence Imaging Experiments.

A Zeiss laser scanning microscope 710 with a 20x objective lens and Zen 2009 software (Carl Zeiss) was used for all confocal fluorescence imaging experiments. FIP-1 was excited using a 488 nm Ar laser ("Green" channel and "FRET" channel) and 543 nm HeNe laser (red channel). "Green" emission was collected using a META detector between 500-535 nm, "FRET" emission was collected using a META detector between 555-611 nm, and "red" emission was collected using a META detector between 555-611 nm. Hoechst 33342 was excited with a 405 nm diode laser, and emission was collected using a META detector between 410-590 nm. Cells were kept at 37 °C throughout imaging experiments, and HBSS (containing calcium and magnesium) was used as the imaging buffer in all experiments. Image analysis and quantification was performed using ImageJ (National Institutes of Health). Quantification of fluorescence intensities were conducted as described previously[67]. Statistical analyses for multiple comparisons were carried out through one-way ANOVA with the Bonferroni correction using the software R.

2.2.10. Fe(II) Supplementation and Chelation Experiments.

250 μM DFO or 1 mM BPS was added to DMEM media containing 10% FBS and glutamax in chambers containing cells and incubated at 37 °C for 8 hours. At this point, media in these wells was replaced with 250 μM DFO or 1 mM BPS containing DMEM media (without FBS and glutamax) and incubated for 90 minutes at 37 °C. DMEM media in non-treated wells was aspirated from chambers containing cells and this was replaced with DMEM media containing 100 μM FAS (prepared from a 20 mM FAS solution in water) or DMEM media and this was incubated for 90 minutes at 37 °C. After 90 minutes, DMEM media was aspirated and cells were washed one time with 500 μL HBSS. Then 500 μL HBSS containing 10 μM FIP-1 (diluted from 5 mM stock) was added to each well and this was incubated at 37 °C for 90 minutes. At this point, buffer was removed and each well was washed 2x with 500 μL HBSS. Then 500 μL of HBSS were added and snapshot images were taken. Cells were then incubated with 1 μM Hoechst 33342 at 37 °C for 10 minutes prior to imaging nuclear staining.

2.2.11. HEK 293T Fe^{2+} Dose Dependence Experiments.

DMEM culture media was aspirated from each chamber containing cells. This was replaced with either 0 μM, 2 μM, 10 μM, or 100 μM FAS in DMEM media (without FBS and glutamax), and cells were incubated in this media for 60 minutes at 37 ºC. After 60 minutes, DMEM media was aspirated and cells were washed 1x with 500 μL HBSS. Then 500 μL HBSS containing 10 μM FIP-1 (diluted from a 5 mM stock in DMSO) was added to each well and this was incubated at 37 ºC for 90 minutes. At this point, buffer was removed and each well was washed 2x with 500 μL HBSS, then 500 μL of HBSS were added and snapshot images were taken.

2.2.12. Ferroptosis Experiments.

MDA-MB-231 cells were cultured in DMEM supplemented with 10% fetal bovine serum (FBS, Hyclone), glutamax (Gibco), and 1% non-essential amino acids (NEAA, Gibco). One day before the experiment, cells were passaged and plated in phenol-red free medium in 4-well Lab Tek borosilicate chambered coverglass slides (Nunc). Media was aspirated and was replaced with 100 µL DMEM media containing 10% FBS and glutamax and either DMSO vehicle, 1.25 µM **21**[46], 1.25 uM **21** + 1 µM ferrostatin-1 (Fer-1), or 1.25 µM **21** + 100 µM DFO at various time points. Cells were treated for 8 hours, at which point media was removed and was washed one time with 500 µL HBSS. Then 500 µL HBSS containing 10 µM FIP-1 (diluted from a 5 mM stock in DMSO) was added to each well and this was incubated at 37 °C for 90 minutes. At this point, buffer was removed and each well was washed 2x with 500 µL HBSS, then 500 µL of HBSS were added and snapshot images were taken.

2.2.13. Flow Cytometric Analysis of HEK 293T Cell Viability using Propidium Iodide (PI) Staining.

Cells were plated in 12-well polystyrene culture plates (Corning). 250 µM DFO or 1 mM BPS was added to DMEM media containing 10% FBS and glutamax in chambers containing cells and incubated at 37 ºC for 8 hours. At this point, media in these wells was replaced with 250 µM DFO or 1 mM BPS containing DMEM media (without FBS and glutamax) and incubated for 90 minutes at 37 ºC. DMEM media in non-treated wells was aspirated from chambers containing cells and this was replaced with DMEM media containing 100 uM FAS (prepared from a 20 mM FAS solution in water) or DMEM media and this was incubated for 90 minutes at 37 ºC. After the incubation was complete, media was removed and 900 uL PBS containing 3 µM propidium iodide (PI) was added to each well. Cells were dislodged by agitation and filtered through 35 µm nylon mesh caps into a 12 x 75 mm polystyrene tube (Corning) for analysis by flow cytometry. Finally, cell viability was calculated as the percentage of PI negative cells.

2.2.14. Analysis of MDA-MB-231 Cell Viability using PrestoBlue Plate Reader Assay.

MDA-MB-231 cells were cultured in DMEM supplemented with 10% fetal bovine serum (FBS, Hyclone), glutamax (Gibco), and 1% non-essential amino acids (NEAA, Gibco). One day before the experiment, cells were passaged and plated in phenol-red free medium on clear-bottom, black 96-well plates at 4.5x104 cells/well. Media was aspirated and was replaced with 100 µL DMEM media containing 10% FBS and glutamax and either DMSO vehicle, 1.25 µM Cmpd 21,1 1.25 µM Cmpd 21 + 1 µM ferrostatin-1 (Fer-1),2 or 1.25 µM Cmpd 21 + 100 µM DFO at various time points. Cells were treated for 8, 10, 12, 16, 18 and 22 hours. At the end of the incubation period, containing-compound media was removed and was replaced with 100 µM DMEM media containing 10% PrestoBlue reagent (ThermoFisher). Cells were incubated for 1 hour at 37 ºC, then fluorescence was read at 590 nm on a plate reader.

2.2.15. Generating Ratio Images.

All quantification of images was done prior to generating ratio images. Ratio images were generated as following. Images were opened as 32-bit images in ImageJ then an ROI was selected in an area containing no cells and the background fluorescence measured in this area was subtracted from the image. A background subtraction was done on both the Green channel and on the FRET channel, then the Green channel was divided by the FRET channel using the Image calculator tool. For visualization, a median filter of 0.2 was applied.

2.3. Results

2.3.1. Design and Synthesis of FIP-1.

Our design of FIP-1 makes use of an endoperoxide moiety prominent in natural antimalarial agents such as artemisinin[436] and synthetic endoperoxide variants[42, 44, 4750]. We envisioned creating an Fe(II)-responsive FRET platform with two fluorophores linked through an endoperoxide core. In the absence of iron, FRET would proceed efficiently through the intramolecular donor and acceptor pair. Fe(II)-mediated cleavage of the endoperoxide bridge would then result in dissociation of the two fluorophores from each other and concomitant loss of FRET signal (Scheme 2.1). We chose a 5-aminomethyl fluorescein (5-AMF) donor and a cyanine 3 (Cy3) acceptor as a FRET pair owing to their good spectral overlap and broad utility as dyes in biological imaging[548-49]. We note that this basic chemical strategy can be generalized to other fluorophore and fluorophore/quencher pairs, in addition to other modalities including photoacoustic, chemiluminescent, bioluminescent, MRI, and PET, for selective detection of iron and other analytes where quenching by a permanent binding event might present a challenge for generating a signal that preserves spatial resolution. When FIP-1 is intact, FRET occurs between 5-AMF and Cy3 when the probe is excited at the fluorescein excitation maximum. Upon Fe(II)-mediated cleavage of the endoperoxide linker, FRET no longer occurs between the dissociated 5-AMF and Cy3 moieties, resulting in an increase in 5-AMF emission at 515 nm. Increases in labile Fe(II) can then be monitored using the ratio of emission profiles for 5-AMF channel and Cy3 channel, which we designate hereafter as Green/FRET ratio.

The synthesis of FIP-1 is described briefly as follows. The dual-functionalized adamantyl-endoperoxide linker was synthesized in five steps from commercial available starting material (Scheme 2.2). 2-Adamantanone-5-carboxylic acid 1 was converted to the methyl ester 2 through a Fisher esterification and this was subsequently reacted with hydroxylamine-hydrochloride to afford oxime ether **3**. Oxime **3** was then reacted with 1,4-cyclohexanedione and ozone in a Griesbaum co-ozonolysis reaction to afford endoperoxide 4. Reductive amination was carried out on endoperoxide **4** followed by subsequent saponification to afford the endoperoxide-carboxylic acid linker **6**. Cy3-NHS-ester and 5-AMF were synthesized using published procedures.(50,51) With these key pieces in hand, Cy3-NHS-ester and 5-AMF were coupled sequentially onto the dual-functionalized linker to yield FIP-1 (Scheme 2.2).

2.3.2. Reactivity and Fe(II) Selectivity of FIP-1 in Aqueous Buffer.

With FIP-1 in hand, its fluorescence response to Fe^{2+} was evaluated in aqueous buffer (50 mM HEPES, pH 7.4). As expected, FIP-1 shows absorption maxima at 495 nm and 545 nm, corresponding to 5-AMF and Cy3, respectively, (Figure 2.1, dashed line) with molar attenuation coefficients of ε495 = 24800 M-1 cm-1 and ε 543 = 27800 M-1 cm-1 (Figure 2.2) and emission maxima at 515 nm and 556 nm (Figure 2.3, dashed line). When exposed to Fe(II), FIP-1 exhibits an increase in 5-AMF-derived emission at 515 nm (Figure 2.3a, solid line and 2.1, solid line). Notably, the increase at 5-AMF donor emission partially obscures the anticipated decrease in Cy3 acceptor emission centered at 556 nm resulting from the loss in intramolecular FRET owing to spectral overlap.

Nevertheless, the overall observed decrease in Green/FRET ratio is consistent with loss of FRET by endoperoxide cleavage with Fe^{2+}, as supported by both UV-Vis signatures (Figure 2.1), and mass spec data that confirm the presence of an intact endoperoxide before Fe^{2+} reaction and 5-AMF and Cy3 derived fluorophore components after Fe^{2+} reaction. FIP-1 reaches saturation for this FRET change within 1 hour when 1 μM FIP-1 is treated with 10 μM Fe^{2+} in aqueous buffer (Figure 2.5a) and exhibits fast reaction kinetics with a pseudo-first order rate constant of 0.0016 s^{-1} (Figure 2.5b). At a concentration of 1 μM FIP-1, FIP-1 is also capable of sensing low levels of Fe^{2+} in aqueous buffer in a dose-dependent manner (Figure 2.6).

We next evaluated the response of FIP-1 for Fe^{2+} compared to a panel of biologically relevant transition, alkali, and alkaline earth metals (Figure 1.1b). The data show that FIP-1 exhibits a highly metal- and oxidation state-specific response to Fe^{2+} and gives no FRET change in the presence of glutathione, the major intracellular reductant (Figure 2.3b). Only Cu+ at 10 μM levels gives a modest response, but FIP-1 is not responsive to lower concentrations of Cu+ (1 μM). These data, combined with the ca. 10-fold higher abundance of iron over copper in the typical eukaroytic cell,[1,50-51] coupled with the relatively high buffering capacity of the cell for copper in the form of glutathione and metallochaperones (pM-fM K_d values),[52-56] suggest FIP-1 has a sufficient *in vitro* selectivity profile for application to labile iron detection in biological systems. Indeed, while FIP-1 responds to addition of 10 μM Fe^{2+} in HEK 293T cells (Figure 2.7), FIP-1 shows no response to addition of 10 μM Cu^{+} in HEK 293T, indicating that FIP-1 is selective for labile iron over Cu^{+} *in cellulo* (Figure 2.8).

2.3.1. Application of FIP-1 to Imaging Labile Iron Pools in Living Cells.

Application of FIP-1 to Imaging Labile Iron Pools in Living Cells. Having established the ability of FIP-1 to respond selectively to physiological Fe^{2+} levels in aqueous buffer, we next explored its ability to respond to changes in Fe^{2+} levels in living cells through ratiometric fluorescence imaging. The data establish that FIP-1 is indeed able to visualize both increases and decreases in intracellular Fe^{2+} levels. HEK 293T cells exposed to 100 μM Fe^{2+} for 90 minutes, treated with FIP-1 for 90 minutes, and then imaged showed a patent increase in Green/FRET ratio over control cells. In contrast, HEK 293T cells pretreated either with 1 mM bathophenanthroline disulfonate (BPS) – a ferrous iron chelator – or with 250μM deferoxamine (DFO) – a ferric iron chelator – for 9.5 hours then stained with FIP-1 for 90 minutes exhibited a decrease in Green/FRET ratio when compared to control cells (Figure 2.9).

As a control, the iron addition and chelation treatments used the above imaging experiments were independently shown to alter total levels of intracellular iron by inductively coupled plasma mass spectrometry (ICP-MS) (Figure 2.10), consistent with the interpretation that FIP-1 is responding to the altered iron levels in these supplementation and chelator

treatments. Furthermore, FIP-1 showed a dose-dependent response with varying levels of Fe^{2+} (Figure 2.7). Finally, cell viability for these treatments was verified by propidium iodide staining, which confirmed that the cells were not significantly affected under these conditions compared to the vehicle control (Figure 2.9).

After verifying that FIP-1 was able to detect both increases and decreases in labile Fe^{2+} pools in a dose-dependent manner in HEK 293T cells, we sought to generalize its applicability to assay labile Fe^{2+} levels in other cell types. Owing to emerging interest in the connections between iron homeostasis and cancer[12, 57-58], we chose to compare the normal human mammary epithelial MCF10A cell line and two cancer lines, the metastatic human breast adenocarcinoma MDA-MB-231 cell line and the human osteocarcinoma U2OS cell line (Figure 3). Interestingly, we observe that the FIP-1 Green/FRET ratio is significantly higher in MDA-MB-231 and U2OS cells under basal states compared to the normal breast cell line MCF10A, consistent with reports that suggest expansion of iron pools in tumor cells[12, 46-478] over normal healthy ones. Moreover, treatment of the two cancer cell lines with 250 μM DFO for 8 h attenuates the FRET responses to levels comparable of the MCF10A cells with or without DFO treatment, presaging that this expanded labile iron pool can be specifically targeted in cancer cells while leaving normal cells relatively unaltered in terms of iron status. Taken together, the data establish that FIP-1 is responsive to changes in endogenous levels of labile Fe^{2+} across multiple cell types and can be potentially used to screen across a variety of cell types.

2.3.5. FIP-1 Enables Identification of Changes in Labile Iron Status in a Model of Ferroptosis.

With results showing that FIP-1 is capable of assaying relative levels of labile iron pools within a given cell type under basal conditions and situations of iron overload or iron deficiency, as well as compare cell types, we sought to explore the application of FIP-1 to directly observe potential changes in labile Fe^{2+} levels in cells undergoing ferroptosis. Ferroptosis refers to a novel and biochemically, genetically, and morphologically distinct form of cell death that can be triggered in cancer cells with a structurally diverse class of small molecules[59]. Cell death was suggested to be iron-dependent, as treatment with iron chelators reverses the death phenotype, and shown to be caused by lipid peroxidation, as lipophilic antioxidants, such as Ferrostatin-1 (Fer-1), can also prevent cell death[59]. Despite the growing recognition of the importance of ferroptosis as a cell death process, precise mechanisms linking labile iron pools and ferroptotic pathways remain insufficiently understood, in part due to a relative lack of tools for directly assaying labile Fe^{2+} in living specimens[60].

Building on the demonstrated ability of FIP-1 to detect endogenous changes in labile Fe^{2+} in MDA-MB-231 cells (Figure 2.11), we turned our attention to linking labile iron fluxes to this common model for ferroptosis. We observed that MDA-MB-231 cells begin to undergo exponential cell death when treated with 1.25 μM compound 21 (35MEW28, a recently re-ported inducer of ferroptosis)[660] after 10-12 hours. For labile iron detection, we imaged cells using FIP-1 at various time points after treatment with compound 21 (Figure 2.12). Interestingly, we observed that the Green/FRET ratio increased 2 hours after treatment as compared to the vehicle control and the signal further increased over time (Figure 2.12a, b). To validate that the ratiometric fluorescence response was derived from changes in the labile iron pool, we co-incubated cells with 21 and 100 μM DFO. Confocal microscopy measurements at the 8 hour time point no longer revealed an increased Green/FRET ratio (Figure 2.12c) compared to control (Figure 2.12a). However, when the cells are co-treated with compound 21 and the lipophilic antioxidant Fer-1, which blocks ferroptosis downstream of where we hypothesize a ferrous iron elevation to occur, we observe a Green/FRET ratio that is equivalent to cells treated with compound 21 alone (Figure 2.12d). As such, the data are consistent with the model that Fer-1 does not alter the mobilization of Fe^{2+} and indicates that the observed change in Green/FRET ratio is not simply an artifact of the process of ferroptosis. Taken together, these imaging results suggest that treatment with compound 21 may alter iron homeostasis to increase labile Fe(II) levels, serving as direct evidence that ferroptosis may be altering labile Fe(II) levels (Figure 2.12).

2.4. Conclusion

To summarize, we have presented the design, synthesis, characterization, and biological applications of FIP-1, a unique first-generation chemical probe for ratiometric detection of Fe^{2+}. FIP-1 operates by a reactivity mechanism in which Fe(II)-dependent cleavage of a bioinspired endoperoxide linker between donor and acceptor fluorophores modulates FRET. FIP-1 is responsive to Fe^{2+} in aqueous buffer with good metal- and oxidation state-selectivity and can report on changes in levels of labile Fe^{2+} pools in HEK 293T cells in a dose-dependent manner. Moreover, aided by its ratiometric response, this synthetic probe can be used to assay relative levels of labile iron across multiple cell types, as demonstrated by comparisons between normal and cancer cell lines under basal and chelator-treated conditions. Finally, FIP-1 provides direct imaging evidence for changes in labile iron status during ferroptosis, opening the door to studies of dynamic iron signaling during this newly recognized form of cell death and other biological processes. The synergistic development and application of FIP-1 and new chemical tools to study transition metal signaling are the focus of current efforts.

2.5. Future Directions

We are currently setting up a high-throughput platform to use FIP-1 to identify kinases that modulate iron homeostasis. Iron homeostasis is known to be altered in a variety of cancers [12-13, 47, 58], and iron homeostasis is altered by modulation of a number of cancer-relevant kinases[61-66]. We hypothesized that there may exist additional kinases that modulate iron homeostasis. As such, we are interested in using FIP-1 in an siRNA kinase screen. If a kinase is important in maintaining iron homeostasis, we hypothesize that knocking down kinase activity

will result in a change in FIP-1 signal. Efforts are still underway to optimize conditions for this screen.

2.6. Acknowledgments

We thank the NIH (GM79465) for supporting this work. A.T.A was partially supported by an NSF Graduate Fellowship and a Chemical Biology Training Grant from the NIH (T32 GM066698). C.J.C. is an Investigator of the Howard Hughes Medical Institute. We thank Alison Killilea and Carissa Tosta (UC Berkeley Tissue Culture Facility) for expert technical assistance. We thank Thomas Brewer, Cheri Ackerman, Marie Heffern, and Lakshmi Krishnamoorthy, as well as Ben Spangler and Adam Renslo, for helpful discussions.

Figures

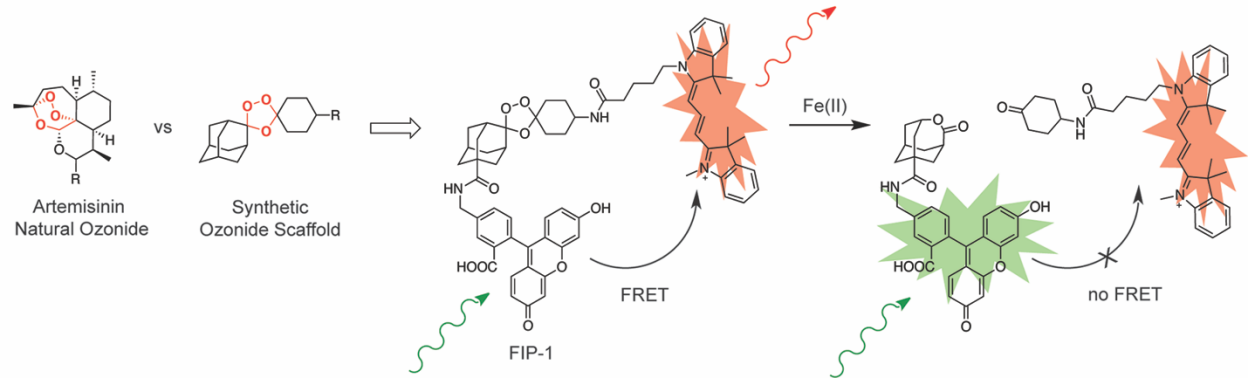

Scheme 2.1. Design of FRET Iron Probe (FIP-1).

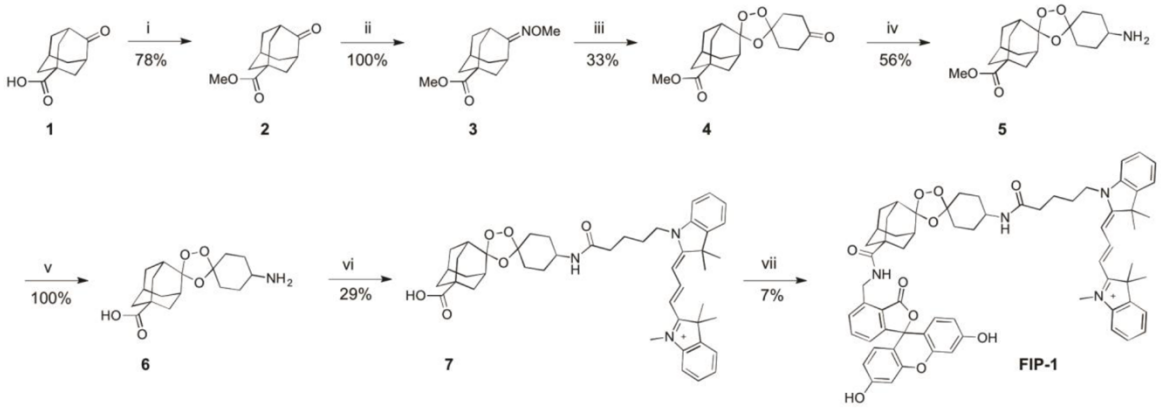

Scheme 2.2. Synthesis of FRET Iron Probe FIP-1[a]

[a]Reagents and conditions: (i) $SOCl_2$, MeOH, 0 °C to r.t., 12 h; (ii) H_2NOMe-HCl, pyridine, r.t., 3 h; (iii) 1,4-cyclohexanedione, O_3, CH_2Cl_2, CCl_4, 0 °C, 2.5 h; (iv) NH_4OAc, $NaBH_3CN$, r.t., 12 h; (v) LiOH, THF, H_2O, r.t., 12 h (vi) Cy3-NHS ester, NEt_3, DMF, 30 °C, 12 h; (vii) 5-aminomethyl fluorescein, HBTU, DIPEA, DMF, r.t., 12 h.

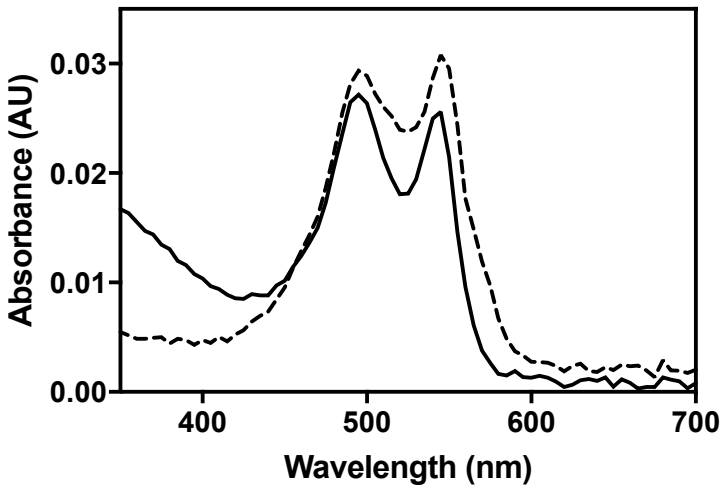

Figure 2.1. (a) UV-Visible spectra of FIP-1. (a) Spectra were obtained in 50 mM HEPES (pH 7.4) with 1 μM FLIP-1 (solid) and after treatment with 10 μM Fe(II).

(a)

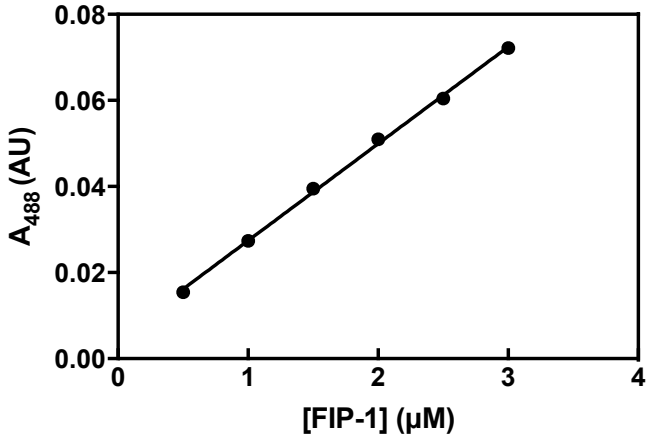

(b)

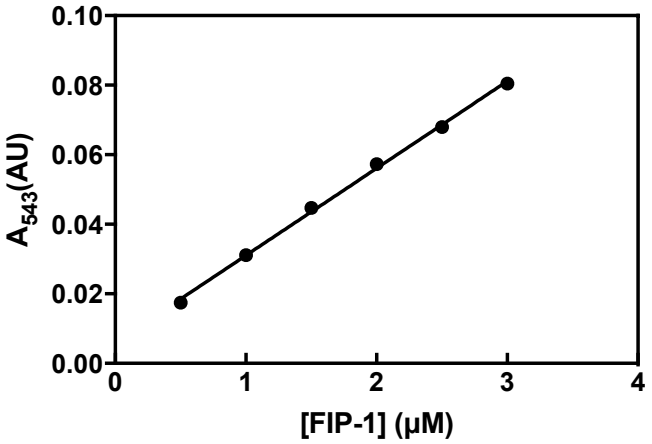

Figure 2.2. Determination of molar attenuation coefficient at (a) λ = 488 nm and at (b) λ = 543 nm. Spectra were obtained in 50 mM HEPES (pH 7.4) with 1 μM FIP-1.

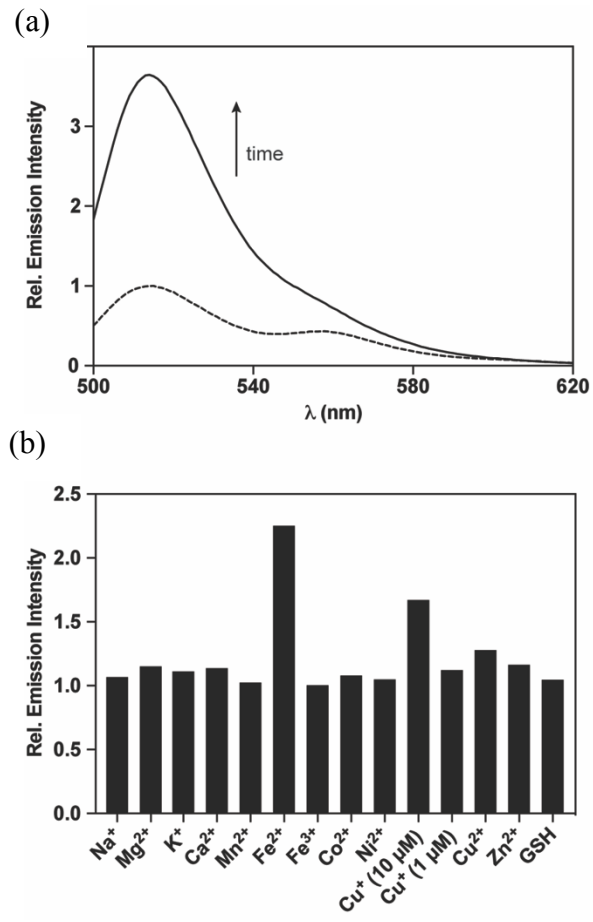

Figure 2.3. (a) Fluorescence intensity of 1 μM FIP-1 before (dashed line) and after (solid line) reaction with 10 μM Fe^{2+} at time = 270 minutes. (b) Fluorescence response of 1 μM FIP-1 to biologically relevant d-block (10 μM) and s-block (1 mM) metals as well as to glutathione (GSH) (5 mM). Manipulations were performed anaerobically and spectra were acquired at 37 °C in 50 mM HEPES (pH 7.4) when monitoring intensity of the 5-AMF donor, with λ_{ex} = 488 nm, collecting emission between 500 – 620 nm.

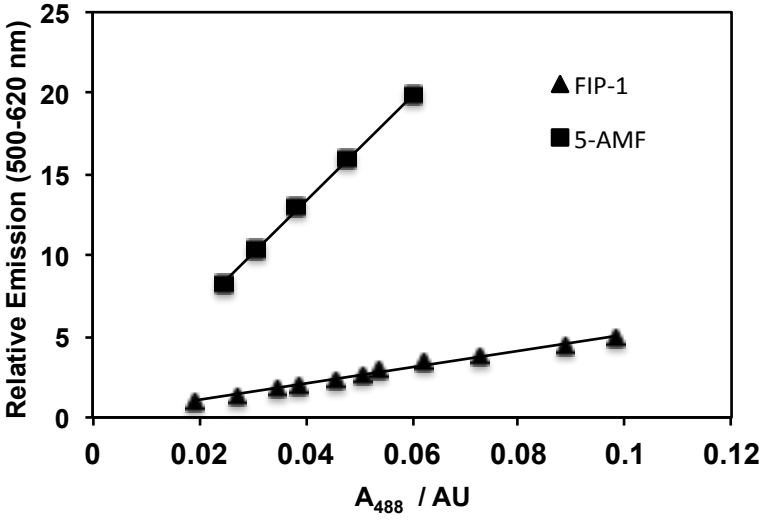

Figure 2.4. Determination of quantum yield for (a) fluorescein portion of FIP-1 and for (b) 5-AMF. The quantum yield for fluorescein portion of FIP-1 was determined to be 0.12 and the quantum yield for 5-AMF was determined to be 0.77. The quantum yield for the Cy3 derivatives is ca. 0.1.[134]

(a)

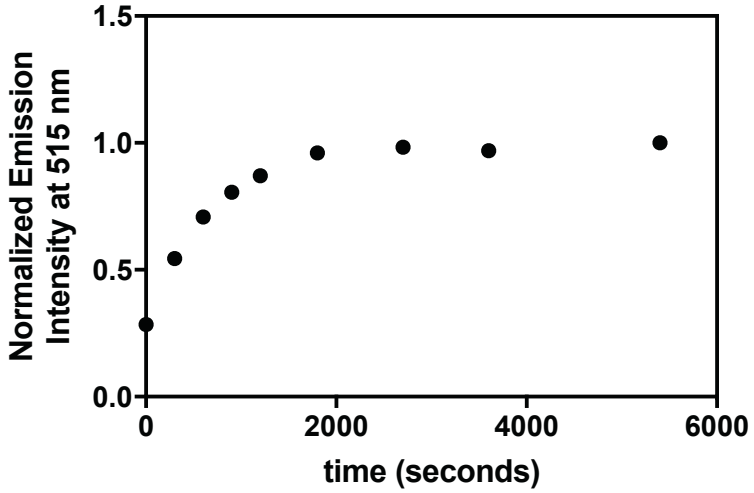

(b)

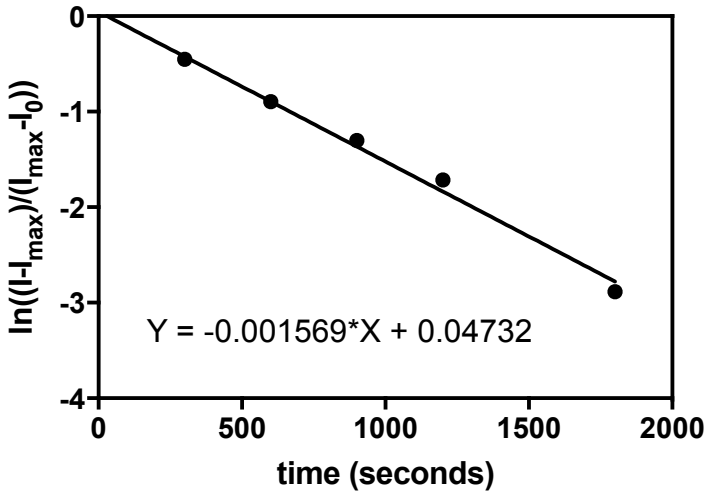

Figure 2.5. (a) Kinetic profile of the reaction between 1 μM FIP-1 and 10 μM Fe^{2+} monitored at 515 nm. Reaction was carried out at 37 ºC in 50 mM HEPES (pH 7.4) with excitation at 488 (b) Linearized integrated rate law, assuming this behaves as a pseudo first order reaction. kobs = 0.00157 ± .000063

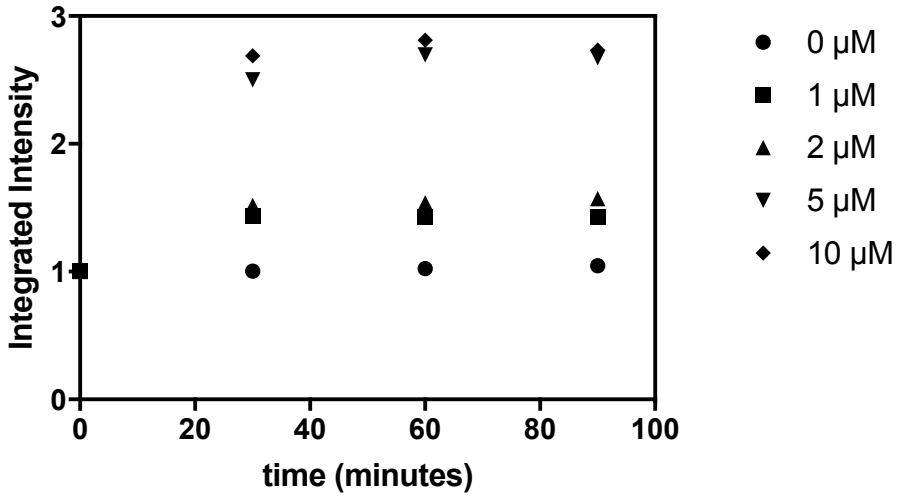

Figure 2.6. Dose dependence of 1 µM FIP-1 response to varying amounts of Fe^{2+}. Data was acquired at 37 ºC in 50 mM HEPES (pH 7.4) with excitation at 488. Emission intensity was integrated over the range of 500-620 nm.

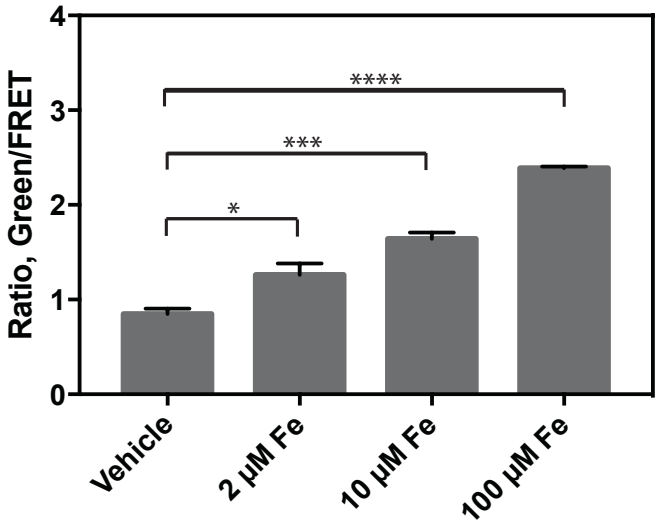

Figure 2.7. Dose dependence to Fe^{2+} addition in HEK 293T cells. HEK 239T cells were treated with 0 μM, 2 μM, 10 μM, or 100 μM FAS in serum-free DMEM media for 60 minutes at 37 ºC, then cells were washed and treated with 10 μM FIP-1 in HBSS for 90 minutes. Images were acquired after 2x HBSS washes. Error bars denote SEM, n=3. Statistical significance was assessed by calculating p-values using one-way ANOVA with the Bonferroni correction in R, * $p < 0.05$, ** $p < 0.01$, *** $p < 0.001$, **** $p < 0.0001$.

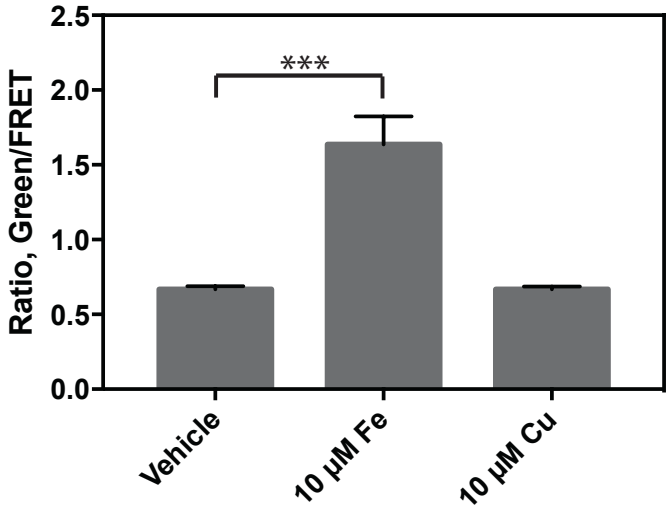

Figure 2.8. Selectivity for Fe^{2+} over Cu^{+} in HEK 293T cells. HEK 239T cells were treated with vehicle control (MilliQ water) or 10 µM FAS or 10 µM $CuCl_2$ in serum-free DMEM media for 90 minutes at 37 ºC, then cells were washed and treated with 10µM FIP-1 in HBSS for 90 minutes. Images were acquired after 2x HBSS washes. Error bars denote SEM, n=2. Statistical significance was assessed by calculating p-values using one-way ANOVA with the Bonferroni correction in R, *** $p < 0.001$.

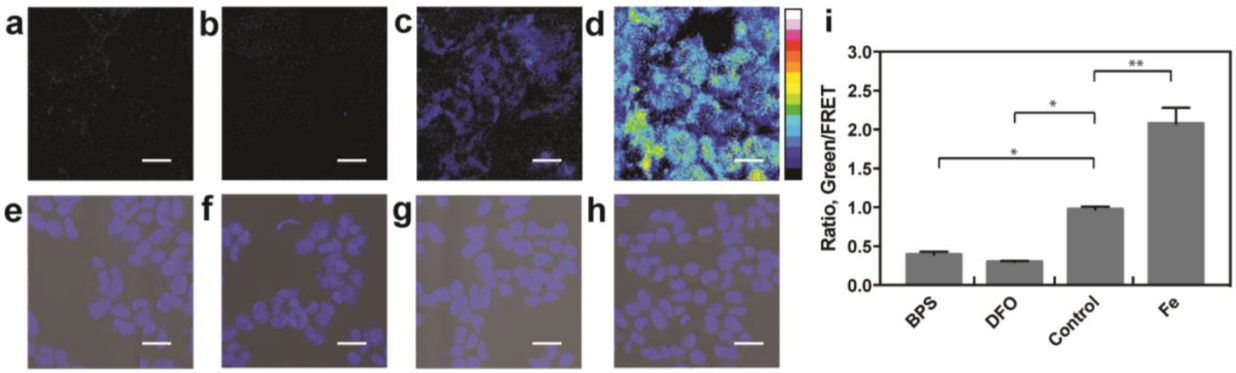

Figure 2.9. Representative ratiometric confocal microscopy images of live HEK 293T cells loaded with FIP-1. Cells were treated with (a) 1 mM bathophenanthroline disulfonate (BPS) for 9.5 hours, (b) 250 μM deferoxamine (DFO) for 9.5 hours, (c) vehicle, or (d) 100 μM ferrous ammonium sulfate (FAS) for 90 minutes. Cells were washed and treated with 10 μM FIP-1 in HBSS for 90 minutes then washed 2x with HBSS before acquiring images. (e-h) Brightfield images of (a-d) overlaid with Hoechst stain. (i) Mean Green/FRET ratios of HEK 293T cells treated with Fe(II) and chelators; error bars denote SEM, n=3. Statistical significance was assessed by calculating p-values using one-way ANOVA with the Bonferroni correction in R, *$p < 0.05$, **$p < 0.01$. Scale bar = 25 μm.

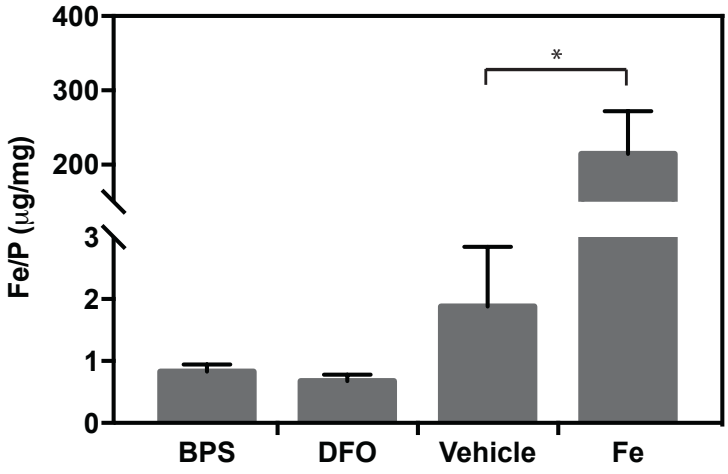

Figure 2.10. Total iron (^{56}Fe) content of control, chelator-treated and iron-supplemented HEK 293T cells. Chelator-treated HEK 293T cells were incubated with DMEM containing 250 μM DFO or 1 mM BPS and 10% FBS and glutamax for 8 hours at 37 ºC, then were incubated for in serum-free DMEM containing 250 μM DFO or 1 mM BPS for 90 minutes at 37 ºC. Iron-supplemented HEK 293T cells were incubated in serum-free DMEM containing 100 μM FAS for 90 minutes at 37 ºC. Cellular ^{56}Fe and phosphorous content was measured by ICP-MS. Error bars denote SEM, n=3. Statistical significance was assessed by calculating p-values using one-way ANOVA with the Bonferroni correction in R, **$p < 0.01$.

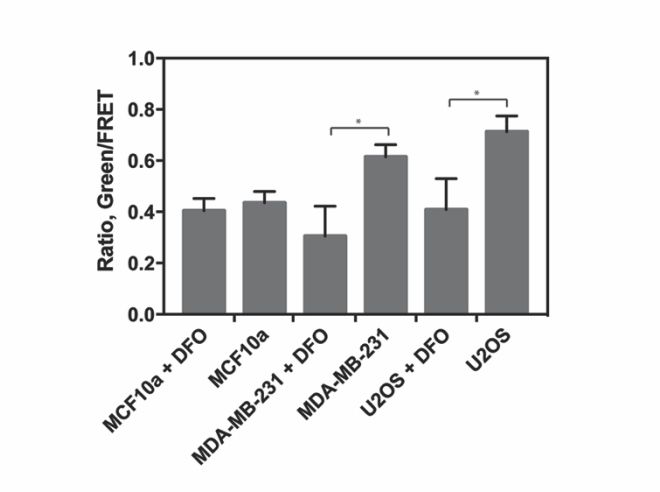

Figure 2.11. Application of FIP-1 to assay labile iron content across a variety of cell lines. Data shown for MCF10A normal breast cells compared to MDA-MB-231 and U2OS cancer cells under basal conditions as well as treated with 250 μM DFO for 8 hours. Cells were washed and stained with 10 μM FIP-1 in HBSS for 90 minutes then washed 2x with HBSS before acquiring images. Mean Green/FRET ratio was obtained for each cell line; error bars denote SEM, n=3. Statistical significance was assessed by calculating p-values using one-way ANOVA with the Bonferroni correction in R, *$p < 0.05$.

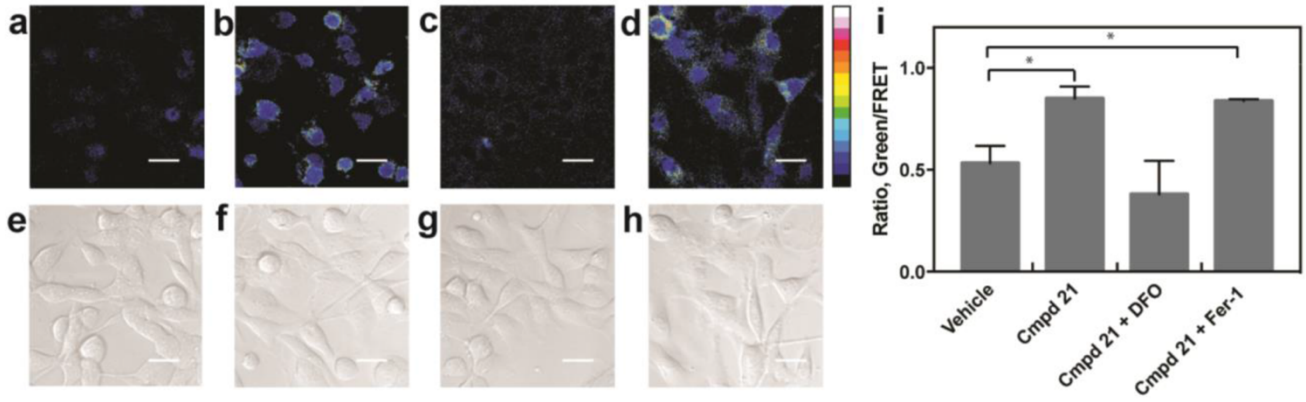

Figure 2.12. FIP-1 enables direct detection of changes in labile iron pools upon induction of ferroptosis. Confocal microscopy of 10 μM FIP-1 in MDA-MB-231 cells treated with (a) vehicle, (b) 1.25 μM compound **21** for 8 hours, (c) 1.25 μM compound **21** + 1 uM Fer-1 for 8 hours, and (d) 1 μM compound **21** + 100 μM DFO for 8 hours. (e) Mean Green/FRET ratios of MDA-MB-231 cells treated with ferroptosis-inducing compounds and inhibitors; error bars denote SEM, n=3. Statistical significance was assessed by calculating p-values using one-way ANOVA with the Bonferroni correction in R, *$p < 0.05$. Scale bar = 25 μm.

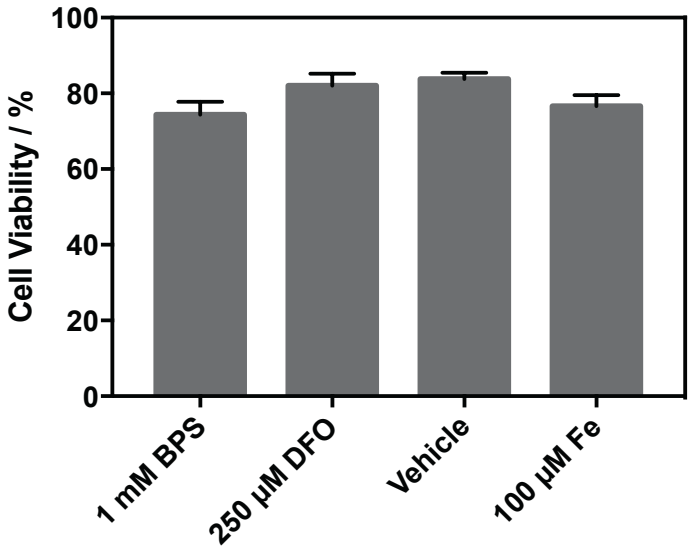

Figure 2.13. Cell viability of HEK 293T cells upon chelator-treatment or iron-supplementation. Chelator-treated HEK 293T cells were incubated with DMEM containing 250 µM DFO or 1 mM BPS and 10% FBS and glutamax for 8 hours at 37 ºC, then were incubated for in serum-free DMEM containing 250 µM DFO or 1 mM BPS for 90 minutes at 37 ºC. Iron-supplemented HEK 293T cells were incubated in serum-free DMEM containing 100 µM FAS for 90 minutes at 37 ºC. Cell viability was measured by propidium iodide (PI assay). Error bars denote SEM, n=3.

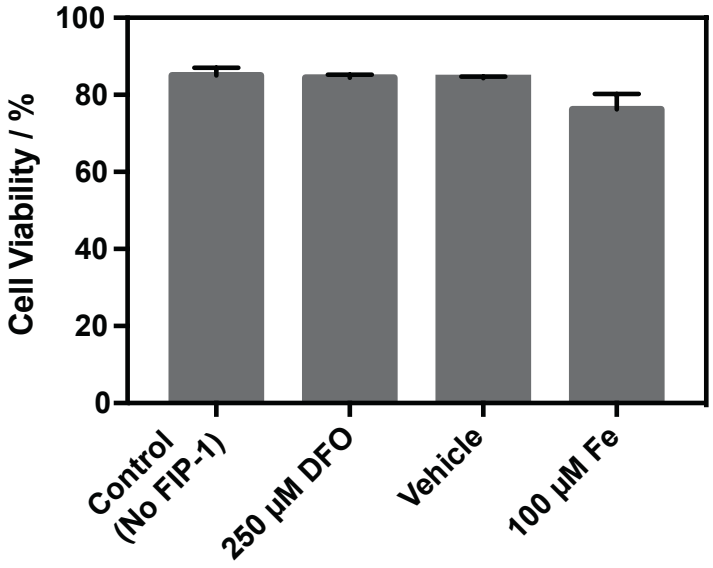

Figure 2.14. Cell viability of HEK 293T cells upon chelator-treatment or iron-supplementation and after treatment with FIP-1. Chelator-treated HEK 293T cells were incubated with DMEM containing 250 µM DFO and 10% FBS and glutamax for 8 hours at 37 ºC, then were incubated for in serum-free DMEM containing 250 µM DFO for 90 minutes at 37 ºC. Iron-supplemented HEK 293T cells were incubated in serum-free DMEM containing 100 µM FAS for 90 minutes at 37 ºC. Media was removed and cells were treated for 90 minutes in HBSS containing 10 µM FIP-1, before washing 1x with HBSS. Cell viability was measured by propidium iodide (PI assay). Error bars denote SEM, n=2.

2.7. References

1. Lippard, S. J.; Berg, J. M., *Principles of Bioinorganic Chemistry*. University Science Books: Mill Valley, CA,: Mill Valley, CA, 1994.
2. Hentze, M. W.; Muckenthaler, M. U.; Andrews, N. C., Balancing acts: molecular control of mammalian iron metabolism. *Cell* **2004,** *117*, 285-297.
3. Theil, E. C.; Goss, D. J., Living with Iron (and Oxygen): Questions and Answers about Iron Homeostasis. *Chem. Rev.* **2009,** *109*, 4568-4579.
4. Aisen, P.; Enns, C.; Wessling-Resnick, M., Chemistry and biology of eukaryotic iron metabolism. *Int. J. Biochem. Cell Biol.* **2001,** *33* (10), 940-959.
5. Cammack, R.; Wrigglesworth, J. M.; Baum, H., *Transport and Storage*. CRC Press: 1989.
6. Johnson, D. C.; Dean, D. R.; Smith, A. D.; Johnson, M. K., Structure, function, and formation of biological iron-sulfur clusters. *Annu Rev Biochem* **2005,** *74*, 247-81.
7. Winterbourn, C. C., Toxicity of iron and hydrogen peroxide: the Fenton reaction. *Toxicol Lett.* **1995,** *82/83*, 969-74.
8. James, S. A.; Robert, B. R.; Hare, D. J.; de Jonge, M. D.; Birchall, I. E.; Jenkin, N. L.; Cherny, R. A.; Bush, A. I.; McColl, G., *Chem. Sci.* **2015,** *6*, 2952-2962.
9. von Haehling, S.; Jankowska, E. A.; van Veldhuisen, D. J.; Ponikowski, P.; Anker, S. D., Iron deficiency and cardiovascular disease. *Nat. Rev. Cardiol.* **2015,** *12*, 659-669.
10. Hare, D.; Ayton, S.; Bush, A.; Lei, P., A delicate balance: Iron metabolism and diseases of the brain. *Front Aging Neurosci* **2013,** *5*, 34.
11. Gerlach, M.; Ben-Shachar, D. B.; Riedere, P.; Youdim, M. B. H., Altered brain metabolism of iron as a cause of neurodegenerative diseases? *J. Neurochem.* **1994,** *63* (3), 793-807.
12. Torti, S. V.; Torti, F. M., Iron and cancer: more ore to be mined. *Nat Rev Cancer* **2013,** *13* (5), 342-355.
13. Wu, K. J.; Polack, A.; Dala-Favera, R., Coordinated regulation of iron-controlling genes, H-ferritin and IRP2, by c-MYC. *Science* **1999,** *283*, 676-9.
14. Pinnix, Z. K.; Miller, L. D.; Wang, W.; D'Agostino, R. J.; Kute, T.; Willingham, M. C.; Hatcher, H.; Tesfay, L.; Sui, G.; Di, X.; Torti, S. V.; Torti, F. M., *Sci. Transl. Med.* **2010,** *2* 43ra56.
15. Toyokuni, S., Role of iron in carcinogenesis: cancer as a ferrotoxic disease. *Cancer Sci.* **2009,** *100* (1), 9-16.
16. Carter, K. P.; Young, A. M.; Palmer, A. E., Fluorescent Sensors for Measuring Metal Ions in Living Systems *Chem. Rev.* **2014,** *114* (8), 4564–4601.
17. Domaille, D. W.; Que, E. L.; Chang, C. J., Sythetic Fluorescent Sensors for Studying to Cell Biology of Metals. *Nat. Chem. Biol.* **2008,** *4*, 168-175.
18. Irving, H.; Williams, R. J. P., The stability of transition-metal complexes. *J. Chem. Soc.* **1953**, 3192-3210.
19. Kemlo, J. A.; Shepherd, T. M., Quenching of Excited Singlet States by Metal Ions. *Chem. Phys. Lett.* **1977,** *47* (1), 158-162.
20. Varnes, A. W.; Dodson, R. B.; Wehry, E. L., Interactions of transition-metal ions with photoexcited states of flavines. Fluorescence quenching studies. *J. Am. Chem. Soc.* **1972,** *94* (3), 946-950.

21. Breuer, W.; Epsztejn, S.; Millgram, P.; Cabantchik, I. Z., Transport of iron and other transition metals into cells as revealed by a fluorescent probe. *J. Am. Phys. Soc.* **1995,** *268*, C1354-C1361.
22. Kakhlon, O.; Cabantchik, Z. I., The labile iron pool: characterization, measurement, and participation in cellular processes. *Free Radic. Biol. Med.* **2002,** *33*, 1037-1046.
23. Au-Yeung, H. Y.; Chan, J.; Chantarojsiri, T.; Chang, C. J., Molecular Imaging of Labile Iron(II) Pools in Living Cells with a Turn-On Fluorescent Probe. *J. Am. Chem. Soc.* **2013,** *135*, 15165-15173.
24. Hirayama, T.; Okuda, K.; Nagasawa, H., A highly selective turn-on fluorescent probe for iron(II) to visualize labile iron in living cells. *Chem. Sci.* **2013,** *4*, 1250-1256.
25. Niwa, M.; Hirayama, T.; Okuda, K.; Nagasawa, H., *Org. Biomol. Chem.* **2014,** *12*, 6590-6597.
26. Hirayama, T.; Tsuboi, H.; Niwa, M.; Miki, A.; Kadota, S.; Ikeshita, Y.; Okuda, K.; Nagasawa, H., A universal fluorogenic switch for Fe(II) ion based on N-oxide chemistry permits the visualization of intracellular redox equilibrium shift towards labile iron in hypoxic tumor cells. *Chem. Sci.* **2017,** *8* (7), 4858-4866.
27. Chan, J.; Dodani, S. C.; Chang, C. J., *Nat. Chem.* **2012,** *4*, 973-984.
28. Aron, A. T.; Ramos-Torres, K. M.; Cotruvo, J., J. A.; Chang, C. J., *Acc. Chem. Res.* **2015,** *48*, 2434-2442.
29. Chen, X.; Tian, X.; Shin, I.; Yoon, J., *Chem. Soc. Rev.* **2011,** *40*, 4783-4804.
30. Yang, Y.; Zhao, Q.; Feng, W.; Li, F., Luminescent chemodosimeters for bioimaging. *Chem Rev.* **2013,** *113*, 192-270.
31. Cho, D. G.; Sessler, J. L., *Chem. Soc. Rev.* **2009,** *38*, 1647-62.
32. Zlokarnik, G.; Negulescu, P. A.; Knapp, T. E.; Mere, L.; Burres, N.; Feng, L.; Whitney, M.; Roemer, K.; Tsein, R. Y., Quantitation of transcription and clonal selection of single living cells with beta-lactamase as reporter. *Science* **1998,** *279*, 84.
33. Lee, M. H.; Kim, J. S.; Sessler, J. L., Small molecule-based ratiometric fluorescence probes for cations, anions, and biomolecules. *Chem. Soc. Rev.* **2015,** *44*, 4185-4191.
34. Grynkiewicz, G.; Poenie, M.; Tsien, R. Y. J., A new generation of Ca2+ indicators with greatly improved fluorescence properties. *Biol. Chem.* **1985,** *260*, 3440.
35. Harootunian, A. T.; Kao, J. P. Y.; Ecker, B. K.; Tsien, R. Y. J., Fluorescence ratio imaging of cytosolic free Na^+ in individual fibroblasts and lymphocytes. *Biol. Chem.* **1989,** *264*, 19458-19467.
36. Borstnik, K.; Paik, I. H.; Shapiro, T. A.; Posner, G. H., Antimalarial chemotherapeutic peroxides: artemisinin, yingzhaosu A and related compounds. *Int. J. Parasitol.* **2002,** *32* (13), 1661-1667.
37. Wang, X.; Creek, D. J.; Schiaffo, C. E.; Dong, Y.; Chollet, J.; Scheurer, C.; Wittlin, S.; Charman, S. A.; Dussault, P. H.; Wood, J. K.; Vennerstrom, J. L., Spiroadamantyl 1,2,4-trioxolane, 1,2,4-trioxane, and 1,2,4-trioxepane pairs: Relationship between peroxide bond iron(II) reactivity, heme alkylation efficiency, and antimalarial activity. *Bioorg & Med Chem Lett* **2009,** *19* (16), 4542-4545.
38. Deu, E.; Chen, I. T.; Lauterwasser, E. M.; Valderramos, J.; Li, H.; Edgington, L. E.; Renslo, A. R.; Bogyo, M., Ferrous iron-dependent drug delivery enables controlled and selective release of therapeutic agents in vivo. *Proc Natl Acad Sci USA* **2013,** *110* (45), 18244-18249.

39. Fontaine, S. D.; DiPasquale, A. G.; Renslo, A. R., Efficient and Stereocontrolled Synthesis of 1,2,4-Trioxolanes Useful for Ferrous Iron-Dependent Drug Delivery. *Org. Lett.* **2014,** *16* (16), 5776-9.
40. Fontaine, S. D.; Spangler, B.; Gut, J.; Lauterwasser, E. M. W.; Rosenthal, P. J.; Renslo, A. R., Drug Delivery to the Malaria Parasite Using an Arterolane-Like Scaffold. *ChemMedChem* **2015,** *10*, 47-51.
41. Abrams, R. P.; Carroll, W. L.; Woerpel, K. A., Five-Membered Ring Peroxide Selectively Initiates Ferroptosis in Cancer Cells. *ACS Chem Biol 11*, 1305-1312.
42. Creek, D. J.; Charman, W. N.; Chiu, F. C.; Prankerd, R. J.; McCullough, K. J.; Dong, Y.; Vennerstrom, J. L.; Charman, S. A., Iron-mediated degradation kinetics of substituted dispiro-1,2,4-trioxolane antimalarials. *J. Pharm. Sci.* **2007,** *96* (11), 2945-2956.
43. Creek, D. J.; Charman, W. N.; Chiu, F. C.; Prankerd, R. J.; Dong, Y.; Vennerstrom, J. L.; Charman, S. A., Relationship between Antimalarial Activity and Heme Alkylation for Spiro- and Dispiro-1,2,4-Trioxolane Antimalarials. *Antimicrob. Agents Chemother.* **2008,** *52*, 1291-.
44. Tang, Y.; Dong, Y.; Wang, X.; Sriraghavan, K.; Wood, J. K.; Vennerstrom, J. L., Dispiro-1,2,4-trioxane Analogues of a Prototype Dispiro-1,2,4-trioxolane: Mechanistic Comparators for Artemisinin in the Context of Reaction Pathways with Iron(II). *J. Org. Chem.* **2005,** *70* (13), 5103–5110.
45. Chang, C. J., Searching for harmony in transition-metal signaling. *Nat. Chem. Biol.* **2015,** *111*, 744–747.
46. Dixon, S. J.; Patel, D. N.; Welsch, M.; Skouta, R.; Lee, E. D.; Hayano, M.; Thomas, A. G.; Gleason, C. E.; Tatonetti, N. P.; Slusher, B. S.; Stockwell, B. R., Pharmacological inhibition of cystine–glutamate exchange induces endoplasmic reticulum stress and ferroptosis. *eLife* **2014,** *3*, e02523.
47. Spangler, B.; Morgan, C. W.; Fontaine, S. D.; Vander Wal, M. N.; Chang, C. J.; Wells, J. A.; Renslo, A. R., A reactivity-based probe of the intracellular labile ferrous iron pool *Nat. Chem. Biol.* **2016,** *12*, 680-685.
48. Norman, D. G. G., R. J.; Uhrin, D.; Tilley, D. M. J., Location of Cyanine-3 on Double-Stranded DNA: Importance for Fluorescence Resonance Energy Transfer Studies. *Biochemistry* **2000,** *39*, 6317–6324.
49. Li, D.; Liu, L.; Li, W., Genetic Targeting of a Small Fluorescent Zinc Indicator to Cell Surface for Monitoring Zinc Secretion. *ACS Chem Biol* **2015,** *10* (4), 1054-1063.
50. Cerchiaro, G.; Manieri, T. M.; Bertuchi, F. R., Analytical methods for copper, zinc and iron quantification in mammalian cells. *Metallomics* **2013,** *5*, 1336-1345.
51. Epsztejn, S.; Kakhlon, O.; Glickstein, H.; Breuer, W.; Cabantchik, Z. I., Fluorescence Analysis of the Labile Iron Pool of Mammalian Cells. *Anal. Biochem.* **1997,** *248* (1), 31-40.
52. Ramos-Torres, K. M.; Koleman, S.; Chang, C. J., Thioether Coordination Chemistry for Molecular Imaging of Copper in Biological Systems. *Isr. J. Chem.* **2016,** *2016* (article ASAP).
53. Cotruvo, J., J. A.; Aron, A. T.; Ramos-Torres, K. M.; Chang, C. J., Synthetic fluorescent probes for studying copper in biological systems. *Chem. Soc. Rev.* **2015,** *44*, 4400-4414.
54. Rubino, J. T.; Franz, K. J., Coordination chemistry of copper proteins: How nature handles a toxic cargo for essential function. *J. Inorg. Biochem.* **2012,** *107* (1), 129-143.
55. Davis, A. V.; O'Halloran, T. V., A place for thioether chemistry in cellular copper ion recognition and trafficking. *Nat. Chem. Biol.* **2008,** *4*, 148-151.
56. Kim, B. E.; Nevitt, T.; Thiele, D. J., Mechanisms for copper acquisition, distribution and regulation. *Nat. Chem. Biol.* **2008,** *4*, 176-185.

57. Bogdan, A. R.; Miyazawa, M.; Hashimoto, K.; Tsuji, Y., Regulators of Iron Homeostasis: New Players in Metabolism, Cell Death, and Disease. *Trends Biochem Sci.* **2016,** *41* (3), 274-286.
58. V., T. S.; Torti, F. M., Ironing out cancer. *Cancer Res.* **2011,** *71*, 1511-4.
59. Dixon, S. J.; Lemberg, K. M.; Lamprecht, M. R.; Skouta, R.; Zaitsev, E. M.; Gleason, C. E.; Patel, D. N.; Bauer, A. J.; Cantley, A. M.; Yang, W. S.; Morrison, B. I.; Stockwell, B. R., *Cell* **2012,** *149* (1060-72).
60. Dixon, S. J.; Lemberg, K. M.; Lamprecht, M. R.; Skouta, R.; Zaitsev, E. M.; Gleason, C. E.; Patel, D. N.; Bauer, A. J.; Cantley, A. M.; Yang, W. S.; Morrison, B. I.; Stockwell, B. R., Ferroptosis: an iron-dependent form of nonapoptotic cell death. *Cell* **2012,** *149* (1060-1072).
61. Zhou, S.; Du, X.; Xie, J.; Wang, J., Interleukin-6 regulates iron-related proteins through c-Jun N-terminal kinase activation in BV2 microglial cell lines. *PLoS One* **2017,** *12* (7), e0180464.
62. Wang, B.; Zhang, J.; Song, F.; Tian, M.; Shi, B.; Jiang, H.; Xu, W.; Wang, H.; Zhou, M.; Pan, X.; Gu, J.; Yang, S.; Jiang, L.; Li, Z., EGFR regulates iron homeostasis to promote cancer growth through redistribution of transferrin receptor 1. *Cancer Lett.* **2016,** *381* (2), 331-340.
63. Seo, Y. A.; Kumara, R.; Wetli, H.; Wessling-Resnick, M., Regulation of divalent metal transporter-1 by serine phosphorylation. *Biochem. J.* **2016,** *473* (22), 4243-4254.
64. Cao, H.; Schroeder, B.; Chen, J.; Schott, M. B.; McNiven, M. A., The Endocytic Fate of the Transferrin Receptor Is Regulated by c-Abl Kinase. *J. Biol. Chem.* **2016,** *291* (32), 16424-16437.
65. Du, F.; Qian, C.; Qian, Z. M.; Wu, X. M.; Xie, H.; Yung, W. H.; Ke, Y., Hepcidin directly inhibits transferrin receptor 1 expression in astrocytes via a cyclic AMP-protein kinase A pathway. *Glia* **2011,** *59* (6), 936-945.
66. Poli, M.; Derosas, M.; Luscieti, S.; Cavadini, P.; Campanella, A.; Verardi, R.; Finazzi, D.; Arosio, P., Pantothenate kinase-2 (Pank2) silencing causes cell growth reduction, cell-specific ferroportin upregulation and iron deregulation. *Neurobiol Dis.* **2010,** *39* (2), 204-210.

Chapter 3

Design and synthesis of a luciferin-based probe for *in vivo* bioluminescence imaging of labile iron and application to a murine model of Acinetobacter baumannii infection

Portions of this work were published in the following scientific journal:

Aron, A. T.;* Heffern, M. C.;* Lonergan, Z. R.;* Vander Wal, M. N.; Blank, B. R.; Spangler, B.; Zhang, Y.; Park, H. M.; Stahl, A.; Renslo, A. R.; Skaar, E. P.; Chang, C. J. In vivo bioluminescence imaging of labile iron accumulation in a murine model of *Acinetobacter baumannii* infection, *Proc. Nat. Acad. Sci. USA,* **2017**, *114*, 12669-12674. (*Denotes equal contribution)

Portions of this work were performed in collaboration with the following persons:

In vitro and *in cellulo* luminescence assays were performed in part by Marie C. Heffern

Abstract

Iron is an essential metal nutrient for all living organisms, yet disruption of its homeostasis, particularly in labile forms that can contribute to oxidative stress, is connected to diseases ranging from infection to cancer to neurodegeneration. Furthermore, iron deficiency is among the most common nutritional deficiencies worldwide. To advance studies of iron in healthy and disease states, we now report the synthesis and characterization of Iron-Caged Luciferin-1 (ICL-1), a bioluminescent probe that enables real-time monitoring of labile iron pools (LIPs) in living animals. ICL-1 utilizes a bioinspired endoperoxide trigger to release D-aminoluciferin for selective reactivity-based detection of Fe^{2+} with metal and oxidation state specificity. The probe can detect physiological changes in labile Fe^{2+} levels in live cells and mice experiencing iron deficiency or overload. Application of ICL-1 in a model of systemic bacterial infection reveals increased iron accumulation in infected tissues that accompany transcriptional changes consistent with elevations in both iron acquisition and retention. The ability to assess iron status in living animals provides a potentially powerful chemical technology for studying the contributions of iron metabolism to physiology and pathology.

3.1. Introduction

Iron is an essential mineral for every form of life, owing in large part to its ability to cycle between different oxidation states for processes such as nucleotide synthesis, oxygen transport, and respiration[1-4]. At the same time, the potent redox activity of iron is potentially toxic, particularly in unregulated labile forms that can trigger aberrant production of reactive oxygen species (ROS) via Fenton chemistry[4]. Indeed, iron deficiency remains one of the most common nutritional deficiencies in the world[5], and aberrant iron levels have been linked to various ailments, including cancer[6-9], cardiovascular[10] and neurodegenerative[11-12] disorders, as well as aging[13]. The situation is even more complex in infectious diseases, where the requirement for iron by both host organism and invading pathogen leads to an intricate chemical tug-of-war for this metal nutrient during various stages of the immune response[14-15].

The foregoing examples provide motivation for developing technologies to monitor biological iron status, with particular interest in methods to achieve in vivo iron imaging in live animal models that go beyond current state-of-the-art assays that are limited primarily to cell culture specimens. In this regard, detection of iron with both metal and oxidation state specificity is of central importance, because while iron is stored primarily in the ferric oxidation state, a ferrous iron pool bound weakly to cellular ligands, defined as the labile iron pool (LIP), exists at the center of highly regulated networks that control iron acquisition, trafficking, and excretion. Indeed, as a weak binder on the Irving-Williams series[16], Fe^{2+} provides a challenge for traditional recognition-based approaches[17] for its detection, and as such we[18-20] and others[21-24] have pursued reactivity-based approaches to sense labile Fe^{2+} stores in cells[25-29]. These tools have already provided insights into iron biology, as illustrated by the direct identification of elevations in LIPs during ferroptosis[30-31], an emerging form of cell death, using the ratiometric iron indicator FIP-1[18].

We now report the design, synthesis, and molecular imaging applications of Iron-Caged Luciferin-1 (ICL-1), a first-generation caged luciferin probe that enables in vivo iron imaging in living animals. Work from our lab and others has demonstrated the utility of caged luciferins in vivo[32-34] for measuring transient small molecules[35-389], enzyme and transporter activities[38-50], protein-protein and cell-cell interactions[46, 51-52], and copper[54]. In ICL-1, we caged D-

aminoluciferin with an Fe^{2+} reactive endoperoxide trigger[18, 20, 53] inspired by antimalarial agents that exhibit Fe^{2+}-dependent pharmacology[54-56]. Thus, ICL-1 was designed to undergo metal- and redox-specific Fe^{2+}-dependent cleavage to generate D-aminoluciferin, which can interact with the firefly luciferase enzyme to produce red light output through a catalytic bioluminescent reaction. ICL-1 is capable of monitoring changes in LIPs in live cells and mice under situations of iron overload and/or deficiency. Application of this technology to a mouse model of systemic *Acinetobacter baumannii* infection, a Gram-negative bacterial pathogen that infects susceptible intensive care unit (ICU) populations, reveals an elevation of LIPs by in vivo imaging that co-registers with increases in total iron as monitored by ex vivo imaging using laser ablation inductively coupled plasma mass spectrometry (LA-ICPMS). This unique tool for imaging iron in living animals provides a platform for probing the contributions of this metal to physiology, aging, and disease.

3.2. Methods

3.2.1. General methods

Reactions using air- or moisture-sensitive reagents were conducted in flame-dried glassware under an inert atmosphere of N_2. When dry solvent was required, solvent was passed over activated alumina and was stored over activated 3Å molecular sieves before use. All other commercially purchased chemicals were used as received (without further purification). 2-Adamantanone and hydroxylamine methyl ester hydrochloride were purchased from AK Scientific (Union City, CA); 6-amino 2-cyanobenzothiazole was purchased from Abblis Chemicals (Houston, TX); all other reagents were purchased from Sigma-Aldrich (St. Louis, MO). 3-Hydroxycyclohexan-1-one was synthesized as described previously[55]. 3-[(tert-butyldiphenylsilyl)oxy]cyclohexan-1-one was synthesized according to published procedures[57]. Silica gel P60 (SiliCycle) was used for column chromatography and SiliCycle 60 F254 silica gel (pre-coated sheets, 0.25 mm thick) were used for analytical thin layer chromatography and visualized by fluorescence quenching under UV light. ^1H and ^{13}C NMR NMR spectra were collected at 298 K in $CDCl_3$ or CD_3OD (Cambridge Isotope Laboratories, Cambridge, MA) at 25 °C on Bruker AVQ-400, AVB-400, AV-500, or AV-600 at the College of Chemistry NMR Facility at the University of California, Berkeley or on Bruker 900 at the QB3 Central California 900 MHz NMR Facility. All chemical shifts are reported in the standard notation of δ parts per million relative to residual solvent peak at 7.26 ($CDCl_3$) or 3.31 (CD_3OD) for ^1H and 77.16 ($CDCl_3$) or 49.00 (CD_3OD) for ^{13}C as an internal reference. Splitting patterns are indicated as follows: br, broad; s, singlet; d, doublet; t, triplet; m, multiplet; dd, doublet of doublets. Low-resolution electrospray mass spectral analyses were carried out using a LC-MS (Agilent Technology 6130, Quadrupole LC/MS and Advion expression-L Compact Mass Spectrometer). High-resolution mass spectral analyses (ESI-MS) were carried out at the College of Chemistry Mass Spectrometry Facility at the University of California, Berkeley.

3.2.2. Probe synthesis and new compound characterization

Endoperoxide (1). The endoperoxide **1** was synthesized following procedures in the literature[57].

Benzothiazole (2). To 2-cyano-6-aminobenzothiazole (0.0616 g, 0.352 mmol), bis(trichloromethyl) carbonate (0.1045 g, 0.352 mmol) and 4-dimethylaminopyridine (0.086 g,

0.7032 mmol) was added 25 mL dry toluene. This mixture was heated to reflux for 3 hours then was cooled to 35 ºC, at which point N_2 was bubbled through the solution for 15 minutes and collected in a KOH trap. At this point, endoperoxide 1 (0.1223 g, 0.44 mmol) was added in 5 mL of dry toluene followed by addition of sodium hydride (0.025 g, 1.09 mmol). The reaction mixture was stirred overnight at 35 ºC under N_2. The reaction was quenched with water then was diluted with ethyl acetate. The aqueous phase was extracted two more times with ethyl acetate and the combined organic layers were washed with a saturated NaCl solution, dried over Na_2SO_4, and concentrated under reduced pressure to afford a brown powder. Purification by silica chromatography (0 → 15 % ethyl acetate in hexanes) yielded **2** as a pale yellow foam. Yield = 135.34 mg, 80 %. ^{1}H NMR (400 MHz, $CDCl_3$, 298 K) δ (ppm): 8.44 (s, 1 H), 8.12 – 8.09 (d, 1 H), 7.34 – 7.30 (dd, 1 H), 6.87 (s, 1 H), 4.95 – 4.86 (m, 1 H), 2.37 – 2.31 (m,1 H), 2.06 – 1.64 (m, 21 H). ^{13}C NMR (101 MHz, $CDCl_3$, 298 K) δ (ppm): 152.5, 148.3, 138.9, 137.3, 134.9, 125.5, 119.8, 113.2, 111.9, 109.7, 108.6, 72.4, 45.5, 40.1, 36.8, 36.4, 36.4, 36.2, 34.9, 34.8, 33.8, 30.8, 30.6, 26.9, 26.5, 24.8, 21.2, 19.8. LRMS calcd. for $C_{25}H_{27}N_3O_5S$ $[M-H]^-$ *m/z* 480.2; found: 480.3.

ICL-1. To a Schlenk tube charged with D-cysteine hydrochloride monohydrate (0.022 g, 0.125 mmol) and K_2CO_3 (0.020 g, 0.15 mmol) in N_2 was added deoxygenated water (0.2 ml), followed by a solution of 3 (0.040 g, 0.0832 mmol) in deoxygenated MeOH (0.6 ml) and dichloromethane (0.6 ml). The solution was stirred under N_2 at room temperature overnight. At this point, the reaction mixture was filtered and the filtrate was neutralized by addition of one equivalent of 1 M HCl. The filtrate was diluted with ethyl acetate and water. The aqueous phase was separated and extracted with three portions of ethyl acetate. The combined organic phases were washed with saturated aq NaCl solution, dried over Na_2SO_4, filtered, and concentrated to afford a yellow oil. The crude material was purified by HPLC on an Agilent Life Sciences SB-C18 Semi-Prep HPLC Column 9.4 x 250 mm (flow rate = 1.5 ml/min, H_2O/MeCN with 0.05% formic acid gradient: 0-50 min, 35% → 100% MeCN in water, 50-65 min, 100% MeCN in water). Yield = 11.43 mg, 24%. ^{1}H NMR (600 MHz, CD_3OD, 298 K) δ (ppm): 8.27 (s, 1 H), 7.95 – 7.94 (d, 1 H), 7.51 – 7.49 (dd, 1 H), 5.41 – 5.38 (s, 1 H), 4.97 (m, 1 H), 3.79 – 3.73 (q, 1 H), 2.36 – 2.33 (m,1 H), 1.99 – 1.65 (m, 22 H). ^{13}C NMR (151 MHz, CD_3OD, 298 K) δ (ppm): 173.3, 167.5, 164.5, 160.3, 155, 150.0, 140.2, 138.4, 125.2, 120.1, 118.1, 112.7, 111.3, 109.9, 79.6, 72.7, 49.9, 49.6, 40.9, 37.8, 35.9, 35.8, 35.7, 34.8, 31.5, 28.3, 27.9, 20.8. HRMS (ESI) calcd. for $C_{28}H_{31}N_3O_7S_2$ $[M-H]^-$ *m/z* = 584.1603; found: 584.1528.

3.2.3. In Vitro *Luminescence Assays*.

Millipore water was used to prepare all aqueous solutions. Incubation of 5 μM of ICL-1 (100x dilution of a 500 μM stock in DMSO) with different metal ions ($MgCl_2$, $CaCl_2$, $MnCl_2$, $FeCl_2$, $FeCl_3$, $CoCl_2$, $NiCl_2$, $Cu(MeCN)_4(PF_6)$, $CuCl_2$ and $ZnCl_2$) was performed in 50 mM HEPES buffer at pH 7.4. Similar experiments were performed with D-aminoluciferin (termed here aminoluciferin; 100 nM, 100x dilution of a 10 μM stock in DMSO) to determine any effects of the metal ion treatments on luciferase activity. At the end of the incubation, 40 μl each of the solution was transferred to a well of a white, opaque half-area 96-well plate (Corning). An equal volume (40 μl) of a solution of luciferase (100 μg/ml, Promega) in 50 mM Tris buffer at pH 7.4, with 10 mM Mg^{2+} ($MgCl_2$), 0.1 mM Zn^{2+} ($ZnCl_2$) and 2 mM ATP was added and mixed well. Bioluminescent signals were measured using a Synergy Mx plate reader at 37°C for 30 min. To determine the reactivity of ICL-1 with iron-containing species, similar experiments were

performed as with the metal selectivity assays, but with iron-bound transferrin (holo-transferrin, holoTf), ferritin, hemin, and hemoglobin. For holoTf, hemin, and hemoglobin, stoichiometric binding of iron was assumed and the species were measured by weight. For ferritin, total iron per mg of ferritin was approximated with the ferrozine assay. ICL-1 or aminoluciferin was incubated with the appropriate amounts of the iron-containing species to achieve 100 μM total iron in the incubation solution with subsequent bioluminescent assays as described.

3.2.4. Cellular Assays.

A Xenogen IVIS Spectrum instrument (Caliper Life Sciences) was used for bioluminescence imaging in all cellular experiments. PC3M-Luc, HEK293-Luc, MDA-MB-293-Luc, and LNCaP-Luc cells were each cultured in DMEM containing 10% FBS. Cells were passaged and plated in black 96-well plate with clear bottoms (Becton, Dickson and Company) to achieve 75% confluence 1 day after plating (or 90% confluence 2 days after plating), and were treated, assayed, and imaged 2 days after plating. For iron treatments, stock solutions of FAS were prepared in millipore water at 20x the final concentration of the treatment. Ninety minutes prior to imaging, the serum-containing DMEM was aspirated from the cells and replaced with 95 μL serum-free DMEM followed by 5 μL of the aqueous solution of FAS and the cells were incubated at 37 ºC.

Chelator treatments were performed as follows. For treatments with BPY, concentrated stocks of BPY (2000x the final concentration of treatment) were prepared in DMSO with brief heating to solubilize the agent. The DMSO stock was diluted 100-fold with millipore water. Ninety minutes prior to imaging, the serum-containing DMEM was aspirated from the cells and replaced with either 100 μL serum-free DMEM (or with FAS-containing DMEM as described) and the cells were incubated at 37 ºC. Thirty minutes prior to imaging, 5 μL of the DMEM (or the FAS-containing DMEM) was removed from the wells and 5 μL of the BPY solutions were added to the wells and the cells were further incubated at 37 ºC. For treatments with DFO and BPS, 20 mM and 50 mM stock solutions were prepared in millipore water and diluted 80-fold and 20-fold with DMEM containing 10% FBS to obtain 250 μM and 1 mM solutions, respectively. The solutions were sterilized by filtration through a 0.2 μm filter. Nine hours prior to imaging, the serum-containing media was aspirated from the cells and replaced with the chelator-containing media and the treated cells were incubated at 37 ºC. Ninety minutes before imaging, the serum-containing chelator treatments were aspirated from the cells and replaced with equivalent concentrations of chelator in serum-free DMEM, and the cells were further incubated at 37 ºC.

To prepare the solutions of ICL-1 for imaging, 0.5 mM (PC3M-Luc, HEK293-luc, and LNCaP-Luc) or 0.25 mM (MDA-MB-231-Luc) solutions of the probe were prepared in DMSO and diluted 40-fold in HBSS (20 and 10 μM final concentrations, respectively). At the end of the treatment times, the cells were aspirated of the chelator- and/or iron-containing media and replaced with the probe-containing HBSS. The plates were immediately imaged for 1 h (for PC3M-Luc and HEK293-Luc) or 30 min (LNCaP-Luc and MDA-MB-231-Luc) with 1 min exposure times and segments with delay times of 1 - 3 min between segments. For control experiments, cells were treated under the same conditions and imaged with 1 μM aminoluciferin.

3.3. Results

3.3.1. Design and Synthesis of Iron-Caged Luciferin-1 (ICL-1)

Our design of ICL-1 involved caging D-luciferin with a 1,2,4-trioxolane scaffold[53] used previously for in vivo delivery of therapeutic payloads in an Fe^{2+}-dependent fashion[58-59]. The excellent pharmacokinetic properties of these therapeutic conjugates suggested that ICL-1 would have suitable in vivo properties for the desired imaging applications. In the conjugate form, ICL-1 is an incompetent substrate for the luciferase enzyme. Upon Fe^{2+}-promoted reduction of the peroxide, however, a cyclohexanone intermediate is formed that spontaneously releases free D-aminoluciferin, which can be transformed by luciferase to produce a bioluminescent signal (Scheme 3.1). D-aminoluciferin imaging can be used as a control for changes in enzyme activity and can be used in parallel for signal normalization. Scheme 2 depicts the synthetic route to ICL-1. Briefly, commercially available 6-amino-2-cyanobenzothiazole is activated using triphosgene, which is subsequently reacted with (±)-*trans*-**1**[55] to yield carbamate **2**. Cyclization of **2** with D-cysteine-HCl affords ICL-1 after HPLC purification.

The design of ICL-1 was inspired by our laboratory's development of Copper-Caged Luciferin-1 (CCL-1) - a Cu^{+}-responsive caged probe that generates D-luciferin and a bioluminescent signal upon interaction with firefly luciferase[60]. Inspired by the fact that application of this probe to a diet-induced model of nonalcoholic fatty liver disease was able to reveal the start of hepatic copper deficiency, we envisioned developing an analogous caged probe for *in vivo* detection of iron, the most abundant transition metal in the human body. We were particularly eager to develop a probe that could be applied to a model of systemic bacterial infection, as iron metabolism in this context remains poorly understood.

3.3.2. Reactivity and Selectivity of ICL-1

With ICL-1 in hand, its Fe^{2+}-dependent reactivity was assessed in aqueous solution buffered to physiological pH (50 mM HEPES, pH 7.4). Treatment of 5 μM ICL-1 with ferrous ammonium sulfate (FAS) as an Fe^{2+} source at concentrations spanning 25 to 100 μM shows a dose-dependent increase in bioluminescent signal in the presence of luciferase (Figure 3.1a, gray bars), saturating at a ca. 7-fold bioluminescent signal enhancement at highest Fe^{2+} concentrations, when incubation is performed aerobically, versus a ca. 30-fold bioluminescent signal enhancement at the same Fe^{2+} concentration, when incubation is performed anaerobically (Figure 3.2). The observed signal increase is Fe^{2+}-dependent, as co-incubation of ICL-1/luciferase solutions with the Fe^{2+} chelator bipyridine results in a decrease in bioluminescence intensity (Figure 1.1A, gray patterned bars). Further control experiments establish that iron-dependent responses are not observed with the parent D-aminoluciferin substrate (Figure 3.3). ICL-1 exhibits high selectivity for Fe^{2+} over other biologically relevant d-block and s-block metals, including redox-active copper and cobalt transition metals (Figure 3.1b). A modest response is observed with free copper salts, as is similarly observed for the related fluorescence probe FIP-1[19]. However, as a typical eukaryotic cell exhibits a ca. 10-fold higher level of iron over copper coupled with the high buffering capacity of copper with glutathione and metallochaperones (pM-fM K_d values)[60-655], the modest response to free copper salts suggests that ICL-1 should have sufficient selectivity to detect alterations in biological ferrous iron levels. Moreover, ICL-1 is highly selective for labile Fe^{2+} over other biologically-relevant forms of iron that are tightly bound to proteins and cofactors. This includes selectivity over transferrin, ferritin, hemin, and hemoglobin, as well as Fe^{3+}, along with reductants, such as

glutathione, N-acetyl cysteine, β-mercaptoethanol, and ascorbic acid (Figure 3.1c), presaging its suitability for assessing LIPs in biological samples.

3.3.3. ICL-1 Detects Changes in Labile Iron Levels in Living Cells

We next sought to evaluate the ability of the ICL-1 probe to detect changes in Fe^{2+} levels in live cells. Initial experiments employed a luciferase-expressing prostate cancer cell line, PC3M-luc, that has been shown previously to respond to TRX-PURO[20], a cellular Fe^{2+} probe based on the same caging moiety used in ICL-1. Cells were supplemented with various concentrations of an iron salt (FAS), iron chelator (BPY), or FAS followed by BPY, then treated with ICL-1 and imaged using an IVIS bioluminescence imaging system (Figure 3.5-3.7). Iron supplementation results in an increase in ICL-1-dependent bioluminescence that can be attenuated by addition of BPY, and iron deficiency induced by treatment with BPY alone results in a decrease in ICL-1 signal relative to basal levels. Notably, ICL-1 exhibits excellent stability in media (Figure 3.4). Additionally, ICL-1 signal is unaffected by short term treatment with an extracellular iron chelator, suggesting that observed ICL-1 reactivity is due to intracellular, as opposed to extracellular, iron. Control experiments with the parent D-aminoluciferin substrate show that this probe is not sensitive to iron status.

The probe was further evaluated in a broader set of luciferase-expressing cell lines and with additional iron chelators. In addition to PC3M-luc, a second prostate cancer cell line (LNCaP-luc), breast cancer cell line (MDA-MB-231-luc), and embryonic kidney cell line (HEK293-luc) were each treated with FAS, the iron chelators desferroxamine (DFO), bathophenanthrolinedisulfonic acid (BPS), or BPY, or a combination of FAS and BPY for ICL-1 imaging (Figure 3.6-3.7). In line with what is observed using PC3M-luc cells, LNCaP-luc, MDA-MB-231-luc, and HEK-293-luc cells supplemented with 100 μM FAS exhibit increased light production relative to untreated control cells, and these increases are attenuated by co-incubation with the iron chelator BPY. Likewise, iron depletion induced by chelator addition results in decreases in ICL-1-dependent bioluminescence in all cell lines tested. Again, control experiments further confirm that D-aminoluciferin signals are not affected by either iron supplementation and/or depletion (Figure 3.7). The collective data establish that ICL-1 can assess labile Fe^{2+} status across a variety of cell types.

3.4. Conclusions

In summary, we have presented the design, synthesis, and characterization of ICL-1, a first-generation bioluminescence probe for in vivo imaging of labile iron stores in living animals. ICL-1 utilizes a bioinspired Fe^{2+}-dependent endoperoxide cleavage reaction to release D-aminoluciferin and generate an increase in bioluminescent signal with high metal and oxidation-state specificity. This probe is capable of monitoring changes in LIPs upon iron supplementation and/or depletion in live cells and animals, enabling the detection of dynamic alterations in Fe^{2+} under physiological and pathological situations.

Additionally, ICL-1 was applied to an *A. baumannii* model of systemic infection to showcase the utility of this probe for interrogating alterations in iron status in vivo. In collaboration, we observed an increase in liver iron that is supported by complementary ex vivo bioluminescent imaging, as well as ICP-MS and LA-ICPMS data for total iron detection.

Consistent with the observed redistributions of hepatic iron and elevations in total hepatic iron, qPCR analyses of isolated liver tissues after infection reveal concomitant decreases in mRNA levels of the iron export protein ferroportin, increased mRNA levels of the secreted factor LCN2, and modulation in the mRNA levels of key iron storage machinery – namely increased FHC and decreased FLC. These transcriptional changes are supported by significant alterations in serum transferrin and ferritin during infection. We hypothesize that such transcriptional alterations can serve as important contributors to changes in labile and total hepatic iron stores. By expanding our ability to monitor iron dynamics from cell culture to living animals, ICL-1 provides a unique chemical tool to study biological contributions of this essential metal nutrient and a starting point for developing next-generation probes for advancing our understanding of metals in biology in vivo.

3.5. Acknowledgements

We thank NIH (GM79645 to C.J.C, AI101171 to E.P.S., and AI105106 to A.R.R., and DK101293 to A.S.) for funding this work. C.J.C. is an Investigator with the Howard Hughes Medical Institute and a CIFAR Senior Fellow. A.T.A thanks the NSF for a graduate fellowship and was partially supported by an NIH Chemical Biology Interface Training Grant (T32 GM066698). M.C.H. thanks the UC President's Postdoctoral Program for a fellowship. Z.R.L. is supported by the NIH Training Program in Environmental Toxicology (T32 ES007028). B.S. acknowledges funding from an NIH Research Training Grant in Chemistry and Chemical Biology (T32 GM064337). We thank Jessica Moore for technical assistance with tissue sectioning.

Figures

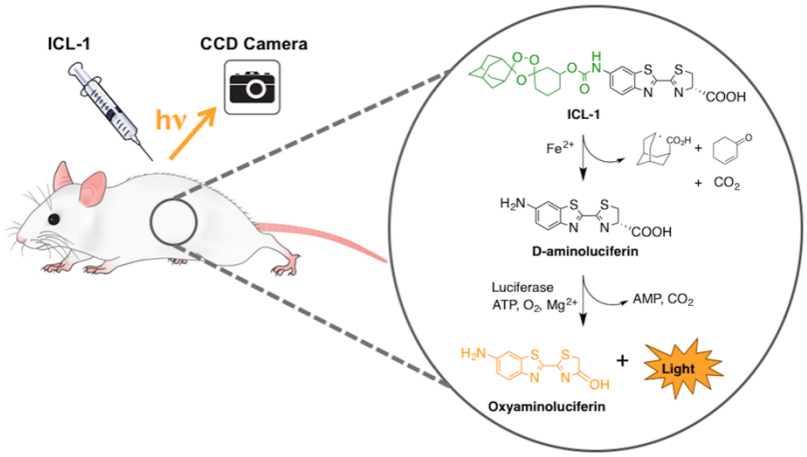

Scheme 3.1. Design scheme for Iron Caged Luciferin 1 (ICL-1).

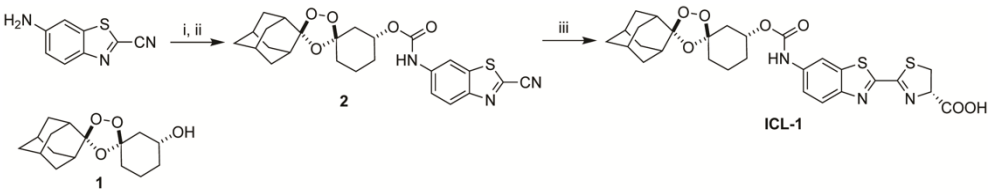

Scheme 3.2. Synthesis of ICL-1[a]**;** [a]Reagents and conditions: (i) triphosgene, 4-DMAP, toluene, 125 °C to 35 °C, 3 h; (ii) **1**, NaH, toluene, 35 °C, 12 h, 80% over two steps; (iii) D-cysteine, K_2CO_3, CH_2Cl_2, MeOH, H_2O, 0 °C, 12 h, 24%.

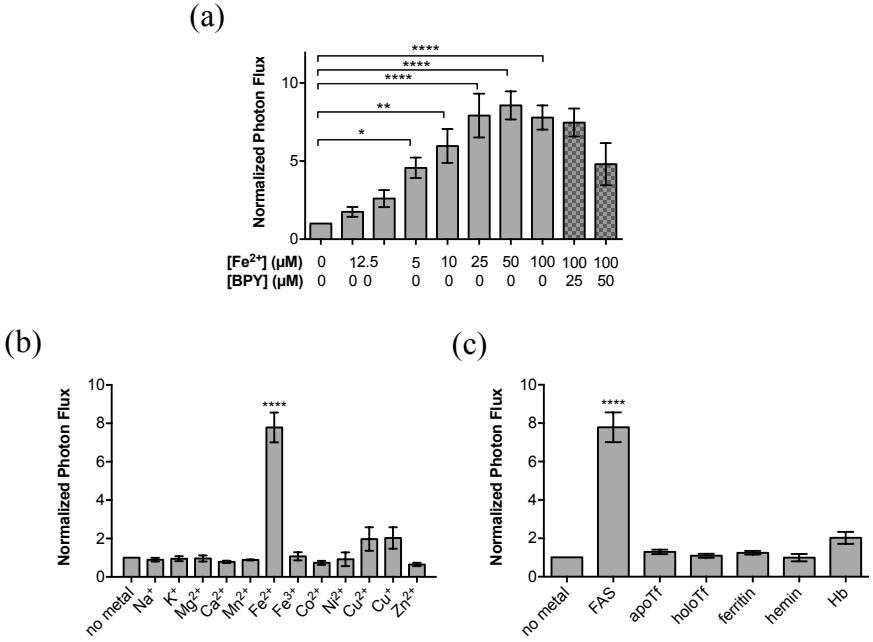

Figure 3.1. ICL-1 selectively responds to Fe^{2+} over other metals and tightly-bound biological iron species with metal and redox specificity. Bioluminescence response of ICL-1 incubated with (a) varying concentrations of Fe^{2+} as the ferrous ammonium sulfate salt (FAS) (gray bars) or 100 μM FAS with 100 μM of the iron chelator bipyridine (BPY, gray patterned bars), (b) various biologically relevant s-block (1 mM) and d-block (100 μM) metal ions, and (c) tightly-bound iron-species of biological relevance, such as transferrin (without iron, apoTf; with iron, holoTf), ferritin, hemin, and hemoglobin (Hb), and reductants, such as glutathione (GSH), N-acetyl cysteine (NAC), β-mercaptoethanol (BME), and ascorbic acid (as. acid). Signals are integrated over 30 min and expressed as photon fluxes normalized to ICL-1 bioluminescence with no treatment (buffer alone). Statistical analyses were performed with one-way analysis of variance (ANOVA) with multiple comparisons to the control with no metal treatment, where *$P \leq 0.05$, **$P \leq 0.01$ and ****$P \leq 0.0001$. Error bars are ± SEM (n = 3).

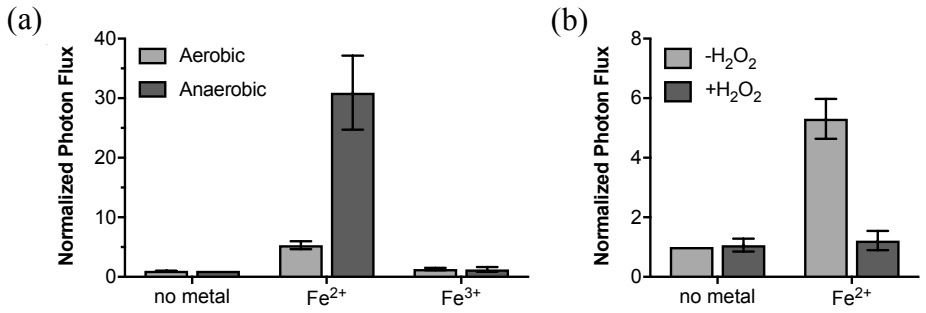

Figure 3.2. ICL-1 selectively responds to Fe^{2+} over other metals and biologically-relevant oxidants. Bioluminescence response of ICL-1 incubated with (a) 100 μM Fe^{2+} or Fe^{3+} in aerobic versus anaerobic incubation conditions, or (b) hydrogen peroxide in the absence and presence of Fe^{2}. Signals are integrated over 30 min and expressed as photon fluxes normalized to ICL-1 bioluminescence with no treatment (buffer alone). Error bars are ± SEM (n = 3).

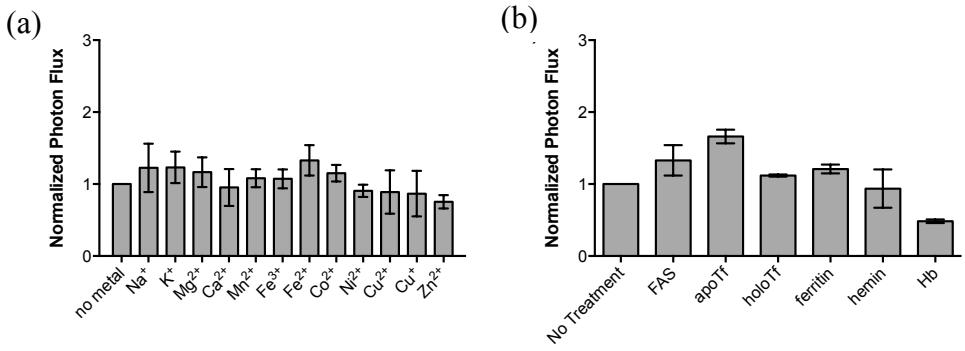

Figure 3.3. The selective response of ICL-1 to ferrous iron is not observed when the same treatments are performed with aminoluciferin. Bioluminescence response of aminoluciferin incubated with (a) various biologically relevant s-block (1 mM) and d-block (100 μM) metal ions and (b) biologically-relevant non-labile iron-containing species, namely transferrin (without iron, apoTf; with iron, holoTf), ferritin, hemin, and hemoglobin (Hb). Signals are integrated over 30 m and expressed as photon fluxes normalized to aminoluciferin bioluminescence with no treatment (buffer alone). Statistical analyses were performed with one-way analysis of variance (ANOVA) with multiple comparisons to the control with no metal treatment, and no statistically significant differences were observed. Error bars are ± SD (n = 3).

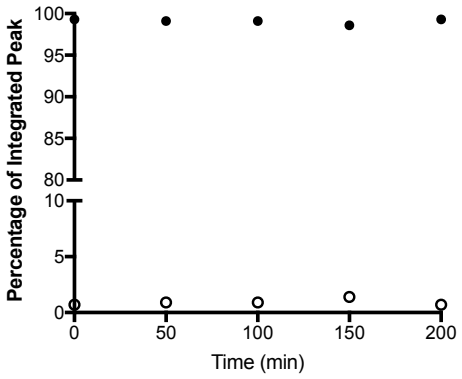

Figure 3.4. ICL-1 exhibits stability of over 200 minutes assayed, as followed by an LCMS assay. ICL-1 dissolved in DMSO was added to HBSS and aliquots were assessed at various time points (t=0, 50, 100, 150, 200 minutes). Over the 200 minutes assayed, no significant uncaging of ICL-1 (solid circles) to D-aminoluciferin (hollow circles) is observed.

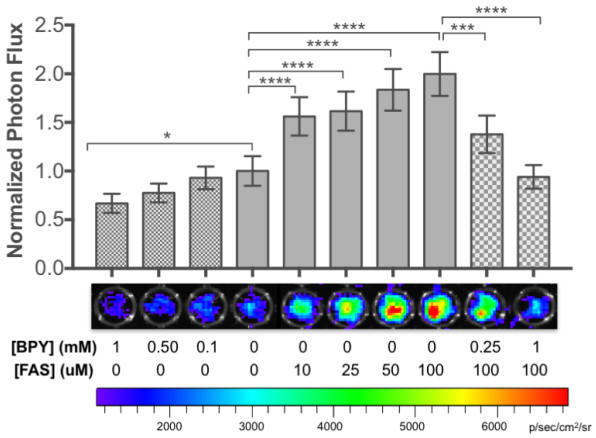

Figure 3.5. Bioluminescent signals from PC3M-luc cells probed with ICL-1. Cells were supplemented with varying concentrations of FAS for 90 min, BPY for 30 min, or a combination the two chemicals followed by addition of ICL-1 (20 μM). Total photon flux was integrated over 1 h and normalized to cells treated with buffer alone. Representative bioluminescence images of PC3M-luc cells with each treatment are shown below the corresponding data bar in the graph. Statistical analyses were performed with one-way analysis of variance (ANOVA) with multiple comparisons to the control with no metal treatment, where *P ≤ 0.05, ***P ≤ 0.001 and ****P ≤ 0.0001. Error bars are ± SD (n = 3 - 5).

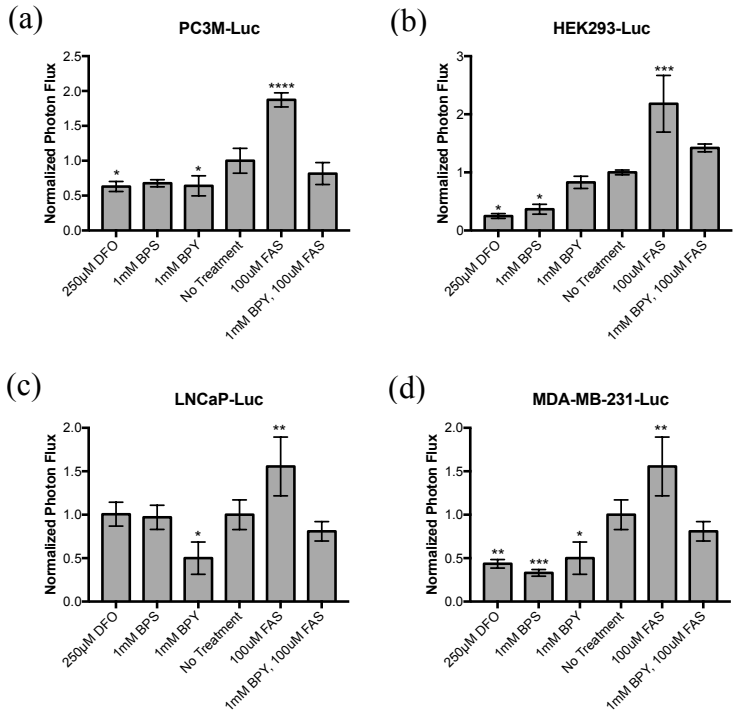

Figure 3.6. Bioluminescent signals from (a) PC3M-Luc, (b) HEK293-Luc, (c) LNCaP-Luc, and (d) MDA-MB-231-Luc cells probed with ICL-1. Cells were supplemented with 250 μM DFO (9 hours), 1 mM BPS (9 hours), 1 mM BPY (30 min), 100 μM FAS (90 min) or both BPY and FAS and imaged with either 20 μM (PC3M-Luc, HEK293-Luc, LNCaP-Luc) or 10 μM (MDA-MB-231-Luc) of ICL-1. Total photon flux was integrated over 1 h (PC3M-Luc and HEK293-Luc) or 30 min (LNCaP-Luc or MDA-MB-231-Luc) and normalized to cells treated with buffer alone. Statistical analyses were performed with one-way analysis of variance (ANOVA) with multiple comparisons to the control with no metal treatment, where *$P \leq 0.05$, **$P \leq 0.01$, ***$P \leq 0.001$ and ****$P \leq 0.0001$. Error bars are ± SD (n = 3 - 5).

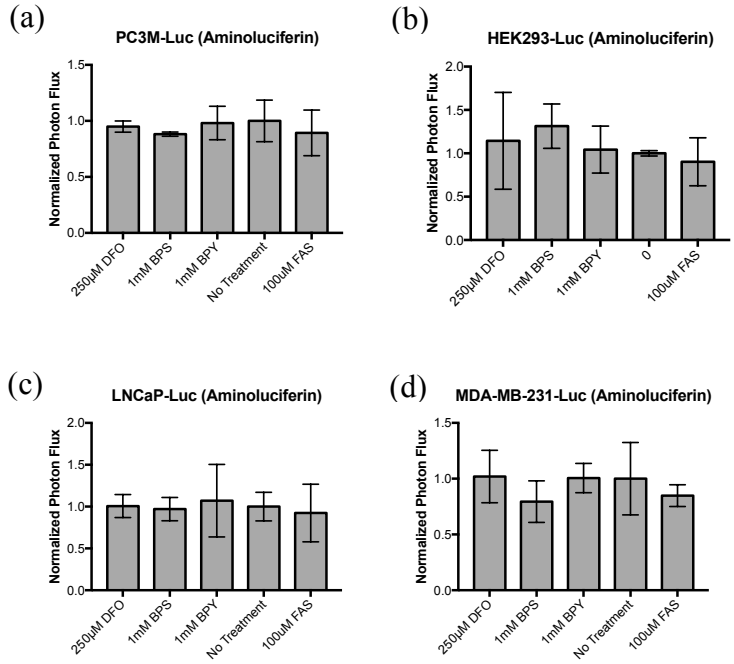

Figure 3.7. Bioluminescent signals from (A) PC3M-Luc, (B) HEK293-Luc, (C) LNCaP-Luc, and MDA-MB-231-Luc cells probed with aminoluciferin. Cells were supplemented with 250 μM DFO (9 hours), 1 mM BPS (9 hours), 1 mM BPY (30 min), 100 μM FAS (90 min) or both BPY and FAS and imaged with either 1 μM amionluciferin. Total photon flux was integrated over 1 h (PC3M-Luc and HEK293-Luc) or 30 min (LNCaP-Luc or MDA-MB-231-Luc) and normalized to cells treated with buffer alone. Statistical analyses were performed with one-way analysis of variance (ANOVA) with multiple comparisons to the control with no metal treatment, and no statistically significant differences were observed. Error bars are ± SD (n = 3 - 5).

3.6. References

1. Cammack, R.; Wrigglesworth, J. M.; Baum, H., *Transport and Storage*. CRC Press: 1989.
2. Johnson, D. C.; Dean, D. R.; Smith, A. D.; Johnson, M. K., Structure, function, and formation of biological iron-sulfur clusters. *Annu Rev Biochem* **2005,** *74*, 247-81.
3. Andrews, N. C., Iron homeostasis: insights from genetics and animal models. *Nat Rev Genet* **2000,** *1* (3), 208-17.
4. Xu, W.; Barrientos, T.; Andrews, N. C., Iron and copper in mitochondrial diseases. *Cell Metab* **2013,** *17* (3), 319-28.
5. Miller, J. L., Iron deficiency anemia: a common and curable disease. *Cold Spring Harb Perspect Med* **2013,** *3* (7).
6. Torti, S. V.; Torti, F. M., Iron and cancer: more ore to be mined. *Nat Rev Cancer* **2013,** *13* (5), 342-355.
7. Wu, K. J.; Polack, A.; Dala-Favera, R., Coordinated regulation of iron-controlling genes, H-ferritin and IRP2, by c-MYC. *Science* **1999,** *283*, 676-9.
8. Pinnix, Z. K.; Miller, L. D.; Wang, W.; D'Agostino, R. J.; Kute, T.; Willingham, M. C.; Hatcher, H.; Tesfay, L.; Sui, G.; Di, X.; Torti, S. V.; Torti, F. M., Ferroportin and Iron Regulation in Breast Cancer Progression and Prognosis. *Sci. Transl. Med.* **2010,** *2* 43ra56.
9. Toyokuni, S., Role of iron in carcinogenesis: cancer as a ferrotoxic disease. *Cancer Sci.* **2009,** *100* (1), 9-16.
10. von Haehling, S.; Jankowska, E. A.; van Veldhuisen, D. J.; Ponikowski, P.; Anker, S. D., Iron deficiency and cardiovascular disease. *Nat. Rev. Cardiol.* **2015,** *12*, 659-669.
11. Hare, D.; Ayton, S.; Bush, A.; Lei, P., A delicate balance: Iron metabolism and diseases of the brain. *Front Aging Neurosci* **2013,** *5*, 34.
12. Gerlach, M.; Ben-Shachar, D. B.; Riedere, P.; Youdim, M. B. H., Altered brain metabolism of iron as a cause of neurodegenerative diseases? *J. Neurochem.* **1994, ,** *63* (3), 793-807.
13. James, S. A.; Robert, B. R.; Hare, D. J.; de Jonge, M. D.; Birchall, I. E.; Jenkin, N. L.; Cherny, R. A.; Bush, A. I.; McColl, G., Direct in vivo imaging of ferrous iron dyshomeostasis in ageing Caenorhabditis elegans. *Chem. Sci.* **2015,** *6*, 2952-2962.
14. Skaar, E. P., The battle for iron between bacterial pathogens and their vertebrate hosts. *PLoS Pathog* **2010,** *6* (8), e1000949.
15. Nairz, M.; Haschka, D.; Demetz, E.; Weiss, G., Iron at the interface of immunity and infection. *Front Pharmacol* **2014,** *5*, 152.
16. Irving, H.; Williams, R. J. P., The stability of transition-metal complexes. *J. Chem. Soc.* **1953**, 3192-3210.
17. Carter, K. P.; Young, A. M.; Palmer, A. E., Fluorescent Sensors for Measuring Metal Ions in Living Systems *Chem. Rev.* **2014,** *114* (8), 4564–4601.
18. Aron, A. T.; Loehr, M. O.; Bogena, J.; Chang, C. J., An Endoperoxide Reactivity-Based FRET Probe for Ratiometric Fluorescence Imaging of Labile Iron Pools in Living Cells. *J. Am. Chem. Soc.* **2016,** *138* (43), 14338-14346.
19. Au-Yeung, H. Y.; Chan, J.; Chantarojsiri, T.; Chang, C. J., Molecular Imaging of Labile Iron(II) Pools in Living Cells with a Turn-On Fluorescent Probe. *J. Am. Chem. Soc.* **2013,** *135*, 15165-15173.

20. Spangler, B.; Morgan, C. W.; Fontaine, S. D.; Vander Wal, M. N.; Chang, C. J.; Wells, J. A.; Renslo, A. R., A reactivity-based probe of the intracellular labile ferrous iron pool *Nat. Chem. Biol.* **2016,** *12*, 680-685.
21. Hirayama, T.; Okuda, K.; Nagasawa, H., A highly selective turn-on fluorescent probe for iron(II) to visualize labile iron in living cells. *Chem. Sci.* **2013,** *4*, 1250-1256.
22. Niwa, M.; Hirayama, T.; Okuda, K.; Nagasawa, H., A new class of high-contrast Fe(II) selective fluorescent probes based on spirocyclized scaffolds for visualization of intracellular labile iron delivered by transferrin. *Org. Biomol. Chem.* **2014,** *12*, 6590-6597.
23. Hirayama, T.; Tsuboi, H.; Niwa, M.; Miki, A.; Kadota, S.; Ikeshita, Y.; Okuda, K.; Nagasawa, H., A universal fluorogenic switch for Fe(II) ion based on N-oxide chemistry permits the visualization of intracellular redox equilibrium shift towards labile iron in hypoxic tumor cells. *Chem. Sci.* **2017,** *Advance Article*.
24. Zastrow, M. L.; Radford, R. J.; Chyan, W.; Anderson, C. T.; Zhang, D. Y.; Loas, A.; Tzounopoulos, T.; Lippard, S. J., Reaction-Based Probes for Imaging Mobile Zinc in Live Cells and Tissues. *ACS Sensors* **2016,** *1*, 32-39.
25. Chan, J.; Dodani, S. C.; Chang, C. J., Reaction-based small-molecule fluorescent probes for chemoselective bioimaging. *Nat. Chem.* **2012,** *4*, 973-984.
26. Aron, A. T.; Ramos-Torres, K. M.; Cotruvo, J., J. A.; Chang, C. J., Recognition- and Reactivity-Based Fluorescent Probes for Studying Transition Metal Signaling in Living Systems. *Acc. Chem. Res.* **2015,** *48*, 2434-2442.
27. Chen, X.; Tian, X.; Shin, I.; Yoon, J., Fluorescent and luminescent probes for detection of reactive oxygen and nitrogen species. *Chem. Soc. Rev.* **2011,** *40*, 4783-4804.
28. Yang, Y.; Zhao, Q.; Feng, W.; Li, F., Luminescent chemodosimeters for bioimaging. *Chem Rev.* **2013,** *113*, 192-270.
29. Cho, D. G.; Sessler, J. L., Modern reaction-based indicator systems. *Chem. Soc. Rev.* **2009,** *38*, 1647-1662.
30. Dixon, S. J.; Lemberg, K. M.; Lamprecht, M. R.; Skouta, R.; Zaitsev, E. M.; Gleason, C. E.; Patel, D. N.; Bauer, A. J.; Cantley, A. M.; Yang, W. S.; Morrison, B. I.; Stockwell, B. R., Ferroptosis: an iron-dependent form of nonapoptotic cell death. *Cell* **2012,** *149* (1060-1072).
31. Dixon, S. J.; Stockwell, B. R., The role of iron and reactive oxygen species in cell death. *Nat Chem Biol* **2014,** *10* (1), 9-17.
32. Li, J.; Chen, L.; Du, L.; Li, M., Cage the firefly luciferin! - a strategy for developing bioluminescent probes. *Chem Soc Rev* **2013,** *42* (2), 662-676.
33. Xu, T.; Close, D.; Handagama, W.; Marr, E.; Sayler, G.; Ripp, S., The Expanding Toolbox of In Vivo Bioluminescent Imaging. *Front Oncol* **2016,** *6*, 150.
34. Adams, S. T., Jr.; Miller, S. C., Beyond D-luciferin: expanding the scope of bioluminescence imaging in vivo. *Curr Opin Chem Biol* **2014,** *21*, 112-20.
35. Chen, P.; Zheng, Z.; Zhu, Y.; Dong, Y.; Wang, F.; Liang, G., Bioluminescent Turn-On Probe for Sensing Hypochlorite in Vitro and in Tumors. *Anal Chem* **2017**, *89*, 5693–5696.
36. Takakura, H.; Kojima, R.; Kamiya, M.; Kobayashi, E.; Komatsu, T.; Ueno, T.; Terai, T.; Hanaoka, K.; Nagano, T.; Urano, Y., New class of bioluminogenic probe based on bioluminescent enzyme-induced electron transfer: BioLeT. *J Am Chem Soc* **2015,** *137* (12), 4010-3.
37. Van de Bittner, G. C.; A., D. E.; Bertozzi, C. R.; Chang, C. J., In vivo imaging of hydrogen peroxide production in a murine tumor model with a chemoselective bioluminescent reporter. *Proc. Natl. Acad. Sci. USA* **2010,** *107*, 21316-21321.

38. Van de Bittner, G. C.; Bertozzi, C. R.; Chang, C. J., Strategy for Dual-Analyte Luciferin Imaging: In Vivo Bioluminescence Detection of Hydrogen Peroxide and Caspase Activity in a Murine Model of Acute Inflammation. *J. Am. Chem. Soc.* **2013,** *135*, 1783-1795.
39. Godinat, A.; Park, H. M.; Miller, S. C.; Cheng, K. H., D. ; Sanman, L. E.; Bogyo, M.; Yu, A.; Nikitin, G. F.; Stahl, A.; Dubikovskaya, E. A., A biocompatible in vivo ligation reaction and its application for noninvasive bioluminescent imaging of protease activity in living mice. *ACS Chem Biol* **2013,** *8*, 987–999.
40. Chang, Y. C.; Chao, P. W.; Tung, C. H., Sensitive luciferin derived probes for selective carboxypeptidase activity. *Bioorg Med Chem Lett* **2011,** *21* (13), 3931-4.
41. Dragulescu-Andrasi, A.; Liang, G.; Rao, J., In Vivo Bioluminescence Imaging of Furin Activity in Breast Cancer Cells Using Bioluminogenic Substrates. *Bioconjugate Chem.* **2009,** *20*, 1660-6.
42. Eiriksdottir, E.; Mager, I.; Lehto, T.; El Andaloussi, S.; Langel, U., Cellular internalization kinetics of (luciferin-)cell-penetrating peptide conjugates. *Bioconjug Chem* **2010,** *21* (9), 1662-72.
43. Henkin, A. H.; Cohen, A. S.; Dubikovskaya, E. A.; Park, H. M.; Nikitin, G. F.; Auzias, M. G.; Kazantzis, M.; Bertozzi, C. R.; Stahl, A., Real-time noninvasive imaging of fatty acid uptake in vivo. *ACS Chem Biol* **2012,** *7* (11), 1884-91.
44. Jones, L. R.; Goun, E. A.; Shinde, R.; Rothbard, J. B.; Contag, C. H.; Wender, P. A., Releasable luciferin-transporter conjugates: tools for the real-time analysis of cellular uptake and release. *J Am Chem Soc* **2006,** *128* (20), 6526-7.
45. Mofford, D. M.; Adams, S. T. J.; Reddy, G. S.; Reddy, G. R.; Miller, S. C., Luciferin Amides Enable in Vivo Bioluminescence Detection of Endogenous Fatty Acid Amide Hydrolase Activity. *J. Am. Chem. Soc.* **2015,** *137* (27), 8684-7.
46. Porterfield, W. B.; Jones, K. A.; McCutcheon, D. C.; Prescher, J. A., A "Caged" Luciferin for Imaging Cell–Cell Contacts. *J. Am. Chem. Soc.* **2015,** *137*, 8656–8659.
47. Rush, J. S.; Beatty, K. E.; Bertozzi, C. R., Bioluminescent Probes of Sulfatase Activity. *ChemBioChem* **2010,** *11* (15), 2096-2099.
48. Vorobyeva, A. G.; Stanton, M.; Godinat, A.; Lund, K. B.; Karateev, G. G.; Francis, K. P.; Allen, E.; Gelovani, J. G.; McCormack, E.; Tangney, M.; Dubikovskaya, E. A., Development of a Bioluminescent Nitroreductase Probe for Preclinical Imaging. *PLoS One* **2015,** *10* (6), e0131037.
49. Yao, H.; So, M. K.; Rao, J., A bioluminogenic substrate for in vivo imaging of beta-lactamase activity. *Angew Chem Int Ed Engl.* **2007,** *46* (37), 7031-4.
50. Zhou, W.; Andrews, C.; Liu, J.; Shultz, J. W.; Valley, M. P.; Cali, J. J.; Hawkins, E. M.; Dieter H. Klaubert Dr.; Robert F. Bulleit Dr.; Dr., K. V. W., Self-Cleavable Bioluminogenic Luciferin Phosphates as Alkaline Phosphatase Reporters. *ChemBioChem* **2008,** *9* (5), 714-718.
51. Cohen, A. S.; Dubikovskaya, E. A.; Rush, J. S.; Bertozzi, C. R., Real-time bioluminescence imaging of glycans on live cells. *J Am Chem Soc* **2010,** *132* (25), 8563-5.
52. Sellmyer, M. A.; Bronsart, L.; Imoto, H.; Contag, C. H.; Wandless, T. J.; Prescher, J. A., Visualizing cellular interactions with a generalized proximity reporter. *Proc. Natl. Acad. Sci. USA* **2013,** *110* (21), 8567-8572.
53. Fontaine, S. D.; DiPasquale, A. G.; Renslo, A. R., Efficient and Stereocontrolled Synthesis of 1,2,4-Trioxolanes Useful for Ferrous Iron-Dependent Drug Delivery. *Org. Lett.* **2014,** *16* (16), 5776-9.

54. Borstnik, K.; Paik, I. H.; Shapiro, T. A.; Posner, G. H., Antimalarial chemotherapeutic peroxides: artemisinin, yingzhaosu A and related compounds. *Int. J. Parasitol.* **2002,** *32* (13), 1661-1667.
55. Tang, Y.; Dong, Y.; Wang, X.; Sriraghavan, K.; Wood, J. K.; Vennerstrom, J. L., Dispiro-1,2,4-trioxane Analogues of a Prototype Dispiro-1,2,4-trioxolane: Mechanistic Comparators for Artemisinin in the Context of Reaction Pathways with Iron(II). *J. Org. Chem.* **2005,** *70* (13), 5103–5110.
56. Creek, D. J.; Charman, W. N.; Chiu, F. C.; Prankerd, R. J.; McCullough, K. J.; Dong, Y.; Vennerstrom, J. L.; Charman, S. A., Iron-mediated degradation kinetics of substituted dispiro-1,2,4-trioxolane antimalarials. *J. Pharm. Sci.* **2007,** *96* (11), 2945-2956.
57. Fontaine, S. D.; Spangler, B.; Gut, J.; Lauterwasser, E. M. W.; Rosenthal, P. J.; Renslo, A. R., Drug delivery to the malaria parasite using an arterolane-like scaffold. *ChemMedChem* **2015,** *2015* (10), 47-51.
58. Lauterwasser, E. M.; Fontaine, S. D.; Li, H.; Gut, J.; Katneni, K.; Charman, S. A.; Rosenthal, P. J.; Bogyo, M.; Renslo, A. R., Trioxolane-Mediated Delivery of Mefloquine Limits Brain Exposure in a Mouse Model of Malaria. *ACS Med Chem Lett* **2015,** *6* (11), 1145-9.
59. Spangler, B.; Fontaine, S. D.; Shi, Y.; Sambucetti, L.; Mattis, A. N.; Hann, B.; Wells, J. A.; Renslo, A. R., A Novel Tumor-Activated Prodrug Strategy Targeting Ferrous Iron Is Effective in Multiple Preclinical Cancer Models. *J Med Chem* **2016,** *59* (24), 11161-11170.
60. Cerchiaro, G.; Manieri, T. M.; Bertuchi, F. R., Analytical methods for copper, zinc and iron quantification in mammalian cells. *Metallomics* **2013,** *5* (10), 1336-45.
61. Epsztejn, S.; Kakhlon, O.; Glickstein, H.; Breuer, W.; Cabantchik, I., Fluorescence analysis of the labile iron pool of mammalian cells. *Anal Biochem* **1997,** *248* (1), 31-40.
62. Rubino, J. T.; Franz, K. J., Coordination chemistry of copper proteins: How nature handles a toxic cargo for essential function. *J Inorg Biochem* **2012,** *107* (1), 129-143.
63. Cotruvo, J. A.; Aron, A. T.; Ramos-Torres, K. M.; Chang, C. J., Synthetic fluorescent probes for studying copper in biological systems. *Chemical Society Reviews* **2015,** *44* (13), 4400-4414.
64. Ramos-Torres, K. M.; Kolemen, S.; Chang, C. J., Thioether Coordination Chemistry for Molecular Imaging of Copper in Biological Systems. *Isr J Chem* **2016,** *56* (9-10), 724-737.
65. Ackerman, C. M.; Lee, S.; Chang, C. J., Analytical Methods for Imaging Metals in Biology: From Transition Metal Metabolism to Transition Metal Signaling. *Analytical Chemistry* **2017,** *89* (1), 22-41.

Chapter 4

Development of a chemoproteomic platform for the identification of copper-binding cysteines

Portions of this work were performed in collaboration with the following persons:

Dr. Cheri Ackerman helped perform chemoproteomics to generate the *in situ* 200 μM Cu-addititon list (Table 4.1) and performed all STAT3 and Keap1 validation experiments.
Tyler Detomasi performed proof-of-concept labeling experiments on Atox1 and validation of TPI.
Tyler Detomasi purified Atox1 with assistance from Dr. Joey Cotruvo.
Dr. Diana Iovan assisted with experiments to generate proteomics lists for 500 μM BCS and 500 μM TEPA treatments (Tables 4.2 and 4.3, respectively) and performed validation on PYCR1.
Dr. Marie Heffern performed CCL-1 imaging of ATN-224 treatment.

4.1. Introduction

Redox-active metals copper and iron are essential for life but can be toxic in excess. As such, cells must precisely regulate uptake and transport of these metals to ensure they are present in the right place at the right time. While copper and iron have been most well studied in the context of enzyme active sites, where they act as static cofactors, several recent studies suggest that redox-active transition metals may also serve as dynamic signals. Our laboratory recently uncovered a novel role for Cu^+ in regulating lipolysis by modulating the activity of phosphodiesterase PDE3B.[1] Additionally, a role for copper in the mitogen activated protein kinase (MAPK) pathway has also been recently elucidated – cellular copper influx was shown to enhance phosphorylation of ERK1/2 through an interaction between copper and MEK1/2.[2-3] These key examples suggest an important and emerging role for copper as a dynamic signaling entity that can interact with cellular proteins to modulate function. Important to note is the fact that these examples were identified by alterations in phenotype in the presence or absence of copper. This phenotypic approach is a thorough but extremely low-throughput way to identify uncharacterized copper-binding proteins. The fact that copper was only recently found to modulate function of these two well-studied enzymes presages the question of whether copper binds to and affects the function of other unknown proteins.

Metalloproteins are estimated to comprise approximately one third to one half of the proteome[4-5]; however, discovering new metal-binding proteins *de novo* is a challenging task. Predicting metal-binding proteins through computational methods is difficult, as one conserved consensus sequence for metal coordination does not exist. While high-throughput approaches are emerging for characterizing novel metalloproteins[5-6], these methods often require specialized equipment and laborious procedures. Recently, a chemoproteomic strategy was developed to identify novel zinc-binding proteins in the human cellular proteomes[7]. This strategy made use of a cysteine-reactive probe for isotopic Tandem Orthogonal Proteolysis Activity-Based Protein Profiling (isoTOP-ABPP)[8] in conditions of high and low zinc to elucidate zinc-binding cysteines. Profiling cysteine residues is useful for elucidating novel zinc-binding proteins because cysteine is one of the most commonly used amino acid residue to bind zinc[9]. Weerapana et al. used isoTOP-ABPP to carry out this study, a technology that is described in detail in Chapter 1. A generalized isoTOP-ABPP workflow is depicted in Figure 1.1. Briefly, isoTOP-ABPP makes use of residue-specific reactive probes that contain either an isotopically-heavy or an isotopically-light tag. By using two different mass tags, residue-labeling under different experimental conditions can be compared directly; Weerapana et al. compared control to zinc-supplemented lysates with untreated control lysates as well as zinc-depleted lysates with untreated control lysates, so as to extract information about zinc-bound cysteine residues.

Cysteine is also a major ligand for copper in cells,[9] so we believed that an isoTOP-ABPP approach would allow us to identify novel cuproproteins in the human proteome. While free cysteine residues are nucleophilic, we hypothesized that copper-cysteine complexation would diminish cysteine nucleophilicity. A decrease in nucleophilicity should minimize interaction with a cysteine-reactive, alkyne-containing probe, resulting in decreased labeling. Subsequent Click chemistry can be used to append a fluorophore for in-gel fluorescence visualization on an SDS-PAGE gel or a cleavable biotin tag for identification by mass spectrometry analysis, which can be used to elucidate Cu-binding cysteine residues. As such, mass spectrometry data can be read out as a ratio of light- to heavy- labeled peptide to generate a list of potential copper-binding proteins. This chapter details our efforts towards using this strategy to profile the copper-binding

proteome. The optimization of cellular treatments and efforts towards validation of potential targets are described herein.

4.2. Materials and methods

4.2.1 Purification of Atox1 and in-gel fluorescence experiments

Atox1 was purified by Tyler Detomasi following published protocols[10] with slight modifications. Iodoacetamide-alkyne in-fluorescence gel experiments were also devised in collaboration with and performed by Tyler Detomasi.

4.2.2 Preparation of human cell line proteome

Cells were maintained by the UC Berkeley Tissue Culture Facility. HEK 293T cells were maintained as a monolayer in exponential growth at 37 °C in a 5% CO_2 atmosphere in Dulbecco's Modified Eagle Medium (DMEM, Gibco) supplemented with 10% fetal bovine serum (FBS, Hyclone), and glutamax (Gibco). One day before harvesting, HEK 293T cells were passaged and plated in DMEM.

4.2.3 isoTOP-ABPP in living cells treated with Cu^+ and ATN-224

The following protocol is described in and modified from Cheri Ackerman's thesis, as it was performed in collaboration.

For Cu addition experiment: HEK 293T cells were plated in 10 cm dishes and were grown to 90% confluence. Each 10 cm dish was harvested as one sample, and each experiment was conducted in quadruplicate. Cells were treated for 1 hr with 200 µM $CuCl_2$ (prepared from a 10 mM stock solution in water) (this is denoted "treated") or with vehicle control (this is denoted "control"). After 1 hr, media was aspirated from plates on ice.

For ATN-224 addition experiment: HEK 293T cells, plated in 10 cm dishes, were grown to 90% confluence. Each proteomics experiment was conducted in quadruplicate, where each 10-cm dish was harvested as one sample. Cells were treated for 1 hr with 50 µM ATN-224 (this is denoted "treated") or with vehicle control (this is denoted "control"). After 1 hr, media was aspirated from plates on ice.

Cells were scraped into 8 mL of cold PBS then were centrifuged at 1400 × g for 5 min. PBS was removed from the cell pellet, then the cell pellet wash washed two additional times with 5 mL PBS per wash. Between each wash, a 1400 × g for 5 min centrifugation was performed. After the final aspiration, cells were brought into the anaerobic chamber for lysis and labeling. Cell pellets were lysed by sonication then insoluble components were removed by centrifugation (16,000 × g, 15 min). Proteomes were quantified by Bradford and diluted to 2.0 mg/ml.

Each sample was then brought to a volume of 500 µL. 5 µL of 10 mM IA-alkyne stock solution (prepared fresh in DMSO) was added to each sample to obtain a 100 µM final concentration. Each sample was then flicked (5x) and allowed to incubate for 1 hr at room temperature in the anaerobic chamber.

Samples were then removed from the anaerobic chamber and were subjected to Click chemistry. A solution of 50 mM TCEP in water was prepared. To each 500 µL of control

sample, 10 µL of 5mM Light Tev-biotin tag was added, and 10 µL of 5mM-Heavy Tev-biotin tag was added to each treated sample. Light and Heavy Tev-biotin tags were obtained from the Nomura laboratory.[8] 10 µL of 50 mM TCEP solution was added, followed by addition of 30 µL of TBTA ligand solution, and finally by addition of 10 µL of 50 mM copper(II) sulfate. Each sample was incubated at room temperature for 1 hr after vortexing.

1 mL cold MeOH (stored at -20 ºC) was added to each sample to stop the reaction. Samples were centrifuged for 5 mins at 16,100 x g (at 4 ºC), then the supernatant was aspirated. Pellets were washed with 500 µL of cold MeOH then were sonicated. After resolubilizing the precipitated pellet, one "treated" sample was added to one "control" sample. The combined sample was centrifuged for 5 mins at 16,100 x g (at 4 ºC) then aspirated. 400 µL of 6 M urea (in PBS) was added to each pellet. Sonication was performed to solubilize insoluble protein, then DTT was added to each sample for a final concentration of 10 mM. Samples were incubated at 65 ºC for 15 minutes, then iodoacetamide was added to afford a final concentration of 20 mM at which point samples were incubated at 37 ºC on a rotator for 30 mins. At this point, 720 µL of PBS was added to each sample. Each sample was subjected to tryptic digest at 37 ºC overnight – $CaCl_2$ was added to each sample at a 1 mM final concentration (12 µL per sample from a 100 mM stock in water) then 1 vial of sequencing grade reconstituted trypsin (Promega, 20 µg trypsin reconstituted in 40 µL Trypsin buffer).

Following overnight tryptic digestion, SDS was added to each sample to yield a final 1% concentration. The pellet was re-suspended then incubated at 65 ºC for 5 mins. 100 µL streptavidin beads (from a 50% slurry solution, Pierce) were transferred into a spin column (BioRad, no resin) and were washed 3x with PBS using a vacuum manifold. Beads were re-suspended in 100 µL PBS and then were added to a 15 mL conical tube in addition to 5.6 mL PBS and sample. Each sample was incubated at room temperature for 3 hours, then was centrifuged at 1000 x g for 5 mins. The supernatant was aspirated, then beads were washed 3x with 10 mL PBS and 3x with 10 mL water. In parallel, beads were washed in TEV buffer and were aspirated using an 18G needle (BD Biosciences). Then 150 µL of TEV buffer and 5 µL TEV protease (Thermo) were added to each sample. Samples were rotated at 30 ºC for 24 hours.

At this point, samples were centrifuged for 15 secs at 3000 x g. Then beads were re-suspended with a blunted P200 pipette tip and were transferred into spin columns (BioRad, no resin). Spin columns were centrifuged for 15 secs at 3000 x g then beads were washed with an additional 150 µL PBS. This afforded a total sample volume of ~ 300 µL. 15 µL formic acid was added to each sample, then each sample was stored at -20 ºC until analysis. Mass spectrometry and data analysis were performed by the Nomura lab following published protocols.[8]

4.2.4 isoTOP-ABPP in cell lysates treated with Cu-chelator or Cu^{+}– anaerobic preparations

For labeling experiments in cell lysates, cells were grown to 100% confluency, then were washed three times and scraped into ice-cold PBS. Centrifugation was performed at 1400 × g for 5 min, then PBS was removed by aspiration from the cell pellet. Cell pellets were brought into the anaerobic chamber for lysis and labeling; cell pellets were lysed by sonication then insoluble components were removed by centrifugation (16,000 × g, 15 min). Proteomes were quantified by Bradford and diluted to 2.5 – 3.5 mg/ml. Then each sample was split in half (one "control" sample and one "treated" sample).

For BCS experiment: 100 mM BCS stock was prepared in water. From this, BCS was added to half of the proteome samples ("treated") to afford a 500 µM BCS concentration. 12.5 µL of water was added to each corresponding 2.5 mL control sample ("control"). Samples were allowed to incubate for two hours at room temperature in the anaerobic chamber.

For TEPA experiment: 100 mM TEPA stock was prepared in water. From this, TEPA was added to half of the proteome samples ("treated") to afford a 500 µM TEPA concentration. 12.5 µL of water was added to each corresponding 2.5 mL control sample ("control"). Samples were allowed to incubate for two hours at room temperature in the anaerobic chamber.

For Cu-addition experiment: 10 µM CuCl in MOPS (from a concentrated stock solution prepared in 0.1 M HCl, 50 mM NaCl) was added to half of the proteome samples ("treated"). 1 µL of 0.1 M HCl, 50 mM NaCl was added to half of the proteome samples ("control"). Samples were allowed to incubate for one hour at room temperature in the anaerobic chamber.

A 10 mM IA-alkyne stock solution (prepared fresh in DMSO) was added to each sample to obtain a final 100 µM concentration. Upon addition, each sample was vortexed then allowed to incubate at room temperature for one hour. Next, each sample was run through a PD-10 desalting column (GE Healthcare), following the pack insert protocol. Fractions containing protein were diluted to 2 mg/mL (4 samples x 500 µL per sample).

Next, each sample was subjected to click chemistry. Briefly, a solution of 50mM TCEP in water is prepared. To each 500 µL of control sample, 10 µL of the 5mM Light Tev-biotin tag was added, and 10 µL of 5mM-Heavy Tev-biotin tag was added to each Cu-treated sample. Light and Heavy Tev-biotin tags were obtained from the Nomura laboratory.[8] Next, 10 µL of the 50mM TCEP solution was added, followed by the addition of 30 µL of TBTA ligand solution, and finally the addition of 10 µL of 50mM Copper (II) Sulfate. After vortexing, each sample was incubated at room temperature for one hour.

Labelled control and Cu-treated samples were combined and centrifuged. At this point, the supernatant was removed and 500 µL cold methanol was added to each sample before sonicating. Samples were centrifuged again, then the supernatant was removed and the above wash and subsequent addition of 500 µL cold methanol was repeated. After removing supernatant, 1 mL 1.2% SDS/PBS (w/v) was added and each sample was then heated to 80-90°C for 5min. Finally, samples were centrifuged before addition of streptavidin-agarose beads. After washing streptavidin-agarose beads, 170 µL slurry was added per sample. The 1 mL sample is transferred into 5 mL PBS containing the bead slurry. The labeled slurry is then rotated at 4° C overnight.

After re-solubilizing the SDS, the samples were centrifuged and supernatant was removed. The beads were washed with 0.2%SDS/PBS (w/v) and the supernant was removed. Next, the beads were transferred to a spin column with 500 µL x2 PBS, then were washed three times with 1 mL PBS and three times with 1 mL water. The washed beads were then transferred using two 250 µL washes of **6** M Urea/PBS solution, then incubated with 25 µL DTT solution (30mg/mL in water) at 65°C for 20 min. After allowing the tube to cool, 25 µL IA solution (74mg/ml in water) was added to each tube and this is incubated for 37°C for 30 min. Finally, each reaction is diluted with 950 µL PBS, centrifuged, and supernatant is removed, then solution of 200 ul of a 2M Urea/PBS solution, 2 µL of 100mM Calcium Chloride in water, and 4 µL of Trypsin solution were added to each tube. This reaction was incubated at 37°C over-night in the shaking incubator

After transferring to a spin column, beads were washed with three times with 500 µL PBS then 3X with 500 µL water, then were transferred with 1 mL of water. Supernatant was removed and the beads were washed with 1 x TEV buffer (140 µL water, 7.5 µL of 20x TEV buffer, 1.5 ul of 100 µM DTT) before a premixed solution of TEV buffer, containing 5 µL of Ac-TEV protease, was added. The reaction was incubated at 29°C incubator overnight with rotation. Finally, the beads were eluted and washed twice with 75 µL of water before adding16 µL of formic acid for mass spectrometric analysis.

4.2.5 Expression and purification of proteins from in-cellulo *$Cu^{+}$and ATN-224-treatment list*

4.2.5.1 Transketolase

The sequence encoding for His_6-thrombin-TKT was ordered as a gBlock (IDT) (Figure 4.2). This gBlock was reconstituted in 100 µL sterile water for a stock concentration of 10 ng/µL. Golden gate cloning was performed, following standard protocol (1 µL 10x T4 ligase buffer with 10 mM ATP, 0.5 µL BSAI HF, 0.5 µL T4 ligase, 1 µL vector, 2 µL TKT gBlock, and 5 µL water) to transfer this fragment into a protein expression vector (pECH003_pKJM145_). Correctness of the introduced gene was confirmed by complete sequencing, using the T7 forward/reverse primers.

BL21(DE3) cells were transformed with this plasmid and expression conditions were optimized. After optimization, a 6x1L culture was grown in the presence of 100 µM thiamine-HCl until OD_{600} = 0.6, then protein expression was induced by introduction of 100 µM IPTG and the culture was grown overnight at 18 ºC, shaking at 220 rpm. Cells were harvested centrifuging at 7000 x g for 15 mins, and the pellet was lysed by homogenization in ~85 mL lysis buffer (25 mM Tris-HCl, pH 8.0, 30 mM NaCl, 20 mM imidazole, 1 mM $CaCl_2$, 0.1 mM ThDP, plus DNAse, lysozyme, benzamidadine HCl, and 1 mM $MgSO_4$). After lysis, the lysate was clarified through ultracentrifugation; lysate was centrifuged for 1 hour at 42,000 x g. Lysate was loaded onto a pre-equilibrated Ni-NTA column (column was equilibrated with 50 mL low imidazole buffer – 25 mM Tris-HCl, pH 8.0, 30 mM NaCl, 20 mM imidazole, 1 mM $CaCl_2$). Then a gradient from 100% low imidazole buffer → 100% high imidazole buffer (25 mM Tris-HCl, pH 8.0, 30 mM NaCl, 200 mM imidazole, 1 mM $CaCl_2$) was run over 500 mL. 30 mL of high imidazole buffer was passed over the column. Fractions were loaded on an SDS-PAGE gel and visualized by Coomassie. Fractions containing protein were pooled (29 mg protein total), exchanged into thrombin cleavage buffer (50 mM Tris-HCl, 100 mM $CaCl_2$) and thrombin cleavage was carried out for 13 h, rotating at room temperature. After cleavage, protein was loaded onto a Ni-NTA column and was eluted with 20 mL of low imidazole buffer. 4.5 mg of pure TKT were isolated – this was concentrated and exchanged into storage buffer (50 mM MOPS, pH 7.6, 100 mM NaCl, 5% glycerol) then frozen in liquid nitrogen and stored at -80 ºC.

4.2.5.2 S-methyl-5'-thioadenosine phosphorylase (MTAP)

Rosetta BL21(DE3)pLysS cells were transformed with His_6-TEV-MTAP plasmid (obtained from Addgene – plasmid #64077) A 4x1 L culture was grown, and this was induced with 100 µM IPTG at OD_{600} = 0.6. After induction, the culture was allowed to grow for 4 hours at 37 ºC. Cells were harvested by spinning at 7000 x g for 5 mins, then the pellet was frozen in liquid N_2. The following day, the pellet was allowed to warm to room temperature and was resuspended in ~85 mL of lysis buffer (20 mM Tris HCl, pH 7.5, 100 mM KCl containing DNAse, lysozyme, & benzamidadine HCl) before lysing by sonication on ice (10 mins in total, 30 sec on, 1 min off, power: 35%). Lysate was clarified by centrifuging for 1 hour at 40,000 x g. After equilibrating a 6 mL Ni-NTA column with 30 mL (5 column volumes, CVs) low imidazole

buffer (15 mM imidazole, 300 mM NaCl, 50 mM phosphate), clarified lysate was loaded onto the column. The column was washed with 100% low imidazole buffer for 30 mL (5 CVs) then a gradient from 0 → 100% high imidazole buffer (250 mM imidazole, 300 mM NaCl, 50 mM phosphate) was run over 470 mL. The column was washed with 100% high imidazole (30 mL), then fractions were loaded on an SDS-PAGE gel and visualized by Coomasise. Fractions containing protein were pooled (60 mg protein total), and a TEV-protease cleavage was carried out for 16 h at 37 ºC. After cleavage, protein was loaded onto a Ni-NTA column and was eluted with 30 mL of low imidazole buffer. 10 mg of pure MTAP protein were obtained – this was concentrated and exchanged into storage buffer (100 mM phosphate, pH 7.4, 2 mM DTT, 5% glycerol) then frozen in liquid nitrogen and stored at -80 ºC.

4.2.6 Metabolomics experiments

2e6 cells were seeded into 60 mm dishes and were allowed to sit overnight. Each sample was prepared from 5 dishes, and experiments were performed in quadruplicate (n=4). For each n, one sample was prepared for analysis of polar metabolites and one sample was prepared for analysis of non-polar metabolites. In the morning, cells were treated with 200 μM $CuCl_2$ (prepared from a $CuCl_2$ stock in water) for 3 hours. After treatment, media was aspirated and cells were scraped into 1 mL cold PBS per dish, transferred to an Eppendorf tube and spun down at 1.5G. The supernatant was aspirated and the pellet was washed with an additional 1 mL cold PBS per sample. This was spun down at 1500 x g, the supernatant was aspirated, and the cell pellet was frozen in liquid N_2.

4.2.7 Validation of Transketolase and MTAP

4.2.7.1 MTAP Activity Assay

Activity assay was adapted from literature procedures.[11] Briefly, 200 μM MTA was added in 100 mM KH_2PO_4, 50 mM HEPES, pH 7.4 buffer in a cuvette. After mixing, 0.1 μM MTAP was added, and reaction was incubated for 40 minutes at 37 ºC. An absorbance reading at 275 nm was obtained every 24 seconds.

4.2.7.2 Transketolase Activity Assay

A coupled enzyme assay with alcohol dehydrogenase (ADH) was adapted from literature procedures.[12]

4.2.3.1 UV-vis titration experiments

UV-vis titration experiments were performed as described previously.[1] Briefly, copper solutions were prepared freshly each day in an anaerobic chamber. Immediately before use, the 70-100 mM CuCl stock solution was diluted 100-fold in a solution of 0.1 M HCl, 1 M NaCl. The CuCl concentration in this stock solution was calculated spectrophotometrically by addition of excess BCS using ε_{483} nm = 13.0 mM^{-1} cm^{-1}. Immediately before the titration, this solution was diluted 10-fold into buffer A (50 mM MOPS, 100 mM NaCl, pH 7.5) and was loaded into a 50 μL Hamilton syringe. The syringe was inserted into a septum-sealed anaerobic cuvette (micro volume, Starna Cells) containing buffer A, 1.5-2.5 μM protein, and 35 μL 0.1 M HCl/1 M NaCl for a total volume of 350 μL. An initial spectrum was acquired (Cary 60 UV-visible spectrophotometer) between 240 and 700 nm with a 1 nm step size. The protein was titrated with 1 μL or 2 μL Cu^+ solution, up to ~40 μL, with 1−2 min between copper addition and spectrum acquisition.

Titrations were analyzed as following – the average absorbance between 650 nm and 700 nm was subtracted from the spectra, then the spectra were corrected for volume change during the course of the titration. Following these corrections, the absorbance at 265 nm was plotted against Cu+ (calculated from the concentration of the ~75−100 μM Cu^+ solution used for the titration, determined using BCS).

4.2.4 SOD activity assay

SOD1 activity assay kit (480 reactions, Cayman Chemical) was used for all SOD1 activity measurements. All experiments were carried out according to recommended protocols provided by Cayman Chemical.

4.2.5 FLAG-Atox1 labeling

Transfections of 6-well plates of HEK 293T cells were performed as described previously.[13] After 24 hours of transfection, cells were treated as indicated (with copper chelator or with in DMEM + glutamax) for 1-2 hours. Each well was washed 1x with 1 mL cold PBS then was scraped into 150 μL cold PBS and transferred into Eppendorf tubes. Cells were sonicated then centrifuged at 16,000 x g for 10 minutes at 4 ºC. Supernatants were transferred, and protein concentration was quantified by Bradford assay then each sample was diluted to 2 mg/mL. Lysate was separated into 50 μL aliquots, and this was treated with 100 μM IA-alkyne (1 μL from 5 mM stock solution in DMSO) for 1 hour at room temperature. 1 μL of 50 mM $CuSO_4$, 3 μL 1.7 of mM Tris[(1-benzyl-1H-1,2,3-triazol-4-yl)methyl]amine (TBTA) in DMSO/^{t}BuOH, 1 μL of 5 mM rhodamine azide (Azide-fluor 545, Sigma-Aldrich) and 1 μL of 14 mg/ml Tris(2 carboxyethyl)phosphine hydrochloride (TCEP) in water were added to each sample. After reaction for 1 hour at room temperature, 1 mL cold acetone (-20°C) was added with 15 μL 100% TCA to precipitate protein. This was performed because FLAG-Atox1 runs with the dye front. After 40 minutes, samples were centrifuged for 15 minutes at 16,100 x g at 4°C. The supernatant was aspirated and an additional 0.5 mL cold acetone was added, then this was centrifuged for 5 minutes at 16'000 x g and 4 ºC. Supernatant was aspirated and protein was dried by boiling for 5 minutes at 95°C before resuspending each pellet in 50 μL-100 μL of 2x loading buffer (with β-mercaptoethanol). This was heated to 95 °C for 5 minutes 2x to resolubilize protein then 15 μL were loaded on a gel then imaged on a GelDoc XR using the Rhodamine setting.

4.2.6 Purification of proteins from anaerobic Cu^+-addition in lysates

4.2.6.1 Thymidine Kinase 1

The sequence encoding for His_6-TEV-TK1 was ordered as a gBlock (IDT) (Figure 4.3). This gBlock was reconstituted in 100 μL sterile water for a stock concentration of 10 ng/μL. Golden gate cloning was performed, following standard protocol (1 μL 10x T4 ligase buffer with 10 mM ATP, 0.5 μL BSAI HF, 0.5 μL T4 ligase, 1 μL vector, 0.5 μL TK1 gBlock, and 6.5 μL water) to transfer this fragment into a protein expression vector (pECH003_pKJM145_). Correctness of the introduced gene was confirmed by complete sequencing, using the T7 forward/reverse primers.

BL21(DE3) cells were transformed with this plasmid and expression conditions were optimized. After optimization, a 3x1L culture was grown until an OD_{600} of 0.6 was reached, then protein expression was induced by introduction of 300 μM IPTG and the culture was grown overnight at 25 ºC, shaking at 200 rpm. Cells were pelleted by centrifugation, resuspended in

lysis buffer (300 mM NaCl, 10% (v/v) glycerol, 25 mM Tris-HCl (pH 7.5), 1% Triton X-100, 2 mM MgCl2 + ½ protease inhibitor tablet) and lysed by sonication (20 minutes, 20 sec on/20 sec off, 50% power). The supernatant was loaded onto a metal chelating Sepharose column charged with nickel ions (GE Healthcare) after pre-equilibrating with 5 CV of buffer A (buffer A = 20 mM Tris, 500 mM NaCl, and 10% glycerol, pH 8.0). Then the column was washed with 30 mL 80% buffer A/ 20% buffer B (buffer B = 20 mM Tris, 500 mM NaCl, 500 mM imidazole, and 10% glycerol, pH 8.0). The column was then incubated three times with 5 ml ATP/$MgCl_2$ solution (5 mM ATP, 5 mM $MgCl_2$, 20 mM Tris, 500 mM NaCl, and 30% glycerol, pH 8.0) for 7 min at 37 °C to remove the 70 kDa chaperone DnaK[14]. After each incubation, the column was washed with 2 CVs of 20% buffer B to remove the contaminant. The protein was then eluted applying a gradient from 40% buffer B (10 mL), to 60% buffer B (10 mL) and another 10 mL of 100% buffer B. 15 fractions were collected, combined, and dialyzed overnight in cleavage buffer (20 mM Tris, 0.5 mM EDTA, 1 mM DTT) (cleavage 1). In the morning, protein was concentrated to 2 mL volume, then cleaved protein was separated from uncleaved protein using Ni-NTA bead batch purification – 4 mL of beads were washed with buffer A. Then protein was added in 2 mL buffer A, this was spun at 1,000 x g for 2 mins and removed. Then the beads were washed with an additional 8 mL of buffer A. This was incubated at 4 ºC for 30 mins, then was spun at 1,000 x g for 2 mins and removed. 2.73 mg protein was obtained; this protein was frozen in liquid nitrogen and stored at -80 ºC.

4.2.7 Follow up on Thymidine Kinase 1

4.2.7.1 GSH-Cu binding bead assay

Based on the fact that Cu-loaded GSH beads can enrich MEK from cell lysates,[2] we wanted to test whether Cu-GSH beads could also be used to enrich TK1 from cell lysates. Copper was immobilized onto GSH by rotating equal volumes (200 µL) GSH Sepharose beads (GE Healthcare) and copper sulfate (200 µL of 50 mM solution in water) at 4ºC for 1 hr. The beads were then washed five times (200 µL x5) with EDTA-free 1% Triton lysis buffer (25 mM HEPES, 100 mM NaCl, 10% glycerol, and 1% Triton X-100) to remove excess unbound copper. The above beads were then used to precipitate TK1 from V5-TK1 expressing HEK 293T cell lysates. Cells were lysed using the following protocol – media was aspirated from each well of a 6-well plate, then each well was washed 2x with 500 µL cold PBS. Then 50 µL 1x RIPA buffer was added to each well. Cells were scraped off of the plate into RIPA buffer, and lysis was allowed to proceed in an Eppendorf for 15 min. Cell debris was pelleted by spinning at 16,000 x *g* for 10 min, then supernatant was removed and protein was quantified using Bradford assay. At this point, 30 µL Cu-GSH beads or GSH beads were added to 30 µL cell lysates and rotated at 4ºC for 2 hr. Supernatant was removed, and beads were washed four times with EDTA-free 1% Triton lysis buffer and pelleted, then the precipitate was re-suspended in LDS loading buffer for immunoblotting. Immunoblotting was performed with TK1 antibody (1:1000 dilution, Cell Signaling Technology #8960) and V5-tag antibody (1:1000, Abcam ab27671).

4.3. Results and Discussion

To verify that reactive cysteine profiling could be used to identify copper-binding proteins, we performed a control proof-of-concept experiment, in which we tested whether Antioxidant Protein 1 (Atox1), a known copper-binding protein, exhibited copper-dependent

labeling. Atox1 is a copper chaperone that shuttles copper from the copper import protein (Ctr1) at the cell membrane to the copper export protein (Atp7) at the Golgi complex. Atox1 contains three surface-exposed cysteines: C12, C15 and C41. The copper-binding site is comprised of C12 and C15, while C41 does not bind copper. We hypothesized that copper binding to Atox1 at C12 and C15 would decrease the reactivity of these cysteines, which could be read out as a decrease in labeling by a cysteine-reactive probe. In order to test this hypothesis, we purified Atox1 (described above) then utilized an iodoacetamide-alkyne (IA-alkyne) probe to label apo-, holo-, and chelator-treated holo- Atox1. Following labeling with IA-alkyne, we performed Click chemistry to append a rhodamine-azide for visualization on an SDS-PAGE gel. Notably, we performed labeling experiments in the anaerobic chamber, as both copper and cysteine residues can react with oxygen and oxidation would complicate results. Indeed, purified apo-Atox1 is labeled by IA-alkyne, while copper-loaded Atox1 exhibits a 70% decrease in labeling (data not shown). This is consistent with the fact that two of three cysteine residues bind copper. In order to verify that this decrease in labeling is due to copper complexation as opposed to formation of a disulfide-bond, for example, we next performed a chelation experiment by applying bathocuproinedisulfonic acid (BCS), a copper chelator, to holo-Atox1 and found that BCS-treatment was indeed able to restore IA-alkyne labeling (data not shown). These proof-of-concept experiments on purified protein were carried out by Tyler Detomasi and gave us confidence that applying a similar workflow for a quantitative mass spectrometry experiment (Click reaction with biotin-azide instead of rhodamine-azide) could yield a list of potential copper-binding proteins.

Towards this end, we performed our initial chemoproteomics experiment (Figure 4.1) in collaboration with the Cravatt lab at the Scripps Research Institute, comparing HEK 293T cells treated *in situ* with 200 μM Cu for one hour to vehicle-treated HEK 293T cells. Cells were harvested and IA-alkyne treatments, Click chemistry, and subsequent processing steps were performed aerobically (a detailed experimental procedure was described previously).[15] Seeking to validate targets identified on the generated list, the following criteria were considered for validation - (1) Light/Heavy ratio > 3 (2) n > 2 (3) labeled cysteine is not found in active site (4) protein has an established activity/functional assay *in vitro* and *in situ* (5) protein has a known biological role (and ideally a known crystal structure). From this list, we performed follow-up validation on STAT3 and Keap1, as described previously[15]. Both STAT3 and Keap1 satisfied the requisite criteria for follow-up, exhibiting ratios >3 (high ratios indicate less labeling in Cu-treated lysates than in control lysates) on cysteines 712/718 and cysteine 288, respectively, and n=3 and n=2, respectively. Validation studies were described in detail previously[15]; however, we were unable to validate either target for direct Cu-binding.

Based on these results (Table 4.1), we decided to narrow our focus to specifically perform validations on enzymes. We had difficulty performing follow-up on transcription factors (such as STAT3), and we reasoned that activity assays would be easier to carry out on enzymes with defined activity assays. We envisioned enzyme activity assays as being more amenable to testing Cu^{+}-specific inhibition or activation. In parallel, we decided to generate a chemoproteomics list from *in cellulo* treatment with a Cu-chelator. We hypothesized that chelator-treatment could identify endogenous copper-binding residues without causing oxidative stress. In a Cu-treatment experiment we observe a decrease in labeling after Cu-addition (Figure 4.2A), whereas treatment with a Cu-chelator should increase labeling of cysteines previously bound to copper (Figure 4.2B). With this rationale, we planned to follow up on proteins that were present on both the Cu-addition and chelation lists. Toward this end, we performed our

second chemoproteomics experiment, in which we treated living cells with 50 μM ATN-224 for one hour. In this experiment, we labeled 4799 cysteine residues corresponding to 135 protein hits (Table 4.2). Based on this, we chose to follow-up on transketolase (TKT) and triose phosphate isomerase (TPI) – two enzymes on the Cu-addition list.

While we hypothesized that we would see significant overlaps on Cu-addition and chelation lists, we saw minimal overlap between the two lists generated. We believed this could be due to the fact that treatment with Cu-chelators will reveal cysteines endogenously bound to Cu, while Cu^+-treatment will reveal cysteines that can bind (but are *not* already bound to) Cu. Given this rationale, we would in fact expect the Cu+ and the chelator-treated lists to be mutually exclusive. In addition to TKT and TPI from the Cu-addition list, we chose to follow up on S-methyl-5'-thioadenosine phosphorylase (MTAP) from the chelation list. These proteins were chosen because they satisfied the criteria for follow-up described above. Tyler Detomasi performed validation studies on TPI (data not shown).

Both TKT and MTAP were expressed and purified using standard Ni-NTA purification techniques followed by cleavage of the His_6-tag. With pure protein in hand (Figures 4.4 and 4.6), the activity of both proteins was tested. To assess activity of MTAP, we monitored the reaction of methyl-5'-thioadenosine (MTA) with phosphate to produce adenine and S-methyl-5-thio-alpha-D-ribose 1-phosphate for a decrease in absorbance at 275 nm. We observed a decrease in absorbance at 275 nm when MTA is treated with enzyme (Figure 4.5). After verifying that the protein was active, we carried out UV-vis Cu+-titration experiments, monitoring absorption at 265 nm. These studies were carried out as described previously;[1] as absorbance at 265 nm corresponds to a Cu^+-cysteine ligation. We observe an increase in absorbance with increasing Cu; however, we observe this same trend in the control sample treated with acid alone (data not shown). For this reason, we did not characterize enzyme kinetics further (we did not obtain values for K_m or for k_{cat}), based on the fact that initial UV-vis Cu^+ titration experiments did not look promising. Unfortunately, TKT also did not seem to be a promising target. Attempts to optimize activity assays were unsuccessful and were ultimately not pursued because UV-vis Cu+ binding assays also did not look promising (data not shown). As with MTAP, we observe a small increase in absorption at 265 nm in both the sample treating with increasing Cu+ and in the sample treated with acid alone. We additionally see increases in all wavelengths tested (including A_{355}, A_{262}, and A_{295}), which suggests that the change in absorbance is not due to Cu^+-cysteine ligation.

Given that we were unable to validate the selected targets, we decided to take a step back to assess whether the treatments performed (1) caused oxidative stress *in cellulo*, which could lead to false positive hits and (2) did indeed modulate Cu levels *in cellulo* (2). In addition to binding cysteine residues, 200 μM Cu *in situ* treatment may cause non-specific cysteine oxidation through the formation of disulfide bonds or other oxidative cysteine modification. Because the formation of a disulfide bond will also result in the loss of cysteine labeling, we cannot differentiate direct Cu-binding from Cu-mediated cysteine oxidation from our initial mass spectrometry experiment. To address point (1) described above, we investigated changes in the GSH/GSSG ratio upon the 200 μM Cu-addition through a metabolomics experiment. We indeed found that this treatment significantly alters cellular redox balance; reduced glutathione (GSH) undergoes a 0.2-fold change (p-value = 3.36E-7) while oxidized glutathione undergoes a 4.25-fold change (p-value = 4.31E-5). As such, we reevaluated our experimental design further and chose to perform treatments in cell lysates prepared anaerobically, as opposed to in living cells.

We performed three experiments to address point (2) described above – first, we measured superoxide dismutase (SOD) activity in control vs. chelator-treated lysates as a proxy for Cu+ levels; second, we assessed labeling of FLAG-Atox1 in an overexpression system; and third, we visualized labile Cu+ with CCL-1. We can use SOD activity as a proxy for Cu^+ levels. We found that 1 hour treatment with ATN-224 did not significantly alter SOD activity (Figure 4.7), while longer treatments are known to decrease SOD activity[16]. This suggests that while our treatment may alter Cu^+ levels, it does not deplete cellular copper enough to affect SOD activity. We also found that labeling of FLAG-Atox1 is not modulated by ATN-224 treatment, which is likely due to the fact that the majority of this protein is not metallated *in cellulo*. We do, however, observe that ATN-224 can restore labelling of FLAG-Atox1 that has been treated with Cu+ (Figure 4.8). Lastly, CCL-1 imaging revealed the 1 hour ATN-224 treatment as having a negligible effect on labile Cu^+ levels (Figure 4.9). Based on three lines of evidence, we did not observe altered cellular Cu-levels after 50 μM ATN-224 treatment for 1 hour. As such, we again reevaluated our experimental strategy.

Because treatment *in cellulo* can cause oxidative stress, changes in protein expression levels/cellular compensation mechanisms, and potential off-target effects, we decided to simplify our strategy for list generation. We hypothesized that treating cell lysates prepared anaerobically with Cu could eliminate these issues. Additionally, we wanted to treat cell lysates with Cu+ and with Cu-specific chelators (Table 4.3). Towards this end, we prepared lysates anaerobically then performed isoTOP-ABPP on lysates treated with Cu^+ and with two chelators – bathocuproinedisulfonic acid disodium salt (BCS) and tris[2-(2-pyridyl)ethyl]amine (TEPA) (Tables 4.3, 4.4 and 4.5, respectively).

Given the fact that validation performed on targets from lists generated previously (from *in cellulo* Cu-addition and chelation treatments) was unsuccessful, we only wanted to follow up on a list that contained multiple positive controls. We envisioned copper-binding cysteines 12 and 15 on Atox1 and cysteines 22, 25, 244, and 246 on copper chaperone for superoxide dismutase (CCS) as being potential positive controls for Cu-binding cysteines. While our BCS and TEPA lists did not contain these positive controls and contained relatively few proteins, our Cu^+-addition list gratifyingly showed differential labeling on both CCS and on Atox1. CCS exhibited a ratio >3 on known copper-binding cysteine 244. Atox1 exhibited a ratio >3 on C41. While this cysteine does not bind copper, we hypothesized that perhaps copper binding at C12 and 15 may alter probe accessibility at C41. Given these positive controls, we began to validate targets on the Cu^+-addition list. The Cu+-addition list contained 164 proteins in the proteome containing a cysteine residue with R>2; with approximately 26 enzymes. The 26 enzymes were from a diverse group of classes, including oxidoreductases, transferases, hydrolases, lyases, and ligases. We focused initial validation efforts on Thymidine Kinase 1 (TK1) and Pyrrolidine-5-carboxylate reductase 1 (PYCR1). Diana Iovan focused on the purification and validation of PYCR1.

TK1 gene was inserted into a vector containing an N-terminal His_6-tag and a TEV cleavage site (Figure 4.10). This was purified using standard Ni-NTA purification techniques followed by a TEV cleavage of His_6-tag (Figure 4.11). Cu-loaded glutathione (GSH)-beads were shown to precipitate MEK1 from cell lysates; we hypothesized that this same assay could be used to precipitate TK1 if this protein indeed binds Cu+. We found that Cu-GSH beads did indeed precipitate TK1 from both HEK 293T cells and HEK 293T cells expressing V5-tagged TK1 (cells were obtained from Prof. Donita Brady) (Figure 4.12). This data suggests that TK1 may bind Cu, and ICP-MS studies are currently underway to further validate this target.

4.4. Conclusion

We developed a chemoproteomic strategy for identifying novel copper-binding cysteines in the human proteome. This strategy was based on the hypothesis that copper-cysteine complexation would diminish cysteine nucleophilicity and diminished nucleophilicity can be read out using a cysteine-reactive, alkyne-containing probe. Decreases in nucleophilicity will result in decreased labeling; as such, we generated a number of different chemoproteomics lists from various copper-addition and chelation treatments *in cellulo* and *in vitro*. We identified a number of caveats associated with a number of our treatments. Namely, we found that oxidative stress occurs when cells are treated with 200 μM Cu. We additionally determined that 50 μM ATN-224 treatment *in cellulo* does not significantly alter labile Cu^+ levels. Given these caveats, we switched from performing treatments *in cellulo* to performing copper-addition and chelation treatments *in vitro*. We found that anaerobic addition of 10 μM Cu^+ to cell lysates yielded a list that contained positive control proteins Atox1 and CCS. Based on this, we moved forward to validate two proteins on this list – TK1 and PYCR1 – and studies are currently underway.

Separately, as our proteomics lists have been difficult to interpret, we plan to take a more focused strategy moving forward. As we are interested in understanding whether copper modulates cellular signaling pathways, one potential strategy would be to use kinase- or ATP-beads to enrich for ATP-binding proteins and kinases. By enriching for ATP-binding proteins first, we hope to increase signal-to-noise in our lists. We hypothesize that by increasing signal-to-noise and focusing on kinase assays, we will avoid previous issues with validation discussed above. Another potential strategy would be to enrich for copper proteins before performing ABPP by using Cu-GSH beads, described above.

Figures

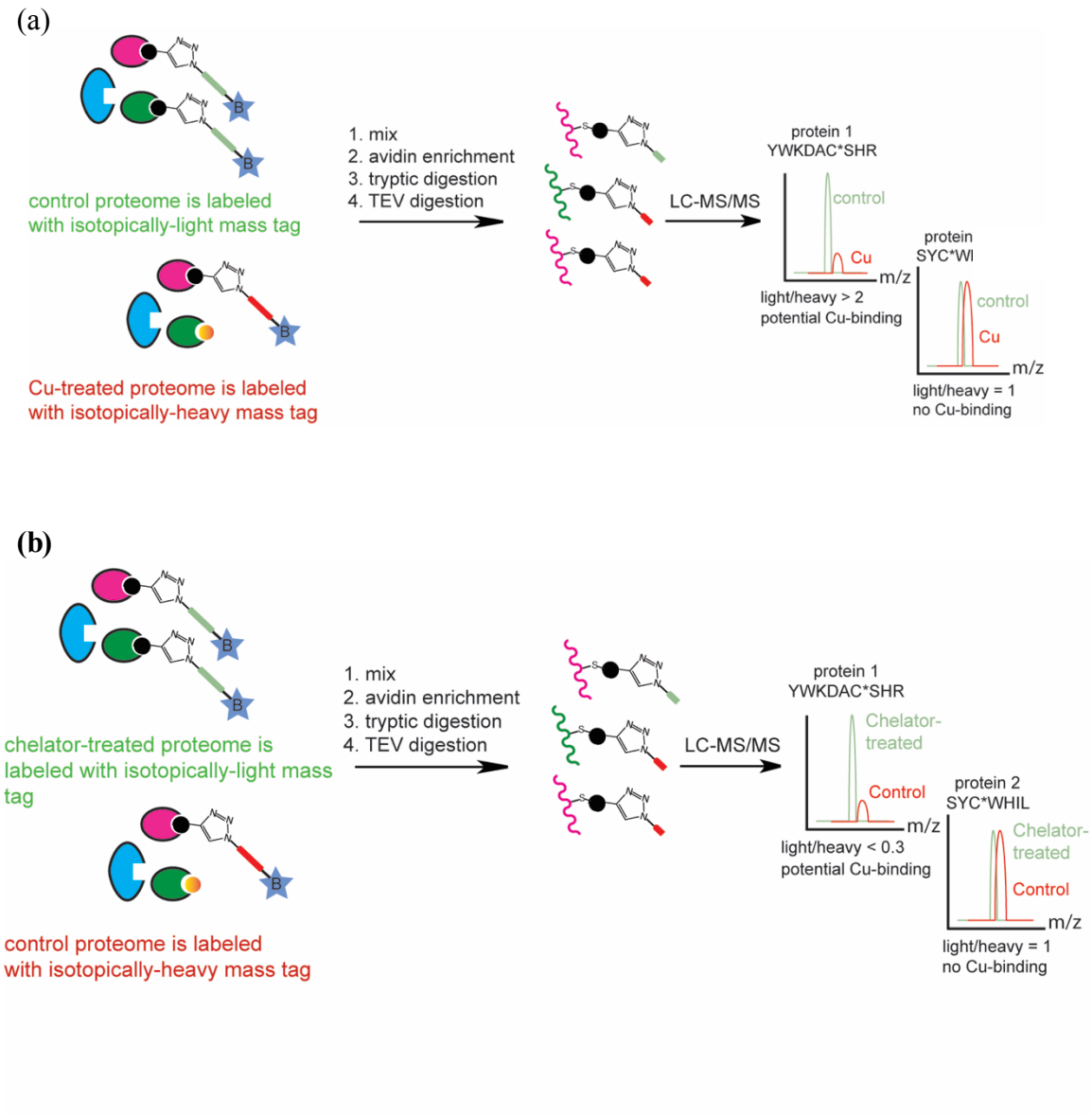

Figure 4.1. isoTOP-ABPP chemoproteomics applied to find novel copper-binding cysteines. (a) Cu-addition or (b) Cu-chelation experiments can be performed. This figure was adapted from the literature.[17]

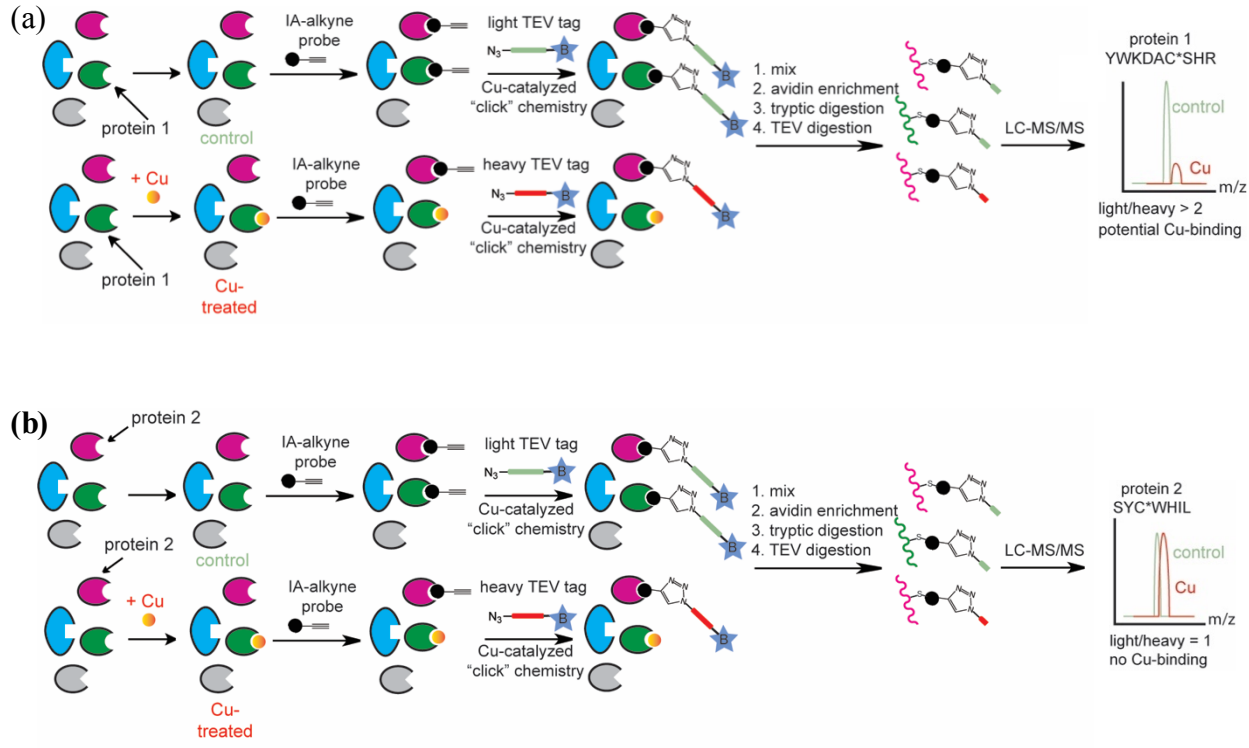

Figure 4.2. (a) A Cu-binding protein, such as the protein depicted in green, will exhibit a light/heavy ratio > 2 while (b) a control protein, such as the protein depicted in pink, will exhibit a light/heavy ratio = 1 in an isoTOP-ABPP experiment. This figure was adapted from the literature.[17]

Uniprot ID	Protein	Ratio	Rep No
P53384	NUBP1	20	2
P07339	CTSD	20	2
Q6PJ69	TRIM65	20	2
Q7RTV0	PHF5A	20	2
Q6FI81	CIAPIN1	20	3
Q9Y3E2	BOLA1	17.95	4
P23921	RRM1	16.58	4
P23921	RRM1	15.95	4
O95793	STAU1	12.75	3
O00244	ATOX1	12.36	4
Q13572	ITPK1	11.51	2
Q3KQU3	MAP7D1	9.85	3
P00441	SOD1	8.96	4
Q9UJY4	GGA2	8.9	2
Q3KQU3	MAP7D1	6.02	3
Q9Y5Y2	NUBP2	4.93	3
Q15005	SPCS2	4.65	2
P54136	RARS	4.37	3
Q9UBB4	ATXN10	4.29	2
P85037	FOXK1	4.09	2
Q96SK2	TMEM209	3.97	2
P40763	STAT3	3.85	3
Q53EZ4	CEP55	3.79	2
Q9Y5Y2	NUBP2	3.71	2
Q9H7E9	C8orf33 UPF0488	3.54	3
Q9C0C2	TNKS1BP1	3.51	2
Q14145	KEAP1	3.51	2
Q147X3	NAA30	3.51	2
Q15365	PCBP1	3.46	4
P17509	HOXB6	3.45	2
Q6FI81	CIAPIN1	3.44	2
Q15365	PCBP1	3.41	4
O14654	IRS4	3.36	2
Q9UHQ1	NARF	3.34	2
O95685	PPP1R3D	3.28	2
P42166	TMPO	3.13	2
P51610	HCFC1	3.13	3
Q9BRA2	TXNDC17	3.12	4
P29401	TKT	3.08	2
H3BVE0	CSCSFR	3	2
P60174	TPI1	3	2
Q9H3K6	BOLA2B	3	2

Table 4.1. Proteomics list obtained when HEK 293T cells were treated with 200 μM Cu for 1 hour (n=4). This list was discussed in detail previously[182].

Uniprot ID	Protein	Ratio	Rep No
Q2M3M2	SLC5A9	0.001898	2
Q9BT17	MTG1	0.025276	2
P13797	PLS3	0.040233	2
Q5JTD0	TJAP1	0.041635	2
A0A087X1L3	KCP	0.044291	2
A0A087X1W5	KIFC1	0.045719	2
C9J1S9	BCS1L	0.0493	2
H0YJ75	PPP2R5C	0.053039	2
P60660	MYL6	0.080718	3
Q92966	SNAPC3	0.092331	2
Q10567	AP1B1	0.103749	2
P49221	TGM4	0.106908	2
A0A087X260	TARDBP	0.108822	3
F5GX32	RAD52	0.115279	2
Q13509	TUBB3	0.116046	2
O15269	SPTLC1	0.117475	2
Q96GS4	C17orf59	0.119301	2
Q5SY74	NSL1	0.136755	3
Q9NQW6	ANLN	0.140617	2
Q9P2D1	Q9HCK8-2	0.14135	3
P17707	AMD1	0.148757	2
O75369	FLNB	0.153626	2
Q13126	MTAP	0.163421	2
O15381	NVL	0.169922	2
Q7Z6Z7	HUWE1	0.170535	2
Q5VZL5	ZMYM4	0.180695	2
Q15393	SF3B3	0.184971	2
Q8WXD5	GEMIN6	0.192722	2
Q8NG31	CASC5	0.195278	2
Q6ZWJ1	STXBP4	0.209763	2
Q9UKA4	AKAP11	0.218092	2
O75439	PMPCB	0.225665	2
Q13564	NAE1	0.229059	2
Q02040	AKAP17A	0.238434	2
O14733	MAP2K7	0.243863	2
P49327	FASN	0.244186	2
Q9P2X3	IMPACT	0.24898	2
Q96EP1	CHFR	0.26151	2
Q9UKT4	FBXO5	0.266332	3
Q9NVN8	GNL3L	0.270958	2
Q10570	CPSF1	0.273265	2
C9JL85	MTPN	0.282683	2
Q9BSC4	NOL10	0.282762	3
A0A0C4DG31	REXO4	0.291581	2
Q9NTM9	CUTC	0.295728	3
Q12802	AKAP13	0.29718	2

Table 4.2. Proteomics list obtained when HEK 293T cells were treated with 50 μM ATN-224 chelation for 1 hour (n=4).

Uniprot ID	Protein	Ratio	Rep No
A0A087WU91	IGHV3-49	354	3
Q9H4B7	TUBB1	340	2
Q9UNH7-2	SNX6	130	2
F8VUV1	DRD2	108	3
Q9H4B0-2	OSGEPL1	106	2
Q7L5Y1	ENOSF1	83	2
C9JZ99	PON3	62	2
P04183	**TK1**	**40**	**2**
Q9NR09	BIRC6	38	3
P40937-2	RFC5	33	2
F8WCP8	SEMA4F	23	2
A8K0R7	ZNF839	19	3
Q9BUH6	PAXX	18	2
Q16763	UBE2S	15	2
B7ZBU3	DDX59	14	2
Q9UBS4	DNAJB11	13	2
Q13158	FADD	11	4
O00244	**ATOX1**	**11**	**2**
Q9BV90	SNRNP25	9	2
Q6ZN17	LIN28B	7	2
Q6FI81	CIAPIN1	7	2
O14893	GEMIN2	7	2
P37268	FDFT1	7	2
P04080	CSTB	6	3
E2QRB3	**PYCR1**	**6**	**2**
O95155	UBE4B	6	2
J3KNF4	**CCS**	**5**	**3**
Q9H081	MIS12	5	2
J3KSM8	RAB31	5	2
P56545	CTBP2	5	2
Q96E09	FAM122A	4	2
Q9Y247	FAM50B	4	2
Q8IY26	PLPP6	4	2
P62979	RPS27A	4	2
Q9Y3T9	NOC2L	4	4
P62979	RPS27A	4	2
K7EIY6	RNF126	4	2
P63244	RACK1	4	4
P17655	CAPN2	4	2
P33993	MCM7	4	2
P53384	NUBP1	3	4
P68431	HIST1H3A	3	2
Q99873	PRMT1	3	2
Q9Y5Y2	NUBP2	3	2
P68366	TUBA4A	3	2

Table 4.3. Proteomics list obtained from 10 μM Cu-addition treatments performed on cell lysates prepared anaerobically. Positive controls and potential interesting hits are highlighted with bold font.

Uniprot ID	Protein	Ratio	Rep No
P62633-2	CNBP	0.01	3
P62633	CNBP	0.02	3
H3BPE7	FUS	0.02	3
Q8N9N5	BANP	0.04	3
C9JGE3	EWSR1	0.05	3
C9JGE3	EWSR1	0.08	3
Q96RG2	PASK	0.09	3
P04406	GAPDH	0.10	3
P62633	CNBP	0.10	3
Q01581	HMGCS1	0.11	3
Q9P2X3	IMPACT	0.11	3
Q13509	TUBB3	0.11	3
P51659	HSD17B4	0.13	3
A0A0C4DGV5	ZRANB2	0.14	3
A0A0C4DGV5	ZRANB2	0.15	3
P22234	PAICS	0.15	3
P36578	RPL4	0.17	3
D6RDI2	LUC7L3	0.18	3
P48735	IDH2	0.19	3
Q15637	SF1	0.21	3
Q96C86	DCPS	0.23	3
Q8NCM8	DYNC2H1	0.23	3
Q9Y5B9	SUPT16H	0.25	2
Q9Y5G8	PCDHGA5	0.26	2
Q99986	VRK1	0.27	2
A0A0D9SF44	R3HCC1	0.28	2
Q13263	TRIM28	0.29	2
P55809	OXCT1	0.29	3
P23497	SP100	0.29	3
A0A0A0MSX9	IARS	0.29	3
Q4JDL3	PTPN20	0.29	2
Q96EQ0	SGTB	0.30	2
Q8NHV4	NEDD1	0.30	2

Table 4.4. Proteomics list obtained from 500 μM BCS treatments performed on cell lysates prepared anaerobically.

Uniprot ID	Protein	Ratio	Rep No
A0A087WT08	ZNF221	0.00	2
A2VEC9	SSPO	0.03	2
P68363	TUBA1B	0.11	3
G5E9C7	MAP2K2	0.16	2
C9JGE3	EWSR1	0.25	2
Q14566	MCM6	0.30	2

Table 4.5. Proteomics list obtained from 500 μM TEPA treatments performed on cell lysates prepared anaerobically.

CGGTCTCCCATGGAGTCCTATCATAAACCCGACCAACAAAAGCTTCAAGCGCTGAA
AGACACAGCTAACCGCCTTCGCATTTCATCCATTCAAGCTACCACAGCGGCAGGTTC
AGGACACCCAACGAGTTGTTGTTCAGCGGCTGAAATCATGGCAGTCTTATTCTTTCA
TACTATGCGTTACAAGAGTCAGGACCCCCGCAATCCTCATAACGACCGTTTTGTGTT
ATCGAAAGGGCACGCTGCGCCTATTCTGTATGCGGTATGGGCGGAAGCTGGCTTCCT
GGCAGAGGCCGAGTTGCTTAACTTGCGTAAAATTTCCTCGGATTTAGACGGCCACCC
AGTGCCAAAGCAGGCGTTCACAGACGTAGCCACCGGATCACTTGGTCAGGGTTTGG
GTGCGGCATGCGGAATGGCTTACACGGGCAAATATTTTGACAAAGCATCTTACCGCG
TCTATTGCCTTTTAGGAGATGGAGAGCTTTCCGAGGGGAGCGTGTGGGAGGCGATG
GCTTTCGCCTCAATTTACAAATTAGATAACTTAGTAGCGATCCTGGACATTAACCGC
CTGGGGCAATCCGATCCCGCCCCGTTACAGCACCAGATGGATATTTACCAGAAACG
CTGCGAAGCGTTTGGGTGGCATGCTATCATTGTCGATGGGCACTCGGTAGAGGAACT
GTGCAAGGCATTCGGGCAGGCCAAGCACCAACCGACAGCGATCATTGCGAAAACCT
TCAAGGGTCGTGGGATCACAGGAGTGGAAGACAAAGAATCATGGCATGGGAAGCCT
TTACCTAAGAACATGGCAGAACAAATTATCCAAGAGATCTATTCCCAAATTCAATCC
AAGAAAAAGATTCTTGCCACGCCACCGCAAGAAGACGCTCCCTCTGTAGACATCGC
CAATATCCGTATGCCTTCCTTACCAAGCTATAAAGTCGGCGATAAGATCGCCACTCG
CAAAGCGTATGGCCAGGCGCTGGCTAAGTTGGGGCATGCGAGCGATCGTATCATCG
CCTTAGATGGAGACACGAAAAATAGCACATTTTCTGAGATTTTTAAGAAGGAACAC
CCAGACCGTTTTATTGAATGTTATATCGCCGAGCAGAATATGGTGAGCATTGCTGTT
GGTTGTGCTACCCGCAACCGCACCGTACCTTTTTGCAGCACATTCGCGGCGTTCTTTA
CCCGCGCTTTTGATCAAATCCGTATGGCAGCTATTTCCGAGTCAAATATTAATTTATG
TGGCAGTCATTGCGGGGTCAGTATTGGTGAGGACGGGCCTTCGCAAATGGCATTGG
AAGACTTAGCCATGTTTCGCAGCGTGCCAACAAGCACAGTTTTCTACCCCAGTGACG
GAGTTGCAACTGAAAAAGCTGTAGAGCTTGCTGCCAATACAAAAGGTATCTGCTTCA
TCCGTACATCTCGTCCTGAGAACGCTATCATTTACAACAACAATGAAGATTTCCAAG
TGGGCCAAGCAAAAGTTGTTCTGAAGAGCAAAGACGATCAAGTGACAGTAATCGGA
GCGGGTGTCACACTGCATGAGGCGTTAGCCGCCGCTGAACTTTTGAAAAAGGAGAA
AATCAACATTCGCGTCTTAGATCCATTTACCATTAAACCCTTAGACCGTAAGTTAATT
CTTGATTCAGCGCGTGCTACTAAAGGCCGCATTTTAACTGTAGAAGACCATTATTAT
GAAGGAGGAATCGGAGAAGCCGTATCGAGTGCAGTTGTGGGGGAACCCGGCATTAC
GGTGACCCATCTGGCGGTCAATCGTGTTCCTCGTTCAGGTAAACCTGCCGAGTTATT
GAAGATGTTCGGGATTGACCGTGACGCGATTGCGCAAGCGGTCCGTGGGCTGATCA
CGAAAGCTCTTGTTCCCCGTGGGTCGTTAGAGCACCACCACCACCACCATTAGTAAA
GGAGACCG

Figure 4.3. Sequence of hTKT-thrombin-His_6 codon optimized gBlock used for expression and purification of TKT. This gene was cloned into a protein expression vector using Golden Gate cloning and BsaI restriction enzyme.

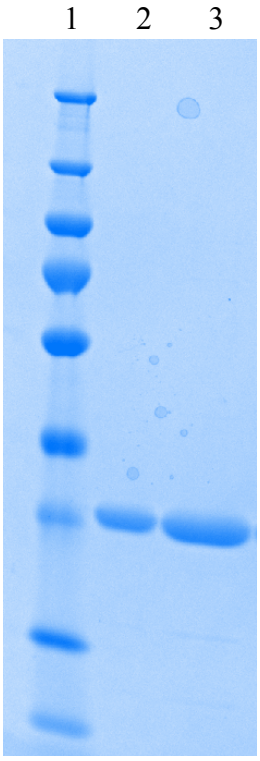

Figure 4.4. Purification of MTAP. SDS-PAGE for purification of MTAP. The lanes represent the following (1) PageRuler Prestained Protein Ladder (Thermo) (2) 5 µL purified MTAP (3) 15 µL purified MTAP, after Ni-NTA column followed by Ni-NTA reverse column.

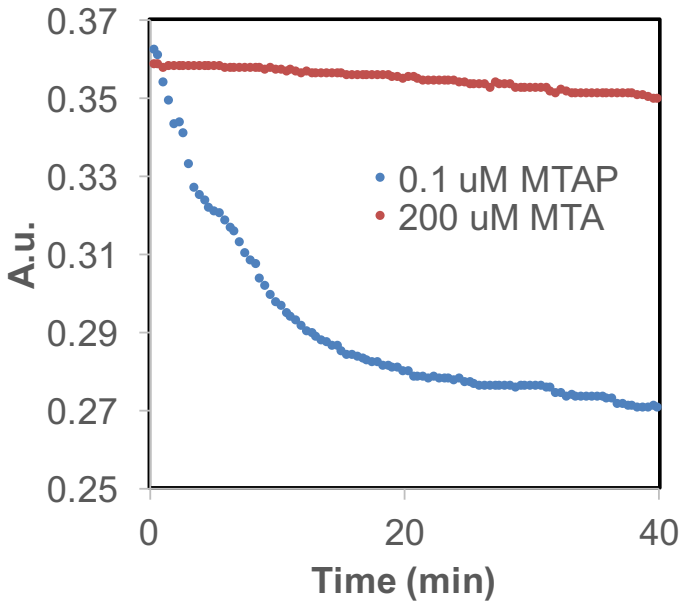

Figure 4.5. MTAP is active, as observed by the decrease in absorbance at 275 nm over time. Full analysis of activity was not performed because UV-vis Cu+ titrations did not look promising. Therefore, K_M and k_{cat} were not obtained.

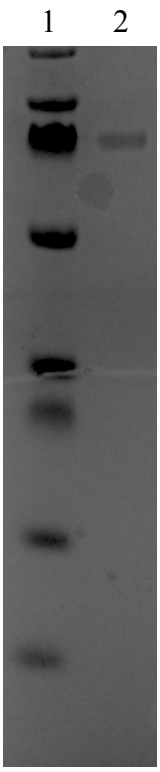

Figure 4.6. Purification of TKT. SDS-PAGE for purification of TKT. The lanes represent the following (1) PageRuler Prestained Protein Ladder (Thermo) (2) 10 µL purified TKT, after Ni-NTA column followed by Ni-NTA reverse column.

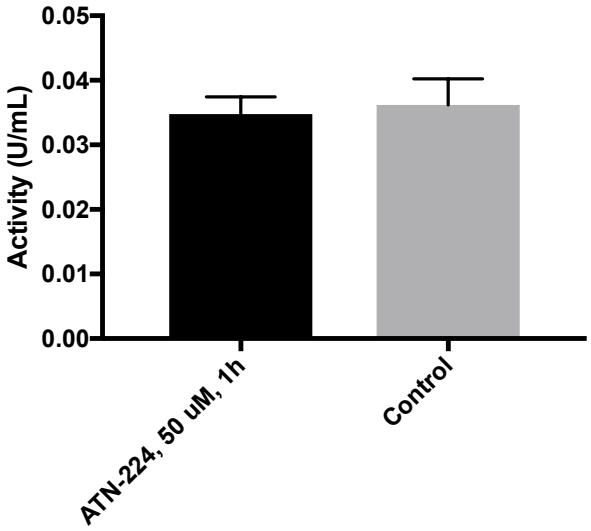

Figure 4.7. SOD activity is not significantly affected by 1 hour 50 μM ATN-224 treatment.

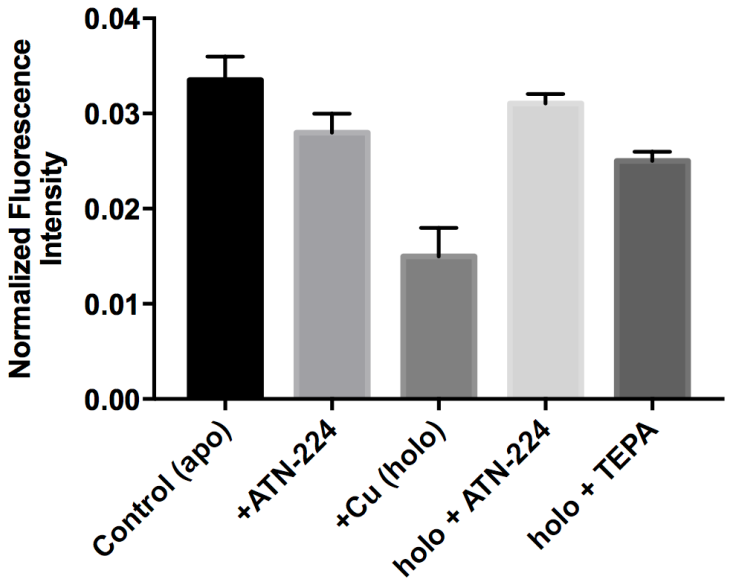

Figure 4.8. Negligible change in labeling is observed when FLAG-Atox1 is treated with ATN-224. However, an increase in labeling is observed when holo-FLAG-Atox1 is treated with ATN-224.

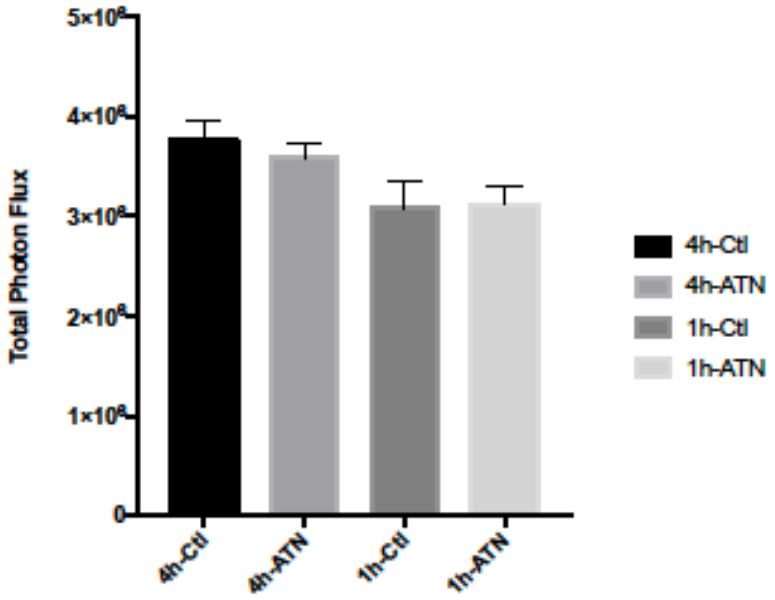

Figure 4.9. HEK 293-luc cells were treated for either 4 hours or 1 hour with 50 μM ATN-224 or with vehicle control, followed by treatment with 25 μM CCL-1 and bioluminescent signal was obtained.

AGGTCTCGCATGCACCACCACCACCACCATGAGAATCTCTATTTCCAGGGCAGCTGC
ATTAACCTGCCCACTGTGCTGCCTGGCTCCCCCAGCAAGACCCGGGGGCAGATCCAG
GTGATTCTCGGGCCGATGTTCTCAGGAAAAAGCACAGAGTTGATGAGACGCGTCCG
TCGCTTCCAGATTGCTCAGTACAAGTGCCTGGTGATCAAGTATGCCAAAGACACTCG
CTACAGCAGCAGCTTCTGCACACATGACCGGAACACCATGGAGGCACTGCCCGCCT
GCCTGCTCCGAGACGTGGCCCAGGAGGCCCTGGGCGTGGCTGTCATAGGCATCGAC
GAGGGGCAGTTTTTCCCTGACATCGTGGAGTTCTGCGAGGCCATGGCCAACGCCGGG
AAGACCGTAATTGTGGCTGCACTGGATGGGACCTTCCAAAGGAAGCCATTTGGGGC
CATCCTGAACCTGGTGCCGCTGGCCGAGAGCGTGGTGAAGCTGACGGCGGTGTGCA
TGGAGTGCTTCCGGGAAGCCGCCTATACCAAGAGGCTCGGCACAGAGAAGGAGGTC
GAGGTGATTGGGGGAGCAGACAAGTACCACTCCGTGTGTCGGCTCTGCTACTTCAAG
AAGGCCTCAGGCCAGCCTGCCGGGCCGGACAACAAAGAGAACTGCCCAGTGCCAGG
AAAGCCAGGGGAAGCCGTGGCTGCCAGGAAGCTCTTTGCCCCACAGCAGATTCTGC
AATGCAGCCCTGCCAACTGATAAACGAGACCT

Figure 4.10. Sequence of His_6-TEV-TK1 gBlock used for expression and purification of TK1. This gene was cloned into a protein expression vector using Golden Gate cloning and BsaI restriction enzyme.

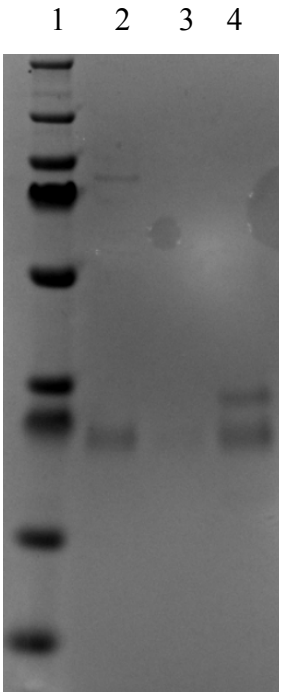

Figure 4.11. SDS-PAGE for purification of TK1. The lanes represent the following (1) PageRuler Prestained Protein Ladder (Thermo) (2) 5 µL low imidazole fraction from TK1 Ni-NTA batch purification (3) 5 µL wash fraction from TK1 Ni-NTA batch purification (4) 5 µL high imidazole fraction from TK1 Ni-NTA batch purification.

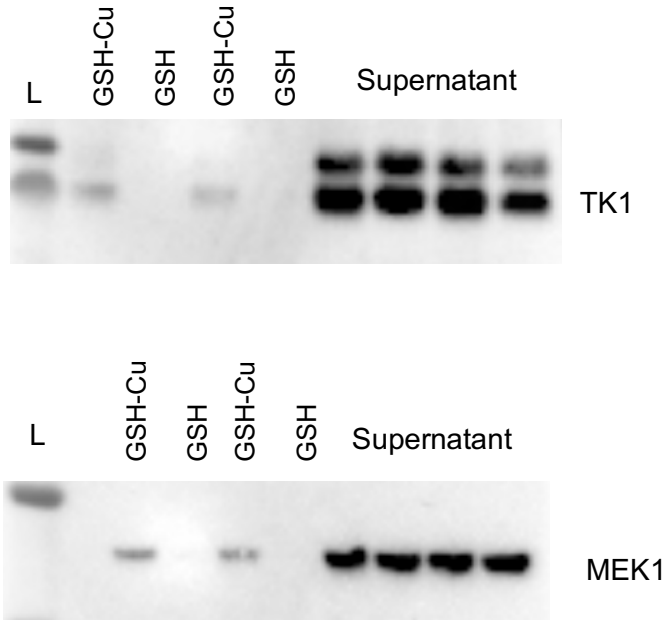

Figure 4.12. TK1 can be enriched by treatment with Cu-GSH beads. (a) V5-TK1 HEK 293T cells are lysed, and lysates are incubated with glutathione (GSH) beads alone or GSH beads that have been pre-treated with $CuCl_2$, then are probed for TK1. (b) V5-TK1 HEK 293T cells are lysed, and lysates are incubated with glutathione (GSH) beads alone or GSH beads that have been pre-treated with $CuCl_2$, then are probed for MEK1.

4.5. References

1. Krishnamoorthy, L.; Cotruvo, J. A. J.; Chan, J.; Kaluarachchi, H.; Muchenditsi, A.; Pendyala, V. S.; Jia, S.; Aron, A. T.; Ackerman, C. M.; Vander Wal, M. N.; Guan, T.; Smaga, L. P.; Farhi, S. L.; New, E. J.; Lutsenko, S.; Chang, C. J., Copper regulates cyclic-AMP-dependent lipolysis. *Nat. Chem. Biol.* **2016,** *12*, 586-592.
2. Turski, M. L.; Brady, D. C.; Kim, H. J.; Kim, B.-E.; Nose, Y.; Counter, C. M.; Winge, D. R.; Thiele, D. J., A Novel Role for Copper in Ras/Mitogen-Activated Protein Kinase Signaling. *Mol Cell Biol* **2012,** *32* (7), 1284-1295.
3. Brady, D. C.; Crowe, M. S.; Turski, M. L.; Hobbs, G. A.; Yao, X.; Chaikuad, A.; Knapp, S.; Xiao, K.; Campbell, S. L.; Thiele, D. J.; Counter, C. M., Copper is required for oncogenic BRAF signalling and tumorigenesis. *Nature* **2014,** *509*, 492-496.
4. Andreini, C.; Bertini, I.; Rosato, A., Metalloproteomes: A Bioinformatic Approach. *Acc. Chem. Res.* **2009,** *42* (10), 1471-1479.
5. Cvetkovic, A.; Menon, A. L.; Thorgersen, M. P.; Scott, J. W.; Poole, F. L. I.; Jenney, F. E. J.; Lancaster, W. A.; Praissman, J. L.; Shanmukh, S.; Vaccaro, B. J.; Trauger, S. A.; Kalisiak, E.; Apon, J. V.; Siuzdak, G.; Yannone, S. M.; Tainer, J. A.; Adams, M. W. W., Microbial metalloproteomes are largely uncharacterized. *Nature* **2010,** *466*, 779-782.
6. Song, Y.; Zhang, H.; Chen, C.; Wang, G.; Zhuang, K.; Cui, J.; Shen, Z., Proteomic analysis of copper-binding proteins in excess copper-stressed rice roots by immobilized metal affinity chromatography and two-dimensional electrophoresis. *BioMetals* **2014,** *27*, 265-276.
7. Pace, N. J.; Weerapana, E., A Competitive Chemical-Proteomic Platform to Identify Zinc-Binding Cysteines. *ACS Chem. Biol.* **2014,** *9* (1), 258-265.
8. Weerapana, E.; Wang, C.; Simon, G. M.; Richter, F.; Khare, S.; Dillon, M. B. D.; Bachovchin, D. A.; Mowen, K.; Baker, D.; Cravatt, B. F., Quantitative reactivity profiling predicts functional cysteines in proteomes. *Nature* **2010,** *468*, 790-795.
9. Lippard, S. J.; Berg, J. M., *Principles of Bioinorganic Chemistry*. University Science Books: Mill Valley, CA,: Mill Valley, CA, 1994.
10. Yatsunyk, L. A.; Rosenzweig, A. C., Cu^+ Binding and Transfer by the N Terminus of the Wilson Disease Protein. *J. Biol. Chem.* **2007,** *282*, 8622-8631.
11. Guan, R.; Ho, M. C.; Brenowitz, M.; Tyler, P. C.; Evans, G. B.; Almo, S. C.; Schramm, V. L., Entropy-driven binding of picomolar transition state analogue inhibitors to human 5'-methylthioadenosine phosphorylase. *Biochemistry* **2011,** *50* (47), 10408 - 10417.
12. Hecquet, L.; Bolte, J.; Demuynck, C., New Assays for Transketolase. *Bioscience, Biotechnology, and Biochemistry,* **1993,** *57*, 2174-2176.
13. Constantin, C. Catching Metalloproteins: Reactive Cysteine Profiling and Metal-targeted Photocrosslinking Probes. Master of Science, Ecole Polytechnique Federale de Lausanne, Lausanne, 2015.
14. Birringer, M. S.; Perozzo, R.; Kut, E.; Stillhart, C.; Surber, W.; Scapozza, L.; Folkers, G., High-level expression and purification of human thymidine kinase 1: quaternary structure, stability, and kinetics. *Protein Expr Purif* **2006,** *47* (2), 506-515.
15. Ackerman, C. M. Detecting, Measuring and Manipulating Copper in Biological Systems. University of California at Berkeley, Berkeley, CA, 2017.
16. Doñate, F.; Juarez, J. C.; Burnett, M. E.; Manuia, M. M.; Guan, X.; Shaw, D. E.; Smith, E. L. P.; Timucin, C.; Braunstein, M. J.; Batuman, O. A.; Mazar, A. P., Identification of

biomarkers for the antiangiogenic and antitumour activity of the superoxide dismutase 1 (SOD1) inhibitor tetrathiomolybdate (ATN-224). *Br J Cancer* **2008,** *98*, 776 - 783.
17. Roberts, A. M.; Ward, C. C.; Nomura, D. K., Activity-based protein profiling for mapping and pharmacologically interrogating proteome-wide ligandable hotspots. *Curr. Opin. Biochem.* **2017,** *43*, 25-33

Appendix 1

Towards the development of fluorescent copper sensors targeted to subcellular organelles

A1.1. Synopsis

Copper is required for sustaining life, in part due to its ability to carry out redox transformations. However, mismanagement of cellular copper pools can result in oxidative stress and damage associated with a variety of pathologies, including metabolic disorders, neurodegenerative diseases, and those associated with aging. For this reason, cellular copper homeostasis is tightly and precisely maintained; however, trafficking of cellular copper is insufficiently understood. In order to better understand cellular copper trafficking mechanisms and subcellular copper distribution, we set out to develop a method for visualizing subcellular changes in Cu^+ by fluorescence imaging. We planned to take advantage of a genetically-encoded protein labelling strategy (i.e. SNAP-tag[1] or HaloTag technology[2]) for site-specific protein labeling with a small molecule Cu^+-responsive dye. In this genetically-encoded protein targeting strategy, a self-labeling protein tag is fused to a protein of interest. If this protein of interest is localized to a unique organelle, this strategy can be used to covalently fix a Cu^+-responsive dye in a precise cellular locale. Similar strategies have found use in the development of targeted hydrogen peroxide,[3] zinc,[4] and magnesium[5] sensors, but the fact that there are at present no targetable Cu^+ sensors points to the difficulty of this task.

Developing a targetable Cu^+ sensor is particularly difficult because of the hydrophobic nature of Cu^+ sensors. Hydrophobic dyes are difficult to wash out of cells, which results in high background in undesired cellular locales. Toward solving this issue, we envisioned combining a hydrophilic fluorophore scaffold with poly(ethylene glycol) (PEG) groups to design a series of protein-targeted Cu^+-responsive dyes that could be washed out of cells more easily (Figure A1.1). Additionally, we envisioned using a chelation-based strategy to visualize changes in the exchangeable pool of Cu^+, as this approach would give us the ability to monitor copper levels through real-time fluorescence movies taken on the confocal microscope. This chelation-based approach makes use of a thioether-rich Cu^+-specific receptor that quenches fluorescence in its apo-form by photoinduced electron transfer (PET). Copper binding events diminish PET, which results in fluorescence enhancement.[6] Early designs of a targetable Cu^+ sensor were based on the functionalization of a boron dipyrromethene (BODIPY) fluorescent scaffold with a handle through which a SNAP-tag reactive benzyl-guanine moiety was appended (data unpublished). While many of the lab's early copper sensors were based on the BODIPY scaffold, this design proved unsuitable for targetable applications due to the collective hydrophobic nature of the BODIPY scaffold, the thioether-rich Cu^+ receptor, and the benzyl-guanine moiety, which precluded probe washout from the cells. With these previous designs in mind, we set out to develop hydrophilic fluorophore scaffolds for targetable Cu^+-sensors. This Appendix describes the development of PEG-containing rhodol scaffolds, and the use of HaloTag protein for targetable Cu^+-sensor development.

A1.2. Methods

A1.2.1. General synthetic and spectroscopic methods

Reactions using moisture- or air-sensitive reagents were carried out in flame-dried glassware under an inert atmosphere of N_2. Solvent was passed over activated alumina and stored over activated 3Å molecular sieves before use when dry solvent was required. All other commercially purchased chemicals were used as received (without further purification). SiliCycle 60 F254 silica gel (pre-coated sheets, 0.25 mm thick) were used for analytical thin layer

chromatography and visualized by fluorescence quenching under UV light. Silica gel P60 (SiliCycle) was used for column chromatography. ^{1}H and ^{13}C NMR NMR spectra were collected at 298 K in CDCl3 or CD3OD (Cambridge Isotope Laboratories, Cambridge, MA) at 25 °C on Bruker AVQ-400, AVB-400, AV-500, or AV-600 at the College of Chemistry NMR Facility at the University of California, Berkeley or on Bruker 900 at the QB3 Central California 900 MHz NMR Facility. All chemical shifts are reported in the standard notation of δ parts per million relative to residual solvent peak at 7.26 ($CDCl_3$) or 3.31 (CD_3OD) for ^{1}H and 77.16 ($CDCl_3$) or 49.00 (CD_3OD) for ^{13}C as an internal reference. Splitting patterns are indicated as fol-lows: br, broad; s, singlet; d, doublet; t, triplet; m, multiplet; dd, doublet of doublets. Low-resolution electrospray mass spectral analyses were carried out using a LC-MS (Agilent Technology 6130, Quadrupole LC/MS and Advion expression-L Compact Mass Spectrometer). High-resolution mass spectral analyses (ESI-MS) were carried out at the College of Chemistry Mass Spectrometry Facility at the University of California, Berkeley.

Milli-Q water was used in the preparation of all aqueous solutions. All spectroscopic measurements were performed in either 20 mM HEPES, pH 7, or in PBS, pH 7.4. Absorption spectra were recorded using a Varian Cary 50 spectrophotometer, and fluorescence spectra were recorded using a Photon Technology International Quanta Master 4 L-format scan spectrofluorometer equipped with an LPS-220B 75-W xenon lamp and power supply, A-1010B lamp housing with integrated igniter, switchable 814 photocounting/analog photomultiplier detection unit, and MD5020 motor driver. Samples for absorption and emission measurements were contained in 1-cm × 1-cm quartz cuvettes with or without septum and sealing caps (1.4-mL or 3.5-mL volume; Starna). Cu+ was delivered in the form of $[Cu(MeCN)_4][PF_6]$ from an acetonitrile stock solution (2 mM).

*A1.2.2. Synthesis of precursor materials for Cu^{+} responsive dyes – intermediate **9***

3,6-Dihydroxy-9H-xanthen-9-one (1) Known compound (**1**) was prepared according to literature procedure.[7]

3,6-Bis(trifluoromethanesulfyloxy)-9H-xanthen-9-one (2) A solution of 3,6-dihydroxy-9H-xanthen-9-one (4.6504 g, 20.38 mmol, 1 eq), N-phenyl bis(trifluoromethanesulfonimide) (19.22 g, 53.8 mmol, 2.64 eq), and N,N-diisopropylethylamine (17.75 mL, 101.89 mmol, 5 eq) in 50 mL DMF was stirred for 1 hour at room temperature. After 1 hour, the reaction was poured into brine, then EtOAc was added. The organic layer was exacted 3 times with EtOAc then combined organic layers were washed again with brine, dried over Na_2SO_4, filtered and concentrated in vacuo. The reaction was then loaded on silica gel for purification by flash column chromatography (10% EtOAc in Hex) to yield compound (**2)** (6 g, 75%) as a white, fluffy solid. ^{1}H NMR (400 MHz, $CDCl_3$) δ (ppm): 8.47-8.44 (d, 2 H), 7.50 (d, 2 H), 7.35 (d, 2 H).

Benzyl 4-(9-oxo-6-(((trifluoromethyl)sulfonyl)oxy)-9*H*-xanthen-3-yl)piperazine-1-carboxylate (3) To 3,6-bis(trifluoromethanesulfyloxy)-9H-xanthen-9-one (3 g, 6.09 mmol, 1 eq) in 10 mL DMSO was added 1-Z-piperazine (1.1753 mL, 6.09 mmol, 1 eq), and this was allowed to proceed for 12 hours. At this point, the reaction was poured into 150 mL water, then the organic layer was exacted 3 times into EtOAc. The combined organic layers were washed with brine, dried over Na_2SO_4, filtered and concentrated in vacuo to yield a dark yellow syrup. The reaction was then loaded on silica gel for purification by flash column chromatography (40% EtOAc in Hex) to

yield compound (**3)** (1.2454 g, 35%). ^{1}H NMR (400 MHz, $CDCl_3$) δ (ppm): 8.39 (d, 1 H), 8.17 (d, 1 H), 7.394 – 7.343 (m, 6 H), 7.26 – 7.24 (m, 1 H), 6.94 – 6.92 (dd, 1 H), 6.71 (d, 1 H), 5.185 (s, 2 H), 4.15 – 4.09 (m, 4 H), 3.47 (s, 4 H).

9-Oxo-6-(piperazin-1-yl)-9*H*-xanthen-3-yl trifluoromethanesulfonate (4) Benzyl 4-(9-oxo-6-(((trifluoromethyl)sulfonyl)oxy)-9*H*-xanthen-3-yl)piperazine-1-carboxylate (0.25 g, 0.444 mmol, 1 eq) was cooled to 0 ºC, then BBr_3 was added dropwise. The reaction was allowed to warm to room temperature, then was quenched with 5 mL of water after stirring for 2 h. This was then poured into 150 mL sat. $NaHCO_3$ and the organic layer was extracted into EtOAc then dried over Na_2SO_4 and filtered. The organic layer is concentrated, then is carried on crude.

(5) Triethylamine (1.1185 mL, 8.02 mmol, 5 eq) was added to compound (4) (0.687 g, 1.603 mmol, 1 eq) in 50 mL DCM. Then Boc_2O (0.4376 g, 2.01 mmol, 1.25 eq) was added and this was stirred for 10 minutes before concentrating and loading on silica gel for purification by flash column chromatography (gradient 20% → 25% → 50% → 75% EtOAc in Hex) to yield compound (5) (0.162 g, 45% over 2 steps). ^{1}H NMR (400 MHz, $CDCl_3$) δ (ppm): 8.41 – 8.39 (d, 1 H), 8.18 – 8.16 (d, 1 H), 7.38 (d, 1 H), 7.27 – 7.24 (m, 1 H), 6.95 – 6.92 (dd, 1 H), 6.71 (d, 1 H), 3.65 – 3.62 (m, 4 H), 3.47 – 3.45 (m, 4 H), 1.505 (s, 9 H).

***Tert*-butyl 4-(6-hydroxy-9-oxo-9*H*-xanthen-3-yl)piperazine-1-carboxylate (6)** Triethylammonium hydroxide (0.626 mL, 0.0009392 mol, 2 eq) was added to compound (5) (0.248 g, 0.4696 mmol, 1 eq) in 3 mL dioxane at room temperature. This was stirred for 45 minutes before concentrating *in vacuo* to yield compound (**6**) (0.186 g).

(7) *tert*-butyl 4-(6-hydroxy-9-oxo-9*H*-xanthen-3-yl)piperazine-1-carboxylate (0.186 g, 0.4696 mmol, 1 eq) was dissolved in 25 mL DCM, followed by addition of imidazole (0.09591 g, 1.4088 mmol, 3 eq), and finally by slow addition of *tert*-Butyldimethylsilyl chloride (0.1456 g, 0.9392 mmol, 2 eq), at which point the color of the solution changed from orange to yellow. The solution was stirred for 1 h, then was concentrated *in vacuo.* The concentrate was then loaded on silica gel for purification by flash column chromatography (10% → 50% EtOAc in Hex) to yield compound (**7)** (0.198 g, 85% over 2 steps). ^{1}H NMR (400 MHz, $CDCl_3$) δ (ppm): 8.20 – 8.17 (m, 2 H), 6.93 – 6.91 (m, 1 H), 6.85 – 6.82 (m, 2 H), 6.75 (m, 1 H), 3.64 (m, 4 H), 3.41 (m, 4 H), 1.5 (s, 9 H), 1.015 (s, 9 H), 0.29 (s, 6 H).

(8) An oven-dried two-neck flask was charged with previously synthesized receptor[8-9] (0.3889 g, 0.7746 mmol, 2 eq) and dry THF then was cooled to -78 °C. A solution of tert-butyllithium in pentane (456 µL, 1.7 M, 0.7746 mmol, 2 eq) was then added dropwise under N_2. This was stirred for 8 min at -78 °C, then (7) (0.198 g, 0.3873 mmol, 1 eq) in dry THF was added and allowed to warm to room temperature over 1 hour. After stirring for 1 hour, the reaction was quenched with 2 N HCl and this was stirred for an additional 30 min. Saturated $NaHCO_3$ was added and the organic layer was extracted with EtOAc (× 3) before the combined organic layers were dried over Na_2SO_4 and concentrated *in vacuo.* The concentrate was then loaded on silica gel for purification by flash column chromatography (5% MeOH in DCM) to yield compound (**8)** (0.051 g). ^{1}H NMR (400 MHz, $CDCl_3$) δ (ppm): 7.35 – 7.33 (m, 2 H), 7.11 – 7.09 (d, 1 H), 6.93 – 6.90 (d, 2 H), 6.80 (s, 1 H), 6.73 – 6.71 (d, 1 H), 6.70 - 6.56 (d, 1 H), 6.44 (s, 1 H), 3.72 (s, 2 H), 3.60 – 3.59 (m, 4 H), 3.45 – 3.44 (m, 4 H), 2.80 (m, 4 H), 2.72 (s, 11 H), 2.59 – 2.53 (q, 4 H), 2.06 (s, 3 H), 1.48 (s, 9 H), 1.25 (t, 6 H).

(9-H) Compound (8) (0.099 g, 0.1289 mmol, 1 eq) was dissolved in 0.5 mL DCM, at which point 0.5 mL trifluoroacetic acid was added; this was stirred at room temperature for 1.5 hours. At this point, 1 mL water was added and stirred for 10 minutes, then poured into saturated $NaHCO_3$, extracted with EtOAc (× 3), washed with brine, then dried over Na_2SO_4 and filtered before concentrating *in vacuo*. The concentrate was then loaded on silica gel for purification by flash column chromatography (5% → 7.5% → 10% MeOH in DCM + 0.05% TEA) to yield compound **(9-H)** (0.062 g, 30% over 2 steps for R = H) Compound (**9-F**) is prepared using the same synthesis (0.0843 g, 29% for R = F over 2 steps). ^{1}H NMR (400 MHz, $CDCl_3$) δ (ppm): 7.37 – 7.34 (m, 2 H), 7.11 – 7.09 (d, 1 H), 6.94 – 6.93 (d, 2 H), 6.84 (s, 1 H), 6.77 - 6.74 (m, 1 H), 6.58 – 6.55 (d, 1 H), 6.46 – 6.46 (m, 1 H), 3.72 (s, 2 H), 3.55 (m, 4 H), 3.17 (m, 4 H), 2.83 – 2.79 (m, 4 H), 2.72 (m, 11 H), 2.59 – 2.54 (m, 4 H), 2.06 (s, 3 H), 1.32 – 1.23 (t, 6 H).

A1.2.3. Synthesis of Cu^+ responsive dyes

Synthesis of SNAP-PEG3-CH5

(10) hydroxyl-PEG6-*tert*-butyl ester (0.100 g, 0.244 mmol, 1 eq) was dissolved in 0.5 mL DCM at 0 ºC, then TEA (0.169 mL, 1.218 mmol, 5 eq) was added. Tosyl chloride (0.0534 g, 0.280 mmol, 1.15 eq) was taken up in 0.5 mL DCM, and added gradually over 10 minutes at 0 ºC with stirring. At this point, the reaction was allowed to warm to room temperature, then was stirred overnight. The reaction was then poured into saturated $NaHCO_3$, extracted with EtOAc (× 3), washed with brine, then dried over Na_2SO_4 and filtered before concentrating *in vacuo* to yield compound **(10)**, which was carried on to the next reaction in its crude form.

(11) Compound **(9-H)** (0.025 g, 0.03592 mmol, 1 eq) was added with Cs_2CO_3 (0.04681 g, 0.1437 mmol, 4 eq) to 1 mL DMF, then compound **(10)** (0.090 g, 0.07184 mmol, 4 eq) was added in 1 mL DMF. This was stirred at 35 ºC overnight. Because the reaction had not gone to completion, KI (0.01193 g, 0.07184 mmol, 2 eq) was added along with additional compound **(10)** (0.0405 g, 0.03592 mmol, 2 eq), and this was stirred overnight at 50 ºC. The reaction was poured into 150 mL brine, then the organic layer was extracted with 50 mL EtOAc x 3. The organic layer was washed with brine, dried with Na_2SO_4 then concentrated *in vacuo*. Crude concentrate was loaded on silica gel for purification by flash column chromatography (10% MeOH in DCM + 0.05% TEA) to yield compound **(11)** (0.029 g, 83%). ^{1}H NMR (400 MHz, $CDCl_3$) δ (ppm): 7.38 – 7.25 (m, 2 H), 7.12 - 7.09 (m, 1 H), 6.95 – 6.89 (m, 2 H), 6.82 (s, 1 H), 6.74 – 6.71 (d, 1 H), 6.59 – 6.55 (d, 1 H), 6.48 (s, 1 H), 3.77 – 3.59 (m, 30 H), 2.85 – 2.70 (m, 22 H), 1.45 (s, 9 H), 1.32 – 1.25 (m, 9 H).

(12) Compound **(11)** (0.0325 g, 0.02986 mmol, 1 eq) was dissolved in DCM in an oven-dried round-bottom flask, then TFA was added dropwise and the reaction was stirred for 2 hrs at room temperature. The reaction was concentrated *in vacuo* to yield compound **(12)** then was carried on crudely.

SNAP-PEG3-CH5 Benzyl-2-chloro-6-aminopyrimide SNAP-tag derivative **A** was synthesized following literature protocols[3]. Compound **(12)** (0.0325 g, 0.03855 mmol, 1 eq), **A** (0.03062 g, 0.1157 mmol, 3 eq), and HATU (0.0513 g, 0.1349 mmol, 3.5 eq) were added to an oven-dried round-bottom flask with 2 mL DMF. Then DIPEA (0.0403 mL, 0.23132 mmol, 6 eq) was added,

and the reaction was stirred at room temperature overnight. The reaction was concentrated *in vacuo*, then was loaded on silica gel for purification by flash chromatography (5% → 7.5% → 10% MeOH in DCM) to yield compound **SNAP-PEG3-CH5**, which was concentrated and further purified by high-performance liquid chromatography (40% → 70% over 20 mins → 100% over 15 mins MeCN in H_2O + 0.05% FA) to yield pure **SNAP-PEG3-CH5** (0.0063 g, 13%). ^{1}H NMR (400 MHz, $CDCl_3$) δ (ppm): 8.27 (s, 1 H), 7.38 – 7.29 (m, 6 H), 7.12 - 7.11 (m, 2 H), 6.97 – 6.95 (m, 2 H), 6.83 (s, 1 H), 6.64 – 6.62 (d, 1 H), 6.55 (s, 1 H), 5.31 (s, 2 H), 4.46 (s, 2 H), 3.77 – 3.520 (m, 28 H), 2.85 – 2.72 (m, 22 H), 2.59 – 2.53 (m, 6 H), 2.06 (s, 3 H), 1.27 – 1.25 (m, 6 H). LRMS calcd. for $C_{64}H_{88}ClN_7O_{10}S_4$ (M+H) 1278.5, found 1278.4.

Synthesis of HALO-CF5

(13) Compound **(9-F)** (0.025 g, 0.0333 mmol, 1 eq) was added with Cs_2CO_3 (0.04344 g, 0.1333 mmol, 4 eq) and KI (0.01106 g, 0.066 mmol, 2 eq) to 1 mL DMF, then *t*-butyl bromoacetate (0.0196 mL, 0.1333 mmol, 4 eq) was added in 2 mL DMF. This was stirred at 35 ºC overnight. The reaction was poured into 150 mL brine, then the organic layer was extracted with 50 mL EtOAc x 3. The organic layer was washed with brine, dried with Na_2SO_4 then concentrated *in vacuo*. Crude concentrate was loaded on silica gel for purification by flash column chromatography (0 → 10% MeOH in DCM) to yield compound (**13**), which was carried on without further purification. ^{1}H NMR (400 MHz, $CDCl_3$) δ (ppm): 7.91 (s, 1 H), 7.75 – 7.74 (m, 1 H), 6.79 – 6.71 (m, 4 H), 6.53 – 6.52 (d, 1 H), 6.43 (s, 1 H), 3.82 (s, 2 H), 3.50 (m, 2 H), 3.19 (s, 2 H), 2.84 – 2.56 (m, 20 H), 1.48 – 1.43 (m, 9 H), 1.27 – 1.25 (m, 6 H).

(14) Compound **(13)** was dissolved in DCM in an oven-dried round-bottom flask, then TFA was added dropwise and the reaction was stirred for 2 hrs at room temperature. The reaction was concentrated *in vacuo* to yield compound **(14)** (0.0159 g, 60% over 2 steps)

HALO-CF5 2-(2-((6-chlorohexyl)oxy)ethoxy)ethan-1-amine **B** was synthesized following literature procedures.[10] Compound **(14)** (0.0159 g, 0.01968 mmol, 1 eq), **B** (0.0132 g, 0.059 mmol, 3 eq), and HATU (0.0262 g, 0.0689 mmol, 3.5 eq) were added to an oven-dried round-bottom flask with 1 mL DMF. Then DIPEA (0.02057 mL, 0.11808 mmol, 6 eq) was added, and the reaction was stirred at room temperature overnight. The reaction was concentrated *in vacuo*, then was loaded on silica gel for purification by flash chromatography (5% → 7.5% → 10% MeOH in DCM) to yield **HALO-CF5** (0.0068 g, 34%). ^{1}H NMR (400 MHz, $CDCl_3$) δ (ppm): 7.94 (s, 1 H), 7.79 – 7.78 (d, 1 H), 6.85 – 6.82 (m, 4 H), 6.63 – 6.59 (d, 1 H), 6.55 (s, 1 H), 3.84 (s, 2 H), 3.59 – 3.45 (m, 12 H), 3.11 (s, 2 H), 2.84 – 2.56 (s, 24 H), 1.28 (m, 6 H).

Synthesis of HALO-PEG1-CF5

(**15**) diethylene glycol (2.5 g, 2.36 mL, 23.558 mmol, 1 eq) was dissolved in 10 mL DMF then NaH (1.03656 g, 25.914 mmol, 1.1 eq) was added slowly, at 0 ºC. This was stirred for 10 minutes at this temperature with stirring, then was warmed to room temperature. At this point, *t*-butyl bromoacetate (3.8263 mL, 25.914 mmol, 1.1 eq) was added and this was stirred overnight for 16 hours. The reaction was concentrated *in vacuo* to yield compound **(15)**, which was carried on to the next reaction in its crude form (4.4993 g, 87%). Spectra match those values reported in literature[11].

(**16**) Compound (**15**) (4.4993 g, 20.427 mmol, 1 eq) was dissolved in 15 mL DCM at 0 ºC, then TEA (14.2 mL, 102.14 mmol, 5 eq) was added. Tosyl chloride (4.6733 g, 24.513 mmol, 1.2 eq) was taken up in 15 mL DCM and added gradually over 10 minutes at 0 ºC with stirring. At this point, the reaction was allowed to warm to room temperature, then was stirred overnight. The reaction was filtered and washed extensively with DCM. Then the filtrate was concentrated *in vacuo* and this was loaded on silica gel for purification by flash chromatography (0% → 40% EtOAc/Hex) to yield (**16**).

(17) Compound **(9-F)** (0.0225 g, 0.0300 mmol, 1 eq) was added with Cs_2CO_3 (0.0391 g, 0.12 mmol, 4 eq) to 1.5 mL DMF, then (**16**) (0.0337 g, 0.09 mmol, 3 eq). This was stirred at overnight at room temperature. At this point KI (0.01 g, 0.060 mmol, 2 eq) was added and the reaction was stirred for an additional 12 hours at 40 ºC. The reaction was poured into 150 mL brine, then the organic layer was extracted with 50 mL EtOAc x 3. The organic layer was washed with brine, dried with Na_2SO_4 then concentrated *in vacuo*. Crude concentrate was loaded on silica gel for purification by flash column chromatography (0 → 10% MeOH in DCM) to yield compound (**17)** (0.0091 g, 34%).

(18) Compound **(17)** was dissolved in DCM in an oven-dried round-bottom flask, then TFA was added dropwise and the reaction was stirred for 2 hrs at room temperature. The reaction was concentrated *in vacuo* to yield compound **(18)** then was carried on in its crude form.

HALO-PEG1-CF5 Compound **(18)** (0.0091 g, 0.01015 mmol, 1 eq), **B** (0.00682 g, 0.03046 mmol, 3 eq), and HATU (0.01544 g, 0.04062 mmol, 4 eq) were added to an oven-dried round-bottom flask with 1 mL DMF. Then DIPEA (0.0106 mL, 0.06093 mmol, 6 eq) was added, and the reaction was stirred at room temperature overnight. The reaction was concentrated *in vacuo*, then was loaded on silica gel for purification by flash chromatography (0% → 10% MeOH in DCM) to yield **HALO-PEG1-CF5** (0.0052 g, 46.5%). ^{1}H NMR (400 MHz, $CDCl_3$) δ (ppm): 7.92 (s, 1 H), 7.76 – 7.75 (d, 1 H), 6.80 – 6.71 (m, 4 H), 6.55 – 6.53 (d, 1 H), 6.45 (s, 1 H), 4.02 (s, 2 H), 3.82 (s, 2 H), 3.73 – 3.45 (m, 26 H), 2.83 – 2.56 (s, 20 H), 1.27 – 1.25 (m, 6 H).

Synthesis of HALO-PEG1.5-CF5

(**20**) Compound (**19**) (0.300 g, 1.0778 mmol, 0.2852 mL, 1 eq) was dissolved in 3 mL DCM at 0 ºC, then TEA (1.494 mL, 5.389 mmol, 5 eq) was added. Tosyl chloride (0.4932 g, 1.2934 mmol, 1.2 eq) was taken up in 3 mL DCM and added gradually over 10 minutes at 0 ºC with stirring. At this point, the reaction was allowed to warm to room temperature, then was stirred overnight. The reaction was filtered and washed extensively with DCM. Then the filtrate was concentrated *in vacuo* and this was loaded on silica gel for purification by flash chromatography (25% → 50% EtOAc/Hex) to yield **(20)**. This compound was carried out without further purification.

(21) Compound **(9-F)** (0.0225 g, 0.03 mmol, 1 eq) was added with Cs_2CO_3 (0.04886 g, 0.15 mmol, 5 eq) to 1.5 mL DMF, then (**20**) (0.0499 g, 0.12, 4 eq) was added. After 6 hours, additional (**20**) (0.025 g, 2 eq) and Cs_2CO_3 (0.024 g, 2 eq) was added. After 16 hours, the reaction was poured into 150 mL brine, then the organic layer was extracted with 50 mL EtOAc x 3. The organic layer was washed with brine, dried with Na_2SO_4 then concentrated *in vacuo.* Crude concentrate was loaded on silica gel for purification by flash column chromatography (2.5% → 10% MeOH in DCM) to yield compound (**21)** (0.0077 g, 28%). ^{1}H NMR (400 MHz, $CDCl_3$) δ (ppm): 7.91 (s, 1 H), 7.76 – 7.74 (m, 1 H), 7.27- 7.26 (m, 1 H), 6.81 – 6.70 (m, 4 H), 6.54 – 6.51 (d, 1 H), 6.43 (s, 1 H), 3.82 (s, 2 H), 3.73 – 3.60 (m, 15 H), 2.83 – 2.48 (s, 28 H), 1.48 – 1.43 (m, 9 H), 1.28 – 1.24 (m, 6 H).

(22) Compound **(21**) was dissolved in DCM in an oven-dried round-bottom flask, then TFA was added dropwise and the reaction was stirred for 2 hrs at room temperature. The reaction was concentrated *in vacuo* to yield compound **(22)** then was carried on in its crude form.

HALO-PEG1.5-CF5 Compound **(22)** (0.0077 g, 0.0081 mmol, 1 eq), **B** (0.005416 g, 0.02421 mmol, 3 eq), and HATU (0.01227 g, 0.03228 mmol, 4 eq) were added to an oven-dried round-bottom flask with 1 mL DMF. Then DIPEA (0.0084 mL, 0.04841 mmol, 6 eq) was added, and the reaction was stirred at room temperature overnight. The reaction was concentrated *in vacuo*, then was loaded on silica gel for purification by flash chromatography (0% → 10% MeOH in DCM) to yield **HALO-PEG1.5-CF5**. ^{1}H NMR (400 MHz, $CDCl_3$) δ (ppm): 7.95 (s, 1 H), 7.71 – 7.69 (m, 1 H), 7.27- 7.26 (m, 1 H), 6.99 – 6.91 (m, 4 H), 6.822 (m, 2 H), 4.07 (s, 2 H), 3.85 (s, 2 H), 3.64 – 3.35 (m, 26 H), 2.83 – 2.52 (s, 22 H), 1.31 – 1.28 (m, 6 H).

Synthesis of HALO-PEG1-CF5-NS4”

2-(Methylthio)ethane-1-thiol Literature protocol was followed and modified slightly, as described.[8] Briefly, 2-(methylthio)ethan-1-ol (10 g, 108.507 mmol, 1 eq) and thiourea (8.259 g, 108.507 mmol, 1 eq) were added to a round-bottom flask in concentrated HBr, and this solution was refluxed at 120 ºC overnight. After neutralizing, the reaction was concentrated *in vacuo*, and this was carried on to the next step.

NS_4” (**24**) Literature protocol was followed and modified slightly, as described.[8] Briefly, sodium metal (2.807 g, 122.128 mmol), was added slowly to 100 mL EtOH. Then 2-(methylthio)ethane-1-thiol (7.93 g, 73.28 mmol) was added, and this was brought to reflux before adding bis(2-chloroethyl)amine (4.359, 24.426 mmol). This compound was carried on to the next step without further purification.

NS_4" Receptor (**26**) Literature protocol was followed[8]; briefly, compound (**24**) (0.529 g, 1.934 mmol), compound (**25**) (1.103 g, 3.869 mmol), KI (0.6423 g, 3.869 mmol), and K_2CO_3 (0.802 g, 5.803 mmol) were added to 10 mL MeCN. Compound **25** was synthesized as described previously.[9] After concentrating *in vacuo*, crude material was purified on silica by flash column chromatography. ^{1}H NMR (400 MHz, $CDCl_3$) δ (ppm): 7.70 (s, 1 H), 7.65 – 7.64 (d, 1 H), 7.42 – 7.41 (d, 1 H), 3.63 (s, 2 H), 2.73 – 2.64 (m, 16 H), 2.1 (s, 6 H).

(8'') An oven-dried two-neck flask was charged with (**26**) (0.3125 g, 0.5980 mmol, 2 eq) and dry THF then was cooled to -78 °C. A solution of tert-butyllithium in pentane (351.78 µL, 1.7 M, 0.59802 mmol, 2 eq) was then added dropwise under N_2. This was stirred for 8 min at -78 °C, then (7) (0.153 g, 0.29901 mmol, 1 eq) in dry THF was added and allowed to warm to room temperature over 1 hour. After stirring for 1 hour, the reaction was quenched with 2 N HCl and this was stirred for an additional 30 min. Saturated $NaHCO_3$ was added and the organic layer was extracted with EtOAc (× 3) before the combined organic layers were dried over Na_2SO_4 and concentrated *in vacuo*. The concentrate was then loaded on silica gel for purification by flash column chromatography (5% MeOH in DCM) to yield compound (**8')** (0.186 g, 75%). ^{1}H NMR (400 MHz, $CDCl_3$) δ (ppm): 7.92 (s, 1 H), 7.76– 7.74 (d, 1 H), 7.27 – 7.26 (d, 1 H), 6.79 – 6.75 (m, 3 H), 6.70 – 6.68 (m, 1 H), 6.54 – 6.53 (dd, 1 H), 6.43 – 6.42 (d, 1 H), 3.82 (s, 2 H), 3.61 – 3.59 (m, 4 H), 3.45 – 3.44 (m, 4 H), 2.84 – 2.68 (m, 16 H), 2.13 (s, 6 H), 1.49 (s, 9 H).

(9'') Compound (**8''**) (0.185 g, 0.2562 mmol, 1 eq) was dissolved in 0.7 mL DCM, at which point 0.4 mL trifluoroacetic acid was added; this was stirred at room temperature for 1.5 hours. At this point, 1 mL water was added and stirred for 10 minutes, then poured into saturated $NaHCO_3$, extracted with EtOAc (× 3), washed with brine, then dried over Na_2SO_4 and filtered before concentrating *in vacuo*. The concentrate was then loaded on silica gel for purification by flash column chromatography (6% → 7.5% MeOH in DCM) to yield compound (**9''**) (0.1003, 60 %).

(**27**) Compound **(9'')** (0.0367 g, 0.05083 mmol, 1 eq) was added with Cs_2CO_3 (0.06625 g, 0.20332 mmol, 4 eq) to 2 mL DMF, then (**16**) (0.0476 g, 0.1271 mmol, 2.5 eq). This was stirred at overnight at 35 ºC. The reaction was poured into 150 mL brine, then the organic layer was extracted with 50 mL EtOAc x 3. The organic layer was washed with brine, dried with Na_2SO_4 then concentrated *in vacuo*. Crude concentrate was loaded on silica gel for purification by flash column chromatography (0 → 3% MeOH in DCM) to yield compound (**17**) . ^{1}H NMR (400 MHz, $CDCl_3$) δ (ppm): 7.92 (s, 1 H), 7.76– 7.74 (d, 1 H), 6.79 – 6.72 (m, 4 H), 6.54 – 6.52 (dd, 1 H), 6.43 (d, 1 H), 4.03 (s, 2 H), 3.83 (m, 2 H), 3.714 – 3.68 (m, 6 H), 3.47 (m, 4 H), 2.85 – 2.69 (m, 24 H), 2.14 (s, 6 H), 1.49 (s, 9 H).

(28) Compound **(27**) was dissolved in 0.3 mL DCM in an oven-dried round-bottom flask, then 0.2 mL TFA was added dropwise and the reaction was stirred for 2 hrs at room temperature. The reaction was concentrated *in vacuo* to yield compound **(28)** (0.0015 g, 34% over 2 steps).

HALO-PEG1-CF5-NS4" Compound **(28)** (0.0015 g, 0.01728 mmol, 1 eq), **B** (0.0116 g, 0.05184 mmol, 3 eq), and HATU (0.0263 g, 0.0691 mmol, 4 eq) were added to an oven-dried round-bottom flask with 1 mL DMF. Then DIPEA (0.018 mL, 0.04841 mmol, 6 eq) was added, and the reaction was stirred at room temperature overnight. The reaction was concentrated *in vacuo*, then was loaded on silica gel for purification by flash chromatography (0% → 3.5% MeOH in DCM) to

yield **HALO-PEG1-CF5** (0.004 g, 23%) ^{1}H NMR (400 MHz, $CDCl_3$) δ (ppm): 7.98 (s, 1 H), 7.82 (d, 1 H), 7.30 – 7.26 (d, 1 H), 6.90 – 6.88 (m, 3 H), 6.69 – 6.59 (m, 2 H), 4.07 (s, 2 H), 3.88 (m, 2 H), 3.74 – 3.48 (m, 17 H), 2.88 – 2.74 (m, 14 H), 2.18 (s, 6 H), 1.38 (s, 9 H).

Purification of HaloTag Protein

50 μL BL21(DE) cells were transformed with 1μL pH6HTN His_6HaloTag T7 Vector. 1 L of BL21(DE) cells were grown at 37 °C until an absorbance of 0.6 at 600 nm was reached. At this point, protein growth was induced by adding 0.1 mM IPTG to the culture. The culture was grown for 3 hours, then cells were pelleted by centrifugation, resuspended in 15 mL lysis buffer and lysed by sonication (12 minutes, 30 seconds on/30 seconds off, 50% power). The lysate was centrifuged at 40,000*g* for 1 hour at 4 °C. The clarified supernatant was loaded onto a metal chelating Sepharose column charged with nickel ions (4 mL resin) after pre-equilibrating with 4 CVs (column volumes) of binding buffer (binding buffer = 50 mM Tris, 300 mM NaCl, 10 mM imidazole). The clarified lysate was loaded onto the column and this was washed with 4 CVs of wash buffer (50 mM Tris, 300 mM NaCl, 20 mM imidazole). Protein was then eluted in 4 CVs elution buffer (50 mM Tris, 300 mM NaCl, 500 mM imidazole) and pure fractions were pooled and collected, then frozen and stored at -80 ºC.

Wash-out Studies

U2OS cells were used for SNAP-PEG3-CH5 studies. The U2OS cell line was chosen because the UC Berkeley Cell Culture facility has U2OS cells that stably express SNAP protein. If preliminary studies looked promising, we envisioned testing our dye in these stable cell lines.

Cells were incubated with 2 μM probe for 15 minutes. After 15 minutes, DMEM media was removed, and this was replaced with fresh, pre-warmed DMEM media. Cells were imaged, then media was exchanged with fresh DMEM media. After 10 minutes, cells were imaged (wash 1). This was repeated two more times (media is exchanged then cells are imaged after 10 minutes to yield results for washes 2 and 3).

Wash-out for HALO series was assessed in HEK 293T cells. Cells were incubated with 1 μM probe for 15 minutes. After 15 minutes, DMEM media was removed, and this was replaced with fresh, pre-warmed DMEM media. Cells were imaged, then media was exchanged with fresh DMEM media. After 15 minutes, cells were imaged (wash 1). This was repeated three more times (media is exchanged then cells are imaged after 15 minutes to yield results for washes 2, 3, and 4).

HaloTag Protein Labeling Studies

For in-gel fluorescence experiments, 100 μL of 2 μM protein in buffer (50 mM HEPES, 5% glycerol, 20 mM imidazole) was treated with 1 equivalent of HALO-PEG1-CH5-NS4'' probe (from a 1 mM stock solution). This was incubated for 30 minutes at 37 ºC. Then 4x LDS loading dye (containing 1% beta-mercaptoethanol) was added and samples were boiled for 15 mins before running on an SDS-PAGE gel. Gel was visualized on a Gel Doc Imager, using Rhodamine fluorescence settings.

For fluorescence experiments, 2 μM protein (in 300 μL total volume) was incubated with HALO-PEG1-CH5-NS4'' probe (1 μL of 1 mM stock solution) for 30 minutes at 37 ºC. This was then concentrated to a volume of 50 μL using a 10K spin filter. In addition to concentrating protein, this filter should remove unbound probe from solution. Protein labeling was verified by ESI-MS (at the QB3 facility). The same protocol was used for preparing labeled protein for Cu+ fluorescence turn-on studies.

Cu+ Fluorescence Studies for Halotag Protein-Probe Conjugate

Buffer (PBS, pH 7.4) was deoxygenated by bubbling a stream of N_2 for 30 minutes. A 2 mM stock solution of probe was prepared in DMSO, and this stock was added to buffer to yield a final concentration of 2 μM probe. Cu+ was added to the buffered solution from a 2 mM Cu+ stock prepared by dissolving $Cu(MeCN)_4PF_6$ in MeCN to yield a final concentration of 2 μM Cu+. The solution was allowed to equilibrate for 3 minutes before taking a fluorescence measurement. All probes in the HALO-CF5 series were excited at 525 nm (abs. max.) and emission was collected from 535 nm to 650 nm (em. max. at 540 nm).

A1.3. Results and Discussion

A1.3.1. Initial efforts using SNAP-tag technology

We initially set out to synthesize a Cu^+-responsive dye appended to a SNAP-tag ligand, as we found previous success applying the SNAP-tag labeling strategy for subcellular detection of H_2O_2.[3] While previous attempts to use Cu^+-responsive dyes appended to a SNAP-tag ligand were unsuccessful due to probe hydrophobicity, we hypothesized that the addition of a long PEG chain could increase the hydrophilicity of the copper dye. Hydrophobicity precludes wash out of unbound dye from cells; we envisioned that the addition of a PEG3 chain could assist in wash out of unbound dye. Towards this end, we synthesized SNAP-PEG3-CH5 from intermediate **9** (Scheme A1.1 and A1.2). We developed a robust synthesis to intermediate **9** – a hydrophilic, rhodol synthon. In addition to its application in genetically-encoded targetable Cu^+-sensor strategies, the synthon can be used for a number of applications, including small-molecule targetable strategies for Cu^+. The presence of the piperidine moiety results in a modular intermediate, as the piperidine amine can participate in nucleophilic or amide-coupling chemistry.

We were able to synthesize SNAP-PEG3-CH5 (Scheme A1.3) from **9**. With SNAP-PEG3-CH5 in hand, we tested the *in vitro* response of this probe to Cu^+. SNAP-PEG3-CH5 exhibits an absorption maximum at 515 nm, an emission maximum at 530 nm, and a 4-fold turn-on to 1 eq Cu+ in PBS (pH 7.4). Given this turn-on response, we next assessed this probe in cells – first assessing the staining pattern in cells without transfection of the SNAP protein. We found that SNAP-PEG3-CH5 exhibits punctate localization in all cell types tested, including HeLa, U2OS (Figure A1.1) and HEK 293T cells. This localization pattern is problematic for a fusion protein application; SNAP-fusion proteins can only be labelled with SNAP-ligand if the ligand is present in the same location as the fusion protein. Given that we are interested in staining proteins in a variety of organelles, we hypothesized that this punctate localization would preclude labeling in other cellular locales. We rationalized that the punctate localization observed was potentially due to the fact that this dye can form micelle-like structures due to the presence of a hydrophobic, aromatic dye core (CH5) and hydrophobic, aromatic ligand (SNAP-tag ligand) in contrast to the hydrophilic PEG3 linker moiety. We next assessed whether unbound probe could be washed out of non-transfected cells. For use in fusion protein applications, unbound probe must either be easily washed out of cells or must be non-fluorescent to ensure signal-to-noise is high. We found that SNAP-PEG3-CH5 was difficult to remove from cells. In fact, fluorescence intensity remains essentially unchanged after four exchanges of media. This is in contrast to probe (**9-H**), which exhibited ~30% in fluorescence intensity after three media exchanges (Figure A1.2). Given these results, we decided to pursue a new strategy based on the HaloTag ligand technology.[2]

A1.3.2. Design of a modular synthetic route for targetable HaloTag Cu^+ sensors

Based on the observed punctate localization of SNAP-PEG3-CH5 and the hypothesis that this could be due to the presence of two aromatic, hydrophobic moieties separated by a hydrophilic linker, we envisioned using the HaloTag ligand technology[2] instead of the SNAP-technology. Because the HaloTag ligand is a PEG-containing alkane-chloride ligand, we hypothesized that appending a HaloTag ligand to our aromatic Cu^+-responsive dye would not cause micelle formation and aggregation – this is in contrast to the SNAP ligand, which it itself π-conjugated and could thus lend itself to further dye aggregation that leads to puncta formation. In switching from SNAP-tag to HaloTag targeting ligand, we made an additional modification to the probe scaffold. Namely, the methyl group on the pendant fluorophore aryl ring was substituted with a trifluoromethyl group, as this modification was found to increase turn-on response to Cu^+.[9] We developed a modular synthetic route to Cu^+-responsive dyes containing the HaloTag-ligand through the hydrophilic rhodol **9**. In developing a small library of dyes containing the HaloTag-ligand, we made compounds with different PEG-linker lengths and additionally altered the Cu-specific receptor moiety (Scheme A1.1). The synthesis of these compounds proceeds through a similar strategy – the HaloTag ligand can be appended to the Cu^+-responsive dye through a PEG-linker (Figures A1.4 – A1.7). In an attempt to reduce hydrophobicity of the NS_4' receptor, we removed two methylene carbons from the receptor of HALO-PEG1-CF5-NS4'' (Scheme A1.7).

A1.3.3. Wash out studies using various Cu^+ sensors in non-transfected HEK 293T cells

With our small library of HaloTag-ligand Cu^+ sensors in hand, we first assessed staining pattern and washout of unbound dye *in cellulo*. Based on previous results (unpublished) and our results with SNAP-PEG3-CH5, we found that these two parameters are difficult to predict based on probe structure alone but are essential in determining whether or not the targetable probe will work to report on subcelluar Cu^+. With HALO-CF5, HALO -PEG1-CF5, HALO-PEG1.5-CF5, and HALO-PEG1-CF5-NS4'' in hand, we were able to comprehensively assess how alterations in PEG chain length affected dye washout. In contrast to SNAP-PEG3-CH5, the HaloTag series of dyes exhibited well-distributed cytosolic staining and could be washed out of cells (Figures A1.3A and B). HALO-PEG1-CF3 and HALO-PEG1-CF3-NS4'' exhibited the best cellular wash out of the series. Based on this data, and the fact that the HALO-PEG1-CF3-NS4'' probe is slightly less hydrophobic, we moved forward to test HALO-PEG1-CF3-NS4'' in protein binding and Cu+ turn-on assays.

A1.3.4. Confirmation of HaloTag labeling and Cu^+-response in vitro

Given that the Halo-CF5 dye series exhibited even staining patterns *in cellulo* and showed suitable washout, we next sought to confirm probe binding to purified HaloTag protein. HaloTag protein was expressed in BL21DE cells and purified as described in the Methods section, using standard Ni-NTA purification techniques. The first attempt at purifying HaloTag protein resulted in the presence of two proteins at similar molecular weight. Unsure of the identity of the second protein band, we attempted an alternate purification, in which we increased imidazole concentration during elution from Ni-NTA column. This modification to purification protocol was able to remove the second truncated band in the gel (Figure A1.4). Before proceeding, we confirmed the identity of this protein by ESI-MS (Figure A1.5A), finding a mass of 39.995 kDa. This mass corresponds to HaloTag protein, as purified directly from *E. Coli* transfected with Promega pH6HTN His_6HaloTag T7 Vector. With purified protein in hand, we were able to confirm that protein is labeled by Halo-CF5, Halo-PEG1-CF5, and Halo-PEG1.5-CF5 probes. We

confirmed this both through in-gel fluorescence experiments (data not shown) and through ESI-MS (Figure A1.5B).

After verifying binding of each of the series of probes to purified HaloTag protein, we were eager to test turn-on response of HaloTag probes to Cu^+ both unbound and bound to purified HaloTag protein. The HALO-CF5 scaffold exhibits an absorption maximum at 525 nm and an emission maximum of 540 nm. We found that HaloTag probes exhibited between a 2- and 4-fold turn-on to one equivalent of Cu^+ in PBS (pH 7.4) the absence of purified protein (Figure A1.6). However, HALO-PEG1-CF5-NS4'' bound to HaloTag protein exhibits a decrease in fluorescence upon addition of one equivalent of Cu^+ (Figure A1.6). This decrease is observed in a variety of buffers, so does not appear buffer dependent. Moreover, hypothesizing that the observed quenching could be due to Cu^+ binding to the His_6-tag present on the HaloTag protein, we performed two separate experiments in which we pre-treated HaloTag protein with one equivalent of Ni^{2+} or with one equivalent of Zn^{2+} to saturate the His_6-tag. In both cases, we still observed no fluorescence turn-on to Cu^+, even when His_6-tag was bound by another metal.

With the above results in hand, we pursued preliminary cell studies on HEK 293T cells transfected with HaloTag plasmid, labeled with probe, and subsequently treated with Cu^+ or chelator. These results were not promising i.e. we saw little change in fluorescence in cells treated with Cu^+ and chelator (data not shown). Based on these results and the quenching observed following Cu^+-treatment *in vitro*, we did not pursue this direction further.

A1.4. Conclusion

In summary, we developed a series of targetable probes for interrogating Cu^+ based on a HaloTag ligand strategy. We ultimately found that when bound to HaloTag protein, probes from this series no longer exhibit a turn-on to Cu^+ but rather show a fluorescence turn-off. We hypothesize this could be due quenching arising from a potential interaction between protein and probe. Based on this result, we plan to utilize a reaction-based strategy for development of targetable- Cu^+ probes. This is in contrast to the chelation-based strategy discussed in this appendix.

Figures

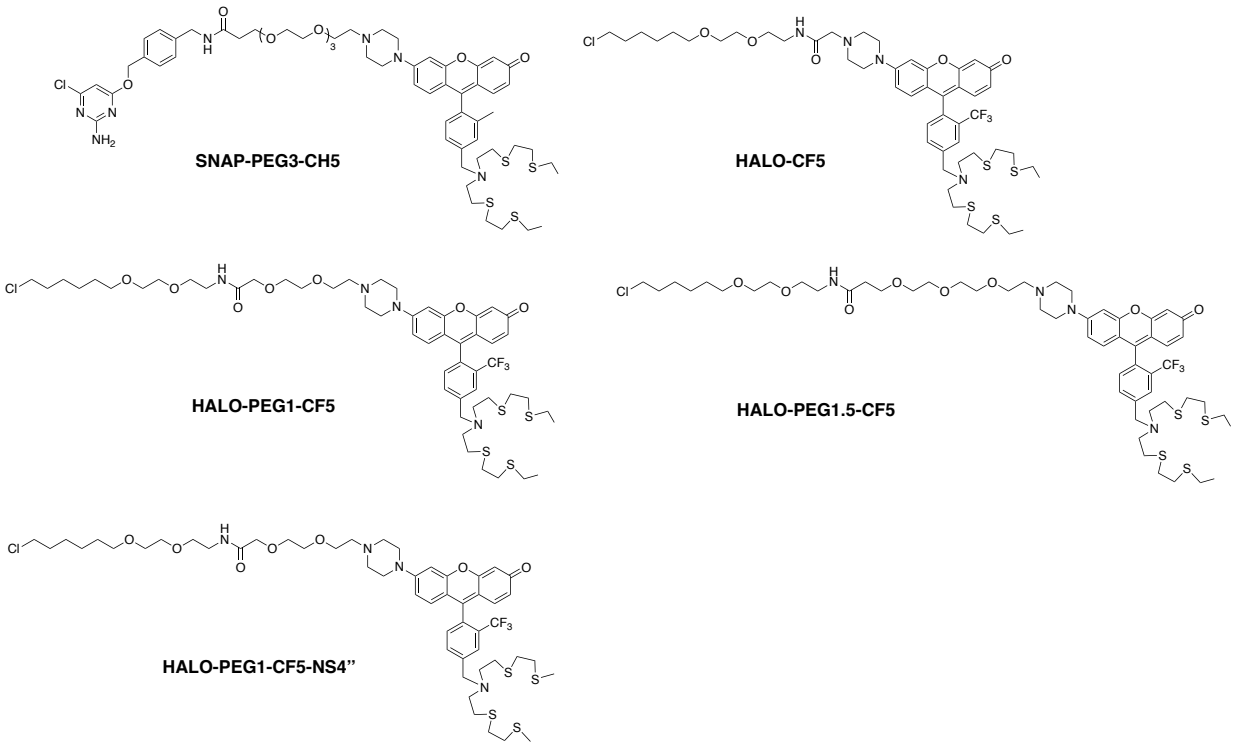

Scheme A1.1. A series of targetable Cu^{+} sensors was synthesized. These include sensors containing both the SNAP-tag and the HaloTag ligands.

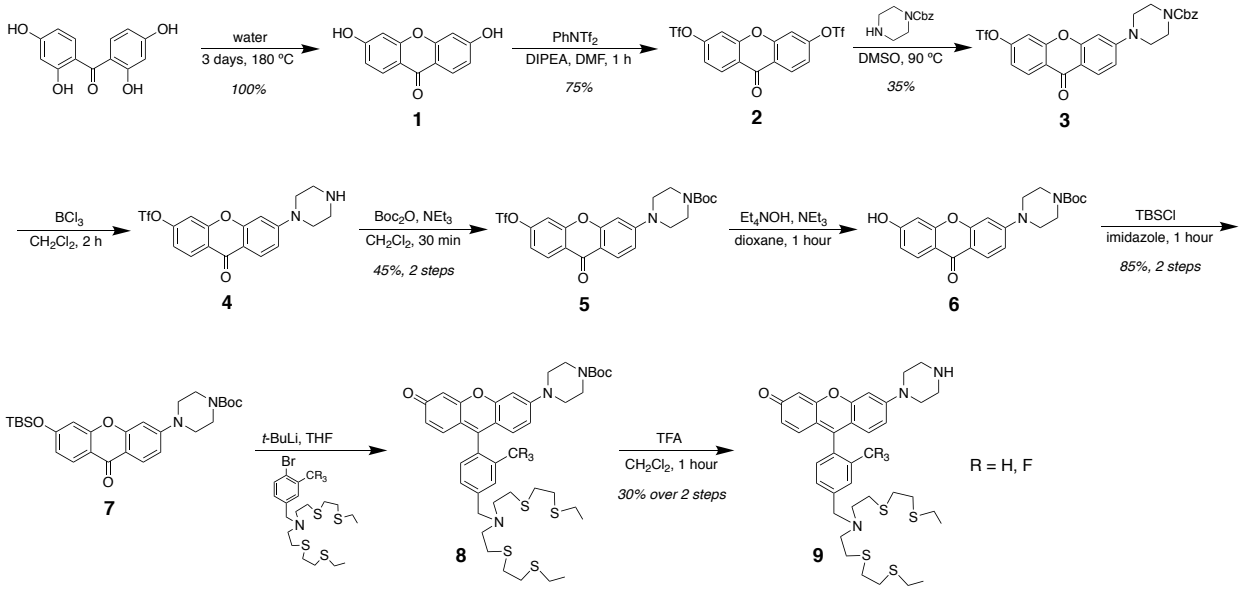

Scheme A1.2 Synthesis of intermediate **9**. This intermediate served as the precursor for a number of the targetable probes synthesized in this Appendix.

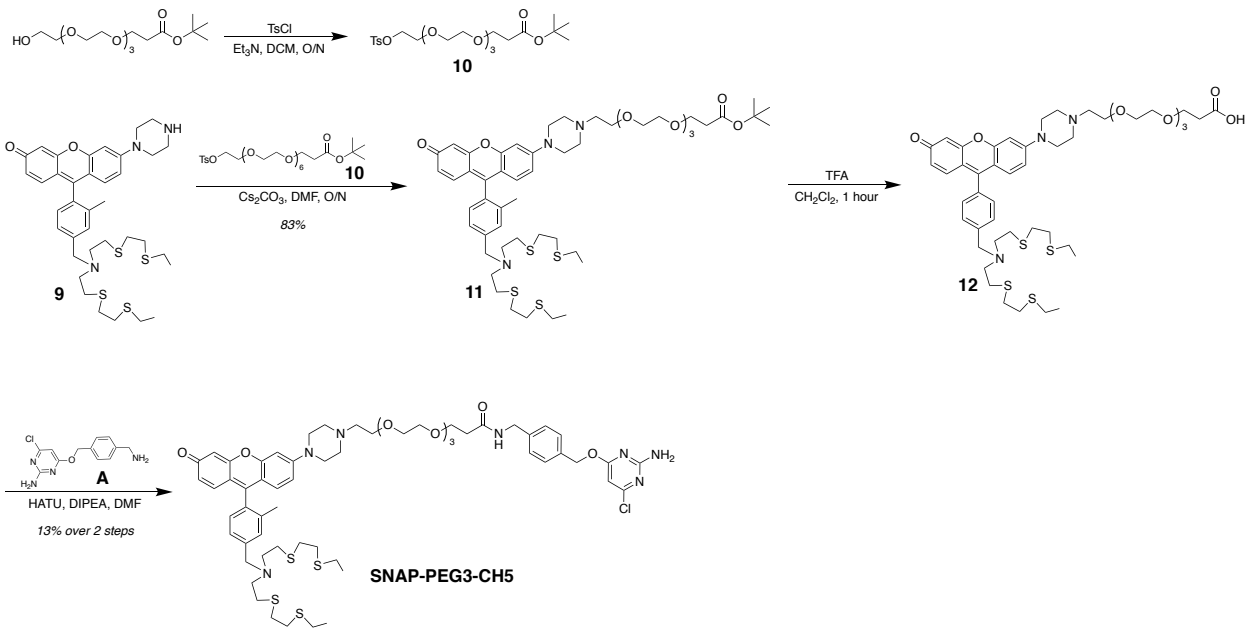

Scheme A1.3. Synthesis of SNAP-PEG3-CH5 probe, from intermediate **9-H** and PEG3 precursor.

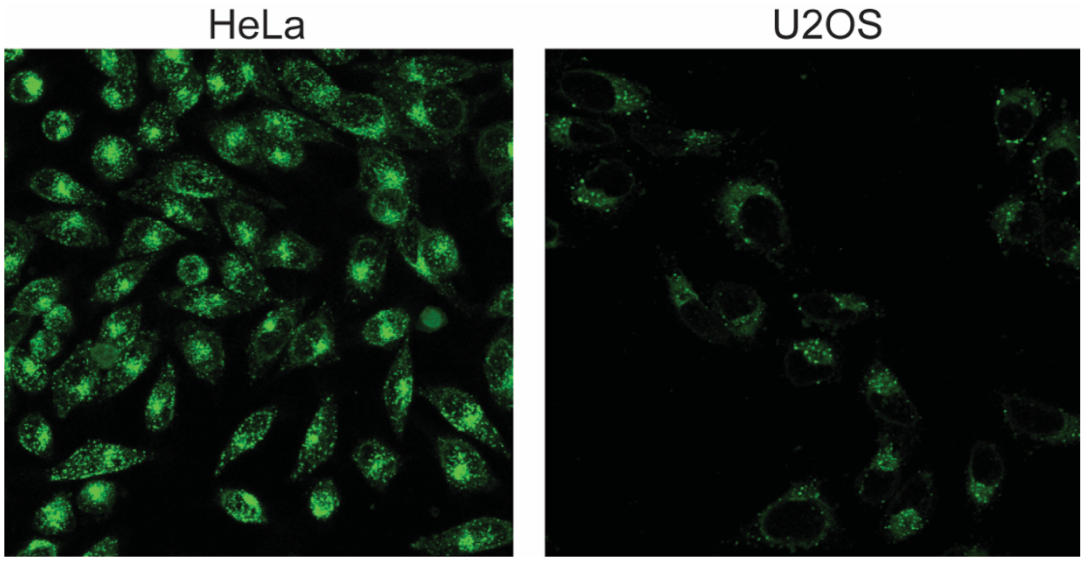

Figure A1.1. SNAP-PEG3-CH5 shows punctate distribution in HeLa and U2OS cells.

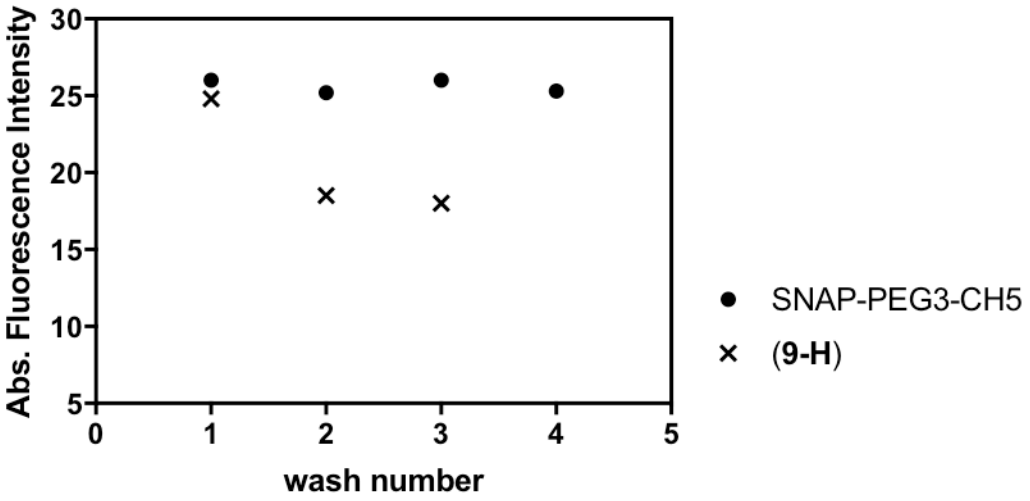

Figure A1.2. Assessing cellular washout of SNAP-PEG3-CH5 versus intermediate (**9-H**) probe in U2OS cells. Unbound SNAP-PEG3-CH5 cannot be readily washed out of cells.

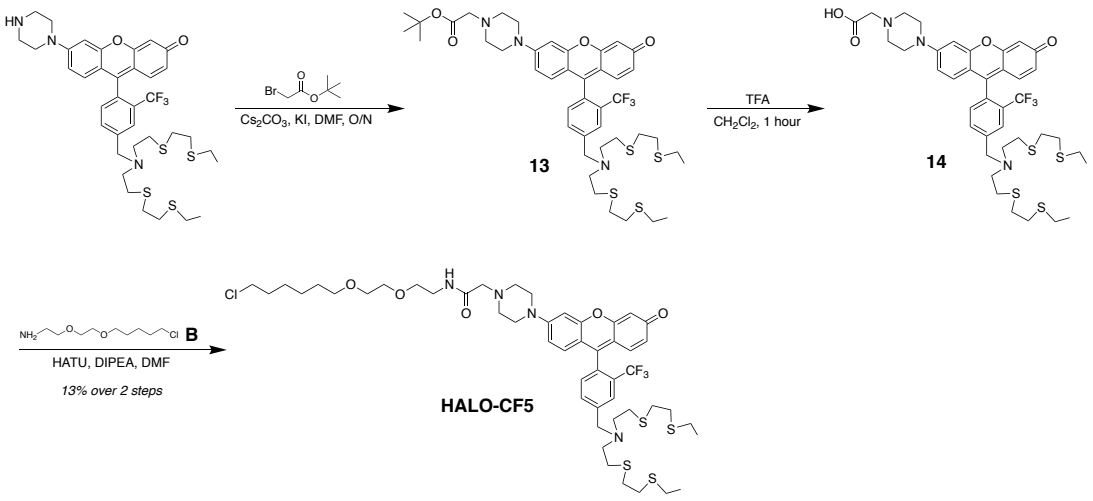

Scheme A1.4. Synthesis HALO-CF5 probe, from intermediate **9-F**.

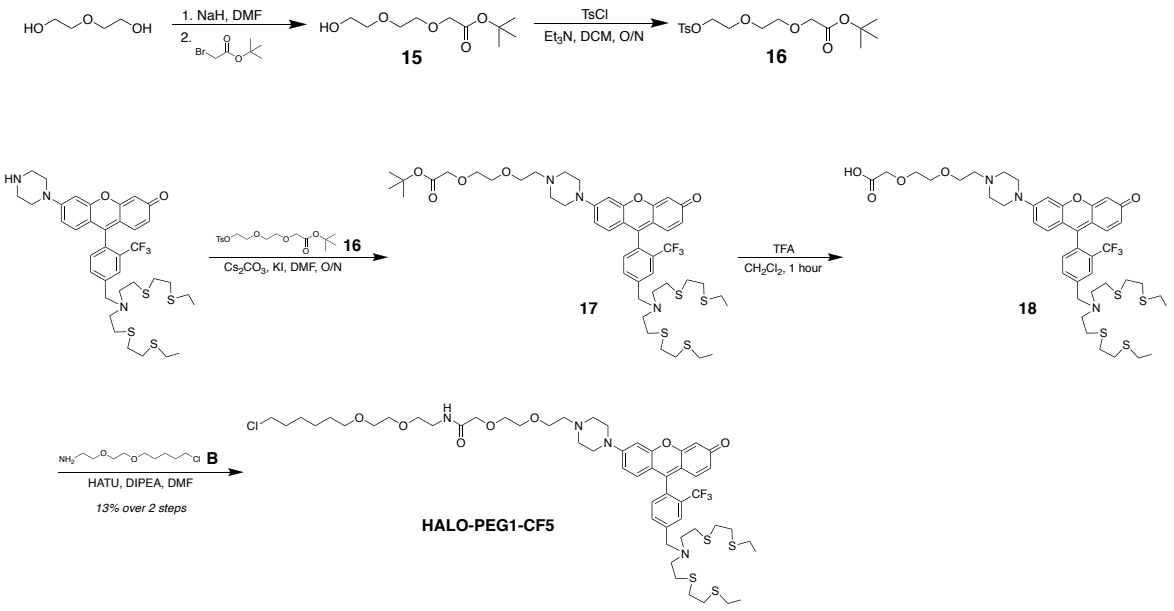

Scheme A1.5. Synthesis HALO-PEG1-CF5 probe, from intermediate **9-F**.

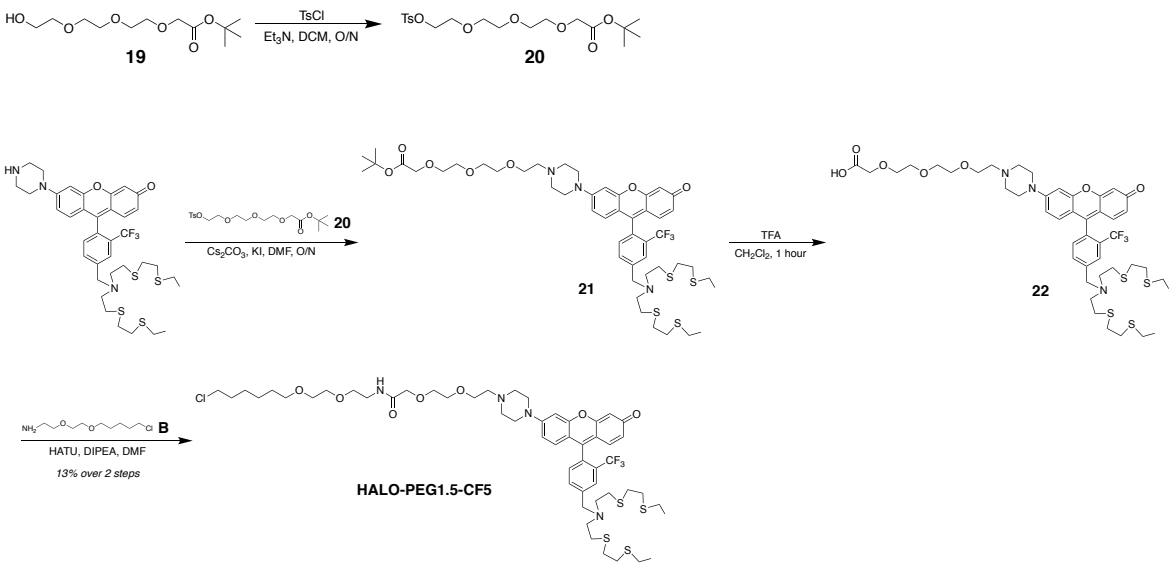

Scheme A1.6. Synthesis HALO-PEG1.5-CF5 probe, from intermediate **9-F**.

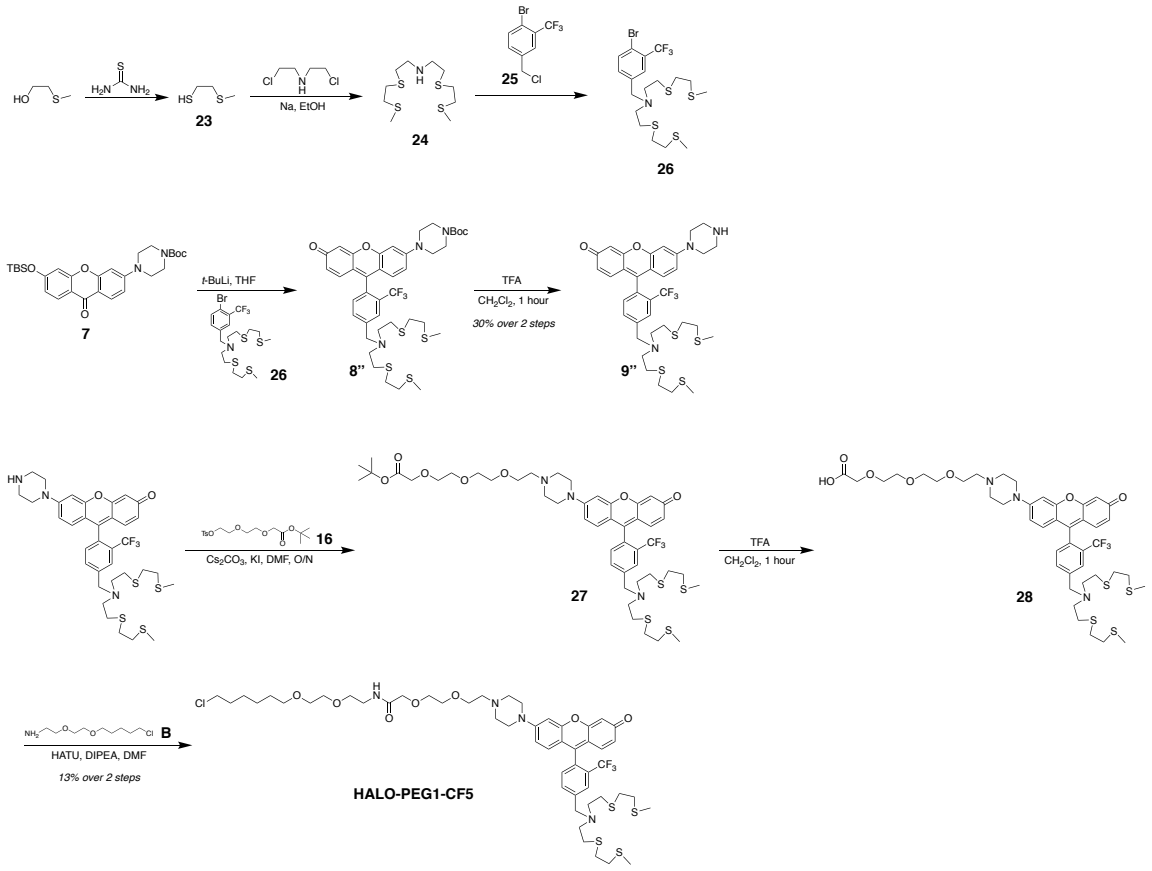

Scheme A1.7. Synthesis HALO-PEG1-CF5-NS4'' probe, from intermediate **9''**.

(a)

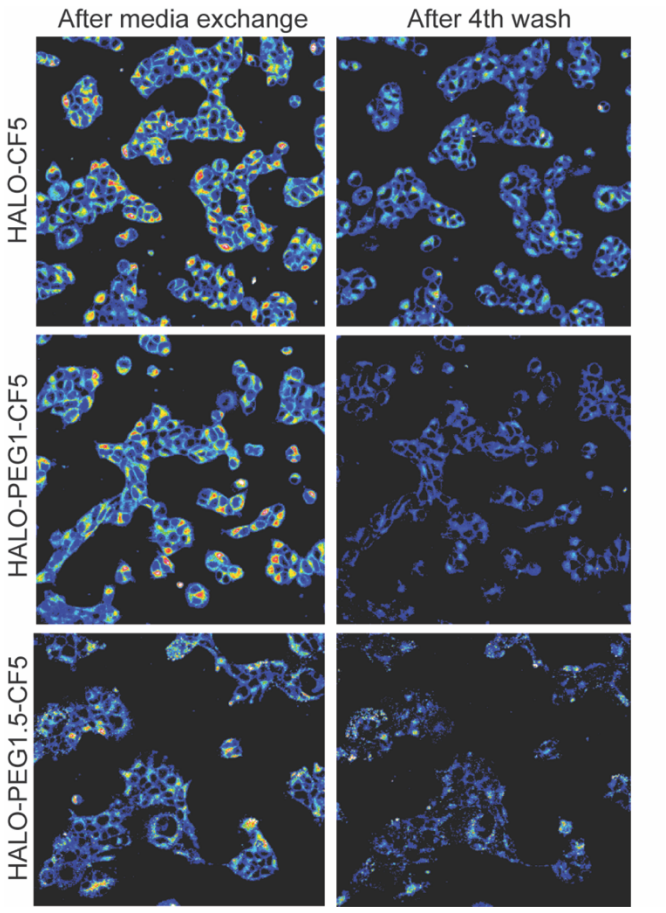

(b)

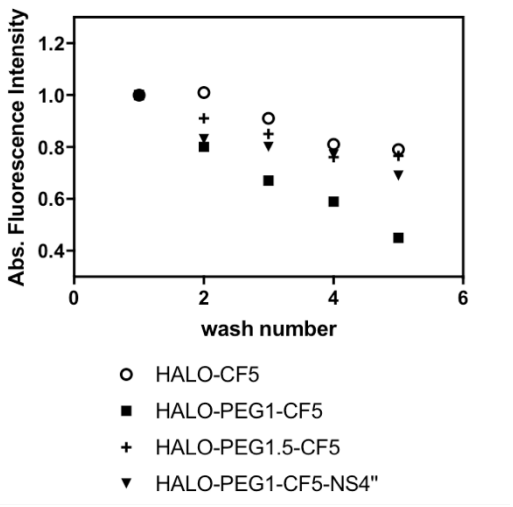

Figure A1.3. (a) Confocal microscopy of 1 μM HaloTag probe (HALO-CF5, HALO-PEG1-CF5, or HALO-PEG1.5-CF5) in HEK 293T cells immediately after media exchange or after 4 washes. (b) Absolute Fluorescence Intensity after each wash for HALO-CF5, HALO-PEG1-CF5, HALO-PEG1.5-CF5, or HALO-PEG1-CF5-NS4'' probe.

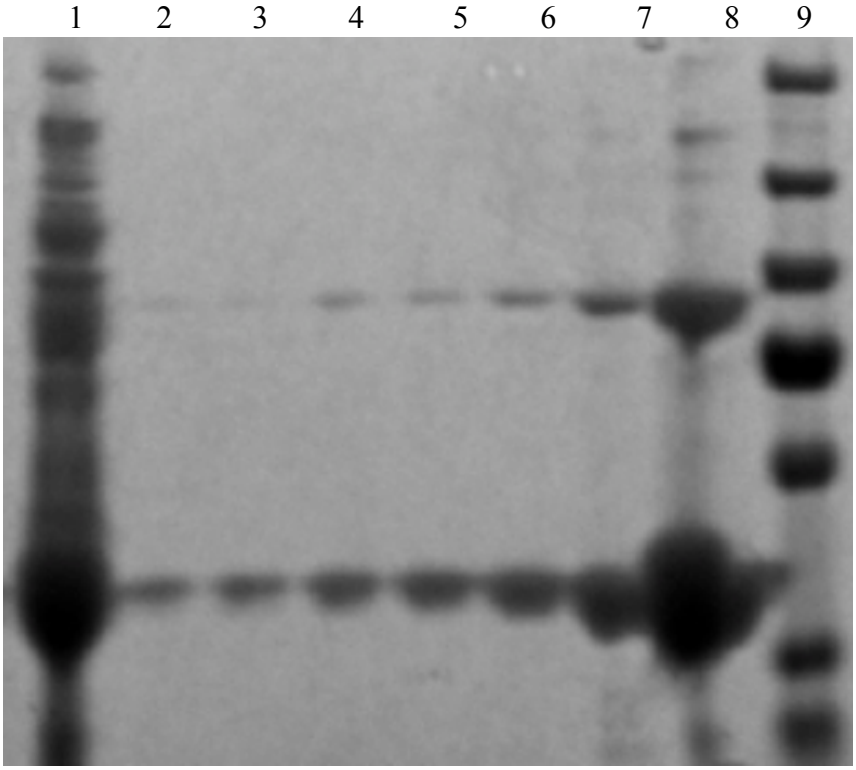

Figure A1.4. HaloTag protein purification gel. Lane 1 is cell extracts, lanes 2 – 8 are fractions 7 – 1, lane 9 is the protein ladder.

(a)

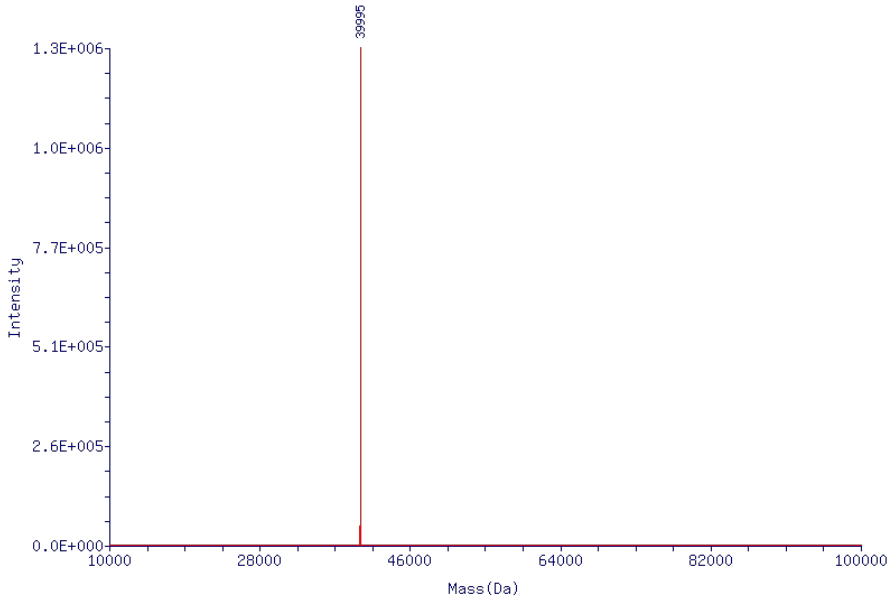

(b)

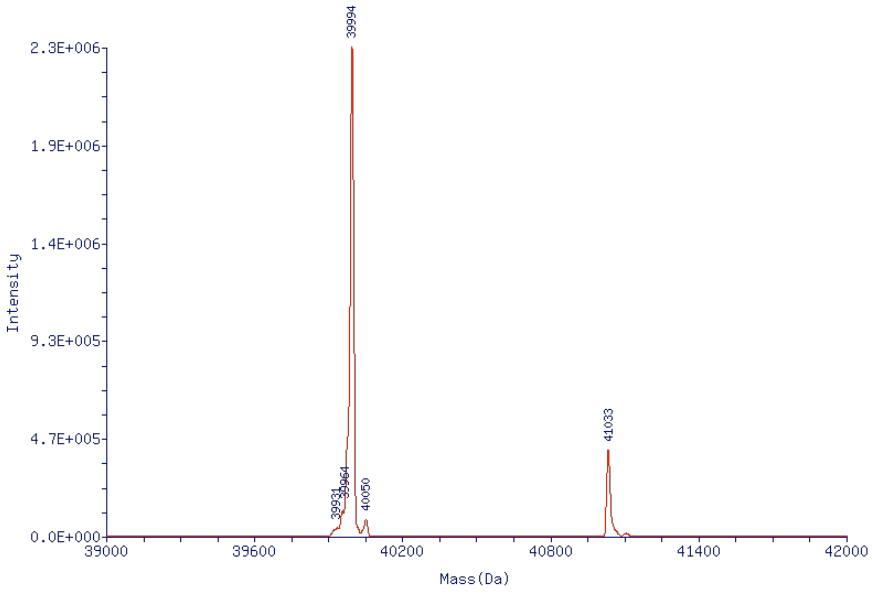

Figure A1.5. (a) ESI-MS of purified HaloTag protein. (b) ESI-MS of purified protein treated with HALO-PEG1-CH5-NS4'' shows that HaloTag protein has been modified by the probe.

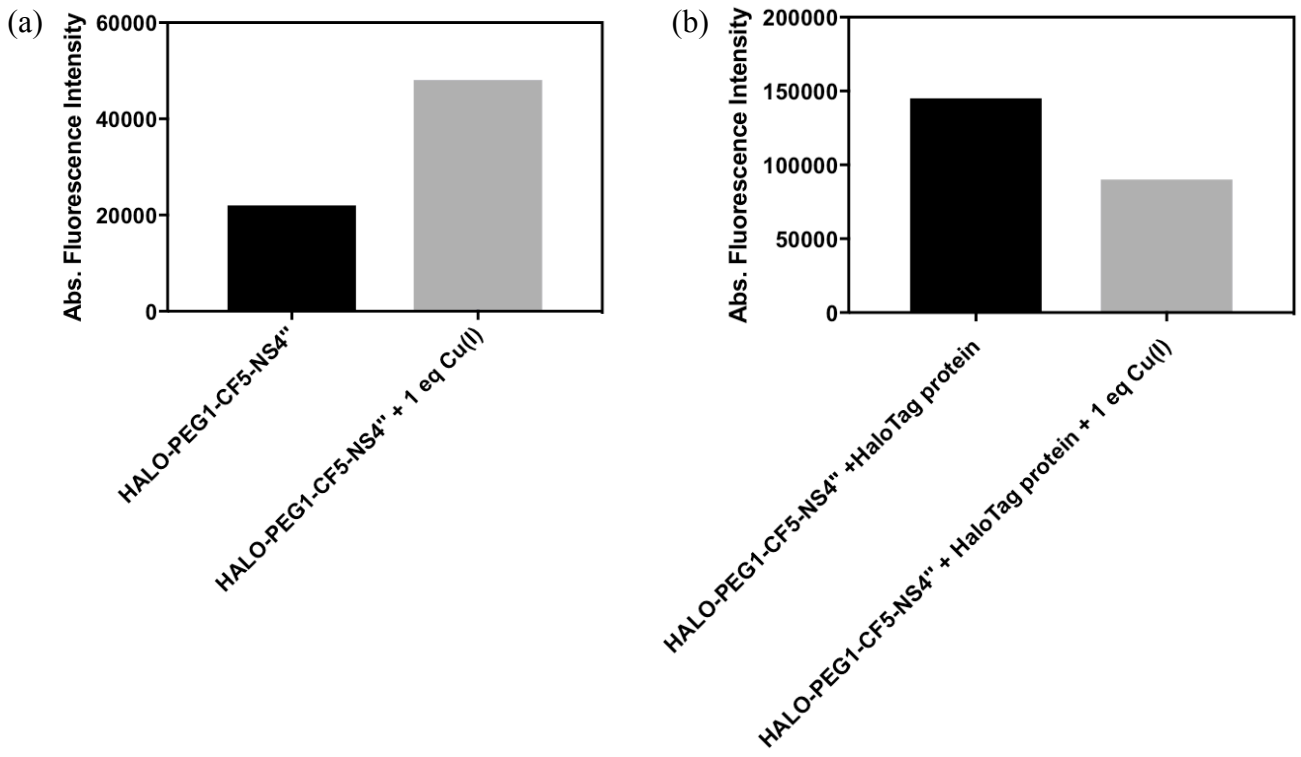

Figure A1.6. Response to 1 equivalent Cu^{+} of (a) HALO-PEG1-CF5-NS4'' and (b) HALO-PEG1-CF5-NS4'' bound to HaloTag protein. Absolute fluorescence intensity is measured at 540 nm.

A1.5. References

1. Gautier, A.; Juillerat, A.; Heinis, C.; Corrêa, I. R. J.; Kindermann, M.; Beaufils, F.; Johnsson, K., An Engineered Protein Tag for Multiprotein Labeling in Living Cells. *Chemistry & Biology* **2008,** *15* (22), 128-136.
2. Los, G. V.; Encell, L. P.; McDougall, M. G.; Hartzell, D. D.; Karassina, N.; Zimprich, C.; Wood, M. G.; Learish, R.; Ohana, R. F.; Urh, M.; Simpson, D.; Mendez, J.; Zimmerman, K.; Otto, P.; Vidugiris, G.; Zhu, J.; Darzins, A.; Klaubert, D. H.; Bulleit, R. F.; Wood, K. V., HaloTag: a novel protein labeling technology for cell imaging and protein analysis. *ACS Chem Biol* **2008,** *3* (6), 373-382.
3. Srikun, D.; Albers, A. E.; Nam, C. I.; Iavarone, A. T.; Chang, C. J., Organelle-Targetable Fluorescent Probes for Imaging Hydrogen Peroxide in Living Cells via SNAP-Tag Protein Labeling. *J. Am. Chem. Soc.* **2010,** *132*, 4455-4465.
4. Li, D.; Liu, L.; Li, W., Genetic Targeting of a Small Fluorescent Zinc Indicator to Cell Surface for Monitoring Zinc Secretion. *ACS Chem Biol* **2015,** *10* (4), 1054-1063.
5. Matsui, Y.; Funato, Y.; Imamura, H.; Miki, H.; Mizukami, S.; Kikuchi, K., Visualization of long-term Mg2+ dynamics in apoptotic cells using a novel targetable fluorescent probe. *Chem Sci* **2017,** *8*, 8255-8264.
6. Zeng, L.; Miller, E. W.; Pralle, A.; Isacoff, E. Y.; Chang, C. J., A Selective Turn-On Fluorescent Sensor for Imaging Copper in Living Cells. *J. Am. Chem. Soc.* **2006,** *128*, 10-11.
7. Krishnamoorthy, L.; Cotruvo, J. A. J.; Chan, J.; Kaluarachchi, H.; Muchenditsi, A.; Pendyala, V. S.; Jia, S.; Aron, A. T.; Ackerman, C. M.; Vander Wal, M. N.; Guan, T.; Smaga, L. P.; Farhi, S. L.; New, E. J.; Lutsenko, S.; Chang, C. J., Copper regulates cyclic-AMP-dependent lipolysis. *Nat. Chem. Biol.* **2016,** *12*, 586-592.
8. Miller, E. W.; L., Z.; Domaille, D. W.; Chang, C. J., Preparation and use of Coppersensor-1, a synthetic fluorophore for live-cell copper imaging. *Nat. Protoc.* **2006,** *1* (2), 824-827.
9. Dodani, S. C.; Firl, A.; Chan, J.; Nam, C. I.; Aron, A. T.; Onak, C. S.; Ramos-Torres, K. M.; Paek, J.; Webster, C. M.; Feller, M. B.; Chang, C. J., Copper is an endogenous modulator of neural circuit spontaneous activity. *Proc. Natl. Acad. Sci. USA* **2014,** *111* (46), 16280 - 16285.
10. Neklesa, T. K.; Tae, H. S.; Schneekloth, A. R.; Stulberg, M. J.; Corson, T. W.; Sundberg, T. B.; Raina, K.; Holley, S. A.; Crews, C. M., Small-molecule hydrophobic tagging–induced degradation of HaloTag fusion proteins. *Nat. Chem. Biol.* **2011,** *7*, 538-543
11. Mills, A. D.; Yoo, C.; Butler, J. D.; Yang, B.; Verkman, A. S.; Kurth, M. J., Design and synthesis of a hybrid potentiator-corrector agonist of the cystic fibrosis mutant protein F508-CFTR. *Bioorg. & Med. Chem. Lett.* **2010,** *20* (1), 87-91.

Appendix 2

New methods for *in vitro* characterization of fluorescent copper sensors and control sensors

Portions of this work were published in the following:

Dodani, S. C.; Firl, A.; Chan, J.; Nam, C. I.; Aron, A. T.; Onak, C. S.; Ramos-Torres, K. M.; Paek, J.; Webster, C. M.; Feller, M. B.; Chang, C. J., Copper is an endogenous modulator of neural circuit spontaneous activity. *Proc. Natl. Acad. Sci. USA* **2014,** *111*, 16280 - 16285.

A2.1. Synopsis

Our laboratory has developed an extensive panel of Cu^+-responsive dyes (Figure A2.1), ranging from the first-generation Copper Sensor 1 (CS1), to ratiometric (RCS1) and organelle-targeted (Mito-CS1), and more recently to hydrophilic second-generation sensors (CF3) and whole animal (CS790 and CCL-1) probes. In order to sufficiently compare these probes, we envisioned developing new *in vitro* models to more thoroughly assess copper-response in biologically relevant *in vitro* systems. New models include testing fluorescence response to Cu^+ and Cu^+-chelation in the presence of cellular components/models including glutathione, liposomes, and BSA. Additionally, we began testing probe response to Cu^+ and Cu^+-chelation in whole cell lysates. This appendix specifically details the optimization of these *in vitro* assays that were performed on two copper sensors, the hydrophobic Copper Sensor 3 (CS3) and the hydrophilic Copper Fluor-3 (CF3) and their corresponding control dyes (Ctl-CS3 and Ctl-CF3, respectively). This appendix presents the results for CF3 and Ctl-CF3.

A2.2. Methods

A2.2.1. Spectroscopic Materials and Methods.

Milli-Q water was used in the preparation of all aqueous solutions. All spectroscopic measurements were performed in either 20 mM HEPES (pH 7) or in PBS (pH 7.4). Absorption spectra were recorded using a Varian Cary 50 spectrophotometer, and fluorescence spectra were recorded using a Photon Technology International Quanta Master 4 L-format scan spectrofluorometer equipped with an LPS-220B 75-W xenon lamp and power supply, A-1010B lamp housing with integrated igniter, switchable 814 photocounting/analog photomultiplier detection unit, and MD5020 motor driver. Samples for absorption and emission measurements were contained in 1-cm × 1-cm quartz cuvettes with or without septum and sealing caps (1.4-mL or 3.5-mL volume; Starna). Cu^+ was delivered in the form of $[Cu(MeCN)_4][PF_6]$ from a 2 mM acetonitrile stock solution.

A2.2.2. Glutathione competition experiments

All manipulations were carried out in an anaerobic chamber (VAC glovebox, Pd catalyst, atmosphere 10% H2 with N2 balance.) Buffer (20 mM HEPES, pH 7) was deoxygenated on a Schlenk line by freeze-pump-thawing before being brought into the anaerobic chamber. Solutions of 5 mM GSH and 2.5 mM GSSG in anaerobic buffer were prepared using 1 and 2 equivalents of sodium hydroxide (from 1 M deoxygenated stock solution) to maintain pH 7. The stock solutions were mixed to yield the indicated GSH/GSSG concentrations in Semi-micro Septum Cap and Screw Cap Starna Fluorometer cells.

A 2-mM stock solution of probe was prepared anaerobically in deoxygenated DMSO. This stock was added to GSH/GSSG-containing buffer to yield a final concentration of 5 μM CF3 (or Ctrl-CF3). After measuring background fluorescence, a 2-mM Cu^+ stock was prepared by anaerobically dissolving Cu(MeCN)4PF6 in deoxygenated MeCN. Cu^+ was added from this stock solution to the buffered solution for a final concentration of 5 μM. Fluorescence intensity was measured five minutes after Cu^+ addition. Neocuproine was prepared as a DMSO stock at 40 mM and added to final concentration of 400 μM. The fluorescence response of 5μM CF3- Cu^+ and 5 μM Ctrl-CF3-Cu^+ complexes to GSH was determined by pre-forming the CF3-Cu^+ or Ctrl-CS3-Cu+ complex from relevant stock solutions. An initial fluorescence spectrum was obtained,

and subsequent scans were taken 5 min after addition of GSH at 0 mM, 0.01 mM, 0.05 mM, 0.1 mM, 0.5 mM, and 1 mM. Solutions of 10 mM and 100 mM GSH in anaerobic buffer were prepared using 1 and 2 equivalents of sodium hydroxide (from1 M deoxygenated stock solution), respectively, to maintain pH 7.

A2.2.3. Probe Response in the Presence of Liposomes

A 2-mM stock solution of CF3 or Ctrl-CF3 was prepared in DMSO, and this stock was added to buffer to yield a final concentration of 2 μM CF3 or Ctrl-CF3. For experiments using DMPC (1,2dimyrisotyl-sn-glycero-3-phosphocholine) as a model liposome forming agent, a DMPC stock solution (10 mM) was prepared in buffer, and this reagent was added to the buffered solution of CF3 or Ctrl-CF3 to afford final DMPC concentrations of 25 μM, 50 μM, 100 μM, and 200 μM. The CF3/DMPC or Ctrl-CF3/DMPC formulation was allowed to equilibrate for 30 min before a fluorescence spectrum was obtained (λex=534 nm, λem collected from 540 to 700 nm). Cu+ was added to the buffered solution from a 2-mM Cu^+ stock prepared by dissolving $Cu(MeCN)_4PF_6$ in MeCN to yield a final concentration of 2 μM Cu^+. A fluorescence scan was obtained after a 15-min equilibration time period, at which point neocuproine was added from a 40-mM stock solution in DMSO to yield a final concentration of 400 μM.

For experiments with commercial, preformed neutral liposomes of well-defined size (FormuMax, DPPC/CHOL 55:45 mol/mol, 100 nm), liposomes were added to the buffered solution of CF3 or Ctrl-CF3 to afford final liposome concentrations of 50 μM, 100 μM, or 200 μM. The CF3/liposome or Ctrl-CF3/liposome formulation was allowed to equilibrate for 6.5 h before a fluorescence spectrum was obtained (λex=534 nm, λem collected from 540 nm to 700 nm). Cu^+ was added to the buffered solution from a 2-mM Cu^+ stock solution prepared by dissolving Cu(MeCN)4PF6 in MeCN to yield a final concentration of 2 μM Cu^+. A fluorescence scan was obtained after a 15-min equilibration time period, at which point neocuproine was added from a 40-mM stock solution in DMSO to yield a final concentration of 400 μM.

A2.2.4. Probe Response in the Presence of BSA

Buffer (20 mM Hepes, pH 7) was rigorously degassed in cycles of evacuation and refilling on a Schlenk line. A 2-mM stock solution of CF3 or Ctrl-CF3 was prepared in DMSO, and this stock was added to buffer to yield a final concentration of 2 μM CF3 or Ctrl-CF3. A 5% BSA (Fisher Scientific; BP1605-100) stock solution was prepared in buffer and was then added to the buffered solution of CF3 or Ctrl-CF3 to afford a 0.1% BSA solution. The CF3/BSA or Ctrl-CF3/BSA solution was allowed to equilibrate for 90 min before a fluorescence scan was obtained (λex=534nm,λemcollected from 540 to 700 nm). Cu^+ was added to the buffered solution from a 2-mM Cu^+ stock prepared by dissolving $Cu(MeCN)_4PF_6$ in MeCN to yield a final concentration of 2 μM Cu^+. A fluorescence scan was obtained, at which point tris[(ethylthio)ethyl]amine (TEMEA) (1) was added from a 50-mMstock solution in DMSO to yield a final concentration of 100 μM.

A2.2.4. Probe Response in Cellular Lysates

All manipulations were carried out in an anaerobic chamber (VAC glovebox, Pd catalyst, 10% H2 in N2 atmosphere). PBS was deoxygenated on a Schlenk line by freeze−pump−thaw cycles before being brought into the anaerobic chamber. HEK293T cells were cultured as described in Chapter 2 and grown until confluent. Cells were washed three times in cold PBS,

harvested by scraping, and subsequently resuspended in an appropriate amount of PBS. The cells were lysed anaerobically by freeze−pump−thaw cycles and then brought into the anaerobic chamber. These lysates were separated by centrifugation at 7,200×gfor 10 min, after which the supernatant was collected and the pellet was discarded. Protein content was quantified by the Bradford assay, and lysates were diluted to a final protein content of 1 mg/mL. Lysates were added to Semi-micro Septum Cap or Screw Cap Fluorimeter cells (Starna). A 2-mM stock solution of CF3 or Ctrl-CF3 was prepared anaerobically in deoxygenated DMSO and this stock solution was added to cell lysates to give a final probe concentration of 2 μM. A 10-mM Cu^+ stock solution was prepared by dissolving $[Cu(MeCN)_4][PF_6]$ in deoxygenated MeCN, and Cu^+ was added from this stock solution to give final Cu^+ concentrations of 10 μM, 50 μM, and 100 μM. Treated lysates were allowed to equilibrate for 45 min, at which point fluorescence intensity was measured (λ_{ex}=534 nm, λ_{em} collected from 540 to 700 nm). Neocuproine was added (from a 1-mM stock to yield a final concentration of 2 μM) to lysates treated with 100μM Cu^+, and fluorescence intensity was measured.

A2.3. Results & Discussion

Glutathione (GSH) is a major cellular metabolite and abundant ligand for labile copper (apparent K_d = 9 x 10^{-12}, where the major species is a 1:1 Cu:GSH complex).[121] Given that the probes developed in our laboratory bind copper in the presence of GSH, we were curious to assess the ability of two probes, CS3 and CF3, to detect Cu^+ *in vitro* in the presence of of GSH at physiological concentrations (1-5 mM). GSH and GSSG levels were altered according to [GSH] + 2[GSSG] = 5 mM. Higher GSH concentrations attenuate the fluorescence response of CF3 to added Cu^+, suggesting that this probe can compete with GSH to sense Cu^+ within the physiological concentration regime. In contrast, control dye, Ctl-CF3, shows no fluorescence dependence on Cu^+ or GSH. Titration of the pre-formed CF3-Cu^+ complex with the copper chelator neocuproine (Figure A2.2) illustrates that complex formation is reversible and that CF3 exhibits a turn-on response to Cu^+ even in the presence of physiological GSH.

In order to assess whether the fluorescence properties of CF3 differ in the presence of hydrophobic proteins and/or lipid membranes versus aqueous buffer, dyes (and their control counterparts) were tested in the presence of neutral liposomes. Unsurprisingly, a fluorescence enhancement is observed upon the addition of DMPC (1,2-dimyrisotyl-sn-glycero-3-phosphocholine) to CF3 – an effect common for many fluorescent organic compounds. Notable, though, is the fact that CF3 displays a further fluorescence enhancement in response to one equivalent of Cu^+ at DMPC concentrations less than or equal to 200 μM. A decrease in fluorescence is observed when copper-chelator neocuproine is added to this solution. On the other hand, Ctl-CF3 is essentially non-responsive to the presence of liposomes. Moreover, fluorescence enhancement of Ctl-CF3 in the presence of all DMPC concentrations tested (10-200 μM) is minimal and is non-responsive to Cu^+ addition and chelation. Likewise, CF3, but not Ctrl-CF3, is able to reversibly respond to copper and chelation in the presence of model liposomes (Figure A2.3).

We additionally showed that CF3, but not its control counterpart, can reversibly respond to copper in the presence of BSA (as a model protein). CF3 shows a fluorescence enhancement in the presence of 0.1% BSA as compared to aqueous buffer. Likewise, Ctl-CF3 also shows an enhancement to BSA but of less magnitude (Figure A2.4). Importantly, addition of Cu^+ to CF3 in the presence of BSA still results in a turn-on response. This enhancement can be reversed by the addition of TEMEA (a Cu^+-chelator). Ctrl-CF3 is non-responsive to addition of copper or

chelator. We speculate that the observed fluorescent enhancement of CF3 in the presence of 0.1% BSA could be in part due to the fact that BSA can bind metals.

Additionally, we showed that CF3, but Ctl-CF3, reversibly responds to copper and chelation within cell lysates. Lysates include a combination of the chemical components (lipids, proteins, and GSH redox buffer/ligands) described above. This series of experiments show that CF3, but not its counterpart control dye, can respond to Cu^+-addition and chelation in the presence of cellular components. These *in vitro* assays can be used to more accurately assess Cu^+-dependent turn on of Cu^+ sensors.

A2.4. Conclusion

This appendix describes new *in vitro* models for assessing copper-response in biologically relevant *in vitro* systems. These *in vitro* systems include testing fluorescence response to Cu^+ and Cu^+-chelation in the presence of cellular components/models such as glutathione, liposomes, and BSA, and testing response in whole cell lysates. While response of CF3 to Cu^+ and Cu^+-chelation varies based on composition of the model solution, this sensor is still able to sense Cu^+ and chelation in the presence of a variety of biologically-relevant model solutions. These *in vitro* assays can be used to more accurately assess Cu^+-turn on of Cu^+ sensors.

Figures

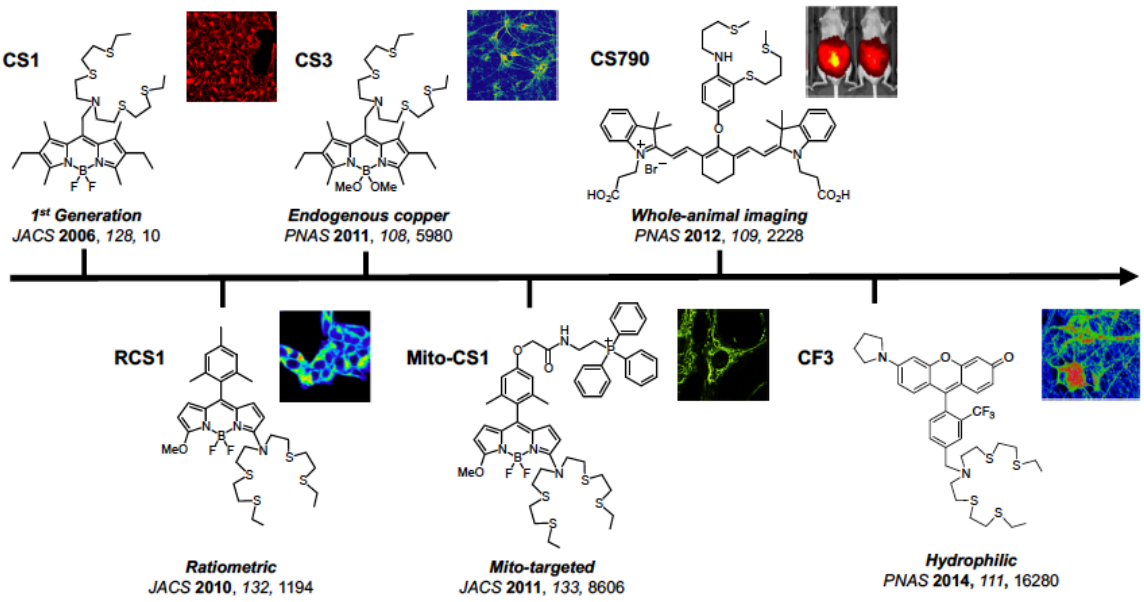

Figure A2.1. Copper probes developed in the Chang laboratory.

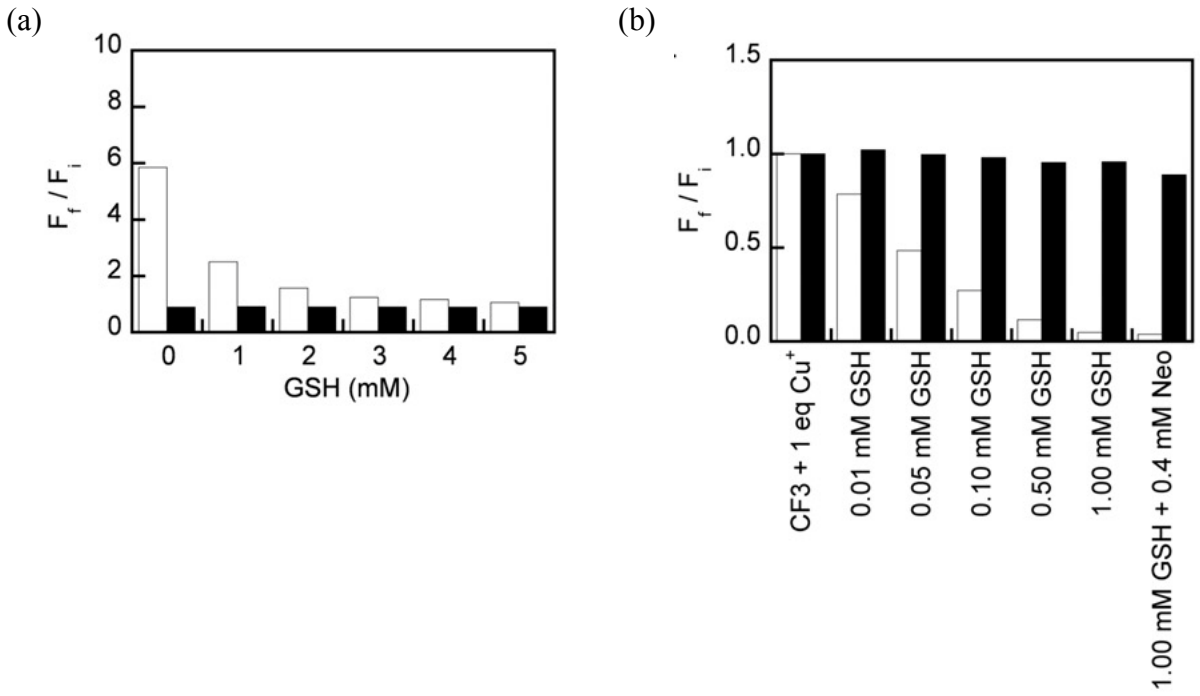

Figure A2.2. (a) Fluorescence response of 5 μM CF3 (white) and Ctrl-CF3 (black) to 5 μM Cu^+ at differing mole ratios of GSH with [GSH] + 2 [GSSG] = 5 mM. Cu^+ was added to the buffer containing GSH/GSSG and CF3 or Ctrl-CF3. Excitation was provided at 534 nm and collected from 540 to 700 nm. Bars represent the final integrated fluorescence response (F_f) over the initial integrated emission (F_i). The data show that higher concentrations of GSH attenuate the fluorescence response of CF3 to added Cu^+, suggesting that CF3 can compete with GSH to sense Cu^+ within physiological concentration regimes. In contrast, Ctrl-CF3 shows no fluorescence dependence on Cu+ or GSH. (b) Fluorescence response of a 5-μM preformed complex of CF3-Cu^+ (white) and 1:1 mixture of Ctrl-CF3 and Cu^+ (black) to GSH (0.01–1 mM) and neocuproine (Neo, 400 μM). Excitation was provided at 534 nm and collected from 540 to 700 nm. Bars represent the final integrated fluorescence response (F_f) over the initial integrated emission (F_i). Titration with the competing GSH ligand demonstrates the reversibility of the CF3- Cu^+ complex.

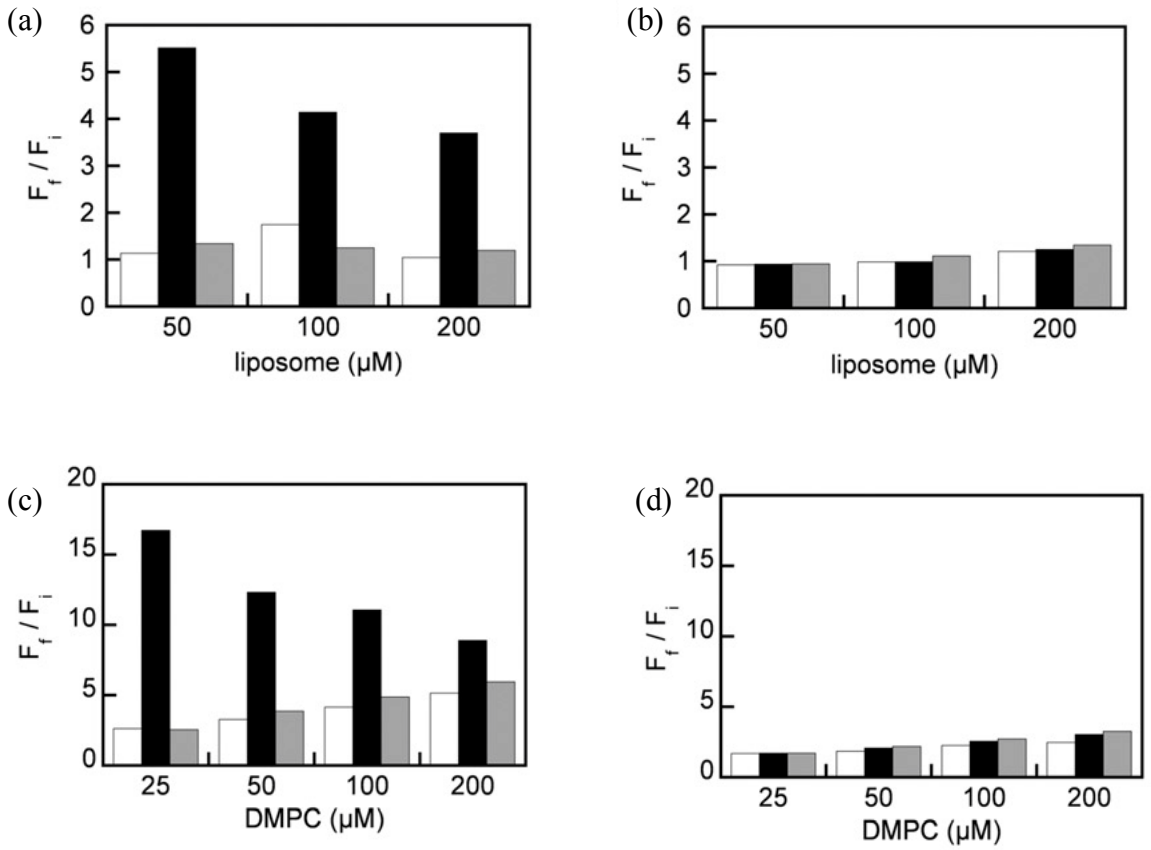

Figure A2.3. Fluorescence response of (a) 2 μM CF3 or (b) 2 μM Ctrl-CF3 in the presence of neutral liposomes (FormuMax, DPPC/CHOL 55:45 mol/mol, 100 nm, 50–200 μM) (white), with subsequent addition of 2 μM Cu^{+} to the solution (black), and a final addition of 400 μM neocuproine (gray). Bars represent the final integrated fluorescence response (F_f) over the initial integrated emission (F_i). Excitation was provided at 534 nm and emission was collected over 540–700 nm. (c) Fluorescence response of 2 μM CF3 or (d) 2 μM Ctrl-CF3 in the presence of 1,2-dimyristoyl-sn-glycero-3-phosphocholine (DMPC, 25–100 μM), a compound used for liposome formation (white), with subsequent addition of 2 μM Cu+ to the solution (black), and a final addition of 400 μM neocuproine (gray). Bars represent the final integrated fluorescence response (F_f) over the initial integrated emission (F_i). Excitation was provided at 534 nm and emission was collected over 540−700 nm.

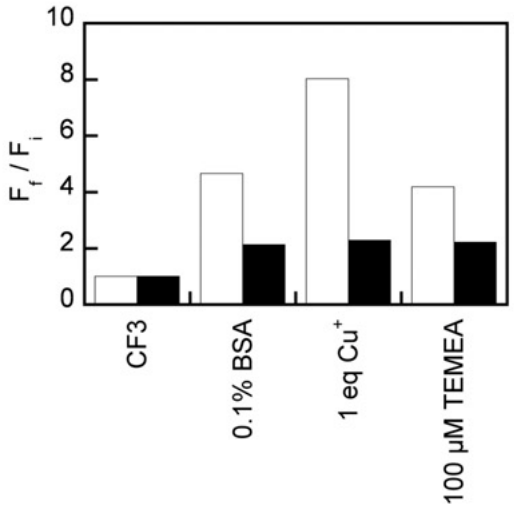

Figure A2.4. Fluorescence response of 2 μM CF3 (white) and 2 μM Ctrl-CF3 (black) in 0.1% BSA and to subsequent addition of 2 μM Cu^+ and 100 μM TEMEA. Bars represent the final integrated fluorescence response (Ff) over the initial integrated emission (Fi). Excitation was provided at 534 nm, and emission was collected over 540–700 nm. The data in J show, unsurprisingly, that both dyes exhibit a fluorescence enhancement in the presence of 0.1% BSA as a model protein compared with pure aqueous buffer. However, only CF3 responds reversibly to addition of Cu^+ in the presence of BSA to give a turn-on response can be subsequently attenuated by the addition of the chelator TEMEA. Neither copper- nor chelator- addition alters the fluorescence responses of Ctrl-CF3.

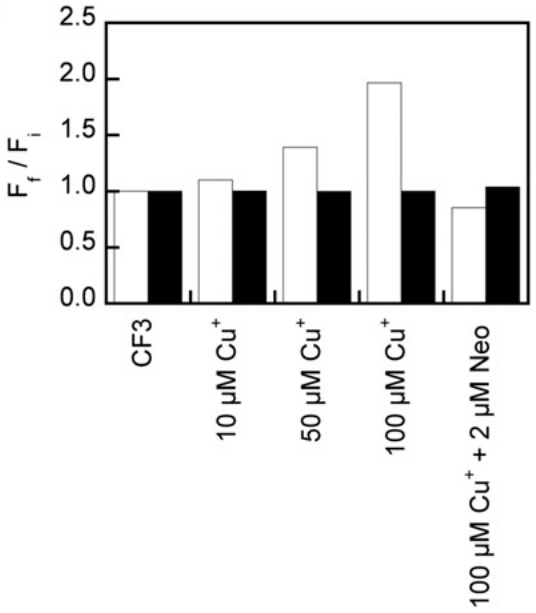

Figure A2.5. Fluorescence responses of 2 μM CF3 (white) and Ctrl-CF3 (black) to 10, 50, and 100 μM Cu^{+}, followed by addition of 2 μM neocuproine in HEK293T cell lysates (protein content of lysates: 1 mg/mL). Bars represent the final integrated fluorescence response (F_f) over the initial integrated emission (F_i). Excitation was provided at 534 nm and emission was collected over 540–700 nm.

Appendix 3

Development of a panel of capped Fe(II)-reactive fluorescent probes

Portions of this work were performed in collaboration with the following persons:

Compounds **6** and **8** were synthesized by Jana Bogena.
Compound **14** was synthesized by Audrey Reeves.

A3.1. Synopsis

Iron is both a required element for all living organisms and is the most abundant transition metal in the human body (1-4); yet despite its central importance, methods for non-invasive detection of labile Fe^{2+} within living cells and other intact biological specimens remain limited. (16,17) While Chapter 2 describes a FRET-based strategy for detection of Fe^{2+}, this appendix describes attempts to develop a modular platform for a series of turn-on fluorescent probes for Fe^{2+}. Developing a turn-on iron probe would be useful as it would be both more synthetically facile then synthesis of the FRET probe and would also be more modular. For example, a turn-on probe could be modified into an organelle targeted probe or a probe of a different excitation/emission wavelength. The work presented in this appendix was inspired by a pro-drug strategy described by Renslo and Bogyo.[1] We envisioned caging phenolic and amine fluorophores with an iron-reactive adamanyl-endoperoxide caging group. It their caged form, fluorophores would be non-fluorescent. We hypothesized that cellular Fe^{2+} would react with the adamantly-endoperoxide to release a ketone intermediate; this intermediate would then undergo ß-elimination to afford the uncaged phenolic or amine fluorophore (Figure A3.1). This appendix describes a series of probes (Figure A3.2) with varied hydrophobicity, cellular retention, leaving group ability, and excitation/emission color for *in vitro* detection of Fe^{2+}. The probes presented in this appendix cannot be used for cellular imaging, as low signal-to-noise precludes their use *in cellulo*.

A3.2. Materials and Methods

A3.2.1. General synthetic methods

Reactions using moisture- or air-sensitive reagents were carried out in flame-dried glassware under an inert atmosphere of N2. Solvent was passed over activated alumina and stored over activated 3Å molecular sieves before use when dry solvent was required. All other commercially purchased chemicals were used as received (without further purification). SiliCycle 60 F254 silica gel (pre-coated sheets, 0.25 mm thick) were used for analytical thin layer chromatography and visualized by fluorescence quenching under UV light. Silica gel P60 (SiliCycle) was used for column chromatography. ^{1}H and ^{13}C NMR NMR spectra were collected at 298 K in CDCl3 or CD3OD (Cambridge Isotope Laboratories, Cambridge, MA) at 25 °C on Bruker AVQ-400, AVB-400, AV-500, or AV-600 at the College of Chemistry NMR Facility at the University of California, Berkeley or on Bruker 900 at the QB3 Central California 900 MHz NMR Facility. All chemical shifts are reported in the standard notation of δ parts per mil-lion relative to residual solvent peak at 7.26 ($CDCl_3$) or 3.31 (CD_3OD) for ^{1}H and 77.16 ($CDCl_3$) or 49.00 (CD_3OD) for ^{13}C as an internal reference. Splitting patterns are indicated as fol-lows: br, broad; s, singlet; d, doublet; t, triplet; m, multiplet; dd, doublet of doublets. Low-resolution electrospray mass spectral analyses were carried out using a LC-MS (Agilent Technology 6130, Quadrupole LC/MS and Advion expression-L Compact Mass Spectrometer). High-resolution mass spectral analyses (ESI-MS) were carried out at the College of Chemistry Mass Spectrometry Facility at the University of California, Berkeley.

*A3.2.2. Synthesis of Trigger **1***

Adamantenone *O*-methyl oxime (1b)
A 500 mL round-bottom flask was charged with adamantanone (3.045 g, 20.29 mmol), methoxyamine hydrochloride (1.845 g, 22.09 mmol), then 45 mL of EtOH were added. Finally, 1.77 mL pyridine (22.09 mmol) were added. The reaction mixture was heated to 90 ºC, then was stirred at this temperature for 3 hours. After 3 hours, the reaction was cooled to room temperature and was concentrated *in vaccuo*, then 50 mL of dichloromethane was added. The organic layer was washed with 1 M HCl (50 mL). The acidified aqueous layer was washed with CH_2Cl_2 two additional times, before washing with acidified brine. The organic layer was dried over anhydrous Na_2SO_4, filtered, then was evaporated to dryness under reduced pressure to afford **1b** in quantitative yield (3.64 g, 100%). Spectra match values reported in literature.[2]

Trioxolane (1c)
Oxime ether **1b** (1.128, 6.29 mmol) and 1,4-cyclohexanedione (1.411, 12.58 mmol) were dried then were added to a flame-dried 100 mL Schlenk flask. Dry pentane (35 mL) and dry CH_2Cl_2 (25 mL) were added and the reaction mixture was stirred at 0 °C for 5 minutes before bubbling ozone through solution for 2 hours at this temperature. At this point, the reaction was purged of ozone, warmed to room temperature, and concentrated. The concentrate was loaded directly on silica gel for purification by silica chromatography (0 → 35% EtOAc/Hex) to yield **1d** as a pale solid. Spectra match values reported in literature.[2]

Lactone (1d)
Trioxolane **1c** (0.4695 g, 1.687 mmol) was added to a small round-bottom flask, followed by addition of *m*-CPBA (0.83165 g, 3.711 mmol) and $NaHCO_3$ (0.2834 g, 3.373 mmol) in 30 mL CH_2Cl_2. This reaction mixture was stirred for 2 days at room temperature. After two days, a white precipitate formed. The reaction is diluted with water (50 mL), then the aqueous layer was extracted with DCM (3 x 50 mL) and the combined organic layers were washed with $NaHCO_3$ (1 x 50 mL) and brine (1 x 50 mL), and finally dried over anhydrous Na_2SO_4, filtered, and concentrated under reduced pressure. The concentrate was loaded directly on silica gel for purification by silica chromatography (0 → 20% EtOAc/Hex) to yield **1d** as a white solid (0.430 g, 87%). Spectra match values reported in literature.[3]

Amide (1e)
Lactone **1d** (0.150 g, 0.5096 mmol) was added to a small round-bottom flask in 2 mL toluene, followed by addition of *n*-propylamine (83.8 µL, 1.019 mmol). This reaction mixture was stirred overnight at 50 ºC. The next morning, solvent was concentrated under reduced pressure; then residue was taken up in DCM and washed with water (1 x 25 mL). The aqueous layer was extracted with DCM (3 x 25 mL) and the combined organic layers were washed with brine (1 x 50 mL), and finally dried over anhydrous Na_2SO_4, filtered, and concentrated under reduced pressure. The concentrate, **1e**, was carried on in its crude form to the next reaction. ^{1}H NMR (400 MHz, $CDCl_3$) δ (ppm): 5.76 (s, 1 H), 5.28 (d, 1 H), 3.78 (m, 2 H), 3.19 (m, 2 H), 2.28 – 1.47 (m, 21 H), 0.90 (t, 3 H).

Tosylated Trigger (1)

Amide **1e** (0.1388 g, 0.3927 mmol) was dissolved in 5 mL DCM under an inert atmosphere of N_2. This solution was cooled to 0 ºC, then TsCl was added portion-wise. The reaction mixture was allowed to warm to room temperature, then was stirred overnight. In the morning, the reaction mixture was filtered and washed with DCM (3 x 25 mL). The reaction mixture was concentrated under reduced pressure, then was loaded directly on silica gel for purification by silica chromatography (0 → 25% EtOAc/Hex) to yield **1** as an oil (0.138 g, 69%).[1]H NMR (400 MHz, $CDCl_3$) δ (ppm): 7.79 (d, 2 H), 7.36 (d, 2 H), 5.305 (s, 1 H), 4.143 (m, 2 H), 3.05 (q, 2 H), 2.48 (s, 3 H), 2.25 – 1.51 (m, 23 H), 0.93 (t, 3 H).

NHS-carbonate trigger (1f)
Amide **1e** (0.1185 g, 0.334 mmol) was dissolved in 2 mL DCM under an inert atmosphere of N_2, then N,N′-Disuccinimidyl carbonate (0.171 g, 0.66 mmol), and 185 µL Et_3N were added. This reaction was stirred overnight, then the reaction mixture was partitioned between H_2O (25 mL) and DCM (25 mL). The aqueous layer next extracted with DCM (3 x 25 mL), the combined organic layers were washed with brine (1 x 25 mL), dried over anhydrous Na_2SO_4, filtered, and concentrated under reduced pressure. NHS-carbonate trigger **1f** was isolated as a crude oil, which was used for subsequent reactions without further purification. [1]H NMR (600 MHz, $CDCl_3$) δ (ppm): 5.757 (s, 1 H), 4.456 (m, 2 H), 3.19 (q, 2 H), 2.837 (s, 4 H), 2.29 – 1.24 (m, 23 H), 0.90 (t, 3 H).

A3.2.3. Synthesis of Phenolic Probe Series (Probes 2, 4, 6, 8, 10)

Compound 2
Tosylated trigger **1** (0.025 g, 0.0591 mmol), 7-hydroxy-4-methylcoumarin (0.0208 g, 0.1182 mmol), and K_2CO_3 (0.0245 g, 0.1773 mmol), were added to a 20 mL vial. Then 2 mL DMF were added and this solution was stirred under an inert atmosphere of N_2 at 55 ºC for 16 hours. After 16 hours, the reaction mixture was poured into brine (20 mL) and extracted with DCM (3 x 20 mL), the combined organic layers were washed with $NaHCO_3$ (1 x 25 mL), dried over anhydrous Na_2SO_4, filtered, and concentrated under reduced pressure. The concentrate was loaded directly on silica gel for purification by silica chromatography (20 → 40% EtOAc/Hex) to yield **2** (0.009 g, 30%). [1]H NMR (400 MHz, $CDCl_3$) δ (ppm): 7.49 (d, 1 H), 6.85 (dd, 1 H), 6.795 (s, 1 H), 5.49 (bs, 1 H), 4.17 (m, 2 H), 3.20 (m, 2 H), 2.40 (s, 3 H), 2.35 – 1.51 (m, 23 H), 0.93 (t, 3 H).

Compound 4
Tosylated trigger **1** (0.0205 g, 0.0403 mmol), fluorescein (0.0403 g, 0.1212 mmol), and K_2CO_3 (0.02514 g, 0.1819 mmol), were added to 2-neck flask. Then 2 mL DMF were added and this solution was stirred under an inert atmosphere of N_2 at 60 ºC for 16 hours. After 16 hours, the reaction mixture was poured into brine (20 mL) and extracted with DCM (3 x 20 mL), the combined organic layers were washed with $NaHCO_3$ (1 x 25 mL), dried over anhydrous Na_2SO_4, filtered, and concentrated under reduced pressure. The concentrate was loaded directly on silica gel for purification by silica chromatography (1% MeOH/DCM) to yield **4**.

Compound 6 2-methyl-4-methoxy-Tokyo Green **6a** was synthesized as described previously.[4] **6a** (0.024 g, 0.0722 mmol) and Cs_2CO_3 (0.094 g, 0.29 mmol) were added to a 50 mL round-bottom flask and this was dried for 2 hours. Then, **1** was added in 1 mL dry DMF to the round-bottom flask, and this reaction mixture was stirred overnight at 50 ºC. After 12 hours, the

reaction was concentrated under reduced pressure, then the concentrate was loaded directly on silica gel for purification by silica chromatography (0 → 10% MeOH/DCM) to yield **6**.

Compound 8 was synthesized by Jana Bogena.[5]

Compound 10

Compound 10b
Cs_2CO_3 (0.03311 g, 0.1016 mmol), $Pd(OAc)_2$ (0.00326 g, 0.0145 mmol), and BINAP were added to an oven-dried tube in 0.5 mL toluene and stirred at room temperature for 5 minutes. Then compound **10a** (0.050 g, 0.0726 mmol) and morphopline (12.56 µL, 0.145 mmol) were added in 0.5 mL toluene, and this reaction mixture was stirred or 30 minutes at room temperature before heating at 100 ºC and stirring at this temperature overnight. After 12 hours, the reaction was diluted by addition of 20 mL DCM then was filtered over celite and concentrated. The concentrate was loaded directly on silica gel for purification by silica chromatography (0 → 40% EtOAc/Hex) to yield **10b** (0.0205 g, 45%). ^{1}H NMR (400 MHz, acetone-d_6) δ (ppm): 7.83 – 7.79 (d, 4 H), 7.46 – 7.43 (m, 6 H), 7.38 (t, 1 H), 7.26 (t, 1 H), 6.82 – 6.78 (m, 3 H), 6.70 – 6.67 (m, 1 H), 6.60 – 6.55 (m, 3 H), 5.25 (s, 2 H), 3.77 – 3.74 (m, 4 H), 3.17 – 3.14 (m, 4 H), 1.11 (s, 9 H).

Compound 10c
Compound 10b (0.0508 g, 0.0881 mmol) was added to a round-bottom flask in THF, then TBAF (97 µL, 0.097 mmol) were added dropwise. This reaction mixture was stirred for 20 minutes then was concentrated under reduced pressure. The concentrate was loaded directly on silica gel for purification by silica chromatography (0 → 50% MeOH/Hex) to yield **10c** (0.012 g, 35%). This was carried on without further purification.

Compound 10
Compound 10c (0.012 g, 0.031 mmol) was added to a round-bottom flask and was dried for 3 hours, before adding Cs_2CO_3 (0.040 g, 0.124 mmol) in 0.5 mL DMF and compound **1** (0.0142 g, 0.0279 mmol) in 0.5 mL DMF. The reaction mixture was stirred overnight at 50 ºC, then was concentrated under reduced pressure. The concentrate was loaded directly on silica gel for purification by silica chromatography (0 → 1% MeOH/Hex) to yield **10** (0.00892 g, 40%). LRMS calcd. for $C_{43}H_{50}O_8N_2$ $[M + H]^+$ 723.3, found 723.3.

Compound 12

Rhodol **12a** (0.018 g, 0.04646 mmol) was added to a round-bottom flask, then compound **1** (0.0212 g, 0.0418 mmol), and Cs_2CO_3 (0.061 g, 0.186 mmol) were added in 1 mL DMF. The reaction mixture was stirred overnight at 50 ºC, then was concentrated under reduced pressure. The concentrate was loaded directly on silica gel for purification by silica chromatography (0 → 1% MeOH/Hex) to yield **12** (0.00817 g, 24%). LRMS calcd. for $C_{43}H_{50}O_8N_2$ $[M + H]^+$ 723.3, found 723.3.

Compound 14

Compound 14 was synthesized by Audrey Reeves. Resorufin sodium salt (0.0147 g, 0.0583 mmol) was added to an oven-dried round-bottom flask filled with N_2, then compound **1** (0.0379 g, 0.0747 mmol), and Cs_2CO_3 (0.0243 g, 0.0747 mmol) were added in 1 mL DMF. The reaction mixture was stirred overnight at 40 ºC, then was concentrated under reduced pressure. The concentrate was loaded directly on silica gel for purification by silica chromatography (0 → 50% EtOAc/Hex) to yield **14** (0.0178 g, 43%).

A3.2.4 Synthesis of Carbamate-Linked Probe Series (Probes 3, 5, 7, 9, 11)

Compound 3

Triphosgene (0.0279 g, 0.09419 mmol) was added to a flamed-dried Schlenk flask in 2 mL dry THF. This was allowed to stir for 10 minutes before adding DMAP (0.01883 g, 0.15413 mmol), then was stirred for an additional 10 minutes. At this point, a white suspension formed. Next, 7-amino-4-methylcoumarin (0.015 g, 0.08563 mmol) was added in 10 mL dry THF over 30 minutes (using a syringe pump), then the temperature of this reaction mixture was brought to 70 ºC and this was heated for 3 hours. After 3 hours, compound **1e** was added, and this reaction was stirred for 8 hours at 40 ºC before concentrating under reduced pressure. At this point, the concentrate was loaded directly on silica gel for purification by silica chromatography (0 → 10% MeOH/DCM) to yield **3** (0.005 g, 10%). ^{1}H NMR (500 MHz, $CDCl_3$) δ (ppm): 9.32 (bs, 1 H), 7.535 (m, 3 H), 6.182 (s, 1H), 5.672 (s, 1 H), 4.369 (m, 2 H), 3.303 (m, 2 H), 2.543 (s, 3 H), 2.423 – 1.546 (m, 22 H), 0.974 (m, 3 H).

Compound 5

Hydroxymethyl rhodamine green

Rhodamine 110 (0.200 g, 0.545 mmol) was dissolved in 6 mL dry THF in an oven-dried flask, then this solution was cooled to -78 ºC and 5.45 mL of a 1 M solution of BH_3 in THF were added dropwise. This solution was warmed to room temperature and stirred overnight. At this point, 147 mg chloranil was added in DCM and this was stirred for an additional hour. The reaction mixture was concentrated under pressure, then the concentrate was loaded directly on silica gel for purification by silica chromatography (0 → 10% MeOH/DCM containing 1% TFA) to yield hydroxymethyl rhodamine green. Spectra matched values reported in literature.[6]

Compound 5

Compound **1f** (0.080 g, 0.2757 mmol) was added in 1 mL DCM to a round-bottom flask containing hydroxymethyl rhodamine green (0.035 g, 0.1103 mmol) in 0.25 mL DCM/1 mL THF. Then DMAP (0.024 g, 0.1985 mmol) was added in 0.25 mL THF along with Et_3N (48 µL). This reaction was stirred at room temperature overnight, then was concentrated under reduced pressure. The concentrate was loaded directly on silica gel for purification by silica chromatography (0 → 5% MeOH/DCM) to yield semi-pure **5**. This was further purified by preparative HPLC (50% MeCN/H_2O + 0.05% FA → 100% MeCN + 0.05% FA). Fractions containing product were combined, extracted into ethyl acetate, and concentrated under reduced pressure to yield pure **5** (0.0096 g, 12.5 %). LRMS calcd. for $C_{43}H_{50}O_8N_2$ $[M + H]^+$ 696.3, found 696.3.

Compound 7
Rhodamine 110 (0.1587 g, 0.43 mmol) was dissolved in 4 mL dry DMF at 0 ºC. NaH (0.02033 g, 0.847 mmol) was added, then this reaction mixture was allowed to warm to room temperature and was stirred for 1 hour before adding compound **1f** (0.1783 g, 0.36 mmol) in 1 mL of dry DMF. This was stirred for 16 h, then the reaction mixture was concentrated under reduced pressure and the concentrate was loaded directly on silica gel for purification by silica chromatography (2:3:5 EtOAc: DCM: Hex → 0 → 10% MeOH/DCM) to yield compound **7**. ^{1}H NMR (600 MHz, CD_3OD) δ (ppm): 8.005 (m, 2H), 7.749 (t, 1 H), 7.709 (t, 1H) , 7.696 (s, 1 H), 7.21 (d, 1 H), 7.047 (d, 1H), 6.657 (s, 1 H), 6.579 (d, 1 H), 6.443 (d, 1 H), 4.304 (t, 1 H), 3.122 (m, 2H), 2.186 – 1.776 (m, 21 H), 1.503 (m, 3 H).

Compound 9
7 (0.0284 g, 0.04 mmol) and K_2CO_3 were dried under reduced pressure overnight. Then 1 mL dry DMF was added, along with NEt_3 (6 µL, 0.044 mmol), and this was stirred for ½ hour. At this point, 4-morpholinecarbonyl chloride (23 µL, 0.30 mmol) were added and this solution was heated to 30 ºC and stirred for 16 hours. The reaction was concentrated under reduced pressure and was loaded directly on silica gel for purification by silica chromatography (0 → 10% MeOH/DCM) to yield crude compound **9**. This was further purified by running a preparative TLC (0 → 10% MeOH/DCM). Colored bands were excised from the silica plate, were extracted with 10% MeOH in DCM and concentrated to yield compound **9**. ^{1}H NMR (600 MHz, $CDCl_3$) δ (ppm): 8.7 (bs, 2 H), 8.006 (d, 1 H), 7.660 – 7.593 (m, 3 H), 7.159 (d, 1H), 7.009 (m, 1 H), 6.830 (s, 1 H), 6.688 (d, 1 H), 6.649 (s, 1 H), 5.569 (s, 1 H), 4.321 (m, 2 H), 3.228 (m, 2 H), 2.366 – 2.313 (m, 6 H), 2.219 – 1.507 (m, 26 H), 0.92 (t, 3 H).

Compound 11
7 (0.0222 g, 0.031 mmol) and DIPEA (21.6 µL, 0.124 mmol) were added to a round-bottom flask in 1 mL THF. Then octyl isocyanate 16.4 µL, 0.093 mmol) was added and this solution was heated to 40 ºC and stirred for 16 hours. The reaction was concentrated under reduced pressure and was loaded directly on silica gel for purification by silica chromatography (0 → 1% MeOH/DCM) to yield crude compound **11**. This was further purified by concentrating and purifying by silica chromatography (0 → 50% EtOAc/Hex) to yield compound **11**. ^{1}H NMR (400 MHz, $CDCl_3$) δ (ppm): 8.80 (bs, 1 H), 8.00 (d, 1 H), 7.62 (m, 2 H), 7.55 (d, 1H), 7.18 (m, 1 H), 7.091 – 7.01 (m, 3 H), 6.95 (s, 1 H), 6.70 (d, 1 H), 6.571 (d, 1H), 5.80 (t, 1 H), 5.248 (m, 1 H), 4.313 (m, 2 H), 3.224 (m, 4 H), 2.34 – 1.25 (m, 32 H), 0.92 (t, 6 H).

Compound 13
The synthesis of compound **1g** is described in Chapter 3. Rhodamine 110 (0.04505 g, 0.1228 mmol) was dissolved in 1.5 mL dry DMF at 0 ºC. NaH (0.0058 g, 0.2404 mmol) was added, then this reaction mixture was allowed to warm to room temperature and was stirred for 1 hour before adding compound **1g** (0.0431 g, 0.1023 mmol) in 1 mL of dry DMF. This was stirred for 16 h, then the reaction mixture was concentrated under reduced pressure and the concentrate was loaded directly on silica gel for purification by silica chromatography (0 → 10% MeOH/DCM). An additional purification was performed by silica chromatography (2% MeOH/DCM) to yield compound **13**. ^{1}H NMR (400 MHz, CD_3OD) δ (ppm): 8.03 - 8.01 (d, 1 H), 7.76 -7.73 (t, 1 H), 7.71 – 7.69 (t, 1H) , 7.60 (s, 1 H), 7.24 - 7.21 (d, 1 H), 7.05 – 7.02 (d, 1H), 6.68 – 6.66 (s, 1 H), 6.59 (d, 1 H), 6.51 – 6.43 (m, 2 H), 4.80 (m, 1 H), 2.26 – 2.23 (m, 1 H), 2.02 – 1.51 (m, 20 H).

A3.2.5. In vitro Fe^{2+} Response

All water and buffers used were degassed by bubbling nitrogen through solutions for 1 hour. A 10 mM stock solution of ferrous ammonium sulfate (FAS) was prepared in degassed MilliQ water. Iron reactivity was assessed in a variety of conditions – (1) in 50 mM HEPES buffer (pH 7.4) alone (2) in 50 mM HEPES buffer (pH 7.4) supplemented with 10% FBS (3) in 50 mM HEPES buffer (pH 7.4) supplemented with DMEM media and (4) in DMEM media supplemented with 10% FBS. All subsequent experiments were performed in 50 mM HEPES buffer.

1-10 μM probe (prepared as a 1-10 μM stock solution in DMSO) was added to 990-999 μL of 50 mM HEPES (pH 7.4) buffer in an air-tight capped cuvette (Starna, see description in Appendix 2). Then 10 μL of Fe (from a 10 mM stock solution prepared in water) or water was added. Reaction was incubated at 37 ºC in a water bath, and fluorescence was measured at various time points.

A3.2.6. In cellulo Fe^{2+} Response

Cell Culture Procedures.

Cells were maintained by the UC Berkeley Tissue Culture Facility. HEK 293T and HepG2/CA3 cells were maintained as a monolayer in exponential growth at 37 °C in a 5% CO2 atmosphere in Dulbecco's Modified Eagle Medium (DMEM, Gibco) supplemented with 10% fetal bovine serum (FBS, Hyclone), and glutamax (Gibco). One day before imaging, HEK 293T cells were passaged and plated in phenol red-free medium on poly-d-lysine-coated 4-well Lab Tek borosilicate chambered coverglass slides (Nunc) at 1.8 x 105 per well. HEK 293T cells were allowed to grow to between 60-75% confluence before imaging. One day before imaging, HepG2/CA3 cells were passaged and plated in phenol red-free medium on poly-d-lysine-coated 4-well Lab Tek borosilicate chambered coverglass slides and were allowed to grow to between 60-75% confluence before imaging.

A3.2.7. Confocal Fluorescence Imaging Experiments.

A Zeiss laser scanning microscope 710 with a 20x objective lens and Zen 2009 software (Carl Zeiss) was used for all confocal fluorescence imaging experiments. Probes were excited using a 488 nm Ar laser or a 543 nm HeNe; emission was collected using a META detector. Cells were kept at 37 °C throughout imaging experiments, and DMEM or HBSS (containing calcium and magnesium) was used as the imaging buffer in all experiments. Image analysis and quantification was performed using ImageJ (National Institutes of Health). Quantification of fluorescence intensities were conducted as described previously.[67]

A3.2.8. Fe(II) Supplementation and Chelation Experiments.

100 μM ferrous ammonium sulfate (FAS) was added to DMEM media containing 10% FBS and glutamax in chambers containing cells and incubated at 37 °C for 24 hours. DMEM media (without FBS and glutamax) containing 1 mM 2,2'-bipyridine (BPY) or 100 μM FAS was incubated for 30-40 minutes at 37 °C. DMEM media in non-treated wells was aspirated and replaced with serum-free media. After 90 minutes, DMEM media was aspirated and cells were washed one time with 500 μL HBSS. Then probe was added in 500 μL DMEM or HBSS at 1-10 μM probe to each well and this was incubated at 37 °C for 1-2 hours. At this point, buffer was removed and each well was washed 1x with 500 μL DMEM or HBSS before acquiring snapshot images.

A3.3. Results and Discussion

Synthesizing the hydroxymethyl rhodamine target (compound **5**) required significant optimization, as hydroxymethyl rhodamines and rhodamines anilines are poor nucleophiles. Optimization included attempts to (1) activate hydroxymethyl rhodamine green with triphosgene in the presence of triethylamine and DMF in DCM (2) activate trigger **1e** with p-nitrophenol chloroformate in the presence of triethylamine and DMAP in DMF (3) activate trigger **1e** with carbonyldiimidazole (CDI) in THF or in MeCN with methyl iodide. Activation of the trigger **1e** with N,N′-disuccinimidyl carbonate and subsequent reaction with hydroxmethyl rhodamine in the presence of DMAP and triethylmaine in THF/DCM afforded the desired compound **5**. Based on this result, we used this strategy to synthesize carbamate-linked probes.

With compound **5** in hand, *in vitro* iron reactivity was assessed in a variety of conditions - (1) in 50 mM HEPES buffer (pH 7.4) alone (2) in 50 mM HEPES buffer (pH 7.4) supplemented with 10% FBS (3) in 50 mM HEPES buffer (pH 7.4) supplemented with DMEM media and (4) in DMEM media supplemented with 10% FBS. We determined that background reactivity occurs in the presence of FBS; we hypothesized this would be the case given that FBS contains iron. We also hypothesized that nucleophiles present in FBS may accelerate the ß-elimination, which would significantly increase fluorescence turn-on. Additionally, we observed diminished turn-on in the presence of DMEM; we rationalized this was due to the fact that components present in DMEM may bind or chelate iron and prevent it from accessing the probe. For this reason, we carried out all subsequent *in vitro* reactivity studies in HEPES buffer and performed all imaging studies with probe in buffer (as opposed to in DMEM), as background hydrolysis was minimal in buffer. Because we still observed background hydrolysis occurring with carbamate-linked probes in buffer, we synthesized a series of ether-linked probes based on the increased stability of ether linkage to hydrolysis. This ether-linked series includes compounds **4**, **10**, and **12**. We found that while these probes exhibited improved stability in HEPES buffer, these probes also exhibited diminished turn-on to Fe^{2+}, likely due to slower reaction kinetics (data not shown).

Based on its performance *in vitro*, compound **5** was tested *in cellulo.* This probe exhibited punctate and lysosomal localization (Figure A3.5). Because we were interested in studying cytosolic iron, lysosomal localization was not desirable for our imaging studies, especially given that Iron Probe 1 (IP-1) is a lysosomal Fe^{2+} probe. Additionally, we did not observe Fe^{2+}-response *in cellulo*; we hypothesized this was due to the fact that our iron-supplementation and chelation treatments were likely altering cytosolic, as opposed to lysosomal, iron. This hydroxymethyl rhodamine scaffold is known to exhibit lysosomal localization; given this, we

next synthesized compound **7**, which we hypothesized would exhibit a more even cytosolic staining pattern due to the presence of the hydrophilic carboxylic acid. Compound **7** performed well *in vitro*, exhibiting a c.a. 40-fold turn-on to 1 mM Fe^{2+} in the presence of 10% FBS/DMEM and a c.a. 10-fold turn-on to 1 mM Fe^{2+} in the presence of 50 mM HEPES (pH 7.5). While this compound exhibited more even cytosolic staining *in cellulo* as compared to compound **5**, it did not exhibit an increase in fluorescence in iron-supplemented cells as compared to control cells. Instead, compound **7** exhibited a fluorescence decrease upon iron-supplementation and a fluorescence increase upon iron-chelation as compared to control cells (Figure A3.6). Given this result, we synthesized a variety of other carbamate-linked dyes, including compound **9**.

With all probes tested *in cellulo*, we observed a decreased fluorescence in iron-supplemented cells (or essentially no change) as compared to control cells (Table A3.1). Compounds **4** and **12** exhibit negligible fluorescence change in cells treated with iron while the remaining probes tested exhibit a turn-off fluorescence to iron in cells (Table A3.1). This is likely due to the fact that ether-linked probes exhibit attenuated reactivity when compared to carbamate-linked probes. Based on these results, we hypothesized that the ketone intermediate or the fluorescent product are diffusing out of cells. This hypothesis would explain why the observed trend was opposite of expected; iron-supplementation would fragment compound **7** into intermediate and subsequently into fluorescent product. If intermediate and product diffuse out of cells, we would observe less fluorescence after iron-supplementation as compared to vehicle-treated cells. The opposite would hold true for chelator-treated cells.

In order to test this hypothesis, we developed a number of probes that we hypothesized would have improved cellular retention. These targets included compounds **11**, **6**, and **8**. We hypothesized compound **11** and the intermediate and product formed in reaction with Fe^{2+} would be retained in cells due to the hydrophobic nature of the octyl group. We envisioned compound **8** would specifically target mitochondria due to the presence of a lipophilic cation.[7] Unfortunately, these cell-trappable probes exhibited low *in vitro* turn-on response to Fe^{2+}, so we were ultimately not able to test this trappability hypothesis using these probes in *in cellulo* (Table A3.1).

Given these results, we wanted to appended the adamantyl-endoperoxide moiety to resorufin to yield compound **14** based on precedent from our laboratory.[8] Bruemmer et al. found that condensation with formaldehyde followed by aza-Cope reaction and subsequent elimination from imine intermediate resulted in an *in cellulo* turn-on to formaldehyde. Based on the similar mechanisms (elimination out of ketone or imine), we hypothesized this strategy could work for *in cellulo* Fe^{2+} detection. We found, however, that while compound **14** exhibited fluorescence turn-on to Fe^{2+} *in vitro* (c.a. 3.75) this compound exhibited the same pattern of *in cellulo* reactivity described for compound **7** above. At this point, we decided to pursue two alternate approaches toward development of turn-on probes for Fe^{2+}.

A3.4 Conclusion

This appendix describes a series of probes (Figure A3.2) with varied hydrophobicity, cellular retention, leaving group ability, and excitation/emission color for *in vitro* detection of Fe^{2+}; however, low signal-to-noise precludes the use of this series *in cellulo*. We believe the low signal-to-noise observed with the probes in this series is due to the slow ß-elimination step, as we hypothesize that ketone intermediate diffuses out of cells before releasing a fluorescent dye. In order to solve this problem, we plan to synthesize a panel of trigger moieties that exhibit enhanced cellular retention (Figure A3.9). We were additionally interested in attaching the

adamantyl-endoperoxide directly to a fluorophore ketone (Figure A3.10); however, synthetic efforts proved unsuccessful due to synthetic difficulties. It is perhaps worth revisiting these targets.

Figures

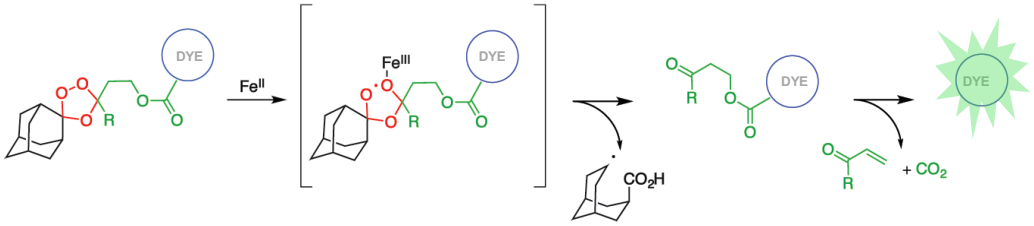

Figure A3.1. Design of ß-elimination turn-on probes for Fe^{2+}. A fluorescent dye is capped with an adamantyl endoperoxide moiety through a self-immolative linker. Reaction of the endoperoxide with Fe^{2+} releases a ketone intermediate, which then undergoes ß-elimination to release a fluorescent dye.

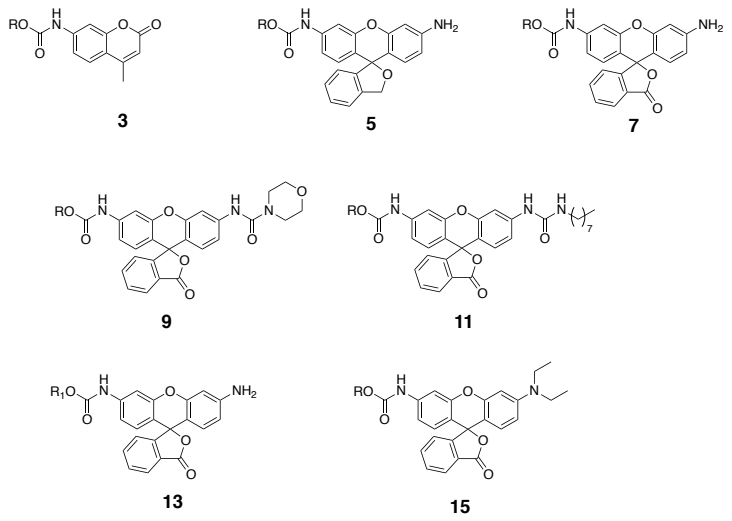

Figure A3.2. A series of probes for *in vitro* detection of Fe^{2+} was developed. These probes utilize an adamantyl-peroxide to cage an amine-containing fluorophore through a carbamate linkage.

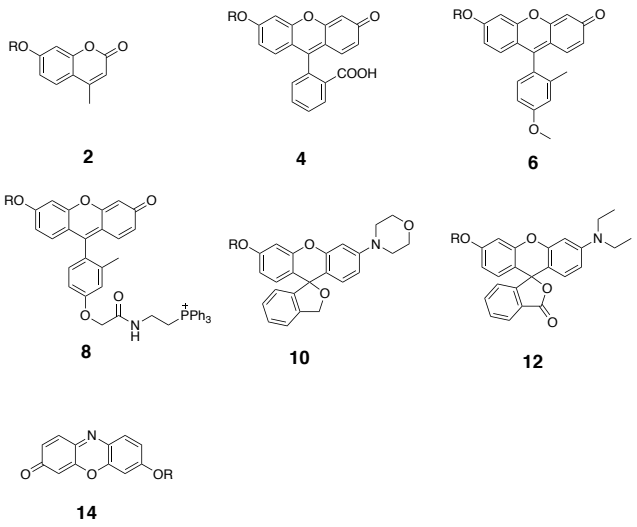

Figure A3.3. A series of probes for *in vitro* detection of Fe^{2+} was developed. These probes utilize an adamantyl-peroxide to cage a phenol-containing fluorophore through an ether linkage.

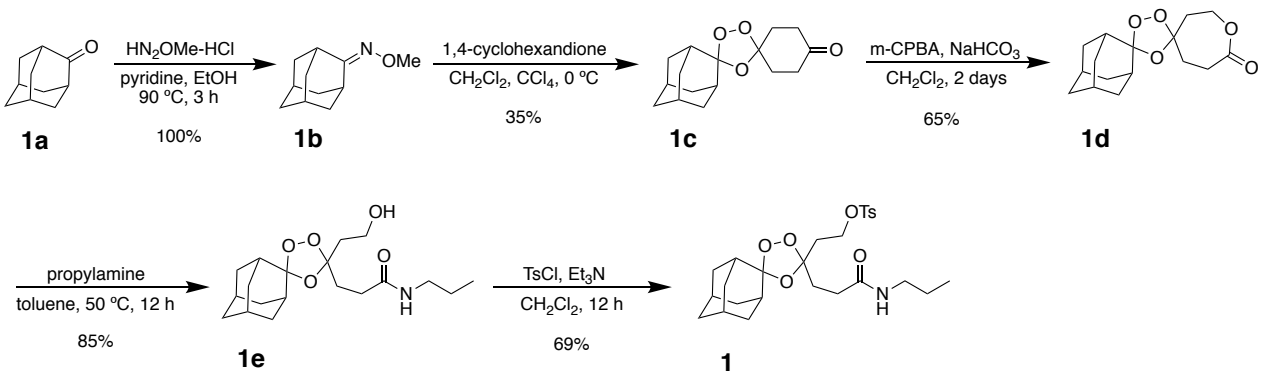

Scheme A3.1. Compound **1** can be synthesized from commercially available adamantanone **1a** in a series of 5 steps.

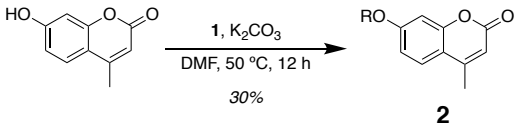

2

Scheme A3.2. Compound **2** can be synthesized from commercially available 7-hydroxymethyl coumarin.

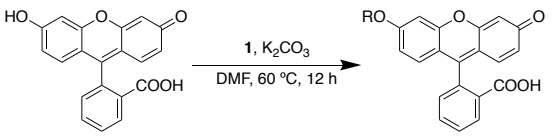

4

Scheme A3.3. Compound **4** can be synthesized from commercially available fluorescein.

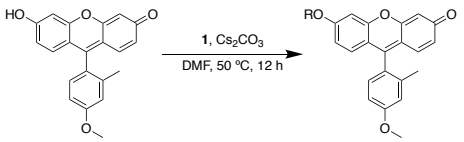

6

Scheme A3.4. Compound **6** can be synthesized from 2-methyl-4-methoxy-Tokyo Green

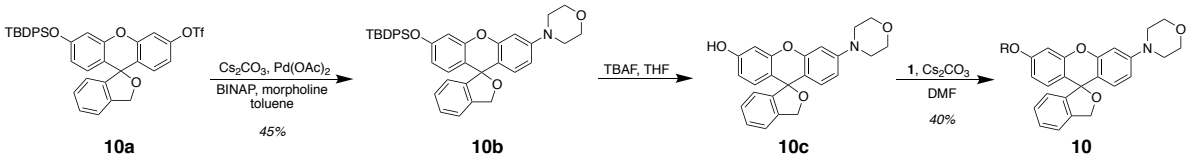

10a 10b 10c 10

Scheme A3.5. Compound **10** can be synthesized from previously synthesized **10a**.

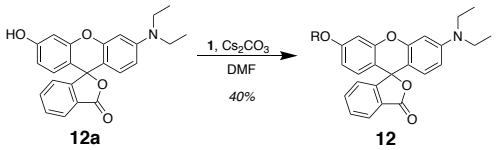

Scheme A3.6. Compound **12** can be synthesized from compound **12a** in a series of 2 steps.

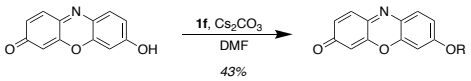

Scheme A3.7. Compound **14** can be synthesized from resorufin.

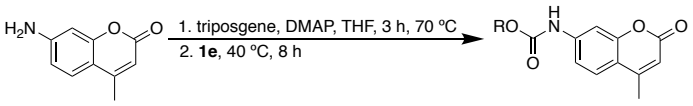

3

Scheme A3.8. Compound **3** can be synthesized from 7-amino-4-methylcoumarin.

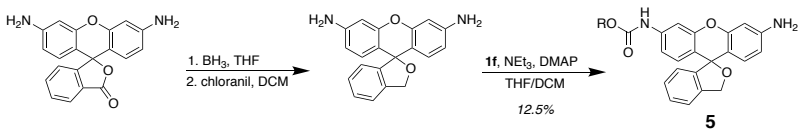

Scheme A3.9. Compound **5** can be synthesized from Rhodamine 110 in 2 steps.

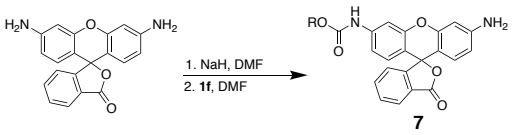

Scheme A3.10. Compound **7** can be synthesized from Rhodamine 110.

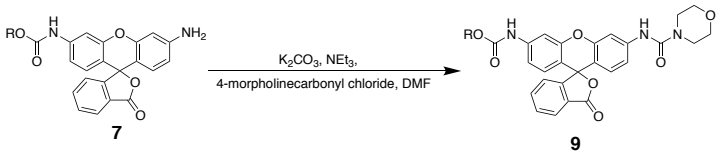

Scheme A3.11. Compound **9** can be synthesized from mono-substituted **7**.

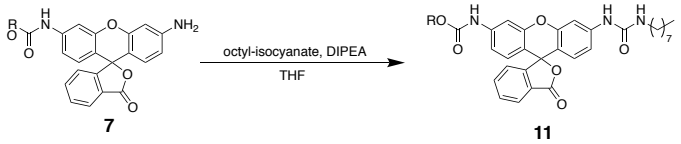

7 11

Scheme A3.12. Compound **11** can be synthesized from mono-substituted **7**.

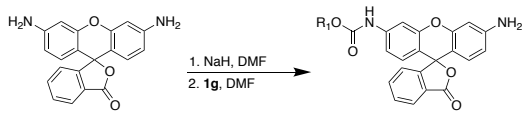

13

Scheme A3.13. Compound **7** can be synthesized from Rhodamine 110.

(a)

Probe	Abs max (nm)	Em max (nm)	*in vitro* Turn-on	Conditions
2	360	450	c.a. 1.2-fold	10uM probe, 100x Fe, 1 h, FBS/DMEM
3	380	450	c.a. 7.4-fold	10uM probe, 100x Fe, 1 h, FBS/DMEM
4	488	515	c.a. 1.7-fold	10uM probe, 5x Fe, 30 min, BSS
5	501	520	c.a. 50-fold	10uM probe, 100x Fe, 1 h, FBS/DMEM
6	488	515	c.a. 35-fold	10uM probe, 100x Fe, 1 h, FBS/DMEM
7	496	517	c.a. 6-fold	10uM probe, 100x Fe, 1 h, HEPES pH 7.5
8	488	515	c.a. 1.1-fold	1uM probe, 20x Fe, 30 mins, HEPES pH 7.5
9	496	517	c.a. 30-fold	
10	525	552	c.a. 8-fold	10uM probe, 100x Fe, 1 h, HEPES pH 7.5
11	488	520	c.a. 1.2-fold	10uM probe, 100x Fe, 1 h, HEPES pH 7.5
12	525	550	c.a. 3.9-fold	10uM probe, 100x Fe, 1 h, HEPES pH 7.5
14	573	585	c.a. 3.8-fold	1uM probe, 100x Fe, 1 h, HEPES pH 7.5

(b)

Probe	*in cellulo* Turn-on	Conditions
2	Not tested	N/A
3	Not tested	N/A
4	5% turn-on to Fe vs. Ctl	HepG2 cells, 100uM Fe treatment, 1 h, 30 mins after probe addition
5	15% turn-on to Fe vs. Ctl	HepG2 cells, 100uM Fe treatment, 24 h, 2 h after probe addition
6	15% turn-off to Fe vs. Ctl	HepG2 cells, 100uM Fe treatment, 1 h, 30 mins after probe addition
7	55% turn-off to Fe vs. Ctl	HepG2 cells, 100uM Fe treatment, 1 h, 30 mins after probe addition
8	Not tested	N/A
9	Not tested	N/A
10	Not tested	N/A
11	10% turn-on to Fe vs. Ctl	HepG2 cells, 100uM Fe treatment, 1 h, 2 h after probe addition
12	37% turn-off to Fe vs. Ctl	HepG2 cells, 100uM Fe treatment, 1 h, 1 h after probe addition
14	40% turn-off to Fe vs. Ctl	HepG2 cells, 100uM Fe treatment, 1 h, 1 h after probe addition

Table A3.1. Compounds **2** - **14** were synthesized for detection of Fe^{2+}. (a) Excitation and emission wavelengths are tabulated, along with *in vitro* turn-on response to Fe^{2+} and the conditions for *in vitro* experiments. (b) *In cellulo* turn-on response to Fe^{2+} and the conditions for those experiments are tabulated as well for probes tested in cells.

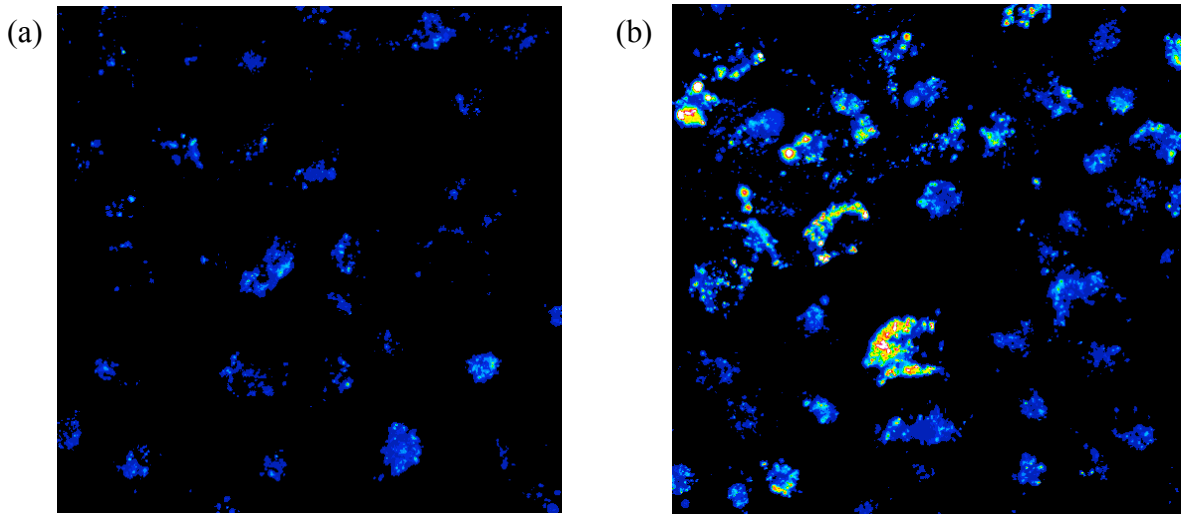

Figure A3.4. 20 μM compound **5** was added and incubated at 37 °C for 1-2 hours. At this point, buffer was removed and each well was washed 1x with 500 μL DMEM before acquiring snapshot images. Lysosomal localization can be observed. (a) Control treatment. (b) 100 μM Fe^{2+} treatment overnight.

(a) 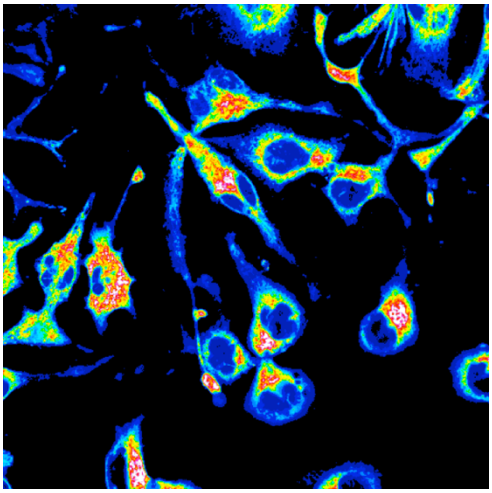 (b) 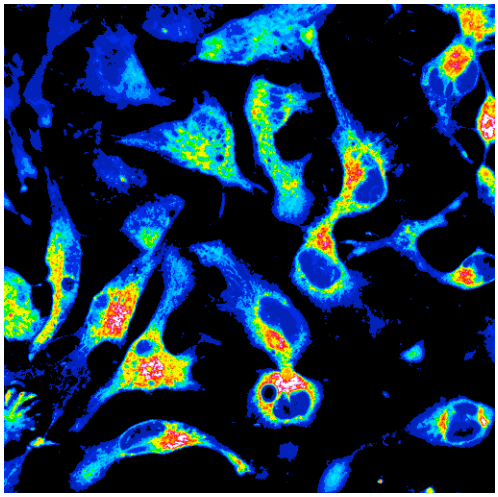

Figure A3.5. 20 μM compound **7** was added and incubated at 37 °C for 1-2 hours. At this point, buffer was removed and each well was washed 1x with 500 μL DMEM before acquiring snapshot images. Localization of compound **7** is cytosolic; however, fluorescence decreases after 1 h Fe^{2+} treatment. (a) Control treatment. (b) 100 μM Fe^{2+} treatment overnight.

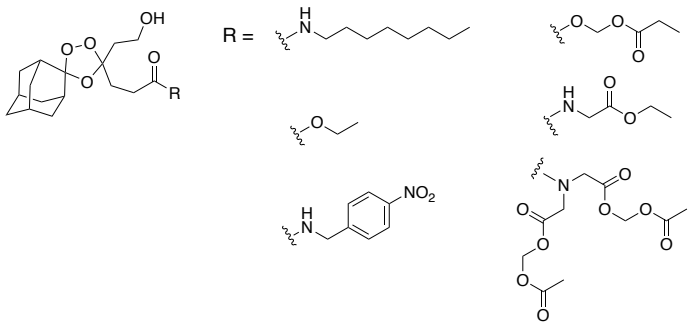

Figure A3.6. We envision modifying the Fe^{2+}-reactive trigger with groups to assist in cellular retention.

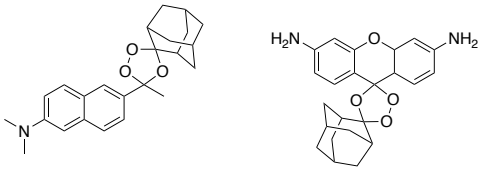

Figure A3.7. We envision synthesizing probes that contain an adamatyl endoperoxide directly appended onto the dye scaffold.

A3.5. References

1. Deu, E.; Chenb, I. T.; Lauterwasserb, E. M. W.; Valderramosa, J.; Lia, H.; Edgingtona, L. E.; Renslob, A. R.; Bogyo, M., Ferrous iron-dependent drug delivery enables controlled and selective release of therapeutic agents in vivo. *Proc. Natl. Acad. Sci. USA* **2013,** *110* (45), 18244-18249.
2. Stocks, P. A.; Bray, P. G.; Barton, V. E.; Al-Helal, M.; Jones, M.; Araujo, N. C.; Gibbon, P.; Ward, S. A.; Hughes, R. H.; Biagini, G. A.; Davis, J.; Amewu, R.; Mercer, A. E.; Ellis, G.; O'Neill, P. M., Evidence for a Common Non-Heme Chelatable-Iron-Dependent Activation Mechanism for Semisynthetic and Synthetic Endoperoxide Antimalarial Drugs. *Angewandte Chemie* **2007,** *46*, 6278-6283.
3. Mahajan, S. S.; Deu, E.; Lauterwasser, E. M. W.; Leyva, M. J.; Ellman, J. A.; Bogyo, M.; Renslo, A. R., A Fragmenting Hybrid Approach for Targeted Delivery of Multiple Therapeutic Agents to the Malaria Parasite. *ChemMedChem* **2011,** *6* (3), 415-419.
4. Urano, Y.; Kamiya, M.; Kanda, K.; Ueno, T.; Hirose, K.; Nagano, T., Evolution of Fluorescein as a Platform for Finely Tunable Fluorescence Probes. *J. Am. Chem. Soc.* **2005,** *127*, 4888-4894.
5. Bogena, J. Synthesis of Novel Fluorescent Probes for Studying Cell Signaling. Ludwig-Maximillians-University Munich, Munich, 2016.
6. Sakabe, M.; Asanuma, D.; Kamiya, M.; Iwatate, R. J.; Hanaoka, K.; Terai, T.; Nagano, T.; Urano, Y., Rational Design of Highly Sensitive Fluorescence Probes for Protease and Glycosidase Based on Precisely Controlled Spirocyclization. *J. Am. Chem. Soc.* **2012,** *135*, 409-414.
7. Murphy, M. P., Targeting lipophilic cations to mitochondria. *Biochim Biophys Acta* **2008,** *1777* (7-8), 1028-1031.
8. Bruemmer, K. J.; Walvoord, R. R.; Brewer, T. F.; Burgos-Barragan, G.; Wit, N.; Pontel, L. B.; Patel, K. J.; Chang, C. J., Development of a General Aza-Cope Reaction Trigger Applied to Fluorescence Imaging of Formaldehyde in Living Cells. *J. Am. Chem. Soc.* **2017,** *139* (15), 5338-5350.

Appendix 4

Development of a platform for identification of metalloproteins using promiscuous photocrosslinking probes

Portions of this work were performed in collaboration with the following persons:

Celine Constantin and Cheri Ackerman; Celine and Cheri performed labelling assays on purified proteins and in cell lysates.
Dr. Chris Parker from the Ben Cravatt laboratory at the Scripps Research Institute (TSRI) performed labelling experiments in whole cells and in cell lysates.

A4.1. Synopsis

Its estimated that metalloproteins comprise approximately one third to one half of the proteome[1-2]; however, discovering new metal-binding proteins *de novo* is difficult. It is challenging to predict metal-binding proteins through computational methods, as there is no one conserved consensus sequence for metal coordination. While high-throughput methods are emerging for characterizing novel metalloproteins[1], these methods often require specialized equipment and laborious procedures. Chapter 4 describes an isoTOP-ABPP workflow developed for profiling cysteine residues that bind copper; this appendix describes an alternative strategy for profiling metalloproteins using ABPP. Instead of profiling amino acid reactivity as an indirect readout of metal-binding, the strategy described in this appendix attempts tag metalloproteins based on interactions between metal center and probe headgroup. We envisioned developing a probe that would contain a metal-chelating headgroup, a photocrosslinking group, and a pull-down handle for protein identification. We envisioned the metal-chelating would provide specificity, the photocrosslinking group would covalently link probe to protein, and the pull-down handle would enable protein identification (Figure A4.1).

A4.2. Materials and Methods

A4.2.1. General synthetic methods

Reactions using moisture- or air-sensitive reagents were carried out in flame-dried glassware under an inert atmosphere of N2. Solvent was passed over activated alumina and stored over activated 3Å molecular sieves before use when dry solvent was required. All other commercially purchased chemicals were used as received (without further purification). SiliCycle 60 F254 silica gel (pre-coated sheets, 0.25 mm thick) were used for analytical thin layer chromatography and visualized by fluorescence quenching under UV light. Silica gel P60 (SiliCycle) was used for column chromatography. ^{1}H and ^{13}C NMR NMR spectra were collected at 298 K in CDCl3 or CD3OD (Cambridge Isotope Laboratories, Cambridge, MA) at 25 °C on Bruker AVQ-400, AVB-400, AV-500, or AV-600 at the College of Chemistry NMR Facility at the University of California, Berkeley or on Bruker 900 at the QB3 Central California 900 MHz NMR Facility. All chemical shifts are reported in the standard notation of δ parts per mil-lion relative to residual solvent peak at 7.26 ($CDCl_3$) or 3.31 (CD_3OD) for ^{1}H and 77.16 ($CDCl_3$) or 49.00 (CD_3OD) for ^{13}C as an internal reference. Splitting patterns are indicated as fol-lows: br, broad; s, singlet; d, doublet; t, triplet; m, multiplet; dd, doublet of doublets. Low-resolution electrospray mass spectral analyses were carried out using a LC-MS (Agilent Technology 6130, Quadrupole LC/MS and Advion expression-L Compact Mass Spectrometer). High-resolution mass spectral analyses (ESI-MS) were carried out at the College of Chemistry Mass Spectrometry Facility at the University of California, Berkeley.

*A4.2.2. Hydroxamic acid probe **2***

Diazarine linker **1** was obtained from our collaborators, Chris Parker & Ben Cravatt at Scripps. Carbonate diimidazole was added to a solution of **1** in 1 mL dry MeCN. This reaction mixture was stirred for 4 hours. At this point, imidazole (0.0164 g, 0.2408 mmol) and hydroxylamine (0.021 g, 0.301 mmol) were added, and the reaction mixture was stirred overnight. After 16 h, the reaction mixture was acidified (to pH 6) by addition of 1 M HCl. The reaction mixture was extracted into EtOAc (3 x 25 mL), washed with brine (1 x 25 mL), then

dried over Na_2SO_4 and filtered before concentrating under reduced pressure. The crude concentrate was further purified by HPLC (5% MeCN/H_2O → 95% MeCN/H_2O) and fractions containing product were lyophilized to yield **2** (0.002 g). ^{1}H NMR (600 MHz, DMSO-d_6) δ (ppm): 10.36 (s, 1 H), 8.73 (bs, 1 H), 2.812 (t, 1 H), 1.960 (m, 2 H), 1.750 (m, 2 H), 1.614 (m, 2 H), 1.546 (m, 2 H).

*A4.2.3. Hydroxyquinoline probe **3***

Diazarine linker **1** (0.013 g, 0.0783 mmol), EDC-HCl (0.0165 g, 0.086 mmol), and HOBt (0.0132 g, 0.086 mmol) were added in 1 mL dry DMF, and this was stirred for 30 minutes; then 5-amino-8-hydroxyquinoline dihydrochloride (0.020 g, 0.086 mmol) and DIPEA (30 μL, 0.1644 mmol) were added and stirred overnight at room temperature. After 16 hours, the reaction was concentrated under reduced pressure and purified by HPLC. The crude concentrate was further purified by HPLC (5% MeCN/H_2O → 95% MeCN/H_2O) and fractions containing product were lyophilized to yield **3** (0.00234 g). ^{1}H NMR (600 MHz, DMSO-d_6) δ (ppm): 9.757 (s, 1 H), 8.842 (m, 1 H), 8.316 (m, 1 H), 7.568 (m, 1 H), 7.399 (m, 1 H), 7.029 (d, 1 H), 2.838 (t, 1 H), 2.34 (m, 2 H), 2.033 (m, 2 H), 1.802 (m, 2 H).

A4.2.4. Labeling purified proteins

All protocols were described previously.[3]

A4.2.5. Labeling cell lysates and cells in situ

Labeling was carried out by Dr. Chris Parker from the Ben Cravatt laboratory at the Scripps Research Institute (TSRI). Labeling was either performed *in situ* (by treating live cells with probe prior to lysis and Click chemistry) or *in vitro* (by treating cell lysates with probe prior to Click chemistry). All treatments were performed as described.[4]

A4.3. Results, Discussion, and Conclusion

Results from experiments on purified protein and in cell lysates were described in detail previously.[3] Before performing mass spectrometry experiments using our probes, we wanted to optimize conditions on purified proteins and demonstrate that hydroxamic acid and hydroxyquinoline probes could be used to label a known metalloprotein in a metal-dependent manner in an *in vitro* model system. We hoped to demonstrate saturation of labeling with increasing probe concentration and a loss of labeling following demetallation of the protein. Toward this end, we tested our probes to see if they could label carbonic anhydrase (CA) and matrix metalloproteinase 2 (MMP2). After spiking CA (1%) into MEF cell lysates (protein concentration of lysates = 1mg/mL), we found that both the hydroxamic acid probe **2** and the hydroxyquinoline probe **3** exhibited weak labeling of CA (Figure A4.2A and B). Labeling of CA exhibited a dose-dependence with both probes. However, we found that probe labeling of CA was not dependent on the presence of Zn in carbonic anhydrase; demetallation of CA[3] did not decrease probe labeling (Figure A4.3).

Due to difficulties characterizing these probes in protein model systems, we decided to test them in metal- and chelator-treated cell lysates. We focused on the hydroxyquinoline probe, as this probe showed better signal. When we compared labeling with of control lysates to Zn-treated and EDTA-treated lysates, we found the emergence of new protein bands (Figure A4.4). Because this data looked potentially promising, our collaborator, Chris Parker from the Ben

Cravatt laboratory at the Scripps Research Institute (TSRI), performed additional labeling either *in situ* (by treating live cells with probe prior to lysis and Click chemistry) or *in vitro* (by treating cell lysates with probe prior to Click chemistry) (data not shown).

We ultimately did not pursue this project further, but it will be informative to run mass spectrometry on hydroxyquinoline-labeled lysates. We additionally plan to synthesize a control probe that cannot bind metals but otherwise has properties similar to the hydroxyquinoline probe. We hope to run mass spectrometry in parallel on lysates labelled with both probes.

Figures

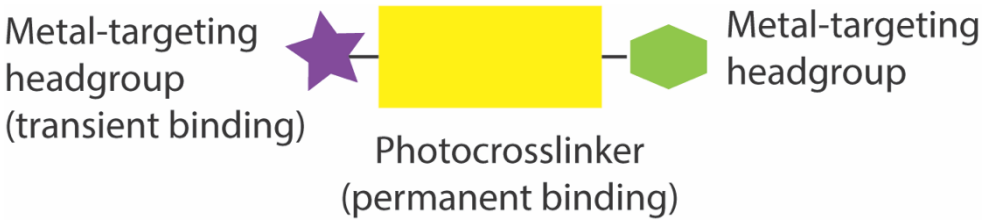

Figure A4.1. Design of metalloprotein-targeted ABPP probes.

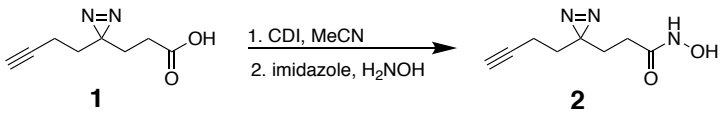

1 **2**

Scheme 4.1 Compound **2** can be synthesized from intermediate **1**, which was obtained from Dr. Chris Parker.

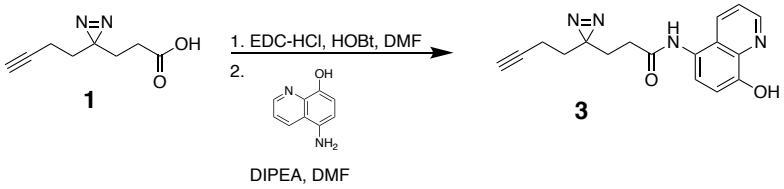

Scheme 4.2 Compound **3** can be synthesized from intermediate **1**, which was obtained from Dr. Chris Parker.

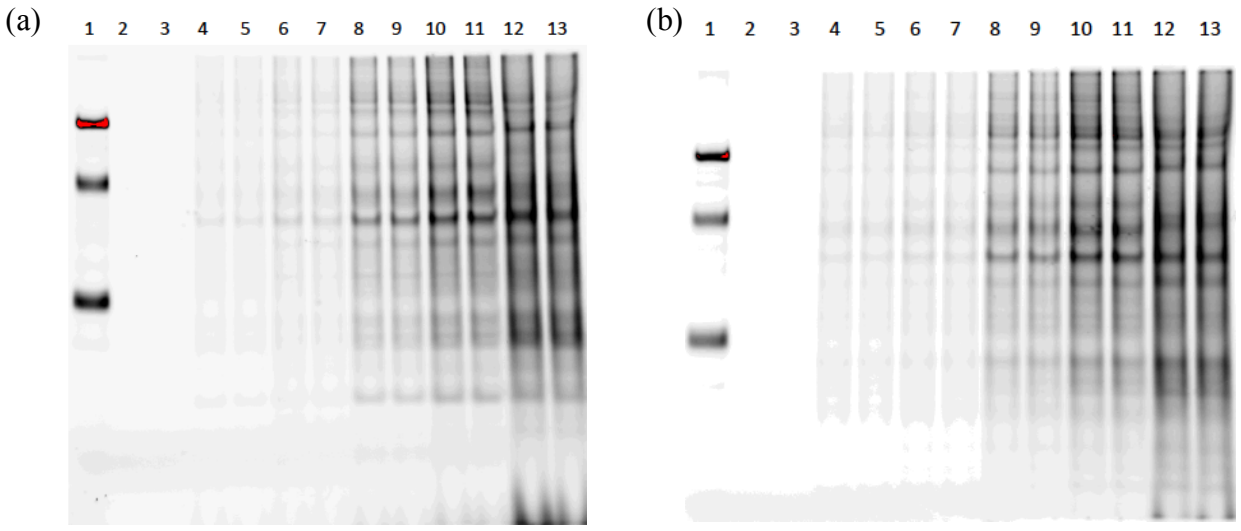

Figure A4.2. (a) Hydroxamic acid probe is titrated in MEF cell lysates (1 mg/mL) with 1% CA. Lanes 2-3 = 0 µM, lanes 4-5 = 5 µM, lanes 6-7 = 10 µM, lanes 8-9 = 50 µM, lanes 10-11 = 100 µM, lanes 12-13 = 500 µM. CA is indicated with an aesterix. (b) Hydroxyquinoline probe is titrated in MEF cell lysates (1 mg/mL) with 1% CA. Lanes 2-3 = 0 µM, lanes 4-5 = 5 µM, lanes 6-7 = 10 µM, lanes 8-9 = 50 µM, lanes 10-11 = 100 µM, lanes 12-13 = 500 µM.

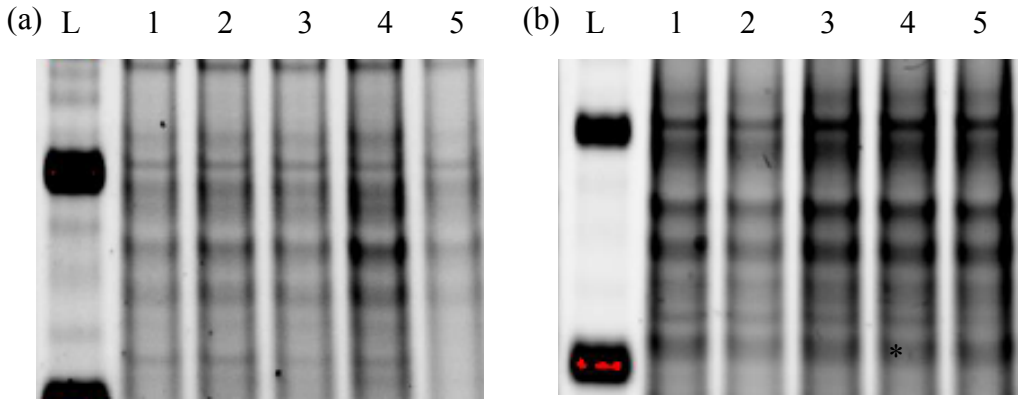

Figure A4.3. (a) Zn-CA (lanes 1-2), apo-CA (lanes 3-4), or no protein (lane 5) is spiked into MEF lysates treated with 1 mM EDTA and subsequently labeled with hydroxamic acid probe. CA is indicated with an aesterix. (b) Zn-CA (lanes 1-2), apo-CA (lanes 3-4), or no protein (lane 5) is spiked into MEF lysates treated with 1 mM EDTA and subsequently labeled with hydroxyquinoline probe.

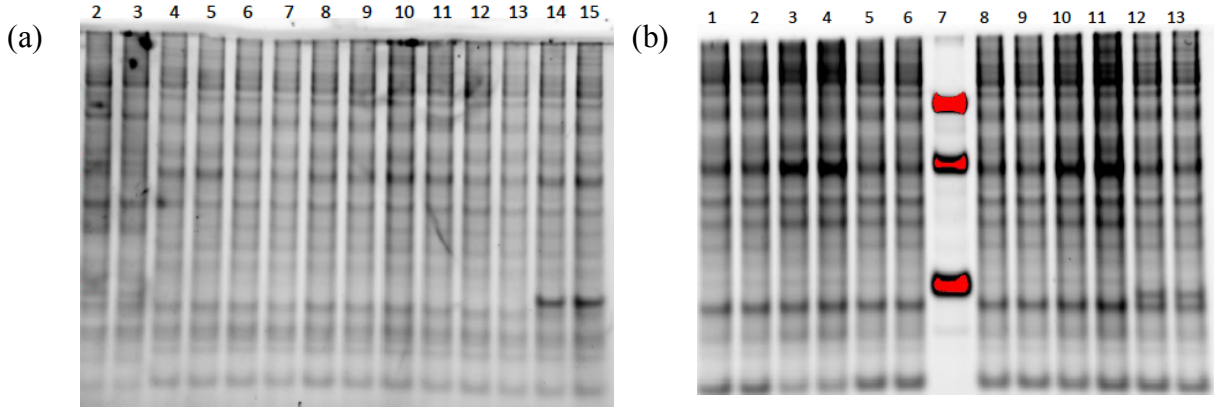

Figure A4.4. (a) 50 µM hydroxamic acid probe is used to label MEF lysates (1 mg/mL). Lanes 2-3 = control, lanes 4-5 = overnight 200 µM Zn-treatment, lanes 6-7 = overnight 1 mM EDTA-treatment, lanes 8-9 = control, lanes 10-11 = 200 µM, 1 h Zn-treatment, lanes 12-13 = 1 mM, 1 h EDTA-treatment. (b) 50 µM hydroxamic acid probe is used to label MEF lysates (1 mg/mL). Lanes 2-3 = control, lanes 4-5 = overnight 200 µM Zn-treatment, lanes 6-7 = overnight 1 mM EDTA-treatment, lanes 8-9 = control, lanes 10-11 = 200 µM, 1 h Zn-treatment, lanes 12-13 = 1 mM, 1 h EDTA-treatment. Overnight treatments were performed in cells; 1 h treatments were performed in lysates.

A4.4. References

1. Cvetkovic, A.; Menon, A. L.; Thorgersen, M. P.; Scott, J. W.; Poole, F. L. I.; Jenney, F. E. J.; Lancaster, W. A.; Praissman, J. L.; Shanmukh, S.; Vaccaro, B. J.; Trauger, S. A.; Kalisiak, E.; Apon, J. V.; Siuzdak, G.; Yannone, S. M.; Tainer, J. A.; Adams, M. W. W., Microbial metalloproteomes are largely uncharacterized. *Nature* **2010,** *466*, 779-782.
2. Andreini, C.; Bertini, I.; Rosato, A., Metalloproteomes: A Bioinformatic Approach. *Acc. Chem. Res.* **2009,** *42* (10), 1471-1479.
3. Constantin, C. Catching Metalloproteins: Reactive Cysteine Profiling and Metal-targeted Photocrosslinking Probes. Master of Science, Ecole Polytechnique Federale de Lausanne, Lausanne, 2015.
4. Parker, C. G.; Galmozzi, A.; Wang, Y.; Correia, B. E.; Sasaki, K.; Joslyn, C. M.; Kim, A. S.; Cavallaro, C. L.; Lawrence, R. M.; Johnson, S. R.; Narvaiza, I.; Saez, E.; Cravatt, B. F., Ligand and Target Discovery by Fragment-Based Screening in Human Cells. *Cell* **2017,** *168* (3), 527-541.